SPACE-CHARGE WAVE THEORY OF INTERACTION GAPS AND MULTI-CAVITY KLYSTRONS WITH EXTENDED FIELDS

by

T. Wessel-Berg

NDRE REPORT NO 32

FORSVARETS FORSKNINGSINSTITUTT

Norwegian Defence Research Establishment

Kjeller - Lillestrøm - Norway

September 1960

PREFACE

This report is the outgrowth of a general study of electron beam interaction phenomena in interaction regions of finite lengths and arbitrary RF field distributions.

The research was initiated while the author was an International Cooperation Administration fellow at the Microwave Laboratory, Stanford University, California, and later continued at the Norwegian Defence Research Establishment, Division for Radar, Bergen.

Some of the results from the earlier parts of the investigation, which have been published elsewhere, are included in considerably revised form. The main parts of the report, however, represent previously unpublished material.

ACKNOWLEDGEMENTS

The author would like to express his appreciation to the Norwegian Defence Research Establishment for permission to publish the present report, and to the Royal Norwegian Council for Scientific and Industrial Research for financial support towards the cost of printing. The author is also grateful to his many associates who took an active interest in the work and contributed in many ways by stimulating discussions and criticism. In particular, the author is indebted to Dr Marvin Chodorow, Stanford University, who originally suggested the topic dealt with in the report.

CONTENTS

GLOSSARY OF SYMBOLS

a_p	Coefficient associated with the gap voltage difference equation, defined by Eq (B. 4)
A	Initial amplitude of the attenuated gap voltage wave in a synchronously tuned multi-cavity klystron, defined by Eq (3. 50)
$\underset{\sim}{A}$	Excitation column vector, defined by Eq (4. 7)
b_e	Small-signal electronic susceptance normalized with respect to G_o, $(b_e = B_e/G_o)$
b_p	Coefficient associated with the gap voltage difference equation, defined by Eq (B. 5)
B	Initial amplitude of the growing gap voltage wave in a synchronously tuned multi-cavity klystron, defined by Eq (3. 51)
$\bar{B}$	Magnetic induction
B_e	Small-signal electronic susceptance, defined by Eq (2. 69)
$\underset{\sim}{B}_{e,S}$	Electronic susceptance matrix associated with the Sth group of gaps, defined by Eq (4. 25)
$\underset{\sim}{C}$	Circuit matrix associated with the two-port representation of a general interaction region, defined by Eq (5. 84)
$\bar{D}$	Electric displacement
$\underset{\sim}{D}_1$, $\underset{\sim}{D}_2$	Drift matrices associated with the two-port representation of a general interaction region, defined by Eqs (5. 70) and (5. 71)
e	Charge of the electron
$\bar{E}$	Electric field intensity
E_b	Space-charge field
E_c	Circuit field
F(x)	Normalized longitudinal RF electric field distribution in a gap, defined by Eq (2. 51)
F_n	The nth space harmonic component of F(x)
g_e	Small-signal electronic conductance normalized with respect to G_o, $(g_e = G_e/G_o)$
G_c	Circuit conductance, $(G_c = \text{Re } Y_c)$
G_e	Small-signal electronic conductance, defined by Eq (2. 69)
G_o	Ratio of DC beam current to DC beam voltage
$\underset{\sim}{G}_{e,S}$	Electronic conductance matrix associated with the Sth group of cavities, defined by Eq (4. 24)
$\bar{H}$	Magnetic field intensity
$\bar{i}$	RF beam current density
I	RF beam current
I_o	DC beam current

$\underset{\sim}{K}$	Matrix representing the two-port of a general interaction region, defined by Eq (5.59)
ℓ	Length of interaction region
$\ell_{s,r}$	Spacing between the centers of the rth gap and the sth gap
$\ell_{s,o}$	Spacing between the input cross-section of the first gap and the center of the sth gap
L	Spacing between two identical groups of cavities
$\underset{\sim}{L}_S$	Position matrix associated with the Sth group of cavities, defined by Eq (4.33)
m	Mass of the electron
M	Complex gap coupling coefficient, defined by Eq (2.53)
M_o	Absolute value of M
M^+	Coupling coefficient of the slow space-charge wave, defined by Eq (2.58)
M^-	Coupling coefficient of the fast space-charge wave, defined by Eq (2.58)
$\overline{M^2}$	Mean square of M_o^+ and M_o^-
$\underset{\sim}{M}_S^+$, $\underset{\sim}{M}_S^-$	Coupling coefficient matrices (line vectors) associated with the Sth group of cavities, defined by Eqs (4.31) and (4.32)
$\underset{\sim}{\overline{M^2}}$	Mean square coupling coefficient matrix, defined by Eq (4.50)
n	Number of half waves, or harmonic number
p	Number of cavities in the multi-cavity klystron
P	Power
P_i	Available input power from the signal generator
P_L	Output power from the klystron
$\mathcal{P}$	Complex power
$\mathcal{P}_p$	Complex power extracted by the beam in the pth interaction region
Q	Unloaded Q-value
Q_e	Electronic Q
Q_{ext}	External Q
Q_L	Loaded Q
R	Plasma reduction factor, ($R = \omega_q/\omega_p$)
R_{sh}	Shunt impedance
R_{sh}/Q	Characteristic impedance of the cavity, defined by Eq (A.10)
S_p	Coefficient associated with the gap voltage difference equation, defined by Eq (3.21)
t	Time
T_p	Coefficient associated with the gap voltage difference equation, defined by Eq (3.22)

u	RF beam velocity
u_o	DC beam velocity
U	RF kinetic voltage, defined by Eq (2.17)
$\underset{\sim}{U}_{S,S}$	Self-admittance matrix in the alternate matrix formulation, defined by Eq (4.75)
$\underset{\sim}{U}_{S,S-1}$	Transfer admittance matrix in the alternate matrix formulation, defined by Eq (4.77)
v	Phase velocity
V	RF gap voltage, defined by Eq (2.52)
V_o	DC beam voltage
$\underset{\sim}{V}$	RF gap voltage column vector, defined by Eq (4.6)
W	RF beam impedance, defined by Eq (2.30)
W_{em}	Stored energy in a resonant cavity
x	Axial co-ordinate measuring distance from the center of each interaction gap
y_1	Normalized input admittance of the first cavity measured at the "detuned short" position, given by Eq (A.7)
$Y_{c,s}$	Circuit admittance of the sth gap, defined by Eq (A.15)
$Y_{e,s}$	Electronic admittance of the sth gap, defined by Eq (2.69)
$[Y_e]_s$	Total electronic admittance of the sth gap including transfer terms, defined by Eq (A.11)
$Y_{s,r}$	Transfer admittance from the rth to the sth gap, defined by Eq (2.67)
$Y_{s,s}$	Self-admittance of the sth gap, $(Y_{s,s} = Y_{c,s} + Y_{e,s})$
$\underset{\sim}{Y}_{c,S}$	Circuit admittance matrix associated with the Sth group of cavities, defined by Eq (4.21)
$\underset{\sim}{Y}_{e,S}$	Electronic admittance matrix associated with the Sth group of gaps, defined by Eq (4.22)
$\underset{\sim}{Y}_{S,R}$	Transfer admittance matrix associated with the Rth and the Sth groups of gaps, defined by Eq (4.36)
$\underset{\sim}{Y}_{S,S}$	Self-admittance matrix of the Sth group of cavities, $(\underset{\sim}{Y}_{S,S} = \underset{\sim}{Y}_{c,S} + \underset{\sim}{Y}_{e,S})$
z	Axial co-ordinate
α_1, α_2	Voltage gain per stage of the attenuated and growing gap voltage waves in synchronously tuned klystrons, given by Eq (3.46)
$\underset{\sim}{\alpha}_S$	Voltage gain matrix of the Sth cavity group, given by Eq (4.71)
β_e	Propagation factor associated with the DC beam velocity, $(\beta_e \triangleq \omega/u_o)$
β_q	Plasma propagation factor
δ	Frequency tuning parameter, defined by Eq (A.8)
Δ	Difference operator, operating on a function of β_e, defined by Eq (2.38)

$\oint$	Sum operator, operating on a function of β_e, defined by Eq (2.39)
ϵ	Velocity parameter, defined by Eq (5.108)
ϵ_o	Permittivity of free space
η_p	Complex voltage gain from the input gap to the pth gap, ($\eta_p = V_p/V_1$)
$\eta_{s,r}$	Voltage gain of the two-gap klystron consisting of the rth and the sth cavities with the intermediate cavities removed or detuned, defined by Eq (3.12)
$\underline{\eta}_{S,R}$	Voltage gain matrix of the Rth and Sth cavity groups with intermediate cavity groups removed, defined by Eq (4.13)
θ	DC transit angle between centers of consecutive gaps
θ_q	Plasma transit angle between centers of consecutive gaps
$\mathscr{M}$	Beam loading parameter, defined by Eq (3.38)
ξ	A parameter proportional to the voltage gain at zero beam loading of a two-cavity klystron, defined by Eq (3.39)
ρ	Space-charge density
φ_1	Phase angle of α_1
φ_2	Phase angle of α_2
$\varphi_{\mathscr{M}}$	Phase angle of $1-2\mathscr{M}$
$\phi(\epsilon)$	A function of ϵ (equal to M_o^2), from which the small-signal electronic conductance can be obtained by means of the difference operator Δ, defined by Eq (5.118)
$\psi(\epsilon)$	A function of ϵ, from which the small-signal electronic susceptance can be obtained by means of the difference operator Δ, defined by Eq (5.119)
ω	Angular frequency
ω_o	Resonant angular frequency
ω_p	Angular plasma frequency
ω_q	Reduced angular plasma frequency
Ω	Space-charge parameter, defined by Eq (5.122)

SPACE-CHARGE WAVE THEORY OF INTERACTION GAPS AND MULTI-CAVITY KLYSTRONS WITH EXTENDED FIELDS

SUMMARY

The report presents an analysis of space-charge wave propagation on a thin electron beam subject to modulation in a series of interaction gaps of arbitrary length and longitudinal RF electric field distribution. Representation of general interaction gaps by two-ports and their possible realization by passive networks are discussed.

Application of the general modulation theory to multi-cavity klystrons with extended interaction fields leads to a generalized small-signal klystron theory which is more rigorous than the conventional theory in the sense that space-charge and density modulation effects in the interaction gaps are properly accounted for.

Analytical formulae for the frequency response are derived using various approaches, including a formulation in terms of self-admittances and transfer admittances associated with the interaction gaps, and a formulation in terms of gap voltage waves.

A number of problems are discussed which appear to be significant for proper understanding of klystron behavior and for practical design of klystrons with extended interaction gaps.

1 INTRODUCTION

The phenomena taking place in electron beam tubes for generation and amplification of electromagnetic power in the microwave region have been the subject of very extensive theoretical and experimental studies during the last few decades. Of the considerable number of various practical devices that have appeared as a result of this study, the tubes known as longitudinal beam amplifiers are probably best known. These are characterized by a long thin electron beam surrounded by an electric circuit that can take many different configurations. The amplification process is basically one in which part of the kinetic energy of the beam is transferred to electromagnetic power by cumulative interaction between space-charge waves propagating on the electron stream and the electromagnetic field of the surrounding circuit. Since a long thin beam is a common feature of these tubes, the characteristics of various types of longitudinal beam amplifiers are mainly determined by the details of the circuit configuration. Typical examples are the traveling-wave tube (1, 2, 3, 4, 5) and the conventional narrow-gap klystron (2, 5, 6, 7), which represent distributed and lumped interaction, respectively. Although the concepts of distributed contra lumped interaction may be useful for qualitative understanding of the interaction processes, the fundamental phenomena of velocity modulation and transit-time effects causing density modulation and power extraction are the same for both. In particular, it should not be implied that distributed and lumped interaction phenomena in general are characteristic for traveling-

wave tubes and klystrons, respectively. Examples can be given of traveling-wave tubes employing transmission lines consisting of coupled narrow-gap cavities essentially similar to klystron cavities, thus exhibiting lumped interaction (8). Conversely, later developments of klystrons make use of extended fields of resonated slow-wave structures for which the interaction is distributed (9,10). Noting that the circuit of the traveling-wave tube is a non-resonant transmission line and that of the klystron a number of separated resonant cavities, the significant differences between the two types of tubes, accounting for their typical operating characteristics, must be ascribed to fundamental differences in the electrical characteristics of the circuits rather than being associated with distributed contra lumped interaction.

Even if historically the klystron is the older of the two, the theory of the various aspects of traveling-wave interaction has reached a more satisfactory state than the theory of the klystron. This situation is probably due largely to the fact that klystron theory has developed along two different lines based on kinematic and space-charge wave approaches, respectively. The original theory of velocity modulation and bunching was a pure kinematic or ballistic approach in which space-charge effects were disregarded (11,12). Later theories introduced corrections accounting for the debunching effects of space-charge in the drift tubes between the gaps (13). Although these corrections essentially are equivalent to a space-charge wave description (14,15) of the drift phenomena in the regions between the gaps, the modulation processes taking place in the gaps themselves are still treated on a kinematic basis using a model with infinitely narrow gaps and introducing correction factors accounting for the small but finite length of the actual interaction gaps. It is not widely recognized, however, that this model is only approximate and does not account fully for the phenomena taking place. The approximations involved are those of neglecting density modulations and space-charge effects in the gaps. In many cases these approximations are serious, particularly in klystrons with high-density beams and extended interaction regions, but also to a lesser extent in conventional narrow-gap klystrons.

The present report is concerned with a small-signal study of interaction gap phenomena and multi-cavity klystrons from a very broad point of view. In presenting the material contained in the report emphasis has been put on generality, and attempts have been made to make the basic assumptions as unrestrictive as possible. A consistent and considerably more general theory than the conventional one is developed by performing a space-charge wave analysis of the interaction processes in a beam traversing an amplifier structure consisting of a number of adjacent but uncoupled interaction regions of arbitrary lengths and arbitrary longitudinal RF field distributions. Through this approach it is possible in the analysis to avoid the rather artificial and unnecessary separation of drift-tube and interaction-gap phenomena that is characteristic of conventional klystron theory.

Even if the theory essentially deals with distributed or extended interaction phenomena and in this respect is related to the theory of traveling-wave tubes, there are

significant differences arising from the types of circuit used. It is characteristic for klystrons as opposed to traveling-wave tubes that the longitudinal RF field distribution in each interaction region is approximately independent of the interaction processes occurring in the region. The normal-mode theory of resonant cavities (2) shows that this assumption is justified provided the cavities have relatively high Q-values, i e large stored energies compared to the power dissipated in the cavities.

The general approach discussed above, using space-charge wave analysis, leads to a consistent small-signal theory which differs from the less complete formulations in several respects: first, both velocity and density modulation phenomena in the interaction regions are properly accounted for; second, space-charge effects in the interaction gaps are included; and third, the theory is considerably more general, comprising interaction regions of arbitrary lengths and arbitrary longitudinal RF field distributions.

These differences between the more rigorous theory of this report and the less complete formulations have many implications that are discussed as they naturally appear in the analysis. Furthermore, apart from the limitations of conventional klystron theory, the present approach appears to be mathematically simpler, and leads to a number of significant results concerning interaction gaps in general and multi-cavity klystrons in particular. The following is a brief account of the main contents in each chapter.

Chapter 2 is concerned with the fundamental modulation phenomena occurring in an electron beam traversing a number of cascaded modulation regions in succession. The RF kinetic energy associated with the beam and conversion of kinetic beam power to electromagnetic power in each region are discussed and shown to be consistent with the small-signal kinetic power theorem (18, 20, 21).

In Chapter 3 application is made of the general space-charge modulation theory of Chapter 2 for a very thorough small-signal study of multi-cavity klystrons with arbitrary, extended interaction fields. General analytical formulae for gain and bandwidth are derived using two different approaches. One leads to a formulation in terms of self-admittances and transfer admittances associated with the interaction regions; this theory is valid for arbitrary, stagger-tuned cavities. The other, which is applicable only to klystrons having synchronously tuned cavities, is a "wave approach" quite analogous to the approach used in the theory of traveling-wave tubes. In this wave formalism, klystron operation is described in terms of growing and attenuated "gap voltage waves" propagating in approximate synchronism with the slow and the fast space-charge waves on the beam.

In this chapter a considerable number of problems are discussed which are important for proper understanding of klystron theory and for practical design of klystrons, such as stability, optimization problems, scaling rules for gain and bandwidth, and reciprocity theorems.

Chapter 4 deals with a further generalization of klystron theory which differs from the theory in Chapter 3 in that klystron performance is described by means of appropriately defined matrix parameters associated with groups of consecutive cavities, rather than by scalar parameters associated with single cavities. The matrix formulation is particularly powerful for solving certain types of problems arising in connection with several klystrons coupled in cascade with common beam, e g evaluation of gain and optimum spacing of two or more cascaded klystrons, periodically stagger-tuned klystrons, and related problems.

Chapter 5 contains a general gap theory of extended interaction regions. Launching of space-charge waves by an extended modulation gap and excitation of an extended-interaction cavity by a modulated beam are studied in considerable detail. The theory includes a discussion of the conditions for which the interaction region couples only to one of the space-charge waves, a situation which has some actuality in connection with fast-wave couplers for low noise parametric amplifiers (24,28). The general gap theory developed in this chapter substantiates the previously discussed objections that must be raised concerning the validity of conventional gap theory.

In the subsequent treatment general two-port representations of interaction regions are given. Representation by a combination of passive, reciprocal networks and transmission lines is discussed and shown to be possible only if the beam loading of the gap vanishes. For this case a practical analog of multi-cavity klystrons is suggested, which is based on transmission lines loaded with passive, lumped resonant circuits (16). The suggested analog appears to have potential uses for optimization of stagger-tuning pattern of multi-cavity klystrons.

The remaining part of Chapter 5 is concerned with a discussion of general properties of the relevant gap parameters, which are the gap coupling coefficients of the slow and the fast space-charge waves, and the electronic admittance. The chapter concludes with presentation of numerical data for these parameters in the special case that the longitudinal RF field distribution is sinusoidal. This is a field distribution of considerable practical interest because it couples strongly to the space-charge waves and can be realized very simply using shorted slow-wave structures which, in general, are characterized by relatively high interaction impedance (9).

The inclusion of numerical data for the sinusoidal field distribution serves as an illustrative example of the possibilities that exist for enhancement of klystron gain and bandwidth by the use of non-conventional interaction regions.

PROPAGATION OF SPACE-CHARGE WAVES ON LINEAR ELECTRON BEAMS IN CASCADED MODULATION REGIONS

Introduction

An exact analysis of the propagation of space-charge waves on longitudinal electron beams of finite cross-sections is extremely difficult. Only approximate solutions based on simplified physical models of the electron beam system can be obtained (14,15). It is found that the beam supports an infinite number of space-charge modes, each consisting of a pair of space-charge waves having propagation factors whose arithmetic averages are approximately equal to the propagation factor associated with the time-average or DC electron velocity. For a thin beam with small lateral extension compared to the wavelengths of the space-charge waves, the lowest-order or fundamental space-charge mode has approximately uniform current and velocity modulations over the entire beam cross-section, whereas the higher-order modes vary rapidly across the beam. For this reason external structures with approximately uniform fields at the position of the beam couple predominantly to the fundamental space-charge mode. This fact allows interaction phenomena between a thin beam and external circuits to be analyzed, disregarding all but the fundamental space-charge mode. This is one of the fundamental assumptions on which the present work is based. The second fundamental assumption is that of small-signal conditions, which is necessary for linearization of the equations describing the interaction phenomena. The assumption of small-signal conditions is not too restrictive to be useful, because longitudinal beam tubes operate in the linear range throughout the larger part of their interaction length except possibly the output region. This is especially true in the upper frequency ranges where efficiency generally is quite low.

In order to avoid mathematical complications that are unessential for an understanding of the physical phenomena, the one-dimensional model of the RF structure and the beam is adopted. This assumption implies that all quantities considered in the analysis are functions of a single spatial co-ordinate, the co-ordinate along the beam. All parameters are thus independent of the co-ordinates transverse to the beam. The one-dimensional small-signal analysis in conjunction with the assumptions stated below leads to a theory in which a signal propagating on the beam can be characterized in terms of two modulation parameters, for example the velocity and current modulations, or suitable linear combinations of these.

The assumptions, stated explicitly, are:

a) The analysis is one-dimensional. The assumption that none of the relevant RF quantities depend on transverse co-ordinates is well satisfied in physical beams if the beam diameter is sufficiently small. In this case both the space-charge field and the external circuit field are approximately uniform over the beam cross-section.

b) A strong longitudinal magnetic focusing field confines the motion of the electrons to lines parallel with the axis.

c) The analysis is non-relativistic. This assumption implies that the acceleration of electrons from RF magnetic fields can be neglected.

d) The electron beam is assumed to drift in a cloud of heavy positive ions exactly neutralizing its time-average or DC space-charge. The ions are assumed to have infinite mass. Thus, they are not accelerated by the RF field and do not contribute to the RF current in the beam.

e) The time-average quantities are independent of the axial co-ordinate. This restriction is required to ascertain that only the fundamental space-charge mode propagates on the beam, since spatial variations in the time-average velocity introduce cross-couplings between the fundamental space-charge mode and higher-order modes.

f) The RF modulation on the beam is treated as a small perturbation of the time-average or DC conditions. The analysis, therefore, is valid under small-signal conditions.

g) Excitations of higher-order space-charge modes are neglected, and a signal on the beam is assumed to propagate only in the fundamental space-charge mode. This assumption is well satisfied for thin beams drifting in a constant DC potential.

h) Interaction between the beam and the external circuit field is treated on a small-perturbation basis, i e with weak coupling between the space-charge field of the beam and the circuit field of the external structure.

The assumption of weak coupling permits a description which essentially is a coupled-mode theory, in which the composite system consisting of the electron beam and the external circuit can be analyzed in terms of the characteristic parameters of the sub-systems, namely the space-charge mode propagating on a freely drifting beam without the external circuit, and the normal modes which are characteristic for the circuit with no beam present.

The coupled-mode formulation, based essentially on the same assumptions as the ones stated above, has been used extensively in the analysis of longitudinal-beam amplifiers such as the traveling-wave tube (1) and the klystron (6). The traveling-wave tube is a typical representative of the class of beam tubes having extended interaction, based on coupling between a space-charge wave propagating on the electron stream and a synchronous circuit wave propagating on a transmission line, while the conventional klystron in a sense represents the other extreme: lumped interaction fields confined to narrow gaps.

In the present work we shall analyze the interaction of space-charge waves with circuit fields which are considerably more general in the sense that the lengths of interaction regions and their longitudinal RF field distributions are quite arbitrary. The analysis naturally divides into two parts. The first part is concerned with the excitation of space-charge waves in the beam by a given circuit field. The appropriate equation describing this relationship is conveniently referred to as the electronic equation, the form of which does not depend on the details of the circuit. The second part of the analysis deals with the excitation of circuit fields by a given space-charge modulation in the beam. This relation is expressed in the circuit equation which generally takes different forms depending on the particular type of circuit used. Simultaneous solution of the electronic equation and the circuit equa-

tion, subject to the proper boundary conditions, yields a consistent solution of the problem of determining the space-charge waves and the circuit fields of the composite system represented by the beam and the circuit coupled together.

2.2 Basic equations governing space-charge flow

In the analysis of electron beam problems it is convenient to adopt a sign convention that results in positive numbers for electron beam velocity, current density, and electron space-charge density. The choice of signs for the various field quantities must be done in a way which is consistent with Maxwell's equations. In the m k s system used throughout this report, these are

$$\begin{aligned} \nabla \times \bar{E} &= -\frac{\partial \bar{B}}{\partial t} \\ \nabla \times \bar{H} &= \bar{i} + \frac{\partial \bar{D}}{\partial t} \\ \nabla \cdot \bar{D} &= \rho \\ \nabla \cdot \bar{B} &= 0 \end{aligned} \qquad (2.1)$$

Obviously, this set of equations is invariant to the following transformations

$$\begin{aligned} \bar{E} &\rightarrow -\bar{E} \\ \bar{H} &\rightarrow -\bar{H} \\ \bar{i} &\rightarrow -\bar{i} \\ \rho &\rightarrow -\rho \\ \bar{u} &\rightarrow \bar{u} \end{aligned} \qquad (2.2)$$

These transformations also leave quantities involving products and ratios of two field quantities invariant, such as energy flow $\bar{E} \times \bar{H}$, impedance E/H etc. The advantage gained by using this sign convention in analyses connected with electron beam problems more than outweighs the minor disadvantages resulting from adopting a sign convention different from the standard form.

Under the small-signal assumption all quantities can be written as a sum of a time-average part and a time-varying part whose amplitude is much smaller than the time-average part. The first-order evaluation of the time-varying quantities results in linear equations. Thus, a sinusoidal excitation of frequency ω causes a sinusoidal response of all time-varying quantities at the same frequency. Under the assumptions stated above we can write, using complex notation

$$E(z,t) = E_o(z) + \mathrm{Re}\,[\,E(z)\,e^{j\omega t}\,] \tag{2.3}$$

$$i(z,t) = i_o(z) + \mathrm{Re}\,[\,i(z)\,e^{j\omega t}\,] \tag{2.4}$$

$$u(z,t) = u_o(z) + \mathrm{Re}\,[\,u(z)\,e^{j\omega t}\,] \tag{2.5}$$

$$\rho(z,t) = \rho_o(z) + \mathrm{Re}\,[\,\rho(z)\,e^{j\omega t}\,] \tag{2.6}$$

where $E(z,t)$, $i(z,t)$, $u(z,t)$ and $\rho(z,t)$ are the longitudinal electric field intensity, the current density, the velocity, and the space-charge density, respectively. Furthermore, $E(z)$, $i(z)$, $u(z)$ and $\rho(z)$ are the small-signal complex amplitudes of the time-varying parts of the same quantities. Using the Eulerian approach, treating the beam as a continuous "fluid", made up of an infinite number of infinitely small particles with an infinitesimal charge, the space-charge flow is governed by the following three equations:

a) The continuity equation

b) The definition of current in terms of velocity and space-charge density

c) The force equation

The continuity equation is given by

$$\frac{\partial i(z,t)}{\partial z} + \frac{\partial \rho(z,t)}{\partial t} = 0 \tag{2.7}$$

Separation in time-average and time-dependent parts yields

$$\frac{\partial i_o(z)}{\partial z} = 0\,, \quad \text{i e} \quad i_o = \text{constant} \tag{2.8}$$

$$\frac{\partial i(z)}{\partial z} + j\omega\,\rho(z) = 0 \tag{2.9}$$

The current is defined by

$$i(z,t) = u(z,t)\;\rho(z,t) \tag{2.10}$$

Neglecting cross-products of second order, we obtain, upon separation in time-average and time-dependent parts

$$i_o(z) = u_o(z)\;\rho_o(z) \tag{2.11}$$

$$i(z) = u_o(z)\;\rho(z) + \rho_o(z)\;u(z) \tag{2.12}$$

In the Eulerian formulation the force equation is given by

$$\frac{du(z,t)}{dt} = \frac{\partial u(z,t)}{\partial t} + u(z,t)\,\frac{\partial u(z,t)}{\partial z} = \frac{e}{m}\,E(z,t) \tag{2.13}$$

where e and m are the charge and mass of the electron, respectively (note that in our notation the electronic charge e is a positive number). Separation of the equation into time-average and time-dependent parts yields

$$\frac{\partial}{\partial z}\left[\tfrac{1}{2}\,u_o(z)^2\right] = \frac{e}{m}\,E_o(z) \tag{2.14}$$

$$j\omega\,u(z) + \frac{\partial}{\partial z}\left[u_o(z)\;u(z)\right] = \frac{e}{m}\,E(z) \tag{2.15}$$

According to our initial assumptions, the time-average quantities do not vary with the axial co-ordinate z. This means that the beam is drifting in a region of constant DC potential V_o which is related to the DC velocity u_o by the equation

$$V_o = \int E_o(z)\,dz = \tfrac{1}{2}\,\frac{m}{e}\,u_o^2 \tag{2.16}$$

Equations (2.8) through (2.15) can be combined to two equations which take on particularly simple forms after introduction of the following variables

$$U(z) = \frac{u_o\,u(z)}{e/m} \tag{2.17}$$

$$\beta_e = \frac{\omega}{u_o} \tag{2.18}$$

The quantity U(z) is the RF kinetic voltage which is proportional to the velocity modulation u(z). The propagation factor β_e is associated with the DC electron velocity u_o.

Substituting from Eqs (2.9) and (2.11) in Eqs (2.15) and (2.12), and introducing the notations defined above, we obtain

$$\left[j\,\beta_e + \frac{\partial}{\partial z}\right] U(z) = E(z) \tag{2.19}$$

$$\left[j\,\beta_e + \frac{\partial}{\partial z}\right] i(z) = \tfrac{1}{2}\,j\,\beta_e\,\frac{i_o}{V_o}\,U(z) \tag{2.20}$$

These two equations, which form the basis for the subsequent analysis, govern the propagation of space-charge waves on a longitudinal electron beam. The first equation is the force equation relating the acceleration to the electric field. The second is essentially the continuity equation, relating the rate of change of the current modulation i(z) to the kinetic voltage modulation U(z).

It is important to notice that the electric field intensity E(z) appearing in Eq (2.19) is the total electric field due to both the charges in the beam and the imposed circuit field. Under the assumption of weak coupling (small perturbation) the superposition principle obtains, that is, the electric field of the composite system is the sum of the electric fields in the modes of the two sub-systems with the coupling

removed. In our case these are the electric fields $E_b(z)$ and $E_c(z)$ of the fundamental space-charge mode on the beam with the external circuit removed, and the appropriate circuit mode, respectively. Thus, we have

$$E(z) = E_b(z) + E_c(z) \tag{2.21}$$

In the next section we shall show that the space-charge field can be eliminated from Eq (2.19) by expressing E_b in terms of the current density i.

2.3 Relation between space-charge field and current density

The space-charge field $E_b(z)$ can be related to the current density $i(z)$ through the use of Maxwell's equations (2.1). We have, by taking the divergence of the curl equation for H

$$\nabla \cdot [\, \bar{i} + j\omega\epsilon_o \bar{E}_b \,] = 0 \tag{2.22}$$

Observing that the current density $\bar{i}$ is directed in the positive z-direction, we have

$$\nabla \cdot \bar{E}_b = -\frac{1}{j\omega\epsilon_o} \frac{\partial i(z)}{\partial z} \tag{2.23}$$

In the truly one-dimensional beam,there are no transverse fields, in which case $\nabla \cdot \bar{E}_b = \partial E_b(z)/\partial z$. Thus, from Eq (2.23)

$$E_b(z) = -\frac{1}{j\omega\epsilon_o} i(z) \tag{2.24}$$

This case requires infinite beam cross-section and has less practical interest than the beam with finite cross-section. In the latter case, the space-charge field has a transverse component E_r, and from Eq (2.23) we find

$$\frac{\partial}{\partial z}\left[E_b(z) + \frac{1}{j\omega\epsilon_o} i(z) \right] = -\frac{1}{r} \frac{\partial}{\partial r} (r E_r) \tag{2.25}$$

This equation serves as an illustration of the fact that the longitudinal field in the finite beam is modified by the transverse fringing field. A rigorous analysis of the finite beam subject to the appropriate boundary conditions (15) shows that the longitudinal space-charge field of the fundamental space-charge mode is obtained by multiplication of the expression in Eq (2.24) by the square of a factor R, the plasma reduction factor, which is always less than unity. The reduction factor depends on the details of the geometry of the beam with its surrounding conducting boundaries, and the propagation factor β_e. Thus, for the finite beam Eq (2.24) must be modified to

$$E_b(z) = -\frac{R^2}{j\omega\epsilon_o}\, i(z) \tag{2.26}$$

In the subsequent analyses we shall assume that the plasma reduction factor R is constant throughout the entire interaction length. Also, according to the basic assumptions stated in the introduction, the beam is sufficiently thin to justify the one-dimensional beam model with no variations of the longitudinal electric field and current density over the beam cross-section. We can then write Eq (2.26) in terms of the complex amplitude of the current I(z) rather than the current density i(z). The equations are further simplified by introducing some new parameters relating to the propagation of space-charge waves, namely the plasma frequency ω_p, the reduced plasma frequency ω_q, the reduced plasma propagation factor β_q, and the RF beam impedance W. These quantities are defined by

$$\omega_p^2 = \frac{e}{m}\,\frac{\rho_o}{\epsilon_o} \tag{2.27}$$

$$\omega_q = R\beta_p \tag{2.28}$$

$$\beta_q = \frac{\omega_q}{u_o} \tag{2.29}$$

$$W = \frac{2V_o\,\beta_q}{I_o\,\beta_e} \tag{2.30}$$

With the use of these definitions the expression for the space-charge field becomes

$$E_b(z) = j\beta_q\, W\, I(z) \tag{2.31}$$

2.4 Beam modulation in general cascaded interaction regions

Substitution of Eq (2.27) through (2.31) in Eq (2.19) and (2.20) results in the following equations between the kinetic voltage U(z), the RF current I(z) and the circuit field $E_c(z)$:

$$\left[j\beta_e + \frac{\partial}{\partial z}\right] U(z) = j\beta_q\, W\, I(z) + E_c(z) \tag{2.32}$$

$$\left[j\beta_e + \frac{\partial}{\partial z}\right] I(z) = j\beta_q\,\frac{1}{W}\, U(z) \tag{2.33}$$

These equations are reminiscent of transmission-line equations, and in fact can be shown to be identical with these in a co-ordinate system moving with the time-average velocity of the beam, provided the circuit field is zero (17).

The first-order coupled "transmission-line" equations above can be combined to yield two second-order differential equations, one for the current and one for the kinetic voltage

$$\frac{\partial^2 I}{\partial z^2} + 2j\beta_e \frac{\partial I}{\partial z} - \left(\beta_e^2 - \beta_q^2\right) I = j\beta_q \frac{1}{W} E_c \qquad (2.34)$$

$$\frac{\partial^2 U}{\partial z^2} + 2j\beta_e \frac{\partial U}{\partial z} - \left(\beta_e^2 - \beta_q^2\right) U = \left(j\beta_e + \frac{\partial}{\partial z}\right) E_c \qquad (2.35)$$

where the explicit dependence of I, U and E_c on the axial co-ordinate z has been omitted. It is noted that the left-hand sides of the two differential equations are identical.

We shall assume that the beam is subject to modulation by the RF fields in a number of cascaded modulation regions as shown schematically in Fig 2.1.

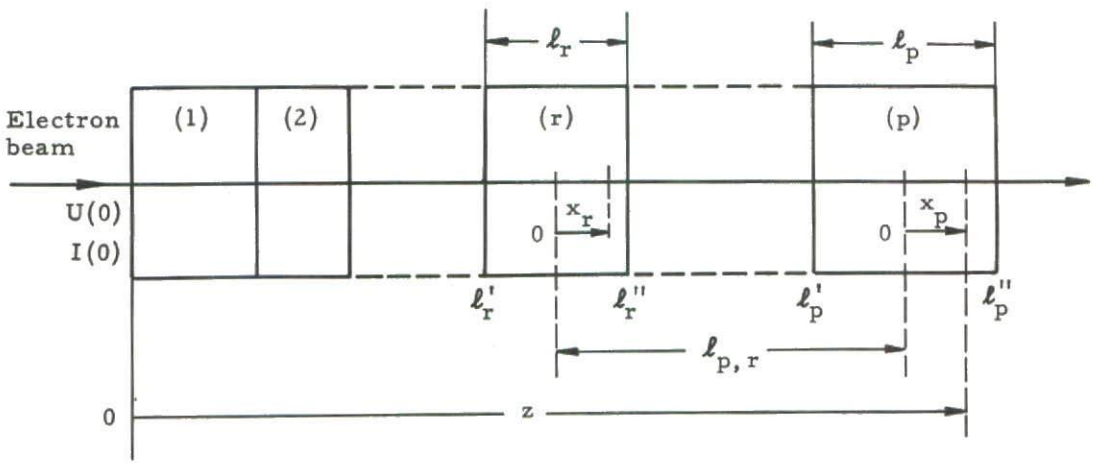

Fig 2.1 Schematic diagram of the arrangement of cascaded, uncoupled modulation regions

The longitudinal RF field distribution and interaction length of each of the p adjacent modulation regions, which supposedly are uncoupled in the absence of the beam, are completely arbitrary and may consequently include field-free drift tubes. For reasons of generality we shall assume that the beam at the entrance to the modulation region (z = 0) has an initial space-charge wave modulation specified by U(0) and I(0). The modulations U(0) and I(0) and their derivatives with respect to z are interrelated through Eqs (2.32) and (2.33).

Equations (2.34) and (2.35) are readily solved by means of Laplace transforms. Using the notation in Fig 2.1, we find

$$I(z) = I(0)\, e^{-j\beta_e z} \cos\beta_q z + j\frac{U(0)}{W} e^{-j\beta_e z} \sin\beta_q z + j\frac{1}{W}\int_0^z E(x) e^{-j\beta_e (z-x)} \sin\beta_q (z-x)\, dx \qquad (2.36)$$

$$U(z) = U(0)\, e^{-j\beta_e z} \cos\beta_q z + jI(0)\, W\, e^{-j\beta_e z} \sin\beta_q z + \int_0^z E(x)\, e^{-j\beta_e (z-x)} \cos\beta_q (z-x)\, dx \qquad (2.37)$$

where the subscript of E(x) has been omitted. In the subsequent analysis considerable simplifications of the algebraic manipulations result through introduction of two operators Δ and $\not\delta$, operating on functions of the electronic propagation constant β_e. These operators are defined by

$$\Delta f(\beta_e) = \tfrac{1}{2} [f(\beta_e + \beta_q) - f(\beta_e - \beta_q)] \tag{2.38}$$

$$\not\delta f(\beta_e) = \tfrac{1}{2} [f(\beta_e + \beta_q) + f(\beta_e - \beta_q)] \tag{2.39}$$

By means of the difference and sum operators Δ and $\not\delta$, the superposition of slow and fast space-charge waves in the cascaded modulation regions is expressed in a particularly simple way. For the following analysis it will be useful to list some of the properties of these operators. They are linear and commutable with respect to differentiation and integration

$$\Delta [\alpha_1 f_1(\beta_e) + \alpha_2 f_2(\beta_e)] = \alpha_1 \Delta f_1(\beta_e) + \alpha_2 \Delta f_2(\beta_e) \tag{2.40}$$

$$\Delta \left[\frac{df(\beta_e)}{d\beta_e} \right] = \frac{d}{d\beta_e} \left[\Delta f(\beta_e) \right] \tag{2.41}$$

$$\Delta \int f(\beta_e, x)\, dx = \int \Delta f(\beta_e, x)\, dx \tag{2.42}$$

with identical results for the sum operator $\not\delta$. Further, the following important relations hold:

$$\mathrm{Re} [\Delta f(\beta_e) \not\delta f(\beta_e)^*] = \tfrac{1}{2} \Delta [f(\beta_e) f(\beta_e)^*] \tag{2.43}$$

$$\mathrm{Im} [\Delta f(\beta_e) \not\delta f(\beta_e)^*] = \tfrac{1}{2} \mathrm{Im} [f(\beta_e + \beta_q) f(\beta_e - \beta_q)^*] \tag{2.44}$$

$$\lim_{\beta_q \to 0} [\Delta f(\beta_e)] = d f(\beta_e) \tag{2.45}$$

$$\lim_{\beta_q \to 0} [\not\delta f(\beta_e)] = f(\beta_e) \tag{2.46}$$

Equations (2.43) and (2.44) are useful in connection with problems involving evaluation of energy flow on the beam, while the relations expressed in Eqs (2.45) and (2.46) provide the link between the space-charge wave theory and kinematic analyses based on the assumption of zero space-charge. For negligible space-charge, operation on a function by the difference operator Δ is equivalent to differentiation, and operation by the sum operator $\not\delta$ leaves the function unchanged.

Expressing Eqs (2.36) and (2.37) by means of the operators Δ and $\not\delta$, we obtain

$$I(z) = I(0)\,\mathcal{S}\left[e^{-j\beta_e z}\right] - \frac{U(0)}{W}\,\Delta\left[e^{-j\beta_e z}\right] - \frac{1}{W}\,\Delta\int_0^z E(x)\,e^{-j\beta_e(z-x)}\,dx \qquad (2.47)$$

$$U(z) = U(0)\,\mathcal{S}\left[e^{-j\beta_e z}\right] - I(0)W\,\Delta\left[e^{-j\beta_e z}\right] + \mathcal{S}\int_0^z E(x)\,e^{-j\beta_e(z-x)}\,dx \qquad (2.48)$$

The integrals on the right-hand sides can be expressed as a sum of integrals over each gap. In doing this it is natural to introduce a separate co-ordinate system for each gap with origin at the center. Following the notation used in Fig 2.1, let x_r be the co-ordinate referring to the rth gap. The relation between x_r and z is then given by the equation

$$x_r = z - \frac{\ell_r' + \ell_r''}{2} \qquad (2.49)$$

Furthermore, it is convenient to express the electric field in each modulation gap as a product of a normalized distribution function $F(x)$ and an amplitude factor V which, by definition, is the RF gap voltage. For the rth gap

$$E(x_r) = F(x_r)\,V_r \qquad (2.50)$$

In the subsequent application of the modulation theory to multi-cavity klystrons with interaction gaps being parts of high-Q cavities, the distribution function $F(x)$ can be chosen real (and V complex). The validity of the general modulation theory of this chapter, however, is not restricted to real values of $F(x)$.

The choice of normalization of the distribution function $F(x_r)$ is irrelevant, and can be specified in any convenient manner. In the present report we shall use the following normalization:

$$\ell_r \int_{-\ell_r/2}^{\ell_r/2} F(x_r)\,F(x_r)^*\,dx_r = 1 \qquad (2.51)$$

where ℓ_r is the length of the rth gap.

Equations (2.50) and (2.51) are equivalent to the following definition of the RF gap voltage V_r:

$$V_r V_r^* = \ell_r \int_{-\ell_r/2}^{\ell_r/2} E(x_r)\,E(x_r)^*\,dx_r \qquad (2.52)$$

which shows that the chosen normalization leads to an rms definition of gap voltage (in the spatial co-ordinate). The often used voltage definition as the line integral

of the RF field, to which Eq (2.52) reduces for a conventional gridded gap with constant RF field, fails in many important cases for which the RF electric field reverses direction within the gap. A typical example is the sinusoidal standing-wave type interaction field which is characteristic for resonated slow-wave structures.

We shall define a coupling coefficient for each gap as the Fourier transform of the normalized RF field. For the rth gap

$$M_r(\beta_e) = \frac{1}{V_r} \int_{-\ell_r/2}^{\ell_r/2} E(x_r) e^{j\beta_e x_r} dx_r = \int_{-\ell_r/2}^{\ell_r/2} F(x_r) e^{j\beta_e x_r} dx_r \quad (2.53)$$

Using these new notations, the RF current and kinetic voltage modulations are readily evaluated from Eqs (2.47) and (2.48). At the position x_p in the last gap these quantities are given by

$$I(x_p) = I(0) \oint \left[e^{-j\beta_e (x_p + \ell_{p,0})} \right] - \frac{U(0)}{W} \Delta \left[e^{-j\beta_e (x_p + \ell_{p,0})} \right]$$

$$- \sum_{r=1}^{p-1} \frac{V_r}{W} \Delta \left[e^{-j\beta_e (\ell_{p,r} + x_p)} M_r(\beta_e) \right] - \frac{V_p}{W} \Delta \left[e^{-j\beta_e x_p} \int_{-\ell_p/2}^{x_p} F(y_p) e^{j\beta_e y_p} dy_p \right] \quad (2.54)$$

$$U(x_p) = U(0) \oint \left[e^{-j\beta_e (x_p + \ell_{p,0})} \right] - I(0) W \Delta \left[e^{-j\beta_e (x_p + \ell_{p,0})} \right]$$

$$+ \sum_{r=1}^{p-1} V_r \oint \left[e^{-j\beta_e (\ell_{p,r} + x_p)} M_r(\beta_e) \right] + V_p \oint \left[e^{-j\beta_e x_p} \int_{-\ell_p/2}^{x_p} F(y_p) e^{j\beta_e y_p} dy_p \right] \quad (2.55)$$

where $\ell_{p,r}$ is the spacing between the centers of the rth and pth gap, and $\ell_{p,0}$ is the distance from the input end ($z = 0$) to the center of the pth gap.

If it is recalled that the operators Δ and $\oint$ express superposition of two waves, the interpretations of the expressions in Eqs (2.54) and (2.55) are straight forward: the current and kinetic voltage in the output gap are expressed as superpositions of slow and fast space-charge waves partly due to the initial beam modulations, and partly originating in the modulation gaps. Two space-charge waves due to the initial current and kinetic voltage modulations I(0) and U(0) propagate along the beam with propagation factors $(\beta_e + \beta_q)$ and $(\beta_e - \beta_q)$ for the slow and fast wave, respectively. These waves propagate unaffected by the modulation fields. On these are superposed the slow and fast waves which are excited by the modulation fields. The slow and fast waves at the position x_p in the output gap due to the modulation at the rth gap are given by

$$I_r(x_p) = -\frac{V_r}{2W}\left[M_r(\beta_e+\beta_q)e^{-j(\beta_e+\beta_q)(\ell_{p,r}+x_p)} - M_r(\beta_e-\beta_q)e^{-j(\beta_e-\beta_q)(\ell_{p,r}+x_p)}\right] \tag{2.56}$$

$$U_r(x_p) = \frac{V_r}{2}\left[M_r(\beta_e+\beta_q)e^{-j(\beta_e+\beta_q)(\ell_{p,r}+x_p)} + M_r(\beta_e-\beta_q)e^{-j(\beta_e-\beta_q)(\ell_{p,r}+x_p)}\right] \tag{2.57}$$

where the Fourier transforms

$$M_r(\beta_e \pm \beta_q) = \int_{-\ell_r/2}^{\ell_r/2} F(x_r)e^{j(\beta_e \pm \beta_q)x_r}\,dx_r \tag{2.58}$$

can be interpreted as the coupling coefficients of the slow and the fast wave, respectively. Since the coupling coefficient $M(\beta_e)$ is a function of β_e, the two coefficients $M_r(\beta_e+\beta_q)$ and $M_r(\beta_e-\beta_q)$ are generally different, meaning that the slow and the fast space-charge waves are excited with different amplitudes. For a given DC beam velocity (β_e given) the difference between the two coupling coefficients tends to increase with increasing β_q. They are identical only if β_q is zero, i e for a beam with negligible space-charge. The significance of the occurrence of two distinct coupling coefficients will become clearer when the power relationships in the gaps are considered. It will be shown that the beam loading is simply related to the two coupling coefficients, being proportional to the difference between their squares.

In the subsequent analysis we shall introduce the following simplified notations:

$$\beta_e + \beta_q = \beta_e^+ \tag{2.59}$$

$$\beta_e - \beta_q = \beta_e^- \tag{2.60}$$

$$M_r(\beta_e+\beta_q) = M_r^+ \tag{2.61}$$

$$M_r(\beta_e-\beta_q) = M_r^- \tag{2.62}$$

and similarly for other quantities associated with the slow and fast space-charge waves. The superscript plus and minus will thus refer to quantities associated with the slow and fast wave, respectively. Although it may be argued that the opposite choice would be preferable, the above superscript notation is more natural in connection with the sum and difference operators $\not\delta$ and Δ used in this report because the superscript then indicates the operation that has to be performed, namely addition or subtraction of β_e and β_q wherever these quantities are involved.

It follows immediately from Eqs (2.56) and (2.57) that the ratios between the kinetic voltage and the current for the two waves are given by minus W and plus W, respectively.

$$U_r(x_p)^+ = -W\, I_r(x_p)^+ \tag{2.63}$$

$$U_r(x_p)^- = W\, I_r(x_p)^- \tag{2.64}$$

which illustrates the characteristic in-phase and out-of-phase relationships between current and kinetic voltage for the two space-charge waves originating in each modulation gap.

2.5 Extraction of power from the electron beam

In this section we shall evaluate the electromagnetic power that is extracted from or imparted to the beam when it flows through the same structure as the one shown in Fig 2.1, consisting of a total of p cascaded interaction regions. Since the interaction regions are not coupled mutually, the power balance for each region can be evaluated separately. As shown in Appendix A, application of the normal-mode theory for resonant cavities (2) gives the following expression for the complex energy flow $\mathcal{P}_p$ to the electron beam from the particular circuit associated with the pth interaction region:

$$\mathcal{P}_p = \frac{1}{2}\int_{-\ell_p/2}^{\ell_p/2} I(x_p)\, E(x_p)^* dx_p = \frac{1}{2} V_p^* \int_{-\ell_p/2}^{\ell_p/2} I(x_p)\, F(x_p)^* dx_p \tag{2.65}$$

where $E(x_p)$ is the circuit field, and $I(x_p)$ is the beam current. It is significant that the space-charge field, according to normal-mode theory, contributes nothing to the energy flow except indirectly through its effect on beam current modulation. By direct substitution of the current from Eq (2.54) in Eq (2.65) we find

$$\begin{aligned}\mathcal{P}_p = {} & \frac{1}{2} I(0)\, V_p^*\, \mathcal{S}\left[M_p^* e^{-j\beta_e \ell_p, 0}\right] - \frac{1}{2}\frac{U(0)}{W} V_p^*\, \Delta\left[M_p^* e^{-j\beta_e \ell_p, 0}\right] \\ & - \frac{1}{2W}\left\{\sum_{r=1}^{p-1} V_r V_p^*\, \Delta\left[M_r M_p^* e^{-j\beta_e \ell_p, r}\right]\right. \\ & \left. + V_p V_p^*\, \Delta \int_{-\ell_p/2}^{\ell_p/2} F(x_p)^* e^{j\beta_e x_p} \int_{-\ell_p/2}^{x_p} F(y_p) e^{j\beta_e y_p}\, dy_p\, dx_p\right\}\end{aligned} \tag{2.66}$$

The increase in beam energy flow in the pth gap is thus a sum of terms due to:

a) Initial current and velocity modulation I(0) and U(0)

b) Modulation in the preceding gaps by the gap voltages V_1, V_2 --- V_{p-1} (transfer terms)

c) Modulation in the pth gap itself (beam loading term)

We shall define appropriate transfer admittances $Y_{p,r}$ and beam loading admittances $Y_{e,p}$ on a <u>voltage-power</u> basis. The transfer admittance $Y_{p,r}$ from the rth to the pth gap is defined by

$$Y_{p,r} = -\frac{1}{W}\Delta\left(M_r M_p^* e^{-j\beta_e \ell_{p,r}}\right) \tag{2.67}$$

The beam loading admittance or the electronic admittance of the pth gap is defined by

$$Y_{e,p} = -\frac{1}{W}\Delta \int_{-\ell_p/2}^{\ell_p/2} F(x_p)^* e^{-j\beta_e x_p} \int_{-\ell_p/2}^{x_p} F(y_p) e^{j\beta_e y_p}\, dy_p\, dx_p \tag{2.68}$$

The circuits considered in this report are resonant cavities; therefore, the phase of the electric field is the same everywhere in the gap, and the distribution function $F(x_p)$ can be chosen real. Under these circumstances Eq (2.68) is readily separated into its real and imaginary parts, with the following result:

$$Y_{e,p} = -\frac{1}{W}\Delta\left\{\tfrac{1}{2}M_p M_p^* + j \int_{-\ell_p/2}^{\ell_p/2} \int_{-\ell_p/2}^{x_p} F(x_p)\, F(y_p) \sin\left[\beta_e (y_p - x_p)\right] dy_p\, dx_p\right\} \tag{2.69}$$

The real part of $Y_{e,p}$ is the beam loading conductance $G_{e,p}$ given by

$$G_{e,p} = -\frac{1}{2W}\Delta\left(M_p M_p^*\right) = \frac{1}{4W}\left[\left|M_p(\beta_e - \beta_q)\right|^2 - \left|M_p(\beta_e + \beta_q)\right|^2\right]$$

$$= \frac{1}{4W}\left[\left|M_p^-\right|^2 - \left|M_p^+\right|^2\right] \tag{2.70}$$

This important relation shows that the beam loading of a gap is equal to the difference between the squares of the coupling coefficients of the fast and the slow space-charge wave divided by four times the RF beam impedance.

Substitution of the admittances defined in Eqs (2.67) and (2.68) in Eq (2.66) yields

$$\mathcal{P}_p = \tfrac{1}{2} I(0)\, V_p^*\, \delta\left[M_p^* e^{-j\beta_e \ell_{p,0}}\right] - \tfrac{1}{2}\frac{U(0)}{W} V_p^* \Delta\left[M_p^* e^{-j\beta_e \ell_{p,0}}\right]$$

$$+ \tfrac{1}{2}\sum_{r=1}^{p-1} V_r V_p^* Y_{p,r} + \tfrac{1}{2} V_p V_p^* Y_{e,p} \tag{2.71}$$

which is the fundamental electronic equation on which is based the space-charge wave analysis of multi-cavity klystrons with arbitrary, extended interaction regions done in Chapters 3 and 4. Before turning our attention to the discussion of klys-

trons we shall evaluate the flow of energy on the beam, using the small-signal kinetic power theorem for longitudinal beams, and show that the results derived in this chapter are consistent with this theorem.

2.6 The small-signal kinetic power theorem for longitudinal electron beams

Amplification of electromagnetic energy in electron beam amplifiers is obtained by conversion of part of the kinetic energy of the electrons to electromagnetic energy. Regardless of details of the amplifier structure, signal level, etc, it follows from power conservation principles that the difference in the average flow of kinetic energy into the structure and out of the structure must be equal to the electromagnetic power delivered to the RF structure surrounding the beam.

It is less obvious that a similar power conservation relation exists between the small-signal solutions of Maxwell's equations. The derivation of this relation for a longitudinal beam starts from Maxwell's equations (2.1). Under the assumptions stated in the introduction to this chapter, all time-dependent quantities can be expressed as the sum of a time-average part and a time-varying part whose amplitude is much smaller than the time-average part, as shown for the z-components in Eqs (2.3) to (2.6). In giving the derivation of the theorem we shall have to consider the transverse components as well. For reasons of generality the assumption of a one-dimensional beam is dropped, but the electron motion is still confined to the z-direction. Therefore, the relevant time-varying vector quantities can be written

$$\bar{E}(\bar{r},t) = \bar{E}_o(\bar{r}) + \mathrm{Re}[\bar{E}(\bar{r})\, e^{j\omega t}] \tag{2.72}$$

$$\bar{H}(\bar{r},t) = \bar{H}_o(\bar{r}) + \mathrm{Re}[\bar{H}(\bar{r})\, e^{j\omega t}] \tag{2.73}$$

$$i(\bar{r},t) = i_o(\bar{r}) + \mathrm{Re}[i(\bar{r})\, e^{j\omega t}] \tag{2.74}$$

$$u(\bar{r},t) = u_o(\bar{r}) + \mathrm{Re}[u(\bar{r})\, e^{j\omega t}] \tag{2.75}$$

$$\rho(\bar{r},t) = \rho_o(\bar{r}) + \mathrm{Re}[\rho(\bar{r})\, e^{j\omega t}] \tag{2.76}$$

where $\bar{r}$ is the radius vector to a given position in the beam.

Upon introduction of these definitions into Maxwell's equations and separation in time-average and time-varying parts, we find for the latter

$$\nabla \times \bar{E}(\bar{r}) = - j\omega\mu_o \bar{H}(\bar{r}) \tag{2.77}$$

$$\nabla \times \bar{H}(\bar{r}) = \bar{a}_z\, i(\bar{r}) + j\omega\epsilon_o \bar{E}(\bar{r}) \tag{2.78}$$

where $\bar{a}_z$ is a unit vector in the z-direction. Equations (2.77) and (2.78) are the small-signal solutions of Maxwell's equations.

Forming the scalar product of $\bar{E}(\bar{r})^*$ and Eq (2.78), then subtracting it from the scalar product of $\bar{H}(\bar{r})$ and the complex conjugate of Eq (2.77), we find

$$- \nabla \cdot [\bar{E}^* \times \bar{H}] = E_z^* i + j\omega [\epsilon_o \bar{E} \cdot \bar{E}^* - \mu_o \bar{H} \cdot \bar{H}^*] \tag{2.79}$$

where the independent variable $\bar{r}$ has been omitted, and E_z is the electric field along the z-axis. Equation (2.79) is the small-signal form of Poynting's theorem for longitudinal beams. The theorem can be transferred to an alternate form, usually referred to as the small-signal kinetic power theorem, first suggested by L J Chu (18) for longitudinal beams and later extended to other beam configurations by others (20,21). The alternate form is obtained by noting that the product $E_z^* i$ can be rewritten by use of the force equation (2.19) and the equation of continuity (2.20). We find

$$E_z^* i = - j\omega \frac{m}{e} \rho_o u u^* + \frac{\partial}{\partial z} (U^* i) \tag{2.80}$$

where U is the kinetic-voltage modulation defined in Eq (2.17), and u is the RF velocity. Noting that

$$\frac{\partial}{\partial z} (U^* i) = \nabla \cdot (U^* i \bar{a}_z) \tag{2.81}$$

we obtain by substitution in Eq (2.79)

$$- \nabla \cdot [\tfrac{1}{2}(\bar{E}^* \times H) + \tfrac{1}{2} U^* i \bar{a}_z] = \tfrac{1}{2} j\omega [\epsilon_o \bar{E} \cdot \bar{E}^* - \mu_o \bar{H} \cdot \bar{H}^* - \frac{m}{e} \rho_o u u^*] \tag{2.82}$$

Equation (2.82) is the complex small-signal kinetic power theorem in differential form. Integration over a volume V bounded by the surface σ gives the integral form of the power theorem:

$$- \oint_\sigma [\tfrac{1}{2}(\bar{E}^* \times \bar{H}) + \tfrac{1}{2} U^* i \bar{a}_z] \bar{n} \, d\sigma = \tfrac{1}{2} j\omega \int_V [\epsilon_o \bar{E} \cdot \bar{E}^* - \mu_o \bar{H} \cdot \bar{H}^* - \frac{m}{e} \rho_o u u^*] dV \tag{2.83}$$

Separation of the equation into its real and imaginary parts gives

$$\mathrm{Re} \oint_\sigma [\tfrac{1}{2}(\bar{E}^* \times \bar{H}) + \tfrac{1}{2} U^* i \bar{a}_z] \bar{n} \, d\sigma = 0 \tag{2.84}$$

$$\mathrm{Im} \oint_\sigma [\tfrac{1}{2}(\bar{E}^* \times H) + \tfrac{1}{2} U^* i \bar{a}_z] \bar{n} \, d\sigma = \tfrac{1}{2}\omega \int_V [\epsilon_o \bar{E} \cdot E^* - \mu_o \bar{H} \cdot \bar{H}^* - \frac{m}{e} \rho_o u u^*] dV \tag{2.85}$$

The interpretation of the small-signal power theorem should be done with some caution since terms involving cross-products and squares of the small-signal amplitudes were neglected in the derivation. As shown by Haus and others (20, 21), the theorem gives the power flow correct to second order in the small-signal quantities.

The real part of the kinetic power theorem (2.84) is a relation between first-order RF quantities, stating that the electromagnetic power extracted from the electron beam inside the volume V is balanced by a net flow into the volume of kinetic energy. The quantity $\frac{1}{2}Ui^{*}\bar{a}_z$ can therefore be interpreted as the complex kinetic-power density $\bar{S}_k$ in the beam.

$$\bar{S}_k = \tfrac{1}{2}U^{*}i\,\bar{a}_z \tag{2.86}$$

With the assumption of a one-dimensional beam the current density i and kinetic voltage U are uniform over the beam cross-section. The real kinetic energy flow on the beam is then given by

$$P = \tfrac{1}{2}\mathrm{Re}(U^{*}I) \tag{2.87}$$

where I is the RF current.

It is immediately obvious from a consideration of Eqs (2.79), (2.84) and (2.26) that the real power extracted by the beam can be evaluated either on the basis of the small-signal Poynting theorem (2.79) as the real part of the volume integral of $\frac{1}{2}E_c^{*}i$ (E_c being the circuit field), or from the kinetic-power theorem (2.83) as the surface integral of the real part of the kinetic-power density $\bar{S}_k$. As shown in detail below, both these methods are equivalent, and neither of them seems to offer computational advantages compared to the other, although conceptionally the introduction of kinetic energy flow associated with the electron beam is appealing.

On the other hand, the surface integral of the <u>imaginary</u> part of the kinetic power density $\bar{S}_k$ is not equivalent to the <u>imaginary</u> part of the volume integral of $\frac{1}{2}E_c^{*}i$. The latter, according to the normal-mode theory of resonant cavities, is the reactive beam power that is balanced by the reactive power in the external cavity, (see for instance the circuit equation (A.7)). Thus, evaluation of the electronic susceptance B_e from the surface integral of the imaginary part of the kinetic power density $\bar{S}_k$ obviously is erroneous. Even if the additional volume integral of $\omega\rho_o uu^{*}m/2e$ in Eq (2.85) were included, the result would be in error by an amount that corresponds to the reactive power associated with the space-charge field E_b. Although not done here, it can be shown that this extra reactive power is associated with energy stored in the <u>electron beam system</u>, oscillating periodically between potential electric energy stored in the space-charge field and kinetic energy associated with the longitudinal RF electron velocity u. This component of reactive power, which plays no active role in the reactive power balance in the circuit itself, accounts for the fact that the space-charge field E_b does not appear in expression (A.5) for the complex power extracted by the beam.

From this discussion it appears that evaluation of the reactive power balance in the circuit-electron beam system should be done with some caution in order not to arrive at erroneous results.

In the following section we shall show that the use of the real small-signal power theorem (2.84) presents an alternate method for derivation of the results in Section 2.5.

2.7 Application of the power theorem to cascaded modulation regions

The real energy flow on an electron beam traversing the cascaded interaction regions shown in Fig 2.1 is readily evaluated from Eq (2.87) substituting the kinetic voltage U and the current I from Eqs (2.54) and (2.55). For simplicity the initial beam modulations U(0) and I(0) are set equal to zero. At the exit cross-section $x_p = \ell_p/2$ of the pth gap, we find that the kinetic energy flow is given by

$$P_{p,2} = \tfrac{1}{2}\mathrm{Re}(U^* I)_{\ell_p/2} = -\frac{1}{4W}\sum_{r=1}^{p}\sum_{q=1}^{p} V_r V_q^* \Delta \left[M_r M_q^* e^{-j\beta_e \ell_{q,r}} \right] \qquad (2.88)$$

This equation can be written in the alternate form

$$P_{p,2} = -\frac{1}{4W}\sum_{r=1}^{p} V_r V_r^* \Delta (M_r M_r^*) - \frac{1}{4W}\sum_{r \neq q}^{p}\sum_{q}^{p} V_r V_q^* \Delta \left[M_r M_q^* e^{-j\beta_e \ell_{q,r}} \right] \qquad (2.89)$$

which shows explicitly the contributions to the beam energy flow from:

a) Interaction in each gap given by the first sum (beam loading terms)

b) Interaction between non-adjacent gaps given by the double sum (transfer loading terms)

According to the small-signal power theorem (2.84) the difference between the kinetic energy flows $P_{p,2}$ and $P_{p,1}$, referred to the output and input cross-sections of the pth gap, respectively, must be balanced by a flow of electromagnetic energy P_p from the pth circuit into the beam. Using Eq (2.89) we obtain

$$\begin{aligned} P_p &= P_{p,2} - P_{p,1} \\ &= -\frac{1}{4W} V_p V_p^* \Delta (M_p M_p^*) - \frac{1}{2W}\,\mathrm{Re}\sum_{r=1}^{p-1} V_r V_p^* \Delta \left[M_r M_p^* e^{-j\beta_e \ell_{p,r}} \right] \end{aligned} \qquad (2.90)$$

By comparison with Eqs (2.67) and (2.70) we find immediately

$$P_p = \mathrm{Re}\left[\tfrac{1}{2} V_p V_p^* Y_{e,p} + \tfrac{1}{2}\sum_{r=1}^{p-1} V_r V_p^* Y_{p,r} \right] \qquad (2.91)$$

Comparison of this equation with the real part of the previously derived electronic equation (2.71), setting $I(0) = U(0) = 0$, shows that these are identical. Thus, evaluation of the real power P_p from Eq (2.65), as done in this paper, is consistent with the small-signal power theorem (2.84). The two methods are therefore equivalent.

A further simple illustration of the significance of the small-signal power theorem is obtained if we consider a single interaction region in which the circuit is loaded by the beam. The beam loading power P is evaluated from Eq (2.70)

$$P = \tfrac{1}{2} V V^* G_e = -\frac{V V^*}{4W} \Delta (M M^*) = -\frac{V V^*}{8W} (M^+ M^{+*} - M^- M^{-*}) \quad (2.92)$$

From the small-signal power theorem (2.84) this power must be balanced by a corresponding increase in kinetic energy flow on the beam leaving the gap. That this is indeed the case is shown by evaluation of the energy flow from Eq (2.89) for the special case of one single interaction gap. Hence, the beam loading power in a single gap is exactly equal to the energy flow on the beam after the gap.

If we consider the kinetic energy carried by each of the two space-charge waves, we find using Eqs (2.87) and (2.64) that the fast wave carries positive energy and the slow wave negative energy, both in the positive direction. In general

$$P^- = \tfrac{1}{2} \mathrm{Re}(U^{-*} I^-) = \frac{1}{2W} U^- U^{-*} = \tfrac{1}{2} W I^- I^{-*} \quad (2.93)$$

$$P^+ = \tfrac{1}{2} \mathrm{Re}(U^{+*} I^+) = -\frac{1}{2W} U^+ U^{+*} = -\tfrac{1}{2} W I^+ I^{+*} \quad (2.94)$$

In the cascaded modulation regions studied in this section the relative contributions to the kinetic power from the two space-charge waves are readily found from Eq (2.88). The fast-wave power is given by

$$P^-_{p,2} = \frac{1}{8W} \sum_{r=1}^{p} \sum_{q=1}^{p} V_r V_q^* M_r^- M_q^{-*} e^{-j(\beta_e - \beta_q)\ell_{q,r}} \quad (2.95)$$

and the slow-wave power by

$$P^+_{p,2} = -\frac{1}{8W} \sum_{r=1}^{p} \sum_{q=1}^{p} V_r V_q^* M_r^+ M_q^{+*} e^{-j(\beta_e + \beta_q)\ell_{q,r}} \quad (2.96)$$

The sum of $P^-_{p,2}$ and $P^+_{p,2}$ is equal to the net RF kinetic power $P_{p,2}$ associated with the beam.

The sign of the net energy flow $P_{p,2}$, given by Eq (2.88), obviously will be determined by the spacings between the modulation gaps and the relative phases of the

gap voltages V_1, V_2, --- V_p that modulate the beam. The preceding analysis is general in the sense that nothing has been assumed concerning the excitation of the gap voltages, whether this is done from external signal generators or by the beam itself. In the particular case of a multi-cavity klystron amplifier studied in the next chapter, the net beam energy flow at some arbitrary position beyond the input cavity is always negative if the amplifier gain exceeds unity. This conclusion follows immediately from the small-signal power theorem (2.84) applied to the structure shown schematically in Fig 3.1, where the input cavity gap is excited from an external signal source and the subsequent "floating" cavities by the RF modulation in the beam itself. Thus, since the initial kinetic energy flow is zero, the kinetic energy flow $P_{p,2}$ immediately after the pth gap is given by

$$P_{p,2} = P_i - P_{c,1} - P_{c,2} - \cdots - P_{c,p} \tag{2.97}$$

where P_i is the input power from the generator and $P_{c,1}$, $P_{c,2}$, --- $P_{c,p}$ are the power dissipated in the p passive cavities or circuits associated with the p gaps. The equation can be written

$$P_{p,2} = P_i \left[1 - \frac{P_{c,1}}{P_i} - \frac{P_{c,2}}{P_i} - \cdots - \frac{P_{c,p}}{P_i} \right]$$

$$= P_i \left[1 - G_1 - G_2 - \cdots - G_p \right] \tag{2.98}$$

where G_1, G_2, --- G_p are the power gains referred to the various cavities. If the structure is to serve as an amplifier, at least one of the G's must exceed unity, which results in negative kinetic energy flow $P_{p,2}$. Of course, the same applies to any longitudinal beam amplifier in which the power gain is obtained by energy transfer from the slow space-charge wave carrying negative energy.

For a more thorough discussion of the physical interpretation of the positive and negative kinetic energy flows associated with the two space-charge waves, the reader is referred to the literature (19, 20, 21).

3 MULTI-CAVITY KLYSTRONS WITH EXTENDED INTERACTION REGIONS

3.1 Introduction

This chapter presents a general small-signal theory of multi-cavity klystrons with arbitrary, extended interaction fields based on the space-charge wave modulation theory in Chapter 2. The generality of the klystron theory presented here thus exceeds that of narrow-gap klystron theory which is obtained as a special case of the general theory. Moreover, the theory is more rigorous than conventional klystron theory, accounting fully for space-charge forces and density modulation effects in the interaction gaps.

The analysis is valid under the same assumptions as those stated in the introduction to Chapter 2. General formulae for the frequency response are derived using an approach based on evaluation of the power balance in each interaction region. This procedure applied to a p-cavity klystron leads to a set of p linear algebraic equations in the p RF gap voltages, which can be solved by standard methods. The solution expresses the voltage gain of a p-cavity klystron very simply in terms of a determinant of order p-1, from which a number of significant results concerning klystron theory can be derived.

Figure 3.1 shows schematically the general type of klystron amplifier that we shall study. The amplifier structure consists of p cascaded interaction regions, each associated with a single resonant cavity. It is characteristic for klystron operation that each cavity is electromagnetically isolated from its neighbors, the only coupling being provided by the electron beam. Since the electron beam by nature is a unilateral transmission system, a signal can be propagated from cavity to cavity only in the forward direction. The propagation of a signal from the output cavity towards the input cavity is therefore prohibited because no possible signal paths exist. This characteristic feature of klystrons as opposed to traveling-wave tubes accounts for the fact that the klystron basically is a stable device, permitting operation at very high gain and power level without danger of oscillations due to feed-back from the output to the input.

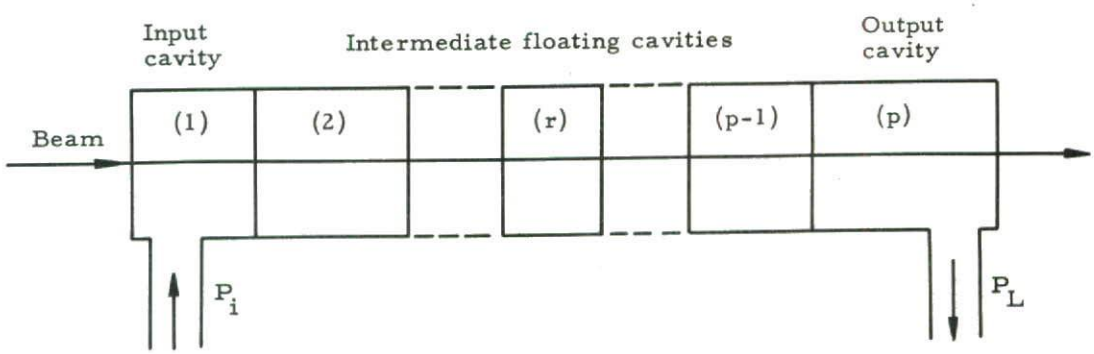

Fig 3.1 Schematic drawing of a multi-cavity klystron with extended gaps

In the klystron shown in Fig 3.1 the signal from the signal source flows through the input transmission line into the first cavity, the input cavity. The RF gap voltage developed across the gap modulates the initially unmodulated electron beam. The signal propagates in the forward direction as space-charge waves on the beam, is amplified by cumulative interaction in the subsequent p-2 intermediate "floating" cavities excited by the beam itself, and is finally extracted in the last cavity, the output cavity, and dissipated in the external load as useful power.

The analysis starts with the power balance in each interaction region, expressed in a relation which we shall refer to as the circuit equation.

3.2 Circuit equations

A general circuit equation for arbitrary resonant cavities interacting with electron beams has been given by Slater (2) in his normal-mode theory of resonant cavities. In Appendix A some of the results from this theory are stated without proof, and rewritten in a form that is suitable for the applications that we have in mind.

In addition to the assumptions stated in Chapter 2 we must introduce additional assumptions concerning the circuits. We shall specify these as resonant cavities characterized by relatively high Q-values, with their resonances sufficiently separated to justify the assumption that only one resonant mode is excited in each cavity. Under these circumstances the circuit equation for a cavity excited by a beam (no excitation from external sources) is particularly simple, as shown by Eqs (A.11) and (A.13) in Appendix A. For the pth cavity we have

$$\mathcal{P}_p = -\tfrac{1}{2} V_p V_p^* Y_{c,p} = -\tfrac{1}{2} V_p V_p^* \left(\frac{Q_p}{R_{sh,p}}\right) \frac{1}{Q_{L,p}} (1 + 2jQ_{L,p}\delta_p) \qquad (3.1)$$

where $\mathcal{P}_p$ is the complex power extracted by the beam in traversing the pth interaction region. From power conservation principles this is equivalent to stating that minus $\mathcal{P}_p$ is the complex power dissipated in the pth resonant cavity and its associated external load. The circuit admittance $Y_{c,p}$ is therefore given by

$$Y_{c,p} = \left(\frac{Q_p}{R_{sh,p}}\right) \frac{1}{Q_{L,p}} (1 + 2jQ_{L,p}\delta_p) \qquad (3.2)$$

The circuit parameters appearing in this equation are all defined in Appendix A for the general type of cavities considered here. The important parameter R_{sh}/Q is the characteristic impedance of the cavity, usually given in this form as the ratio of the shunt impedance and the Q-value; Q_L is the loaded Q; and δ is the frequency tuning parameter defined by

$$\delta_p = \tfrac{1}{2}\left(\frac{\omega}{\omega_p} - \frac{\omega_p}{\omega}\right) \approx \frac{\omega - \omega_p}{\omega_p} \qquad (3.3)$$

where ω is the frequency of excitation and ω_p the resonant frequency associated with the particular normal mode in which the cavity is operating.

It should be noted that the circuit equation (3.1) does not hold for the input cavity which is excited from an external source. In this case the modified circuit equation (A.12) is the appropriate one.

3.3 General formulae for multi-cavity klystron gain

Derivation of general expressions for the gain of a klystron is now a relatively simple matter from considerations of the power balance in the gaps. Simultaneous solution of the electronic equation (2.71), with the initial modulations I(0) and U(0) set equal to zero, and the circuit equation (3.1) yields the following relation between the p complex gap voltages V_1, V_2, --- V_p:

$$\sum_{r=1}^{p-1} V_r Y_{p,r} + V_p (Y_{c,p} + Y_{e,p}) = 0 \qquad (3.4)$$

This equation holds for p equal to or larger than two. Therefore, starting with the second cavity we can write a set of (p-1) linear homogeneous equations in p gap voltages. This set can be transformed to a non-homogeneous set with p-1 unknowns by dividing through in all equations by V_1. For convenience let the voltage gain η_p of the p-cavity klystron be defined by

$$\eta_p = \frac{V_p}{V_1} \qquad (3.5)$$

Since the RF gap voltages in general are complex, the voltage gain η_p will be a complex quantity. Further, let us define a self-admittance $Y_{p,p}$ as the sum of the circuit admittance $Y_{c,p}$ and electronic admittance $Y_{e,p}$.

$$Y_{p,p} = Y_{c,p} + Y_{e,p} \qquad (3.6)$$

Using these notations, we obtain the following set of p-1 linear equations in η_2, η_3, --- η_p:

$$\sum_{r=2}^{q} Y_{q,r} \eta_r = - Y_{q,1} \qquad q = 2, 3, ---, p \qquad (3.7)$$

where the transfer admittances $Y_{q,r}$ and the self-admittances $Y_{q,q}$ are obtained from Eqs (2.67), (2.69), (3.2) and (3.6). For convenience, the admittances are repeated here:

$$Y_{q,r} = - \frac{1}{W} \Delta \left[M_r M_q^* e^{-j\beta_e \ell_{q,r}} \right] \qquad r \neq q \qquad (3.8)$$

$$Y_{q,q} = \left(\frac{Q_q}{R_{sh,q}}\right) \frac{1}{Q_{L,q}} (1 + 2jQ_{L,q}\delta_q)$$

$$- \frac{1}{W} \Delta \left\{ \tfrac{1}{2} M_q M_q^* + j \int_{-\ell_q/2}^{\ell_q/2} \int_{-\ell_q/2}^{x_q} F(x_q) F(y_q) \sin\left[\beta_e (y_q - x_q)\right] dy_q \, dx_q \right\} \quad (3.9)$$

Using matrix notation, the set of equations (3.7) can be written

$$\begin{bmatrix} Y_{2,2} & 0 & 0 & \cdots & 0 \\ Y_{3,2} & Y_{3,3} & 0 & \cdots & 0 \\ Y_{4,2} & Y_{4,3} & Y_{4,4} & \cdots & 0 \\ & & & & 0 \\ Y_{p,2} & Y_{p,3} & \cdots & Y_{p,p-1} & Y_{p,p} \end{bmatrix} \begin{bmatrix} \eta_2 \\ \eta_3 \\ \eta_4 \\ \vdots \\ \eta_p \end{bmatrix} = - \begin{bmatrix} Y_{2,1} \\ Y_{3,1} \\ Y_{4,1} \\ \vdots \\ Y_{p,1} \end{bmatrix} \quad (3.10)$$

The fact that the coefficient matrix is triangular is a manifestation of the unilateral nature of the amplifying process in a klystron. The beam modulations or RF gap voltage at some position along the beam are not affected by the gap voltages in any of the subsequent gaps.

The solution of Eq (3.10) can be written as the following determinant:

$$\eta_p = \begin{vmatrix} \eta_{2,1} & -1 & 0 & \cdots & 0 \\ \eta_{3,1} & \eta_{3,2} & -1 & \cdots & 0 \\ \eta_{4,1} & \eta_{4,2} & \eta_{4,3} & \cdots & 0 \\ \vdots & & & & \vdots \\ & & & -1 & 0 \\ \eta_{p-1,1} & \eta_{p-1,2} & \cdots & \eta_{p-1,p-2} & -1 \\ \eta_{p,1} & \eta_{p,2} & \cdots & \eta_{p,p-2} & \eta_{p,p-1} \end{vmatrix} \quad (3.11)$$

where the elements appearing in the determinant are the negative ratios of the transfer admittances and the self-admittances

$$\eta_{s,r} = -\frac{Y_{s,r}}{Y_{s,s}} \tag{3.12}$$

We shall refer to (3.11) as the gain determinant of the multi-cavity klystron. Using standard rules for expansion of determinants, the voltage gain can also be written as a multiple sum

$$\eta_p = \sum_{s_1=2}^{p} \sum_{s_2=s_1+1}^{p} \cdots\cdots \sum_{\substack{s_{p-2}= \\ s_{p-3}+1}}^{p} \eta_{p,s_{p-2}} \eta_{s_{p-2},s_{p-3}} \cdots \eta_{s_2,s_1} \eta_{s_1,1} \tag{3.13}$$

As examples, let us write explicitly the voltage gains of klystrons having two, three, and four cavities, respectively. We obtain

$$\eta_2 = \eta_{2,1} \tag{3.14}$$

$$\eta_3 = \eta_{3,2} \eta_{2,1} + \eta_{3,1} \tag{3.15}$$

$$\eta_4 = \eta_{4,3} \eta_{3,2} \eta_{2,1} + \eta_{4,2} \eta_{2,1} + \eta_{4,3} \eta_{3,1} + \eta_{4,1} \tag{3.16}$$

This procedure can be continued in an obvious way for p larger than four. By noting that the gain of the two-cavity amplifier is equal to $\eta_{2,1}$, a very useful interpretation can be made of the general gain expression (3.11) or (3.13). Each of the factors $\eta_{s,r}$ appearing in Eq (3.13) represents the gain of a two-cavity klystron consisting of cavity r and s. If the product under the multiple summation sign contains q such factors, it represents the gain of an amplifier chain consisting of q independent two-cavity amplifiers coupled in cascade. This product is conveniently referred to as the cascade gain. Thus, by definition, the cascade gain of the chain of q cavities including the input cavity and the output cavity but otherwise selected arbitrarily from the total of p cavities, is given by

$$\eta(1, s_1, s_2 \cdots\cdots s_{q-2}, p) = \eta_{p,s_{q-2}} \eta_{s_{q-2},s_{q-3}} \cdots \eta_{s_2,s_1} \eta_{s_1,1} \tag{3.17}$$

Substitution in Eq (3.13) yields

$$\eta_p = \sum_{s_1=2}^{p} \sum_{s_2=s_1+1}^{p} \cdots\cdots \sum_{\substack{s_{p-2}= \\ s_{p-3}+1}}^{p} \eta(1, s_1, s_2 \cdots\cdots s_{p-2}, p) \tag{3.18}$$

From these relations the following procedure for evaluation of the overall voltage gain of a multi-cavity klystron can be given: the cascade gain of an arbitrarily selected set of two or more cavities including the input and the output cavity is evaluated using Eq (3.17). The overall voltage gain η_p of the klystron is then equal

to the sum of the cascade gains of all possible sets that can be selected. The procedure is illustrated in Fig 3.2 for a five-cavity klystron.

In the general case the number of terms in the sum (3.18) is easily determined using standard methods for expansion of the determinant (3.11), selecting one factor from each line and row. Starting from the first line, the number of possible combinations is obtained as the following product:

$$S = 2(3-1)(4-2)(5-3) \text{ ----- } (p-1-p+3)$$

or $$S = 2^{p-2} \text{ terms} \qquad (3.19)$$

In other words, the number of terms in the general expression for the voltage gain is doubled for each added cavity. In special cases some of the cascade terms $\eta_{s,1}$ may be zero, under which circumstances the total number of terms is correspondingly lower than that given by Eq (3.19).

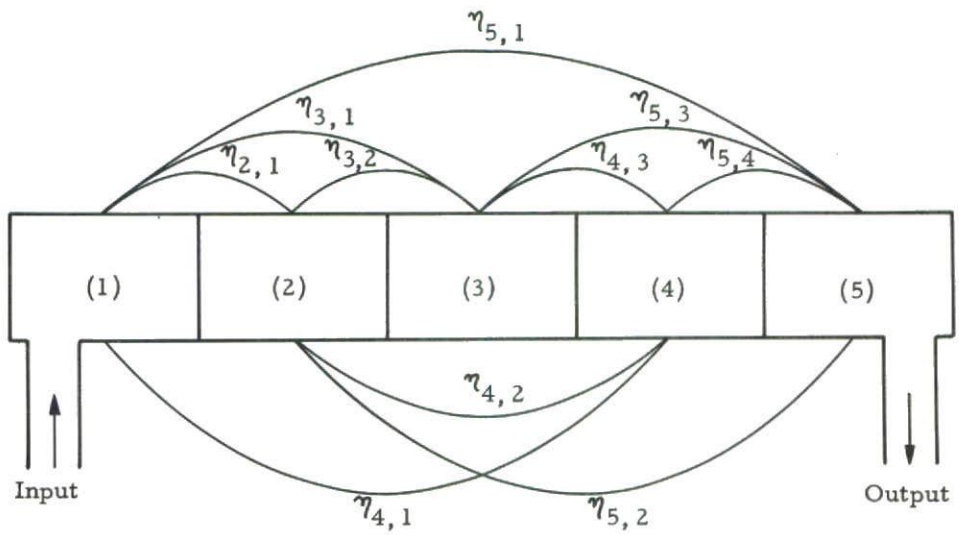

Fig 3.2 Figure showing the possible signal paths in a five-cavity klystron amplifier. The voltage gain is given by: $\eta_5 = \eta(1,2,3,4,5) + \eta(1,2,3,5) + \eta(1,2,4,5) + \eta(1,3,4,5) + \eta(1,2,5) + \eta(1,3,5) + \eta(1,4,5) + \eta(1,5)$

From these results it is clear that the gain function η_p of a multi-cavity klystron is considerably more complicated than the gain function of conventional cascaded band-pass amplifiers. This is due to differences in the mechanism of the amplifying process. In the conventional cascaded amplifier there is only one signal path between the input and output, and the overall gain is the product of the gains of all the stages. In the klystron the excitation of the output cavity is the sum of modulation components proportional to the gap voltages at all preceding gaps (see Eqs (2.54) and (2.55)). The interaction between non-adjacent gaps results in multiple signal paths from input to output, and the overall gain is the sum of the cascade gains over all possible signal paths.

This characteristic of the klystron complicates the synthesis of stagger-tuned multi-cavity klystrons with prescribed band-pass curve, or gain as function of frequency, because the multiple signal paths may cause signal cancellations at complex frequencies other than zero and infinite frequency, which are characteristic for the conventional cascaded amplifier.

It has been shown that the pole-zero concept of modern network theory provides a useful basis for the analysis and design of narrow-gap multi-cavity klystrons (22). Because the results for the general-type klystron analyzed here are identical in form, the pole-zero method is applicable in this general case as well.

From an examination of the determinant (3.11) we can draw the following conclusions concerning the poles and zeros of the gain function: the positions of the poles in the complex frequency plane, i e the complex frequencies for which the gain is infinite, are determined by the zeros of the self-admittances.

$$Y_{r,r} = 0 \qquad (r = 1, 2, \text{---} p) \tag{3.20}$$

The positions of the poles are thus determined by the resonant frequencies and the loaded Q's of the cavities (including beam loading). The number of poles obviously corresponds to the number of cavities (the pole due to the input cavity self-admittance $Y_{1,1}$ is not represented in the voltage gain η_p, but appears in the power gain expression (3.86)). Excluding the trivial zeros at infinite frequency, the number of possible zeros in the gain function η_p, i e the number of complex frequencies for which the gain is zero, is easily determined from the determinant (3.11), or better still, Eq (3.117). In the non-degenerate case the number of zeros is p-2, i e equal to the number of intermediate floating cavities. From examination of the gain determinant (3.117), it is observed that the positions of the zeros depend on all the transfer admittances and the positions of the poles associated with the (p-2) intermediate, floating cavities. The problem of tuning a p-cavity klystron may then be considered in terms of adjusting the p poles and the p-2 dependent zeros in such a way as to achieve a desired frequency response (23). In the present report we shall not deal any further with this method.

3.4 Alternate form of the gain determinant

The determinant (3.11) specifying the voltage gain of a p-cavity klystron can be transformed to an alternate form by taking appropriate linear combinations of the columns. The linear combination is the same as the one used in Eq (B.2) Appendix B, leading to the difference equation (3.34). If we anticipate the results of the next section, the alternate form of the determinant is most easily arrived at using the procedure shown below. Let us define explicitly the coefficients appearing in the difference equation (3.34).

$$S_p = -\frac{1}{Y_{p,p}} \left[a_p Y_{p-2,p-2} + b_p Y_{p-1,p-2} + Y_{p,p-2} \right] \tag{3.21}$$

$$T_p = -\frac{1}{Y_{p,p}}\left[b_p Y_{p-1,p-1} + Y_{p,p-1}\right] \tag{3.22}$$

where a_p and b_p are constants given in Appendix B. Expressed in terms of the coefficients S_p and T_p, the difference equation takes the following form, valid for $p \geq 4$:

$$S_p \eta_{p-2} + T_p \eta_{p-1} - \eta_p = 0 \tag{3.23}$$

If we form a new set of linear equations using Eq (3.23) for $p \geq 4$, and the original set (3.10) for $p < 4$, we obtain

$$\begin{bmatrix} -1 & 0 & 0 & 0 & \cdots & 0 \\ \eta_{3,2} & -1 & 0 & 0 & \cdots & 0 \\ S_4 & T_4 & -1 & 0 & \cdots & 0 \\ 0 & S_5 & T_5 & -1 & \cdots & 0 \\ \multicolumn{6}{c}{\cdots\cdots\cdots\cdots\cdots\cdots\cdots\cdots} \\ 0 & 0 & \cdots & S_p & T_p & -1 \end{bmatrix} \begin{bmatrix} \eta_2 \\ \eta_3 \\ \eta_4 \\ \eta_5 \\ \vdots \\ \eta_p \end{bmatrix} = - \begin{bmatrix} \eta_{2,1} \\ \eta_{3,1} \\ 0 \\ 0 \\ \vdots \\ 0 \end{bmatrix} \tag{3.24}$$

which has the solution

$$\eta_p = \begin{vmatrix} \eta_{2,1} & -1 & 0 & 0 & 0 & \cdots & 0 \\ \eta_{3,1} & \eta_{3,2} & -1 & 0 & 0 & \cdots & 0 \\ 0 & S_4 & T_4 & -1 & 0 & \cdots & 0 \\ 0 & 0 & S_5 & T_5 & -1 & \cdots & 0 \\ \multicolumn{7}{c}{\cdots\cdots\cdots\cdots\cdots\cdots\cdots\cdots\cdots\cdots\cdots\cdots} \\ \multicolumn{4}{c}{\cdots\cdots\cdots\cdots} & 0 & S_{p-1} & T_{p-1} & -1 \\ 0 & 0 & 0 & \cdots & 0 & 0 & S_p & T_p \end{vmatrix} \tag{3.25}$$

The only non-zero elements of this determinant are the elements along three adjacent diagonal lines.

The determinants (3.11) and (3.25) represent two alternate but equivalent formulae for evaluation of the voltage gain. As we have seen, expansion of the determinant (3.11) leads to a superposition of terms that are naturally interpreted as represent-

ing the cascade gains of the various possible signal paths from the input cavity to the output cavity. The study of synchronously tuned multi-cavity klystrons made in sections 3.7 - 3.10 shows that expansion of the alternate determinant (3.25) leads to a formulation in terms of growing and attenuated "gap voltage waves". In this formulation the terms representing interactions between non-adjacent gaps are incorporated in the parameters expressing the overall exponential variation of the gap voltage waves.

3.5 Criterion stating the condition for stability

The solution (3.11) of the set of equations (3.10) is finite only if the system determinant is non-vanishing, i e if

$$D = Y_{2,2}\, Y_{3,3}\, Y_{4,4} \text{ --- } Y_{p,p} \neq 0 \qquad (3.26)$$

In other words, η_p is finite if all the self-admittances in Eq (3.26) are different from zero. If the additional requirement is made that the RF gap voltage V_1 of the input gap be finite, we also have that $Y_{1,1} \neq 0$. Therefore, we must have

$$Y_{r,r} \neq 0 \qquad (r = 1, 2, \text{ --- } p) \qquad (3.27)$$

The physical meaning of these conditions is quite evident. By definition, the self-admittance $Y_{r,r}$ of the rth cavity is the sum of the circuit admittance $Y_{c,r}$ and the electronic admittance $Y_{e,r}$. The vanishing of this sum is exactly the required condition for start of self-supported monotron oscillations in the rth cavity. Because the present linearized theory does not allow for saturation effects, the theory therefore predicts an increase of gain towards infinity as the oscillation condition $Y_{r,r} = 0$ is approached.

From consideration of the physical system, the mathematical condition (3.27) can be further specialized to yield the following criterion for stable operation:

$$\mathrm{Re}\, Y_{r,r} = G_{r,r} = G_{c,r} + G_{e,r} > 0 \qquad (r = 1, 2, \text{ --- } p) \qquad (3.28)$$

In other words, the magnitude of the beam loading conductance, if negative, must be less than the circuit conductance. This condition is generally satisfied in klystrons of conventional design using narrow-gap cavities, and normally there are no instability problems arising from this cause in such klystrons. However, as shown by theory, and also demonstrated experimentally (9), this is not correct in the general case of klystrons having extended interaction regions. Here, the electronic conductance tends to increase with the length of interaction gaps and may assume sufficiently large negative values to cause oscillations. Actually, the stability criterion (3.28) imposes a restriction on the gap lengths and thus on the ultimate performance of klystrons with extended interaction regions.

3.6 Cascade gain approximation

Although the voltage gain of the p-cavity klystron is given by a relatively complicated expression containing the sum of 2^{p-2} products, various approximations of the exact formula can be derived. Of particular interest in this connection is the approximation in which interactions between non-adjacent gaps are disregarded. Such an approximation leads to a formula for gain that is in cascade form:

$$\eta_p \approx \eta_{p,p-1}\, \eta_{p-1,p-2} \text{ ----- } \eta_{3,2}\, \eta_{2,1} \tag{3.29}$$

The approximation involved in Eq (3.29) is small only if the voltage gain per stage is large compared to the number of cavities. In order to show the correctness of this statement we assume for simplicity identical cavities with identical gain per stage, i e $\eta_{p,p-1} = \eta_{p-1,p-2} = \text{---} \eta_{2,1}$. In this case the cascade gain approximation (3.29) gives

$$\eta_p = \eta_{s+1,s}^{p-1} \tag{3.30}$$

where s can be chosen arbitrarily. An approximate criterion of the approximation involved in this expression can be obtained by comparing it with the p-2 products in the exact formula (3.13) containing one factor less. Each of these identical products represents the cascade gain from the input to the output with one of the intermediate cavities removed. The sum of the products is given by

$$\Delta\eta_p = (p-2)\eta_{s+1,s}^{p-3}\, \eta_{s+2,s} \tag{3.31}$$

Forming the ratio of the expressions in Eqs (3.31) and (3.30) we find

$$\frac{\Delta\eta_p}{\eta_p} = (p-2)\, \frac{\eta_{s+2,s}}{\eta_{s+1,s}^2} \tag{3.32}$$

Thus, we arrive at the conclusion that the cascade gain approximation holds if

$$\frac{\eta_{s+1,s}^2}{\eta_{s+2,s}} \gg p-2 \tag{3.33}$$

which reduces to the condition stated previously if $\eta_{s+1,s}$ and $\eta_{s+2,s}$ are of the same order of magnitude.

This discussion leads to the conclusion that the cascade approximation of the voltage gain given in Eq (3.29) hardly is of much value when p exceeds a few cavities, except possibly in special cases for which the spacings are such that the interactions between every second cavity cancel (plasma transit angle equal to π).

In section 3.8 we shall study the special case of klystrons having identical, synchronously tuned cavities and derive an alternate formula for klystron gain which

also is in cascade form and, moreover, is valid for any number of cavities because the derivation is done without disregarding the interactions between non-adjacent gaps.

3.7 General difference equation for voltage gain of multi-cavity klystrons having arbitrarily tuned cavities

For klystrons with a relatively large number of cavities the general formula (3.18) for voltage gain involves the sum of a considerable number of terms that are all complex numbers. A discussion of the various factors that affect the gain is therefore extremely difficult except on a qualitative basis. It seems natural to look for a simpler formulation that lumps all these terms into mathematically simpler expressions, perhaps a formulation similar to the wave description used in the theory of traveling wave tubes. Although such an approach seems quite out of the question in the general case with stagger-tuned cavities, the wave formalism nevertheless is possible in special cases for which the cavities are tuned according to a specific pattern, such as synchronous tuning and periodic tuning. Admittedly, these very special tuning schemes are less interesting than the more general stagger-tuning. Nevertheless, the wave formalism applied to these special cases results in simple gain formulae that are interesting and illuminating, first because the approach leads to considerable insight into the physical mechanism behind the amplifying process in a klystron, and second because many of the conclusions that can be drawn concerning the effect of the various relevant parameters on klystron gain also are qualitatively correct for stagger-tuned klystrons.

The approach used in the following analysis differs from that of the preceding sections in that the voltage gain is obtained by solving a linear second-order homogeneous difference equation, which is satisfied by the gap voltages of the klystron. As shown in Appendix B, the RF gap voltages of three consecutive cavities are linked together by the following quite general second-order difference equation or recurrence formula, valid for any gap parameter combinations and tunings of the individual cavities:

$$Y_{p,p}\eta_p + [b_p Y_{p-1,p-1} + Y_{p,p-1}]\eta_{p-1} + [a_p Y_{p-2,p-2} + b_p Y_{p-1,p-2} + Y_{p,p-2}]\eta_{p-2} = 0$$

$$p = 4, 5, 6 \text{ -------} \qquad (3.34)$$

The quantities a_p and b_p given by Eqs (B.4) and (B.5) as well as the self-admittances and the transfer admittances appearing in the coefficients of this difference equation are given by the characteristic parameters associated with the cavities (p-2), (p-1), and p only. Equation (3.34) holds for p equal or larger than four. If p is less than four, the linear relationships between the gap voltages are obtained directly from Eq (3.7).

If the parameters and spacings of the individual cavities constituting the klystron are chosen in an arbitrary fashion, no simple analytical solution of Eq (3.34) is

possible, although in this case the recurrence form of the difference equation is particularly well adopted for numerical calculations on a digital computer. On the other hand, analytical solutions can be found in some special cases for which the coefficients in Eq (3.34) are specified functions of the independent variable p.

We shall solve the difference equation for the two cases which appear to be the simplest ones, namely:

a) Constant coefficients, corresponding to synchronously tuned cavities and identical spacings between the gaps

b) Periodic coefficients, corresponding to a periodically repeated but otherwise arbitrary stagger-tuning

The procedure followed in solving the above difference equation for these two cases is essentially the same as that known for differential equations having constant coefficients and periodic coefficients, respectively.

In case a) the wave-type solution is readily obtained as a linear combination of two exponential functions whose exponents are given in terms of the cavity parameters by a second-order algebraic equation. In case b) it can be shown, using a theorem similar to Floquet's theorem in the theory of differential equations with periodic coefficients (25), that the solution is a linear combination of two products, each of which is given by an exponential function multiplied by a periodic function with periodicity equal to the number of cavities in the periodically repeated stagger-tuning pattern. The exponents are obtained as the solution of a determinantal equation, the order of the determinant being equal to the number of cavities in the period. Noting that the solution of the equivalent mathematical problem in the theory of differential equations with periodic coefficients involves an infinite determinant, it appears that the solution of a difference equation with periodic coefficients is simpler than that of a differential equation of the same type.

In this chapter we shall study only klystrons with synchronous tuning. The analysis of periodic stagger-tuning is done in Chapter 4 using matrix algebra.

3.8 Gain of synchronously tuned multi-cavity klystrons in terms of growing and attenuated gap voltage waves

The assumption of constant coefficients in the difference equation (3.34) requires identical cavities, synchronous tuning, and equal spacings, i e:

$$
\begin{aligned}
Y_{p,p} &= Y_{p-1,p-1} = \text{--} = Y \\
Y_{p,p-1} &= Y_{p-1,p-2} = \text{--} = Y_{2,1} \\
G_{e,p} &= G_{e,p-1} = \text{--} = G_e \\
\ell_{p,p-1} &= \ell_{p-1,p-2} = \text{--} = \ell \\
M_p^+ &= M_{p-1}^+ = \text{--} = M^+ \\
M_p^- &= M_{p-1}^- = \text{--} = M^-
\end{aligned}
\qquad (3.35)
$$

The derivations in Appendix B show that the difference equation (3.34) in this particular case simplifies to the following:

$$\eta_p - 2e^{-j\beta_e \ell}\left[\left(1 - \frac{G_e}{Y}\right)\cos\beta_q\ell - j\frac{\overline{M^2}}{2WY}\sin\beta_q\ell\right]\eta_{p-1} + e^{-j2\beta_e\ell}\left[1-2\frac{G_e}{Y}\right]\eta_{p-2} = 0$$

$$p = 4,5,6, \text{------} \tag{3.36}$$

where the beam loading G_e is given by Eq (2.70), and $\overline{M^2}$ is the average value of the squares of the coupling coefficients of the slow and the fast space-charge waves.

$$\overline{M^2} = \tfrac{1}{2}\left(|M^+|^2 + |M^-|^2\right) \tag{3.37}$$

For convenience, let us introduce the following dimensionless quantities:

$$\varkappa = \frac{G_e}{Y} \tag{3.38}$$

$$\xi = \frac{\overline{M^2}}{2WY} \tag{3.39}$$

$$\theta_q = \beta_q\ell \tag{3.40}$$

$$\theta = \beta_e\ell \tag{3.41}$$

The ratio of the parameters $\varkappa$ and ξ is given by

$$\frac{\varkappa}{\xi} = \frac{|M^-|^2 - |M^+|^2}{|M^-|^2 + |M^+|^2} \leq 1 \tag{3.42}$$

which shows that $\varkappa$ normally is much less than ξ, except in the special cases for which the gap field couples mainly to one of the space-charge waves. Upon substitution of the parameters $\varkappa$, ξ, θ, and θ_q in the difference equation (3.36) it takes the form

$$\eta_p - 2e^{-j\theta}\left[(1-\varkappa)\cos\theta_q - j\xi\sin\theta_q\right]\eta_{p-1} + e^{-j2\theta}(1-2\varkappa)\eta_{p-2} = 0$$

$$p = 4,5,6, \text{------} \tag{3.43}$$

The solution of the equation is obtained by setting

$$\eta_p = e^{-j\theta(p-1)}\ \alpha^{p-1} \tag{3.44}$$

Substitution in Eq (3.43) yields the following algebraic equation for α:

$$\alpha^{p-3}\left\{\alpha^2 - 2\alpha\left[(1-\varkappa)\cos\theta_q - j\xi\sin\theta_q\right] + 1 - 2\varkappa\right\} = 0 \tag{3.45}$$

Besides the trivial solution α equals zero, the equation has two solutions α_1 and α_2 given by

$$\left.\begin{matrix}\alpha_1\\ \alpha_2\end{matrix}\right\} = (1-\varkappa)\cos\theta_q - j\xi\sin\theta_q \pm j\left\{1 - 2\varkappa - [(1-\varkappa)\cos\theta_q - j\xi\sin\theta_q]^2\right\}^{\frac{1}{2}} \quad (3.46)$$

The general solution of Eq (3.43) is a linear combination of the two particular solutions. Hence

$$\eta_p = e^{-j\theta(p-1)}\left(A\alpha_1^{p-1} + B\alpha_2^{p-1}\right) \quad (3.47)$$

$$p = 2, 3, \text{---}$$

It should be noted that Eq (3.43) holds only when p is larger than or equal to four. For the case that p equals four it relates η_4, η_3 and η_2, and the solution (3.47) is therefore applicable to any of these, i e for p equals two and upwards.

The constants A and B are specified by the initial conditions, i e the gains η_2 and η_3 of the two first stages, which can be calculated from Eqs (3.14) and (3.15). Expressing η_2 and η_3 in terms of the parameters $\varkappa$, ξ, θ and θ_q, we obtain from these equations

$$\eta_2 e^{j\theta} = -2(\varkappa\cos\theta_q + j\xi\sin\theta_q) \quad (3.48)$$

$$\eta_3 e^{j2\theta} = -2(2\xi^2\sin^2\theta_q + j\xi\sin 2\theta_q - 2j\varkappa\xi\sin 2\theta_q - 2\varkappa^2\cos^2\theta_q + \varkappa\cos 2\theta_q) \quad (3.49)$$

Substitution in Eq (3.47) results in two linear equations in the unknowns A and B. By solving we find

$$A = \frac{j\varkappa\cos\theta_q - \xi\sin\theta_q - j\varkappa/\alpha_1}{\left\{1 - 2\varkappa - [(1-\varkappa)\cos\theta_q - j\xi\sin\theta_q]^2\right\}^{\frac{1}{2}}} \quad (3.50)$$

$$B = -\frac{j\varkappa\cos\theta_q - \xi\sin\theta_q - j\varkappa/\alpha_2}{\left\{1 - 2\varkappa - [(1-\varkappa)\cos\theta_q - j\xi\sin\theta_2]^2\right\}^{\frac{1}{2}}} \quad (3.51)$$

The constants A and B are generally different. For the special case that the beam loading is zero ($\varkappa = 0$) we have that A = -B.

Substitution of the expressions α_1, α_2, A, and B in Eq (3.47) yields a formula that expresses the voltage gain of a synchronously tuned klystron in terms of the three dimensionless parameters $\varkappa$, ξ and θ_q defined in Eqs (3.38), (3.39) and (3.40). The parameters can be interpreted physically by noting that $\varkappa$ is proportional to the beam loading, ξ is equal to one half the maximum voltage gain of a two-cavity klystron (cavities spaced a quarter of a plasma wave length), and θ_q is the plasma transit angle between consecutive cavities.

The general nature of the complete solution evidently is in the form of two gap voltage "waves" where the exponential gains per stage of the two waves are given by

the absolute values of α_1 and α_2, respectively. Without making a detailed study of the rather complicated expressions for α_1 and α_2 it is possible to make some general statements concerning the nature of the two waves. First, introducing complex vector notations, we have

$$\alpha_1 = |\alpha_1| \, e^{j\varphi_1} \tag{3.52}$$

$$\alpha_2 = |\alpha_2| \, e^{j\varphi_2} \tag{3.53}$$

$$1 - 2\mathcal{K} = 1 - 2\frac{G_e}{Y} = 1 - 2\frac{G_e}{Y_c + G_e} = \frac{Y_c - G_e}{Y_c + G_e} = |1 - 2\mathcal{K}| \, e^{j\varphi_{\mathcal{K}}} \tag{3.54}$$

In the last equation we have made the small unessential approximation of including the electronic susceptance B_e in the circuit admittance, for instance by making an appropriate small detuning of the cavity. Also note that $\varphi_{\mathcal{K}}$ is the phase angle of $1-2\mathcal{K}$, rather than $\mathcal{K}$. At the resonance frequency $\varphi_{\mathcal{K}}$ obviously is zero.

It follows immediately from Eq (3.45) that the two solutions α_1 and α_2 satisfy the following relations:

$$\alpha_1 \alpha_2 = |\alpha_1| \, |\alpha_2| \, e^{j(\varphi_1 + \varphi_2)} = 1 - 2\mathcal{K} = |1 - 2\mathcal{K}| \, e^{j\varphi_{\mathcal{K}}} \tag{3.55}$$

$$|\alpha_1||\alpha_2| = |1 - 2\mathcal{K}| \tag{3.56}$$

$$\varphi_1 + \varphi_2 = \varphi_{\mathcal{K}} \tag{3.57}$$

The two components of the general solution (3.47) can thus be written

$$\eta_{p,1} = A \left| \frac{1 - 2\mathcal{K}}{\alpha_2} \right|^{p-1} e^{-j(\theta + \varphi_2 - \varphi_{\mathcal{K}})(p-1)} \tag{3.58}$$

$$\eta_{p,2} = B \, |\alpha_2|^{p-1} \, e^{-j(\theta - \varphi_2)(p-1)} \tag{3.59}$$

The following general comments can be made about the nature of the solutions: From the fact that the beam-loading parameter $\mathcal{K}$ normally is quite small, it follows from Eq (3.56) that the product of $|\alpha_1|$ and $|\alpha_2|$ is approximately equal to unity. Therefore, since $|\alpha_2|$ is the larger of the two, we conclude that the two components $\eta_{p,1}$ and $\eta_{p,2}$ represent attenuated and growing waves, respectively. The two waves propagate with phase velocities slightly different from the DC beam velocity. In the numerical analysis in the next section it is shown that φ_2 is always negative, and since $\varphi_{\mathcal{K}}$ is approximately zero, the attenuated wave has a phase shift $\theta + \varphi_2$ per stage, meaning that the wave is traveling faster than the beam. Conversely, the growing wave with a phase shift $\theta - \varphi_2$ per stage travels slower than the beam. It is shown later that if the gap spacing is chosen

such as to maximize the gain ($\theta_q = \pi/2$), the two gap voltage waves are in exact synchronism with the fast and the slow space-charge waves propagating on the beam. These results are in accordance with what might be expected from considerations of the interaction mechanism in terms of coupling between circuit modes carrying positive energy and space-charge modes carrying either positive or negative energy. Synchronization of the circuit mode with the slow space-charge wave carrying negative energy results in waves with growing amplitudes; synchronization with the fast wave carrying positive energy results in attenuated waves.

Another significant point noted from Eq (3.55) is the fact that the product $\alpha_1 \alpha_2$ is independent of the spacing of the cavity gaps. Furthermore, the product is also independent of all cavity and gap parameters provided the beam loading is zero or negligible. Thus, any optimization of cavity parameters and gap spacing that maximizes the amplitude of the growing wave is accompanied by a corresponding minimum in the amplitude of the attenuated wave.

The attenuated wave, which is essential for matching input conditions, attenuates very rapidly, particularly if the gain per stage is high. Therefore, beyond a few stages from the input gap, the attenuated wave is negligibly small, and there the overall voltage gain is equal to the growing wave $\eta_{p,2}$ given by Eq (3.59). Actually, for practical klystrons with gain per stage exceeding a few decibels the attenuated wave is negligible already at the second gap, as shown by the subsequent numerical calculations. For most practical purposes, therefore, the voltage gain of a synchronously tuned p-cavity klystron is given by Eq (3.59) which is in simple cascade form, i e the overall voltage gain is expressed as the product of p-1 factors α_2, each representing the complex voltage gain of one of the identical p-1 stages. It is significant that the derivation of this cascade gain formula is done without disregarding terms arising from interactions between non-adjacent gaps. The gain per stage α_2 is the result of contributions both from cascade interaction between adjacent gaps and interaction between non-adjacent gaps. Equation (3.59) therefore is superior to the approximate cascade gain formula (3.29) derived previously in section 3.6 by throwing away the terms arising from interaction between non-adjacent gaps. On the other hand, the wave approach leading Eq (3.59) is applicable only for the synchronous case, a limitation that does not apply to Eq (3.29).

A comparison of the two formulae for the synchronous case is interesting because it illustrates how the gain and the phase shift per stage are affected by interactions between non-adjacent gaps. According to the approximate equation (3.29) the voltage gain per stage is simply the voltage gain η_2 of a two-cavity klystron, which in the present notation is given by Eq (3.48). For this discussion it is sufficient to assume the frequency equal to the resonant frequency, in which case ξ is real, and to neglect the beam loading factor $\mathcal{K}$ which normally is much less than ξ. In this case Eq (3.48) yields

$$|\eta_2| \approx 2\xi \sin \theta_q \tag{3.60}$$

$$\text{Arg } \eta_2 = -(\theta + \pi/2) \tag{3.61}$$

where ξ is real. Thus, the simplified approach based on cascade interaction alone indicates a phase shift per stage of $-(\theta + \pi/2)$ regardless of the plasma transit angle θ_q. The extra phase shift of $\pi/2$ per stage in addition to θ is explained from the fact that the RF beam current that excites the gap voltage is in time quadrature to the RF velocity modulation in the preceding gap. This argument, of course, is correct only if the RF beam modulations due to previous gaps are neglected, as is done in deriving the approximate equation (3.29).

The numerical data given in the next section (Fig 3.6) reveals that the voltage gain per stage $|\alpha_2|$, obtained using the wave approach, is higher than the gain per stage $|\eta_2|$ evaluated from the cascade approximation. We can therefore draw the conclusion that at least for synchronous tuning the cascade approximation (3.29), neglecting interaction between non-adjacent gaps, underestimates the voltage gain per stage. The enhancement of voltage gain over that evaluated on the basis of cascade interaction alone must be due to favourable phases of the extra current components arising from interactions between non-adjacent gaps. It is significant that the increase in gain is accompanied by a change in the phase shift per stage from $-(\theta + \pi/2)$, predicted by the cascade approximation towards the value $(\theta + \theta_q)$, (see Fig 3.4). The latter would be the expected phase shift if the gap voltage wave were in synchronism with the slow space-charge wave. Since the amplifying process is based on power transfer from the slow space-charge wave to the circuit, the above results are in qualitative agreement with what might be expected from physical reasoning.

The detailed numerical data presented in the next section substantiates the above qualitative discussion, and allows us to draw conclusions concerning many important questions in multi-cavity klystron theory such as the effect of beam loading on gain and bandwidth, optimum gap spacing, etc.

3.9 Numerical data for gain and phase shift per stage

In addition to the general comments and discussion given in the last section concerning the general nature of the two gap voltage waves of a synchronously tuned klystron, we shall present a number of graphs plotted from numerical data calculated on an electronic computer. The graphs serve a twofold purpose, first that of providing some of the required information for the previous general discussion, and second, they are useful for practical design purposes.

All the quantities shown in the graphs are functions of three independent variables which are ξ, $\mathcal{K}$ and θ_q defined in Eqs (3.38) to (3.40). At the resonant frequency the quantities ξ and $\mathcal{K}$ are both real. We note that for frequencies below resonance ξ and $\mathcal{K}$ have positive imaginary parts, and vice versa. Furthermore, according to Eq (3.42) the ratio $\mathcal{K}/\xi$ is real, and the phases of ξ and $\mathcal{K}$ are therefore the same.

In Fig 3.3 are shown the absolute values of α_1 and α_2 evaluated from Eq (3.46) and plotted vs the gap spacing θ_q. The parameters ξ and $\varkappa$ are chosen real, i e the curves refer to resonance, which of course is the case having most interest. Each curve is labelled with two numbers, referring to ξ and $\varkappa$ respectively. Three different values of ξ are chosen: 0.5, 2, and 5, corresponding to low, intermediate, and high gain per stage, respectively. Each of the values of ξ is combined with three different values of the beam loading parameter: 0.2, zero, and -0.2.

The phase angles φ_1 and φ_2 of α_1 and α_2 are shown in Fig 3.4 for the same real values of the parameters ξ and $\varkappa$.

Figure 3.5 shows $|\alpha_1|$ and $|\alpha_2|$ for two different frequencies located symmetrically with respect to the resonant frequency.

Figure 3.6 shows the ratio $|\alpha_2|/|\eta_2|$ for the same real values of ξ as those in Fig 3.4, and $\varkappa = 0$ (zero beam loading).

The graphs in Fig 3.7 are the absolute values of the initial values A and B of the attenuated and growing gap voltage waves for the same real values of ξ and $\varkappa$ as those in Fig 3.3.

In addition to the general comments made in the last section concerning the relative magnitudes of the growing and the attenuated waves, a study of the curves in Figs 3.3 to 3.7 in connection with Eqs (3.46) to (3.51) allows one to draw a number of significant conclusions concerning synchronously tuned multi-cavity klystrons. These are the following.

3.9.1 Optimum gap spacing

First we observe from Fig 3.3 that the gain per stage $|\alpha_2|$ at <u>resonance</u> is maximum when the gap spacing is equal to a quarter of a plasma wavelength ($\theta_q = \pi/2$), regardless of the beam loading. The same conclusion concerning the value of the optimum gap spacing is reached if we discuss the gain of two-cavity and three-cavity klystrons directly from Eqs (3.48) and (3.49) rather than using the wave formalism. It should be pointed out that, although this optimum is predicted by the simple conventional klystron theory, the result is not at all obvious because the simple theory does not account properly for interaction between non-adjacent gaps and density modulation effects within the gaps.

The curves shown in Fig 3.5 for complex values of ξ and $\varkappa$, i e for frequencies different from the resonant frequency, in this case two frequencies located symmetrically on each side of the resonant frequency ($\mathrm{Arg}\,\xi = \mathrm{Arg}\,\varkappa = \pm\pi/4$), indicate a shift in the optimum gap spacing from $\pi/2$ towards smaller values if $\omega < \omega_{res}$, and a shift towards higher values if $\omega > \omega_{res}$. In these two cases the cavity impedance is inductive and capacitive, respectively. The two curves are symmetrically located with respect to $\theta_q = \pi/2$, a property that can also be proved directly from Eq (3.46). Thus, besides maximizing the gain at resonance, the gap spacing $\theta_q = \pi/2$ results in a frequency response curve that is <u>symmetric</u> with respect to the mid frequency.

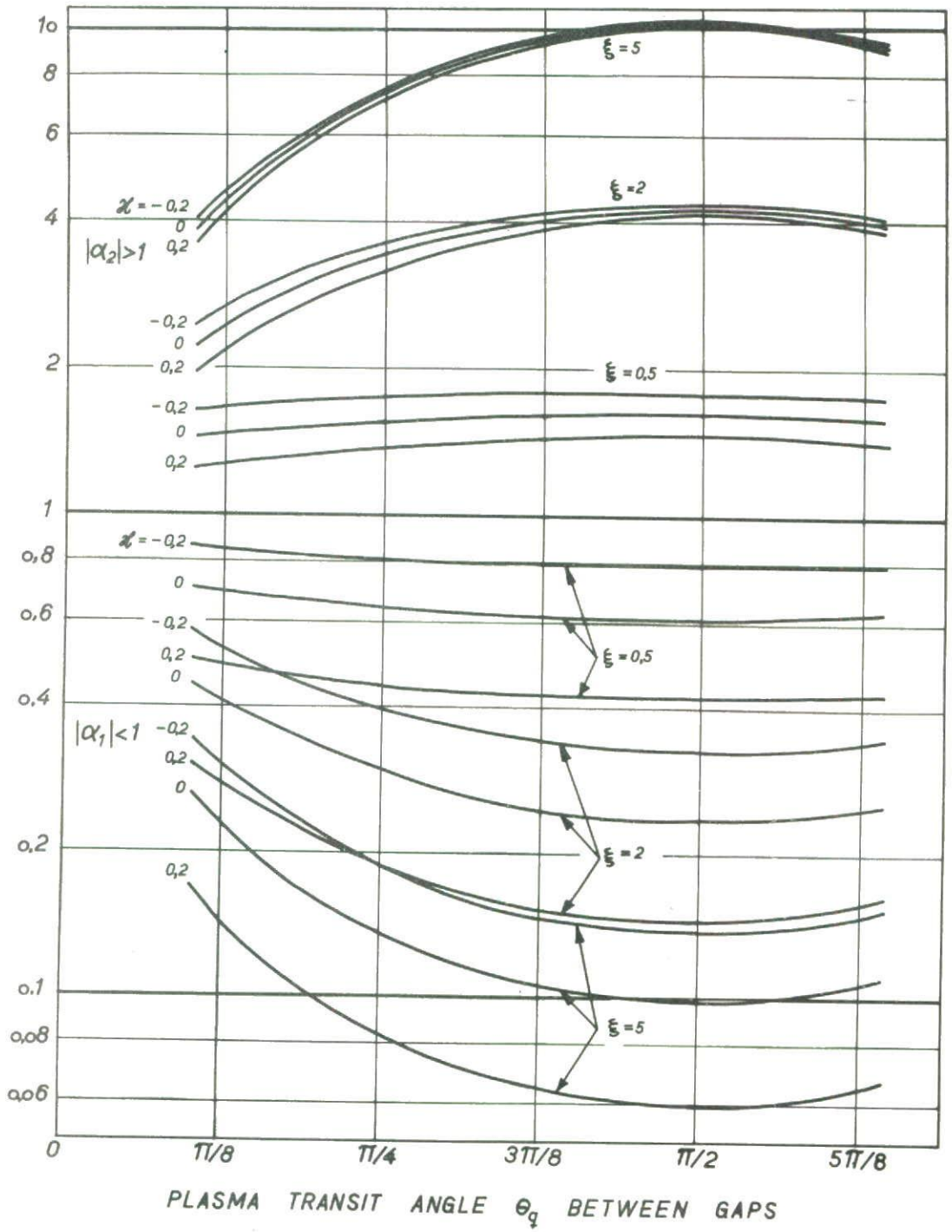

Fig 3.3 Voltage gain per stage of a synchronously tuned multi-cavity klystron at resonance. The curves show the attenuated and the growing gap voltage waves $|\alpha_1|$ and $|\alpha_2|$ plotted vs the gap spacing θ_q for $\xi = 0.5$, 2, and 5; $\chi = -0.2$, zero, and 0.2.

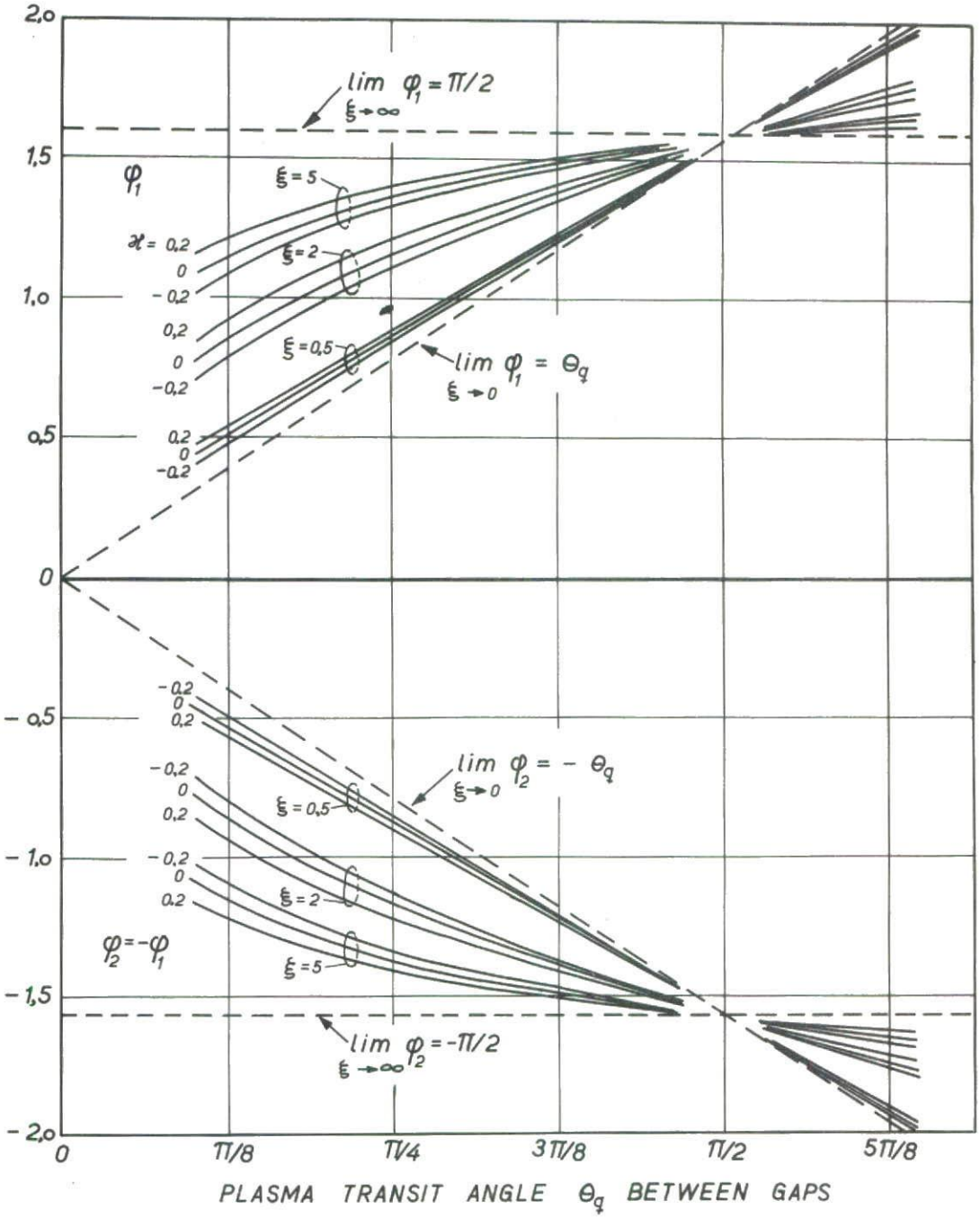

Fig 3.4 Phase shifts per stage φ_1 and φ_2 of the attenuated and growing gap voltage waves of a synchronously tuned multi-cavity klystron at resonance. The curves are plotted vs the gap spacing θ_q for ξ = 0.5, 2, and 5; $\varkappa$ = -0.2, zero, and 0.2.

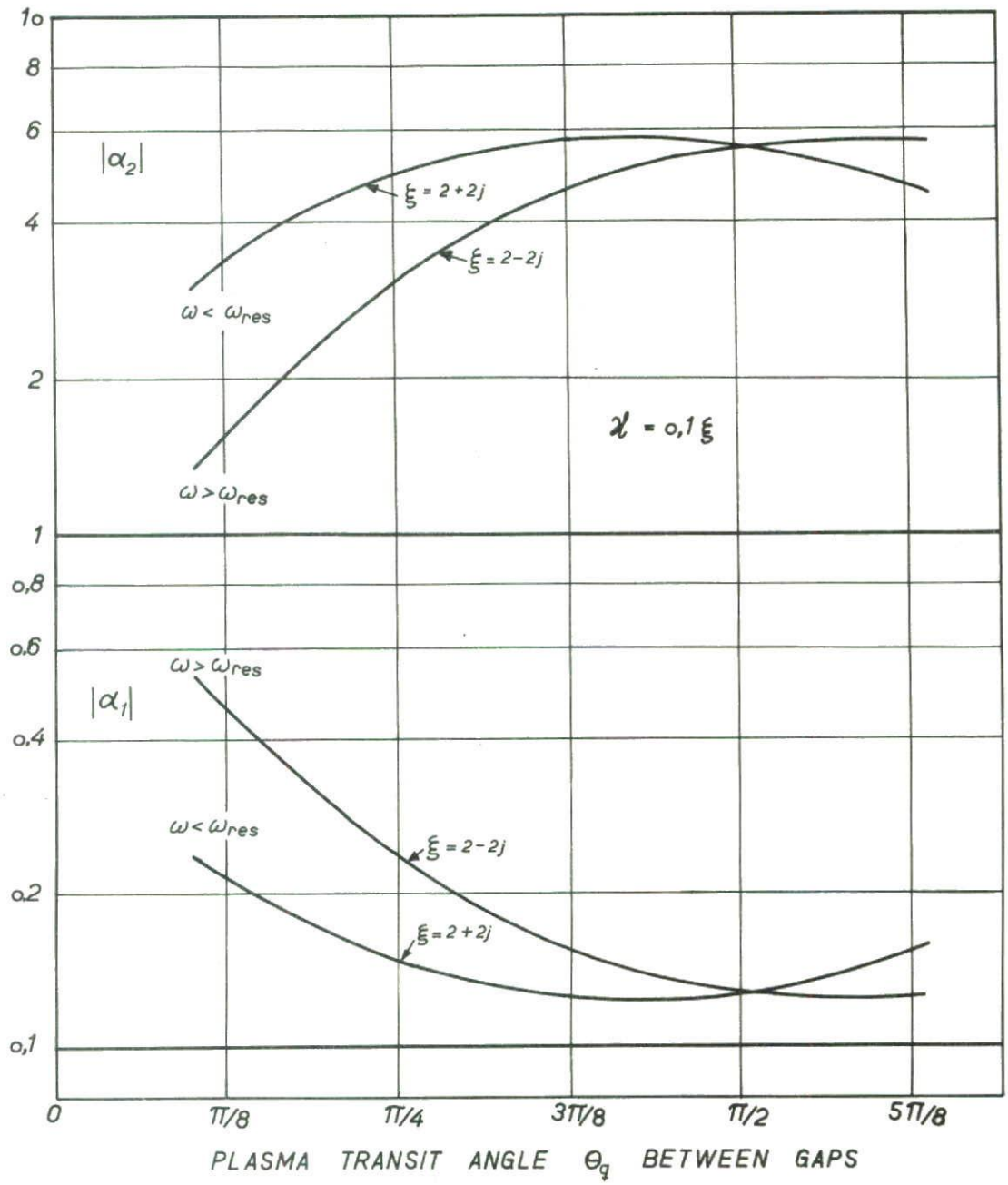

Fig 3.5 Voltage gain per stage of a synchronously tuned multi-cavity klystron for two frequencies located symmetrically on each side of the resonant frequency. The curves show the attenuated and growing waves plotted vs θ_q for $\xi = 2 \pm 2j$ and $\chi/\xi = +0.1$.

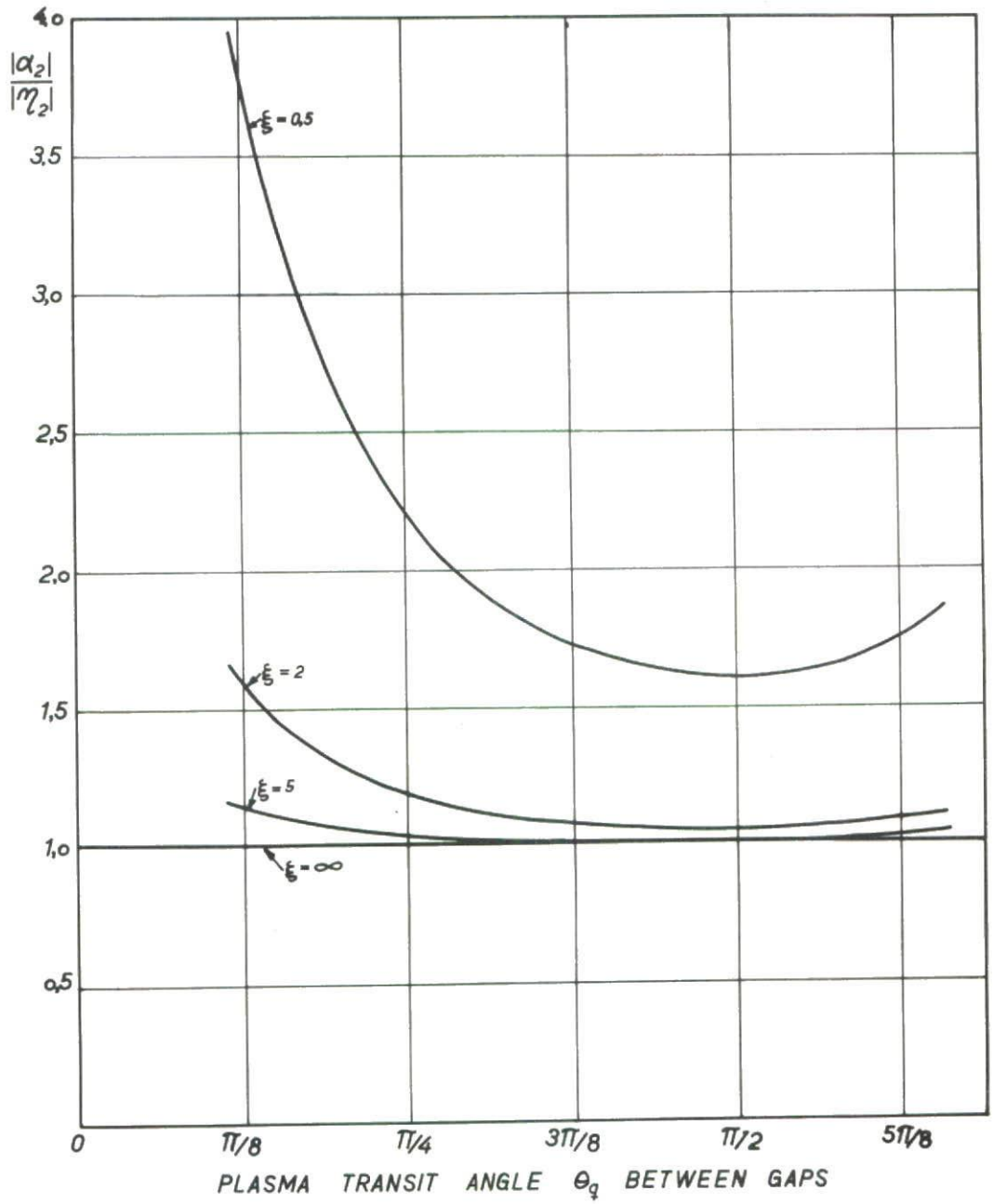

Fig 3.6 Curves demonstrating the enhancement of gain per stage due to interaction between non-adjacent gaps for a synchronously tuned multi-cavity klystron. The ratio $|\alpha_2|/|\eta_2|$ is plotted vs θ_q for $\xi = 0.5$, 2, and 5; $\delta = 0$.

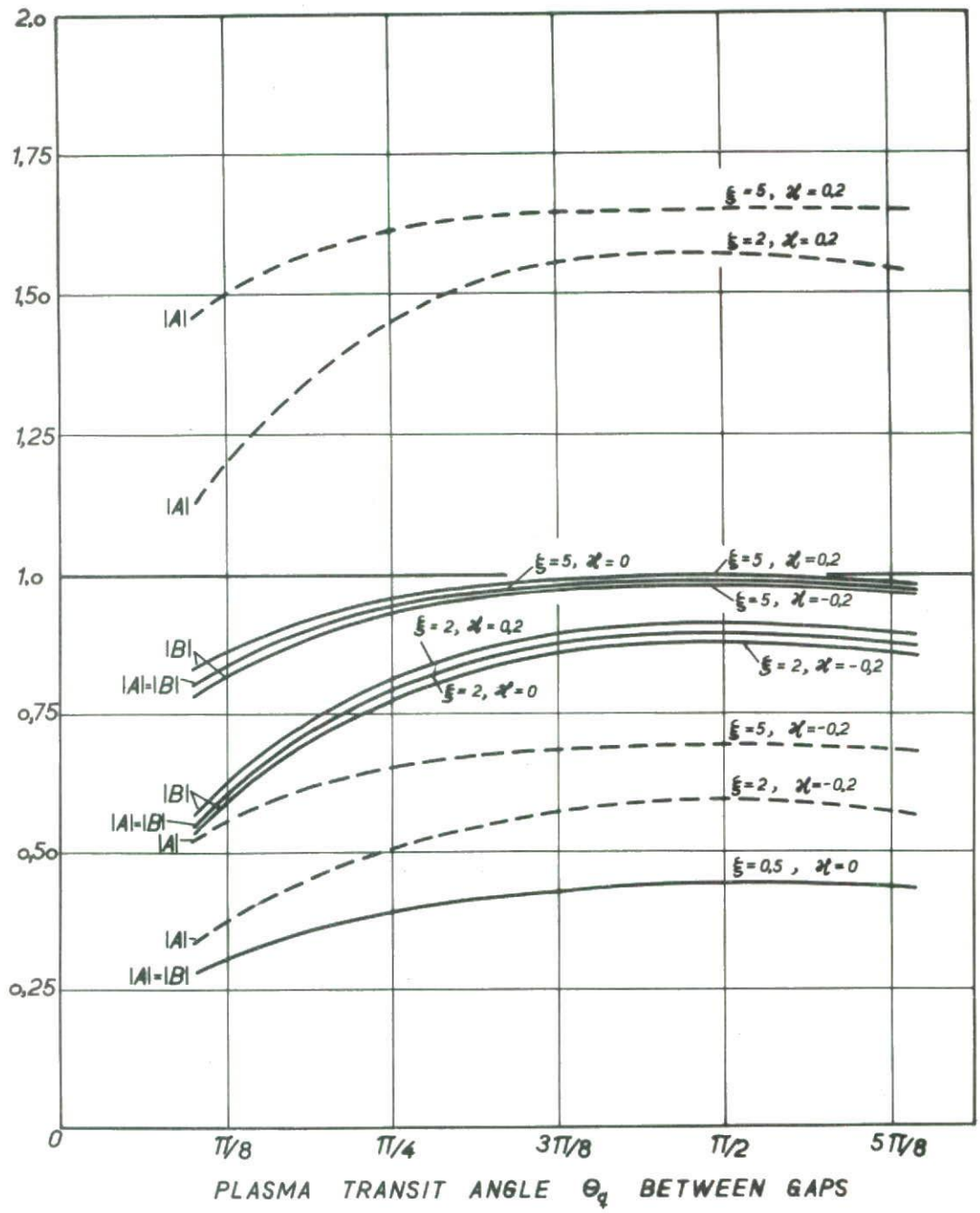

Fig 3.7 The absolute values of the initial amplitudes A and B of the gap voltage waves plotted vs the gap spacing θ_q for $\xi = 0.5$, 2, and 5: $\varkappa = -0.2$, zero, and 0.2

It should be noted that the statements concerning optimum gap spacing do not apply to the more interesting case of non-synchronous tuning. The optimum gap spacings of a stagger-tuned klystron will be modified, depending on the details of the stagger-tuning arrangement and, furthermore, on the frequency to which the optimization is referred. Although this question is an interesting one, it does not seem probable that very much could be gained by a further optimization of drift lengths of stagger-tuned klystrons, and it is beyond the scope of this paper to attack this very complicated problem which appears to be intimately related to the problem of optimization of stagger-tuning pattern with respect to gain and bandwidth.

3.9.2 Gain and phase shift per stage

Setting $\theta_q = \pi/2$, corresponding to optimum gap spacing for synchronous tuning, we can easily write the analytical expressions for the maximum voltage gain. In this connection it is interesting to determine both $|\eta_2|_{max}$, $|\eta_3|_{max}$, and $|\alpha_2|_{max}$ from Eqs (3.48), (3.49) and (3.46), respectively. We find

$$|\eta_2|_{max} = 2\xi \tag{3.62}$$

$$|\eta_3|_{max} = 4\xi^2 - 2\varkappa \tag{3.63}$$

$$\left.\begin{matrix} |\alpha_1|_{min} \\ |\alpha_2|_{max} \end{matrix}\right\} = \left[1 - 2\varkappa + 2\xi^2 \mp 2\xi\,(1 - 2\varkappa + \xi^2)^{\frac{1}{2}}\right]^{\frac{1}{2}} \tag{3.64}$$

Comparison of Eqs (3.62) and (3.64) yields the following result already stated in the general discussion in the previous section:

$$|\alpha_2|_{max} > |\eta_2|_{max} \qquad \text{if } \varkappa < \tfrac{1}{2} \tag{3.65}$$

Since the condition $\varkappa < \frac{1}{2}$ is equivalent to $G_e < G_c$, the inequality (3.65) can be interpreted as meaning that the interaction between non-adjacent gaps always enhances the voltage gain at synchronism provided the electronic conductance G_e is less than the circuit conductance G_c. Of course, this statement is correct only if the attenuated gap voltage wave can be neglected. A case for which the attenuated wave cannot be disregarded is the three-cavity klystron. We have namely from Eqs (3.62) and (3.63)

$$|\eta_3|_{max} < |\eta_2|^2_{max} \qquad \text{if } \varkappa > 0 \tag{3.66}$$

meaning that for positive beam loading the maximum voltage gain of the three-cavity klystron is less than the product of the gains of each of the stages considered alone, a result which is in apparent contradiction to the inequality (3.65). The explanation for the discrepancy is first of all that in this case the attenuated wave can-

not be neglected; its phase at the third gap is opposite that of the growing wave and reduces the overall gain. Second, in the discussion of gain on the basis of Eq (3.59) the initial amplitude B has been disregarded; evidently this is not permitted for klystrons with only a few stages.

The curves in Fig 3.3 and perhaps particularly those in Fig 3.6 show that enhancement of voltage gain due to interaction between non-adjacent gaps actually becomes more pronounced as θ_q departs from the optimum value $\theta_q = \pi/2$, particularly for small values of ξ. For high gain per stage (ξ large) the ratio $|\alpha_2|/|\eta_2$ approaches unity regardless of θ_q, as predicted by the cascade approximation (3.29). For small gain per stage (ξ small) the ratio becomes increasingly large as ξ approaches zero.

These results show that the gain of a klystron with relatively closely spaced gaps ($\theta_q \ll \pi/2$) is considerably higher than anticipated from the cascade formula (3.29), particularly if the cavities are heavily loaded (small ξ) and tuned to a frequency above the signal frequency (see Fig 3.5). Only a more thorough investigation of this scheme could answer the question as to whether gain and bandwidth obtained in this way are comparable to those of ordinary stagger-tuned klystrons.

Next, let us consider the phase shift per stage at resonance where $\varphi_1 + \varphi_2 = 0$. The curves in Fig 3.4 show that φ_2, the phase shift per stage of the growing gap voltage wave, has a value between the plasma transit angle $-\theta_q$ and $-\pi/2$, depending mainly on the parameter ξ and, to a lesser extent, on the beam loading parameter $\mathcal{N}$. For high gain per stage (ξ large) φ_2 approaches $-\pi/2$ which is the value predicted from the cascade approximation neglecting interaction between non-adjacent gaps. For small gain per stage (ξ small), φ_2 approaches $-\theta_q$ in which case the growing gap voltage wave is in exact synchronism with the slow space-charge wave regardless of the gap spacing θ_q. The cascade approximation is therefore, as expected, grossly in error for small gain per stage.

Besides being a function of ξ, the phase shift per stage depends to a lesser extent on the beam loading parameter $\mathcal{N}$ except at the optimum gap spacing $\theta_q = \pi/2$, in which case $\varphi_2 = -\pi/2$ regardless of beam loading. At this gap spacing the growing gap voltage wave is in synchronism with the slow space-charge wave and the attenuated wave in synchronism with the fast space-charge wave. It thus appears that optimization of gap spacing with respect to gain is synonymous with providing synchronism between the growing gap voltage wave and the slow space-charge wave.

3.9.3 Effect of beam loading on gain and bandwidth

If we return to the study of the curves in Fig 3.3, we are able to make a statement concerning the effect on gain and bandwidth of the beam loading, and answer the question whether cavity loading by circuit loss or by the beam is preferable. In this connection it is significant that the beam loading is not properly accounted for

by simply adding the beam loading conductance G_e to the circuit admittance Y_c, as is claimed in the conventional klystron theory. If this were correct, it would be quite irrelevant as far as gain and bandwidth are concerned whether the cavities were loaded with circuit loss or by the beam. It follows from the more rigorous theory developed in this report that the beam loading conductance G_e in addition to appearing in parallel with the circuit admittance also enters into the transfer admittance $Y_{r,s}$, as is apparent for instance from Eq (B. 9) in Appendix B.

Noting that the bandwidth is specified mainly by the value of the self-admittance $Y = Y_e + Y_c$, which determines the effective loaded Q, the gain will depend explicitly on the beam loading G_e through the transfer admittance even if Y, and thus the bandwidth, is kept constant. In the present wave description, this point manifests itself by the fact that with constant ξ (meaning constant Y and therefore constant bandwidth) the gain is a function of the beam loading parameter $\varkappa$, which is proportional to G_e. A study of Fig 3. 3 or of Eqs (3.63) and (3.64) reveals that the quantities $|\eta_3|_{max}$ and $|\alpha_2|_{max}$ increase as the beam loading parameter $\varkappa$ decreases provided ξ and thus the bandwidth are kept constant. Therefore, the rather important conclusion pertaining to synchronously tuned multi-cavity klystrons can be made that loading of cavities by circuit loss is preferable to beam loading. For a given bandwidth (Y constant) the highest gain is achieved using negative beam loading compensated by sufficient circuit loss. Evidently, in this case the density modulations occurring in the interaction gaps in addition to the normal velocity modulations have favourable phases and contribute to enhance the overall gain.

Another observation made from the curves in Fig 3. 3 is that negative beam loading causes a general broadening of the maxima. Therefore, also in this respect negative beam loading is beneficial because the gain will be a less critical function of gap spacing.

Even if the beam loading generally affects the gain and bandwidth as described, the magnitude of the effect is quite small, as clearly observed from Fig 3. 3, because $\varkappa$ normally is much smaller than ξ, and only approaches ξ in extreme cases for which the cavities couple mainly to one of the space-charge waves.

From physical reasoning it seems natural to expect that the discussed possible enhancement of gain at constant bandwidth due to negative beam loading should be accompanied by a change in the phase shift per stage φ_2 in a direction which brings the growing gap voltage wave nearer to synchronism with the slow space-charge wave. That this is indeed the case is shown clearly by the curves in Fig 3.4.

3.9.4 Relative phases of the growing and attenuated gap voltage waves

To conclude the presentation of numerical data for synchronously tuned klystrons, the absolute values of the initial values A and B of the attenuated and growing gap voltage waves are plotted in Fig 3. 7 for the same combinations of the para-

meters ξ and $\varkappa$ as those in Figs 3.3 and 3.4. Over the appreciable range of parameters shown in the graphs, both $|A|$ and $|B|$ are of the order of unity, a fact that permitted us to disregard these factors in the previous discussions. The difference between the phase angles of $|A|$ and $|B|$ is exactly equal to π ($A = -B$) for zero beam loading, and approximately equal to π for moderate values of the ratio $\varkappa/\xi$.

In conclusion we shall show that the growing wave and the attenuated wave are in phase at the gaps for which p is even, and out of phase at the gaps for which p is odd. At least this statement is correct for gaps with optimum spacing $\theta_q = \pi/2$ and zero beam loading. Since in this case $A = -B$, $\varphi_1 = -\varphi_2 = \pi/2$, and $|\alpha_1| = 1/|\alpha_2|$, Eq (3.47) reduces to the following expression:

$$|\eta_p| = |B| \left[|\alpha_2|^{p-1} + (-1)^p \, |\alpha_2|^{1-p} \right] \tag{3.67}$$

which shows that the above statement is correct. Thus, for a three-cavity klystron (p=3) the attenuated wave subtracts from the growing wave at the third gap, explaining the fact previously discussed that the voltage gain in this case is less than the product of the gains of its two stages considered alone (see Eqs (3.62) and (3.63)).

3.10 Space-charge waves in synchronously tuned klystrons

As a supplement to the discussion in the last sections of gap voltage waves in synchronously tuned klystrons, it is instructive to study the growth of the associated space-charge waves that propagate on the electron stream. Since the kinetic voltage components U^+ and U^- of the two space-charge waves are simply related to the current components I^+ and I^- through the RF beam impedance W, it suffices to study the current wave, which in the general case is given by Eq (2.54). Noting that the initial modulations I(0) and U(0) are zero, and using the notations defined in the last sections, we obtain

$$I_p = -\frac{1}{W} \sum_{r=1}^{p} V_r \, \Delta \left[M \, e^{-j\theta(p-r+\frac{1}{2})} \right] \tag{3.68}$$

where I_p is the RF beam current at the output cross-section of the pth gap, and $\theta = \beta_e \ell$ as before is the electronic transit angle between the centers of two adjacent gaps. We shall study the slow and the fast waves I_p^+ and I_p^- separately. Expansion of Eq (3.68) by means of the difference operator Δ yields

$$I_p^+ = -\frac{M^+}{2W} \, e^{-j(\theta+\theta_q)(p+\frac{1}{2})} \sum_{r=1}^{p} V_r \, e^{j(\theta+\theta_q)r} \tag{3.69}$$

$$I_p^- = +\frac{M^-}{2W} \, e^{-j(\theta-\theta_q)(p+\frac{1}{2})} \sum_{r=1}^{p} V_r \, e^{j(\theta-\theta_q)r} \tag{3.70}$$

These formulae are quite general and hold for any stagger-tuning if the proper gap voltages V_r are inserted in the equations. We shall, however, refrain from a general study which is quite involved and rather confine the discussion to one special case for which unessential details are avoided and the mathematical formulae are particularly simple, namely a synchronously tuned klystron having optimum gap spacings ($\theta_q = \pi/2$).

If the synchronously tuned klystron is operated at the resonant frequency, the gap voltage V_r is readily determined from Eq (3.47) by noting that in this case $\varphi_1 = -\varphi_2 = \pi/2$, and both A and B are real. Thus, for $r \geq 2$

$$V_r = \eta_r V_1 = e^{-j\theta(r-1)} V_1 \left[A|\alpha_1|^{r-1} e^{j\frac{\pi}{2}(r-1)} + B|\alpha_2|^{r-1} e^{-j\frac{\pi}{2}(r-1)} \right] \qquad (3.71)$$

where the real constants A and B are of the order of unity.

Substitution in Eqs (3.69) and (3.70) yields for the two components of the current

$$I_p^+ = -\frac{M^+ V_1}{2W} e^{-j(\theta+\frac{\pi}{2})(p-\frac{1}{2})} \left[1 + B\sum_{r=2}^{p} |\alpha_2|^{r-1} + A\sum_{r=2}^{p} (-|\alpha_1|)^{r-1} \right] \qquad (3.72)$$

$$I_p^- = -\frac{M^- V_1}{2W} e^{-j(\theta-\frac{\pi}{2})(p-\frac{1}{2})} \left[1 + B\sum_{r=2}^{p} (-|\alpha_2|)^{r-1} + A\sum_{r=2}^{p} |\alpha_1|^{r-1} \right] \qquad (3.73)$$

Since the quantities inside the brackets are real, the phase shifts per stage of the slow and the fast current components I_p^+ and I_p^- are given by $\theta + \pi/2$ and $\theta - \pi/2$, respectively, corresponding to propagation factors $\beta_e + \beta_q$ and $\beta_e - \beta_q$, as expected.

The amplitudes of I_p^+ and I_p^- grow from gap to gap in accordance with the sum of the geometrical series inside the brackets. Of these the α_2-series represents the current modulation due to the growing gap voltage wave, and the α_1-series the current modulation due to the attenuated gap voltage wave. By evaluation of the series it follows immediately that each of the components I_p^+ and I_p^- is the sum of <u>three</u> current waves: one wave having constant amplitude, one growing wave, and one attenuated wave. Some distance beyond the input gap no significant error is made if the constant-amplitude wave and the attenuated wave are neglected compared to the growing wave. Making this approximation, we find

$$I_p^+ \approx -\frac{BM^+ V_1}{2W} \frac{|\alpha_2|^p}{|\alpha_2| - 1} e^{-j(\theta+\frac{\pi}{2})(p-\frac{1}{2})} \qquad (3.74)$$

$$I_p^- \approx -\frac{BM^- V_1}{2W} \frac{(-|\alpha_2|)^p}{|\alpha_2| + 1} e^{-j(\theta-\frac{\pi}{2})(p-\frac{1}{2})} \qquad (3.75)$$

The equations show quite clearly that the amplitude of the slow wave I_p^+ exceeds that of the fast wave I_p^-, as is expected from the small-signal kinetic power theorem (see section 2.7). From a study of Eqs (3.69) to (3.73) it is readily seen why the slow space-charge wave grows more rapidly than the fast wave. The growing gap voltage wave modulating the beam is in synchronism with the slow space-charge wave and the effect on the slow wave I_p^+ is therefore cumulative, i e the contributions from each gap add in phase, shown by the fact that all the terms in the α_2-series in Eq (3.72) have the same sign. On the other hand, the phase of the growing gap voltage wave is unfavourable for modulation of the fast space-charge wave. The modulation in one particular gap tends to cancel that of the preceding gap, as indicated by the fact that the sign of the terms in the α_2-series in Eq (3.73) alternates between plus and minus. The net amplitude growth of the fast space-charge wave is therefore smaller than that of the slow wave.

The additional small modulations given by the α_1-series in Eqs (3.72) and (3.73) are caused by the attenuated gap voltage wave which is in synchronism with the fast space-charge wave. Therefore, the small current modulations due to the attenuated gap voltage wave are cumulative for the fast wave and alternating between plus and minus for the slow wave.

The relative magnitudes of I_p^+ and I_p^- depend, furthermore, on the coupling coefficients M^+ and M^-. Since the amplifying mechanism is one by which RF power is coupled to the cavities along the stream from the slow space-charge wave carrying negative kinetic energy, the occurrence of a growing slow wave is quite essential. The fast wave, however, increases its amplitude at the expense of power, and serves no useful purpose in the amplifying process. The fast wave could be eliminated altogether by arranging matters such that the gaps couple only to the slow space-charge wave, in which case $M^- = 0$. We would then have a klystron in which the slow wave is the only one occurring. If the practical problem of designing gaps that couple only to the slow wave is disregarded (although design of such couplers seems entirely feasible), such a hypothetical klystron would be characterized by gaps having negative beam loading, which would require sufficient cavity loss to avoid self-oscillations. The gain would be almost independent of gap spacing and be somewhat larger than that of a similar klystron with zero or positive beam loading, according to the discussion given in the previous two sections. It appears improbable, however, that the small improvement in gain and bandwidth would justify the added complexity.

3.11 General expression for power gain

The power gain of a multi-cavity klystron is determined by establishing the proper relationships between the input power and output power and the RF gap voltages of the input and output cavities by means of the formulae given in Appendix A.

3.11.1 Relation between input power and gap voltage

The RF energy from the signal source flows through a transmission line into the input cavity, as indicated in Fig 3.8a. The equivalent circuit shown in Fig 3.8b, referred to the position in the transmission line known as the "detuned short" position, is correct for any resonant cavity provided the cavity is excited in only one of its resonant modes.

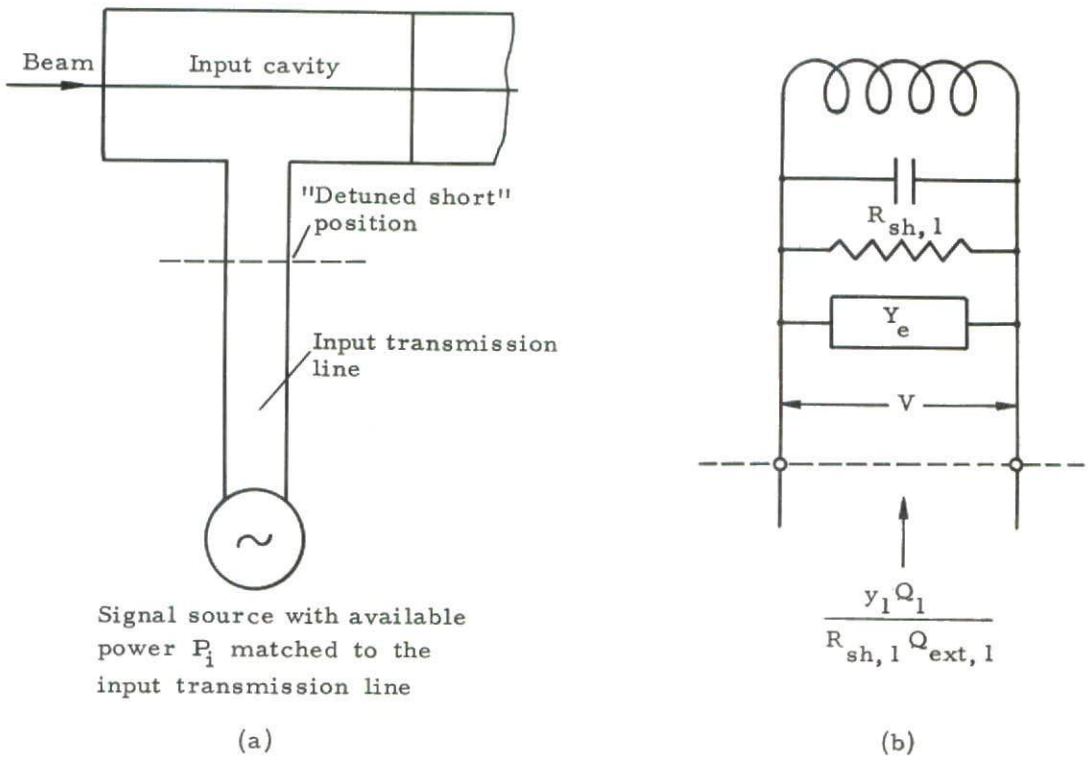

Fig 3.8 Configuration of the input cavity and signal source
(a) Input cavity excited from a signal source with available power P_i
(b) Equivalent lumped-parameter circuit

The input admittance y_1, normalized with respect to the characteristic admittance of the transmission line and referred to the detuned short position, follows from Eq (A.12) in Appendix A. In the present notation the equation takes the form

$$y_1 = Q_{ext,1}\left(2j\delta_1 + \frac{1}{Q_1} + \frac{R_{sh,1}}{Q_1} Y_{e,1}\right) \tag{3.76}$$

where $Q_{ext,1}$ is a measure of the coupling from the input transmission line to the cavity, δ_1 is the frequency-tuning parameter defined in Eq (3.3), Q_1 is the unloaded Q, $R_{sh,1}/Q_1$ is the characteristic impedance of the cavity, and $Y_{e,1}$ is the electronic admittance. The loaded Q of the input cavity by definition is given by

$$\frac{1}{Q_L} = \frac{1}{Q_1} + \frac{1}{Q_{ext,1}} \tag{3.77}$$

Substituting Eq (3.77) in Eq (3.76) and using Eq (3.2), we can express the normalized input admittance y_1 in terms of the self-admittance $Y_{1,1} = Y_{c,1} + Y_{e,1}$ in the following way:

$$y_1 = Q_{ext,1} \frac{R_{sh,1}}{Q_1} Y_{1,1} - 1 \tag{3.78}$$

Although it normally is desirable to adjust the normalized admittance to unity at resonance by appropriate choice of coupling between guide and cavity (adjustment of $Q_{ext,1}$), the general case characterized by arbitrary input admittance will first be considered. The assumption will be made that the signal source impedance is matched to the input transmission line, so that the entire available power P_i is transferred to the cavity and the beam when the normalized input admittance y_1 is unity. Such an assumption does not restrict the generality of the results. If y_1 is not unity, some of the power is reflected at the input terminal, only part of it being transmitted into the cavity. For this transmitted complex power we shall use the notation $\mathcal{P}_i$. From elementary considerations of reflections at the input terminal, the following relation between the available power P_i, the transmitted complex power $\mathcal{P}_i$, and the normalized input admittance is obtained:

$$\mathcal{P}_i = P_i \frac{4y_1}{(1+y_1)(1+y_1^*)} \tag{3.79}$$

where here, as throughout the paper, complex power is defined on the basis of the product of current and the conjugate of voltage.

The transmitted complex power $\mathcal{P}_i$ may be related to the RF gap voltage V_1 through the self-admittance $Y_{1,1}$ by noting that the power is dissipated in this admittance minus the coupled admittance from the input transmission line.

$$\mathcal{P}_i = \tfrac{1}{2} V_1 V_1^* \left(Y_{1,1} - \frac{Q_1}{R_{sh,1}} \frac{1}{Q_{ext,1}} \right) \tag{3.80}$$

Combination of Eqs (3.78), (3.79) and (3.80) yields the desired relation between the available power P_i of the signal source and the RF gap voltage V_1:

$$P_i = \frac{1}{8} V_1 V_1^* \frac{R_{sh,1}}{Q_1} Q_{ext,1} Y_{1,1} Y_{1,1}^* \tag{3.81}$$

3.11.2 Optimization of the input coupling

At a given available power P_i the maximum input gap voltage V_1 at resonance is obtained for a certain optimum value of $Q_{ext,1}$ which can be determined from Eq (3.81) by differentiation. It should be noticed that resonance is defined as the frequency at which the imaginary part of the self-admittance $Y_{1,1}$, rather than the imaginary part of the circuit admittance $Y_{c,1}$ alone, is zero. Using Eqs (3.6) and (3.9) we find the optimum condition

$$\left(\frac{Q_{L,1}}{Q_{ext,1}}\right)_{opt} = \frac{1}{2}\,\frac{R_{sh,1}}{Q_1}\,Q_{L,1}\,G_{1,1} = \frac{1}{2}\left(1 + \frac{G_{e,1}}{G_{c,1}}\right) \tag{3.82}$$

where $G_{1,1}$ is the real part of $Y_{1,1}$; $G_{e,1}$ as before is the electronic conductance; and $G_{c,1}$ is the loaded circuit conductance $Q_1/(R_{sh,1}\,Q_{L,1})$. An alternative way of writing the optimum input condition (3.82) is the following:

$$\frac{1}{R_{sh,1}} + G_{e,1} = \frac{Q_1}{R_{sh,1}}\,\frac{1}{Q_{ext,1}} \tag{3.83}$$

which is easily interpreted as meaning that the sum of the unloaded circuit conductance and the electronic conductance must equal the transformed external conductance, i e the generator conductance. This, of course, means that the generator is matched to the cavity and the beam. We can easily convince ourselves that if the optimum condition (3.82) is fulfilled, the input admittance y_1 given by Eq (3.78) is equal to unity, and all the available power P_i of the generator is therefore transmitted to the cavity and the beam.

If the beam loading is zero, the optimum condition simply is $Q_{L,1}/Q_{ext,1} = \frac{1}{2}$. This situation is normally referred to as critical coupling. In this case the two space-charge waves are excited with equal amplitudes, and the net power required for their excitation is zero. Seen from the generator, the cavity behaves as if the beam were not present.

With positive beam loading the amplitude of the fast space-charge wave exceeds that of the slow wave, and a net positive power is required for their excitation. Therefore, optimum power transfer occurs at a coupling stronger than the critical coupling, $Q_{L,1}/Q_{ext,1} > \frac{1}{2}$. Conversely, if the input gap has negative beam loading, the amplitude of the slow space-charge wave exceeds that of the fast wave, and a net positive power is extracted from the beam. The optimum input condition is obtained for weaker coupling, $Q_{L,1}/Q_{ext,1} < \frac{1}{2}$.

With optimum coupling Eq (3.81), relating the available power P_i and the RF gap voltage V_1, reduces to

$$P_i = \frac{1}{4}\,V_1 V_1^*\,\frac{Y_{1,1}\,Y_{1,1}^*}{G_{1,1}} \tag{3.84}$$

It is interesting to study what happens if by some means the beam loading is made larger, but otherwise the cavity parameters $R_{sh,1}/Q_1$ and Q_1 are kept constant. In order to maintain the optimum condition given by Eq (3.83), the transformed generator conductance must be correspondingly increased through reduction of the external Q, by making the coupling between input transmission line and cavity stronger. If the beam loading becomes sufficiently large, the optimum external Q will be approximately equal to the loaded Q, meaning that the larger part of the overall cavity loading is due to external loading and beam loading, both being approximately equal in magnitude. In this limiting case for which

$Q_{ext,1} \approx Q_{L,1} \ll Q_1$, a negligible amount of the available power P_i is dissipated in the input cavity itself. The main part of P_i is transferred to the electron beam and propagates in the forward direction in the form of an excess modulation of the fast space-charge wave relative to the slow wave. This discussion has some relevance to problems encountered in connection with fast-wave cavity couplers for beam parmetric amplifiers (24), as discussed more thoroughly in Chapter 5.

3.11.3 Relation between output power and gap voltage

As already done for the input cavity, we shall next establish a corresponding relation between output gap voltage and output power. It will be assumed that the output transmission line carrying the useful power from the output cavity (cavity no. p) is terminated in a matched external load. This assumption does not in any sense restrict the generality of the results. The power P_L dissipated in the external load is then simply given by

$$P_L = \tfrac{1}{2} V_p V_p^* \frac{Q_p}{R_{sh,p}} \frac{1}{Q_{ext,p}} \tag{3.85}$$

which is the required relation.

The power gain, defined as the ratio of the output power P_L dissipated in the external load and the available power P_i of the signal source, is obtained by division of Eqs (3.85) and (3.81). Recalling that the ratio V_p/V_1 is the voltage gain η_p, we obtain

$$\frac{P_L}{P_i} = 4\eta_p \eta_p^* \frac{Q_p}{R_{sh,p}} \frac{Q_1}{R_{sh,1}} \frac{1}{Q_{ext,1} Q_{ext,p}} \frac{1}{Y_{1,1} Y_{1,1}^*} \tag{3.86}$$

This equation is quite general, holding for arbitrary input and output couplings, and also for large-signal operation, if by η_p is meant the actual large-signal voltage gain. In the present report we are concerned only with the small-signal performance, in which case η_p is given by the formulae derived previously in this chapter.

3.11.4 Optimization of output coupling at small-signal level

The output coupling can be adjusted to maximize the power gain in the same fashion as previously done for the input coupling. Remembering that the voltage gain η_p contains the self-admittance $Y_{p,p}$ of the output cavity as a common denominator (see Eq (3.13)), we obtain the following condition stating the optimum output coupling at resonance and small-signal level:

$$\left(\frac{Q_{L,p}}{Q_{ext,p}} \right)_{opt} = \frac{1}{2} \frac{R_{sh,p}}{Q_p} Q_{L,p} G_{p,p} = \frac{1}{2} \left(1 + \frac{G_{e,p}}{G_{c,p}} \right) \tag{3.87}$$

It is significant that the optimum small-signal output coupling is identical with the optimum input coupling given by Eq (3.82).

If the external Q's of both input and output cavities are adjusted to their optimum small-signal values according to Eqs (3.82) and (3.87), we find from Eq (3.86) that the corresponding maximum small-signal power gain is given by

$$\frac{P_L}{P_i} = \eta_p \eta_p^* \frac{G_{1,1} G_{p,p}}{Y_{1,1} Y_{1,1}^*} \tag{3.88}$$

At resonance this equation simplifies to

$$\frac{P_L}{P_i} = \eta_p \eta_p^* \frac{G_{p,p}}{G_{1,1}} \tag{3.89}$$

Hence, for optimized input and output couplings at small-signal level, the power gain is equal to the square of the voltage gain if the input and output cavities are identical ($G_{1,1} = G_{p,p}$). High-efficiency operation of practical tubes at large-signal level requires stronger output coupling than that indicated by Eq (3.87). In this case the power gain is given by the general Eq (3.86) rather than Eq (3.88).

3.12 Bandwidth considerations

Simple expressions for the bandwidth of a multi-cavity klystron cannot be given even for the simple case that all the cavities are identical and synchronously tuned. This difficulty is due to the complicating effect of interaction terms between non-adjacent cavities. A rough idea of the expected bandwidth can be obtained by considering a special case for which the interaction terms between non-adjacent cavities can be disregarded, namely a klystron having large gain per stage compared to the number of cavities. In this case the cascade gain approximation (3.29) holds. If for simplicity the assumption is made that all the cavities including the input and output cavities are identical, the small-signal power gain is obtained from Eq (3.88), yielding

$$\frac{P_L}{P_i} = \left(\eta_{2,1} \eta_{2,1}^*\right)^{p-1} \frac{G_{1,1} G_{p,p}}{Y_{1,1} Y_{1,1}^*} \tag{3.90}$$

where the voltage gain per stage $\eta_{2,1}$ is given by Eq (3.12)

$$\eta_{2,1} = -\frac{Y_{2,1}}{Y_{2,2}} \tag{3.91}$$

Since, by our assumption, $Y_{1,1} = Y_{2,2} = \cdots Y_{p,p}$, Eq (3.90) reduces to

$$\frac{P_L}{P_i} = (Y_{2,1} Y_{2,1}^*)^{p-1} \frac{G_{1,1}^2}{(Y_{1,1} Y_{1,1}^*)^p} \tag{3.9}$$

In this expression the only quantity changing rapidly with frequency is the self-admittance $Y_{1,1}$. Therefore, the frequencies for which the power gain is reduced to half its value at resonance are given by the relation

$$\left(\frac{Y_{1,1}\, Y^{*}_{1,1}}{G^{2}_{1,1}} \right)^{p} = 2 \tag{3.93}$$

Neglecting the slow variation of the beam loading admittance with frequency, we obtain the following expression for the relative bandwidth (subscripts are omitted):

$$\frac{\Delta\omega}{\omega_o} = \delta_1 - \delta_2 = \left(1 + \frac{R_{sh}}{Q}\, Q_L\, G_e \right) \frac{1}{Q_L} \left(2^{1/p} - 1 \right)^{\frac{1}{2}} \tag{3.94}$$

If the number of cavities exceeds two, the following approximation holds to within three per cent:

$$2^{1/p} = e^{(1/p)\log 2} \approx 1 + \frac{1}{p} \log 2 \tag{3.95}$$

We shall also define an <u>electronic Q</u> by the relation

$$\frac{1}{Q_e} = \frac{R_{sh}}{Q}\, G_e \tag{3.96}$$

Substitution of Eqs (3.95) and (3.96) in Eq (3.94) yields

$$\frac{\Delta\omega}{\omega_o} \approx \frac{0.83}{p^{\frac{1}{2}}} \left(\frac{1}{Q_L} + \frac{1}{Q_e} \right) = \frac{0,83}{p^{\frac{1}{2}} Q_L} \left(1 + \frac{Q_L}{Q_e} \right) \tag{3.97}$$

Thus the relative bandwidth is inversely proportional to the <u>total loaded Q</u> (including the electronic Q) and the square root of the number of cavities. The effect of positive beam loading is to <u>increase</u> the bandwidth, of negative beam loading to <u>decrease</u> the bandwidth. The modified bandwidth due to beam loading is accompanied by a corresponding change in the power gain in the opposite direction. This is easily observed from Eq (3.92), which at resonance can be written

$$\frac{P_L}{P_i} = \left(Y_{2,1}\, Y^{*}_{2,1} \right)^{p-1} \left[\frac{(R_{sh}/Q) Q_L}{1 + Q_L/Q_e} \right]^{2(p-1)} \tag{3.98}$$

Hence, if the bandwidth is increased by a certain factor due to positive beam loading, the power gain per stage becomes smaller by the square of this factor, and vice versa. These phenomena obviously are caused by regenerative effects in the individual cavities. The bandwidth becomes vanishingly small and the gain extremely high in the limiting case for which the beam loading is negative and its magnitude sufficiently large to cause the klystron to operate just below the start of oscillations. This situation occurs when the sum of the electronic Q and the loaded Q approaches zero.

Since the beam loading and therefore the electronic Q are functions of the DC beam velocity, gain and bandwidth of a klystron with appreciable beam loading will be a function of the DC beam voltage. The above discussion shows that the gain and bandwidth are expected to vary in opposite directions as the beam voltage is varied.

In the theory of cascaded band-pass amplifiers it is convenient to define a gain-bandwidth factor GB as the product of the relative bandwidth and the square root of the power gain per stage

$$GB = \frac{\Delta\omega}{\omega_o}\left(\frac{P_L}{P_i}\right)^{\frac{1}{2(p-1)}} \qquad (3.99)$$

In the cascade approximation of multi-cavity klystron gain discussed here, the gain-bandwidth factor is readily evaluated from Eqs (3.97) and (3.98). We find

$$GB = \frac{0.83}{p^{\frac{1}{2}}}\,\frac{R_{sh}}{Q}\,\left|Y_{2,1}\right| \qquad (3.100)$$

which shows explicitly that the factors containing the beam loading or the electronic Q have cancelled out, rendering the gain-bandwidth factor substantially constant and independent of regenerative effects. It should not be implied, however, that the gain-bandwidth factor is entirely independent of beam loading, because the transfer admittance $Y_{2,1}$ contains a term proportional to the beam loading (see for instance Eq (B.9), Appendix B). As discussed previously, this term is due to the small density modulation taking place in the gaps in addition to the velocity modulation.

3.13 General rules for scaling of the frequency band at constant gain

The expressions for bandwidth derived in the previous section are approximate because interactions between non-adjacent gaps are neglected. A discussion of bandwidth for synchronous tuning, taking full account of these terms, is rather difficult, and even more so for the general case of klystrons with arbitrary, stagger-tuned cavities. We shall refrain from a discussion of the rather involved problems encountered in the analysis and synthesis of frequency response functions with stagger-tuned cavities. Instead, we shall confine our attention to the discussion of a particular problem which is solvable, namely that of scaling the frequency band at constant small-signal power gain.

Using the general gain formulae (3.86) and (3.11), we find that the power gain vs frequency depends on a number of parameters or parameter combinations, listed as follows:

Input cavity (s=1) :

$$M_1^+ , \quad M_1^- , \quad \left(\frac{R_{sh,1}}{Q_1} Q_{ext,1} \right) , \left(\frac{R_{sh,1}}{Q_1} \frac{Q_{L,1}}{W} \right) , \quad (Q_{L,1}\, \delta_1)$$

Intermediate cavities (s=2, 3, ----- p-1) :

$$M_s^+ , \quad M_s^- , \quad \left(\frac{R_{sh,s}}{Q_s} \frac{Q_{L,s}}{W} \right) , \quad (Q_{L,s}\, \delta_s) \tag{3.101}$$

Output cavity (s=p) :

$$M_p^+ , \quad M_p^- , \quad \left(\frac{R_{sh,p}}{Q_p} Q_{ext,p} \right) , \left(\frac{R_{sh,p}}{Q_p} \frac{Q_{L,p}}{W} \right) , \quad (Q_{L,p}\, \delta_p)$$

Note that these expressions include the effect of beam loading through the coupling coefficients M^+ and M^-. The gain obviously stays constant if all the M-parameters and the products inside the parentheses are kept constant. Within the limitation indicated by this requirement the parameters can be scaled. We shall show that the frequency response curve at constant gain is scaled by a factor k in bandwidth provided all the loaded Q's are scaled in the ratios $1/k$, all the characteristic impedances R_{sh}/Q in the ratio k, and the stagger-tuning pattern scaled as described below. If the scaled parameter values are indicated by primes, we obtain, using for each cavity the condition $Q_L \delta$ = constant

$$\frac{Q_{L,1}}{Q'_{L,1}} = \frac{Q_{L,2}}{Q'_{L,2}} = \text{---} = \frac{Q_{L,p}}{Q'_{L,p}} = \frac{\delta'_1}{\delta_1} = \frac{\delta'_2}{\delta_2} = \text{---} \frac{\delta'_p}{\delta_p} = k \tag{3.102}$$

Within the accuracy of the approximate expression for δ given in Eq (3.3) we obtain from Eq (3.102)

$$\frac{\omega' - \omega'_{0,1}}{\omega - \omega_{0,1}} = \frac{\omega - \omega'_{0,2}}{\omega - \omega_{0,2}} = \text{----} = \frac{\omega' - \omega'_{0,p}}{\omega - \omega_{0,p}} = k \tag{3.103}$$

where $\omega_{0,1}$, $\omega_{0,2}$, --- $\omega_{0,p}$ are the original resonant frequencies, and $\omega'_{0,1}$, $\omega'_{0,2}$, --- $\omega'_{0,p}$ are the scaled resonant frequencies. By successive subtractions of both numerators and denominators in the various fractions of Eq (3.103), the frequencies ω and ω' cancel, and we obtain the new, scaled stagger-tuning pattern expressed in terms of the new resonant frequency of the first cavity and the original resonant frequencies.

$$\frac{\omega'_{0,2} - \omega'_{0,1}}{\omega_{0,2} - \omega_{0,1}} = \frac{\omega'_{0,3} - \omega'_{0,1}}{\omega_{0,3} - \omega_{0,1}} = \text{-----} = \frac{\omega'_{0,p} - \omega'_{0,1}}{\omega_{0,p} - \omega_{0,1}} = k \tag{3.104}$$

The new frequency ω' is related to the original frequency ω by

$$\omega' - \omega'_{0,1} = k(\omega - \omega_{0,1}) \tag{3.105}$$

showing that the frequency band is increased by the factor k. It should be noted that the scaling rules still hold if the location of the new response curve is shifted in the frequency band relative to the original one.

Furthermore, since from (3.101) the product $(R_{sh}/Q)(Q_L/W)$ must be constant for each cavity, the scaled values are given by

$$\frac{(R_{sh,1}/Q_1 W)'}{R_{sh,1}/Q_1 W} = \text{-----} = \frac{(R_{sh,p}/Q_p W)'}{R_{sh,p}/Q_p W} = k \tag{3.106}$$

This means that the product of the characteristic impedance R_{sh}/Q and the inverse RF beam impedance $1/W$ must be scaled in the ratio k.

The scaling discussed here further requires that the coupling coefficients M^- and M^+ of the two space-charge waves are maintained at their original values in each gap.

$$\begin{aligned} M_s^{-\prime} &= M_s^- \\ M_s^{+\prime} &= M_s^+ \end{aligned} \qquad s = 1, 2 \text{ ---}, p \tag{3.107}$$

Provided the RF field distribution in each cavity is maintained, the requirements stated in Eq (3.107) imply that the propagation factors β_q and β_e remain the same (see Eq (2.58)). This again imposes a slight restriction on the possible scaling of the RF beam impedance W, defined in Eq (2.30), since the scaling must be done without affecting the propagation factors.

The requirements expressed in Eqs (3.106) and (3.107) are equivalent to having a constant ratio between the cavity admittance and the electronic admittance or the transfer admittance.

It is noticed from (3.101) that two additional requirements must be fulfilled, namely the scaling of external Q's at the input and output cavities. These requirements are rather trivial, however, because no frequency dependent quantities are involved.

The above discussion shows that if the stagger-tuning pattern of a given klystron is already optimized with respect to gain and bandwidth, a further increase in bandwidth at constant gain can only be obtained through:

a) Higher characteristic impedances R_{sh}/Q of the cavities

b) Lower characteristic beam impedance W

These results demonstrate quite clearly the significance of the characteristic impedances of the cavities and the beam in multi-cavity klystron theory and design. In this connection it should be pointed out that the characteristic impedance R_{sh}/Q generally increases with the interaction length. For example R_{sh}/Q of a shorted slow-wave structure having sinusoidal RF field distribution is proportional to the number of standing waves, while the coupling coefficients are substantially independent of this number. Therefore, the use of such structures offers definite possibilities of marked improvement in bandwidth over that obtained with conventional narrow-gap klystrons (9).

The scaling problem discussed above, characterized by constant gain and scaled frequency band, seems to be the only one that can be discussed in simple terms. If we ask what happens if the loaded Q's, or the characteristic impedances are scaled independently, no simple answers can be given to these questions, except for special cases in which interaction between non-adjacent gaps and the beam loading can be disregarded. The difficulties encountered in such a discussion are due to the fact that the relative contributions to the gain from the various terms in the general formula (3.11) depend on the loaded Q's and the (R_{sh}/Q)'s in a rather complicated manner. Thus, the following general statement can be made:- In a multi-cavity klystron, separate scaling of all the loaded Q's, or of all the characteristic impedances R_{sh}/Q, does not result in a simple scaling of bandwidth or gain, except in the case discussed above for which the scalings of the parameters are interconnected in the way prescribed by Eqs (3.102) through (3.107). Although not done here, it may be shown that this same conclusion can be drawn from a treatment of the same scaling problem in terms of poles and zeros of the gain function in the complex frequency plane.

To conclude the discussion of bandwidth, we shall emphasize the unique role played by the input and output cavities relative to the intermediate floating cavities. This difference is quite clear already from the pole-zero description of the response function (22, 23). Each of the p cavities contributes to one of the p poles in the complex frequency plane, while the p-2 zeros depend only on the p-2 intermediate cavities, and not on the input and output cavities. In our formulation this point manifests itself by the fact that the self-admittances $Y_{1,1}$ and $Y_{p,p}$ of the input and output cavities are common factors in the denominators of all the 2^{p-2} cascade terms (3.17) adding up to the overall gain (see Eqs (3.18) and (3.86)), and thus can be brought outside as multiplicative factors.

On the other hand, each of the self-admittances $Y_{2,2}$ --- $Y_{p-1,p-1}$ of the intermediate cavities is found only in 2^{p-3} of the total of 2^{p-2} cascade terms (3.17), i e in exactly half the total number of terms. Thus, it appears plausible that the frequency response will depend more strongly on the loaded Q's of the input and output cavities than on the loaded Q's of the intermediate, floating cavities. The practical consequence of this fact is that the required bandwidths of the input and output cavities should be of the same order as the desired frequency band of the multi-cavity klystron, while no such restrictions on the bandwidths of the intermediate cavities are necessary. In practice, therefore, the frequency responses

of the input and output cavities should be sufficiently broad to be considered as constant. The actual frequency response of the entire klystron amplifier will then be determined mainly by the general voltage gain function (3.11), i e by the parameters of the intermediate floating cavities and the details of their stagger-tuning.

3.14 Reciprocity theorems for multi-cavity klystrons and interaction gaps with distributed interaction

In this section some very important reciprocity theorems will be proved, pertaining to general, extended interaction gaps and multi-cavity klystrons using cavities with such gaps. The theorems are concerned with the reciprocity relations for reversed direction of electron flow through the gaps. We shall show that by reversing the electron flow, the following theorems hold:

a) For any gap s the coupling coefficients M_s^+ and M_s^- of the slow and the fast space-charge waves transfer to their complex conjugates M_s^{+*} and M_s^{-*}.

b) For any gap s the electronic admittance $Y_{e,s}$ and the self-admittance $Y_{s,s}$ are invariant with respect to reversed flow.

c) The transfer admittance $Y_{r,s}$ between any two gaps s and r is invariant with respect to reversed flow, i e $Y_{r,s} = Y_{s,r}$.

d) For any arbitrarily stagger-tuned multi-cavity klystron with arbitrary, extended interaction gaps the power gain over the entire frequency band remains the same if the beam is reversed and the roles of the input and output transmission lines are interchanged such that in the new configuration the electromotive force of the generator appears in series with the original output load, and the original generator impedance serves as the new output load.

As a corollary to theorem d), we have the following theorem:

e) Assume that the cavities with their gaps are arranged symmetrically with respect to the plane half way between the input and the output gap. Then, for each stagger-tuning pattern characterized by the resonant frequencies $\omega_1, \omega_2, \omega_3 \cdots \omega_p$, there exists a second, different stagger-tuning pattern having exactly the same power gain vs frequency. The second pattern is obtained from the first by reversing the order of tuning, i e the new resonant frequencies are $\omega_p, \omega_{p-1}, \cdots \omega_1$.

3.14.1 Reciprocity relation for the coupling coefficient

The coupling coefficients M^- and M^+ are given by Eq (2.58)

$$\left.\begin{matrix} M^+ \\ M^- \end{matrix}\right\} = \int_{-\ell/2}^{\ell/2} F(x)\, e^{j(\beta_e \mp \beta_q)x}\, dx \qquad (3.108)$$

where $F(x)$ is the normalized longitudinal RF field distribution in the gap. If primed quantities refer to the situation with reversed electron flow, we have from Fig 3.9

$$F'(x) = F(-x) \qquad (3.109)$$

therefore

$$\left.\begin{matrix}(M^+)'\\(M^-)'\end{matrix}\right\} = \int_{-\ell/2}^{\ell/2} F'(x)\, e^{j(\beta_e \mp \beta_q)x}\, dx = \int_{-\ell/2}^{\ell/2} F(-x)\, e^{j(\beta_e \mp \beta_q)x}\, dx \qquad (3.110)$$

Changing sign of the integration variable x, we obtain

$$\left.\begin{matrix}(M^+)'\\(M^-)'\end{matrix}\right\} = \int_{-\ell/2}^{\ell/2} F(x)\, e^{-j(\beta_e \mp \beta_q)x}\, dx = \begin{cases} M^{+*} \\ M^{-*} \end{cases} \qquad (3.111)$$

which proves theorem a).

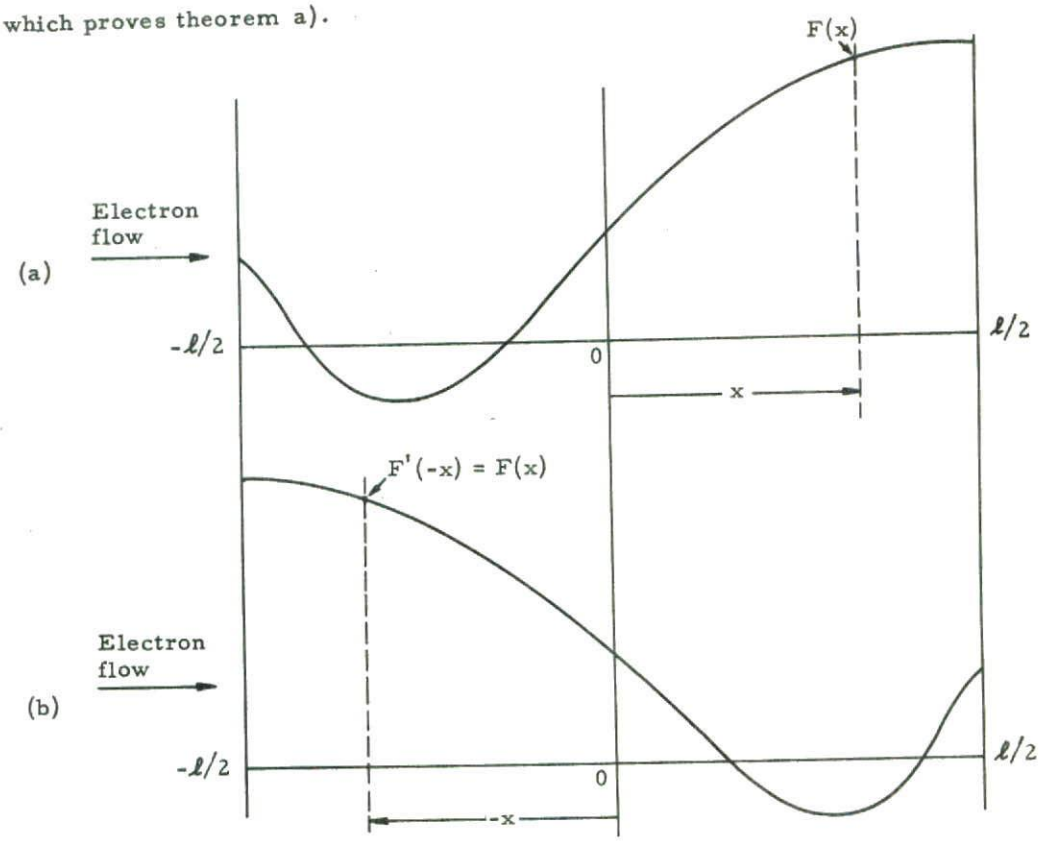

Fig 3.9 Longitudinal RF field distributions

(a) Example of RF field distribution of a gap with electron flow in original direction

(b) RF field distribution of the same gap with electron flow reversed

3.14.2 Reciprocity relation for the electronic admittance

The electronic admittance Y_e of a gap is given by Eq (2.68). Since a cavity interaction gap is characterized by real values of F(x), we have

$$Y_e = -\frac{1}{W}\,\Delta \int_{-\ell/2}^{\ell/2} F(x)\, e^{-j\beta_e x} \int_{-\ell/2}^{x} F(y)\, e^{j\beta_e y}\, dy\, dx \qquad (3.112)$$

where Δ is the difference operator defined in Eq (2.38). For the reversed beam we find, using Eq (3.109)

$$Y'_e = -\frac{1}{W}\Delta \int_{-\ell/2}^{\ell/2} F(-x)\, e^{-j\beta_e x} \int_{-\ell/2}^{x} F(-y)\, e^{j\beta_e y}\, dy\, dx$$

Changing signs of the integration variables x and y, we obtain

$$Y'_e = +\frac{1}{W}\Delta \int_{-\ell/2}^{\ell/2} F(x)\, e^{j\beta_e x} \int_{\ell/2}^{x} F(y)\, e^{-j\beta_e y}\, dy\, dx$$

Partial integration transforms the double integral to

$$Y'_e = -\frac{1}{W}\Delta \int_{-\ell/2}^{\ell/2} F(x)\, e^{-j\beta_e x} \int_{-\ell/2}^{x} F(y)\, e^{j\beta_e y}\, dy\, dx = Y_e \qquad (3.113)$$

which proves theorem b).

Since the circuit admittance Y_c obviously is independent of the direction of electron flow, it is hereby also proved that the self-admittance $Y_{s,s}$ for any cavity s is invariant with respect to reversed flow.

$$Y'_{s,s} = Y'_{e,s} + Y'_{c,s} = Y_{s,s} \qquad (3.114)$$

3.14.3 Reciprocity relation for the transfer admittance

The transfer admittance $Y_{s,r}$ <u>from gap r to gap s</u>, $(r < s)$ is given by Eq (2.67)

$$Y_{s,r} = -\frac{1}{W}\Delta\left(M_r M_s^* e^{-j\beta_e \ell_{s,r}}\right) \qquad (3.115)$$

Evidently, with reversed flow, the transfer admittance $Y'_{r,s}$ <u>from gap s to gap r</u> is given by

$$Y'_{r,s} = -\frac{1}{W}\Delta\left(M'_s M'^*_r e^{-j\beta_e \ell_{r,s}}\right)$$

Since $\ell_{s,r}$ is equal to $\ell_{r,s}$, and the primed coupling coefficients satisfy theorem a) stated in Eq (3.111), we obtain

$$Y'_{r,s} = -\frac{1}{W}\Delta\left(M_r M_s^* e^{-j\beta_e \ell_{s,r}}\right) = Y_{s,r} \qquad (3.116)$$

which proves theorem c).

3.14.4 Reciprocity relation for the power gain

The proof of this apparently important theorem is based on theorems a), b) and c) already proved. Let us first consider the voltage gain η_p of a p-cavity klystron, which from Eqs (3.11) and (3.12) can be written as the following determinant:

$$\eta_p = \frac{(-1)^{p-1}}{Y_{2,2}Y_{3,3}\cdots Y_{p,p}} \begin{vmatrix} Y_{2,1} & Y_{2,2} & 0 & 0 & \cdots & 0 \\ Y_{3,1} & Y_{3,2} & Y_{3,3} & 0 & \cdots & 0 \\ \vdots & \vdots & & & & \vdots \\ Y_{p-1,1} & Y_{p-1,2} & \cdots & Y_{p-1,p-2} & Y_{p-1,p-1} & \\ Y_{p,1} & Y_{p,2} & \cdots & Y_{p,p-2} & Y_{p,p-1} & \end{vmatrix} \qquad (3.117)$$

If the direction of electron flow is reversed and the cavity resonant frequencies maintained at their original values, the new voltage gain η_p' can be evaluated from the same general equation. The original gap indices are retained, i e the new input gap has the index p, the second gap index (p-1), etc. We find

$$\eta_p' = \frac{(-1)^{p-1}}{Y_{1,1}Y_{2,2}\cdots Y_{p-1,p-1}} \begin{vmatrix} Y'_{p-1,p} & Y'_{p-1,p-1} & 0 & 0 & \cdots & 0 \\ Y'_{p-2,p} & Y'_{p-2,p-1} & Y'_{p-2,p-2} & 0 & \cdots & 0 \\ \vdots & \vdots & & & & \vdots \\ Y'_{2,p} & Y'_{2,p-1} & \cdots & Y'_{2,3} & Y'_{2,2} & \\ Y'_{1,p} & Y'_{1,p-1} & \cdots & Y'_{1,3} & Y'_{1,2} & \end{vmatrix} \qquad (3.118)$$

The next step is to show that the determinants appearing in Eqs (3.117) and (3.118) are identical. This result follows very simply using theorem c) on all the transfer admittances in one of the determinants, and then interchanging rows and columns. Therefore, the ratio between the voltage gains η_p' and η_p for the reversed and original directions of flow is given by

$$\frac{\eta_p'}{\eta_p} = \frac{Y_{p,p}}{Y_{1,1}} \qquad (3.119)$$

The equation shows that the voltage gains are the same in the two cases except for a trivial impedance transformation equal to the ratio between the self-admittances of the output and input cavities.

We shall prove next that the power gain with reversed flow is exactly the same as the power gain for the original direction of flow. The proof follows very simply from Eq (3.86), which is valid for arbitrary input and output loads. For the original direction we have

$$\frac{P_L}{P_i} = 4\eta_p \eta_p^* \frac{Q_p}{R_{sh,p}} \frac{Q_1}{R_{sh,1}} \frac{1}{Q_{ext,1} Q_{ext,p}} \frac{1}{Y_{1,1} Y_{1,1}^*} \tag{3.120}$$

With reversed beam and input and output interchanged, we obtain from the same formula

$$\left(\frac{P_L}{P_i}\right)' = 4\eta_p' \eta_p^{*'} \frac{Q_1}{R_{sh,1}} \frac{Q_p}{R_{sh,p}} \frac{1}{Q_{ext,p} Q_{ext,1}} \frac{1}{Y_{p,p} Y_{p,p}^*} \tag{3.121}$$

On account of Eq (3.119), the following identity obviously holds:

$$\left(\frac{P_L}{P_i}\right)' = \frac{P_L}{P_i} \tag{3.122}$$

which proves theorem d).

Theorem e) follows immediately as a corollary to theorem d). By symmetric arrangement of cavities with respect to the center cavity, it is quite evident that the klystron with reversed beam and the cavities maintained at the original resonant frequencies is equivalent to the original klystron with cavities tuned in the reversed order.

As an example, this theorem shows that a stagger-tuning pattern in which the first cavities are tuned to lower frequencies and the subsequent cavities to higher frequencies, results in exactly the same power gain and frequency response as the reversed tuning pattern in which the first cavities are tuned to the higher frequencies and the subsequent cavities to the lower frequencies. It should be borne in mind, however, that all the theorems a) to e) hold under small-signal conditions only. For efficiency reasons one would in practice prefer the pattern in which the next to last cavity is tuned to a relatively high frequency, since this in general enhances the large-signal bunching and thus the efficiency.

4 MULTI-CAVITY KLYSTRON THEORY FORMULATED IN TERMS OF MATRICES ASSOCIATED WITH CAVITY GROUPS

4.1 Introduction

The present chapter is concerned with a further generalization of klystron theory based on a reformulation of the results of Chapter 3, expressing these by means of appropriately defined matrix parameters associated with groups of consecutive cavities rather than by scalar parameters associated with single cavities. We shall find that this approach leads to a theory describing klystron performance in terms of matrix relations which are formally identical to the scalar relations derived in Chapter 3, which can be obtained as a special case of the more general theory of this chapter.

The matrix formulation is particularly powerful for solving certain types of problems arising in connection with several klystrons coupled in cascade with common beam, such as evaluation of the overall gain of two or more cascaded klystrons, or of periodically stagger-tuned klystrons, and other related problems.

4.2 General matrix formulation

In the present analysis it is slightly more convenient operating with RF gap voltages, rather than normalizing these with respect to the input gap voltage V_1 as was done in the analysis in Chapter 3 (Eqs (3.5) through (3.18)). The analysis will be based on the set (3.4) of p-1 linear equations in the p RF gap voltages V_1, V_2, --- V_p. The additional equation required to make the set complete is furnished by Eq (3.81) relating the input gap voltage V_1 and the input power P_i.

$$P_i = \frac{1}{8} V_1 V_1^* \frac{R_{sh,1}}{Q_1} Q_{ext,1} Y_{1,1} Y_{1,1}^* \tag{4.1}$$

Let us define a complex quantity a, whose absolute value squared is proportional to the input power P_i.

$$aa^* = 8 \frac{P_i}{Q_{ext,1}} \frac{Q_1}{R_{sh,1}} \tag{4.2}$$

Equation (3.4) together with (4.1) form the following complete set of linear equations:

$$\begin{aligned}
&Y_{1,1} V_1 = a \\
&Y_{2,1} V_1 + Y_{2,2} V_2 = 0 \\
&Y_{3,1} V_1 + Y_{3,2} V_2 + Y_{3,3} V_3 = 0 \\
&\text{----------} \\
&Y_{p,1} V_1 + Y_{p,2} V_2 + \text{---} + Y_{p,p} V_p = 0
\end{aligned} \tag{4.3}$$

In matrix form this set of equations can be expressed as

$$\underset{\sim}{Y}\,\underset{\sim}{V} = \underset{\sim}{A} \tag{4.4}$$

where the triangular admittance matrix $\underset{\sim}{Y}$ of order p is given by

$$\underset{\sim}{Y} = \begin{bmatrix} Y_{1,1} & 0 & 0 & 0 \text{ -------- } 0 \\ Y_{2,1} & Y_{2,2} & 0 & 0 \text{ -------- } 0 \\ Y_{3,1} & Y_{3,2} & Y_{3,3} & 0 \text{ -------- } 0 \\ & & & \\ \text{----------} & & & \\ & & & \\ Y_{p,1} & Y_{p,2} & Y_{p,3} \text{ --- } Y_{p,p-1} & Y_{p,p} \end{bmatrix} \tag{4.5}$$

The voltage matrix $\underset{\sim}{V}$ and the excitation matrix $\underset{\sim}{A}$ in Eq (4.4) are column vectors given by

$$\underset{\sim}{V} = \begin{bmatrix} V_1 \\ V_2 \\ \cdot \\ \cdot \\ \cdot \\ \cdot \\ V_p \end{bmatrix} \tag{4.6}$$

$$\underset{\sim}{A} = \begin{bmatrix} a \\ 0 \\ \cdot \\ \cdot \\ \cdot \\ \cdot \\ 0 \end{bmatrix} \tag{4.7}$$

Under the assumption that the admittance matrix $\underset{\sim}{Y}$ is non-singular (Det $\underset{\sim}{Y} \neq 0$, satisfying the stability criterion (3.27)), the solution of Eq (4.4) is

$$\underset{\sim}{V} = \underset{\sim}{Y}^{-1}\,\underset{\sim}{A} = \frac{\hat{\underset{\sim}{Y}}}{\text{Det } \underset{\sim}{Y}}\,\underset{\sim}{A} \tag{4.8}$$

where $\hat{\underset{\sim}{Y}}$ is the adjoint matrix. Solving with respect to the output gap voltage V_p, we find

$$V_p = \begin{vmatrix} 1 & 0 & 0 \text{ ---------- } & V_1 \\ -\eta_{2,1} & 1 & 0 \text{ ---------- } & 0 \\ -\eta_{3,1} & -\eta_{3,2} & 1 \text{ ---------- } & 0 \\ \text{----------} & & 1 & 0 \\ -\eta_{p,1} & -\eta_{p,2} \text{ ---------- } & -\eta_{p,p-1} & 0 \end{vmatrix} \tag{4.9}$$

where $\eta_{s,r}$ is given by Eq (3.12). If V_p is divided by $V_1 = a/Y_{1,1}$, Eq (4.9)

reduces properly to Eq (3.11) as required. After these introductory remarks we shall turn to the problem stated in the introduction to this chapter, namely that of lumping consecutive cavities together in groups and considering the composite set of gaps belonging to each group as one interaction region, as indicated in Fig 4.1. As before, we shall use small letters for indices referring to the sequence of cavities: 1, 2, 3, --- s, ---(p-1), p, and capital letters for indices referring to the sequence of cavity groups: 1, 2, 3, --- S, --- P.

The decomposition into cavity groups is done by observing that the triangular admittance matrix $\underset{\sim}{Y}$ given by Eq (4.5) can be partitioned into a number of sub-matrices using the procedure indicated in Fig 4.2. Here, the sub-matrices along the diagonal are all triangular matrices of orders corresponding to the number of cavities lumped together in the particular groups associated with the sub-matrices.

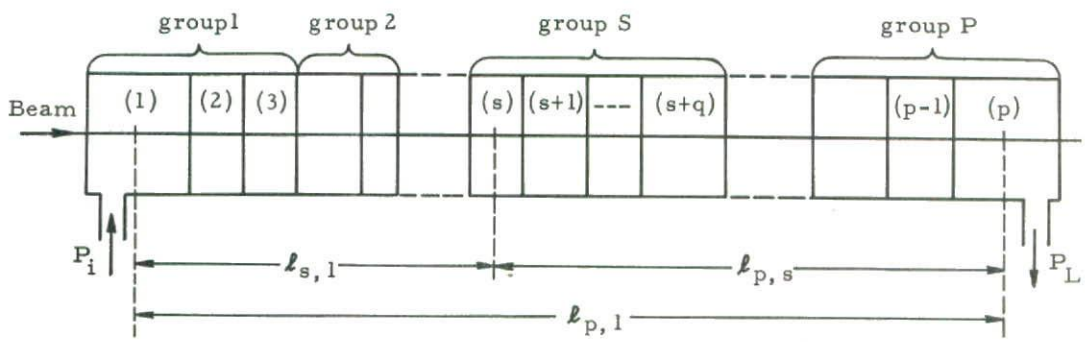

Fig 4.1 Schematic drawing indicating the procedure followed in lumping cavities together in groups

$$\underset{\sim}{Y} = \begin{bmatrix} \underset{\sim}{Y}_{1,1} & \underset{\sim}{0} & \cdots & \underset{\sim}{0} & \cdots & \underset{\sim}{0} & \cdots & \underset{\sim}{0} \\ \underset{\sim}{Y}_{2,1} & \underset{\sim}{Y}_{2,2} & \cdots & \underset{\sim}{0} & \cdots & \underset{\sim}{0} & \cdots & \underset{\sim}{0} \\ \vdots & \vdots & & \vdots & & \vdots & & \vdots \\ & & & \underset{\sim}{Y}_{R,R} & \cdots & \underset{\sim}{0} & \cdots & \underset{\sim}{0} \\ & & & \vdots & & \underset{\sim}{0} & \cdots & \underset{\sim}{0} \\ \underset{\sim}{Y}_{S,1} & \underset{\sim}{Y}_{S,2} & \cdots & \underset{\sim}{Y}_{S,R} & \cdots & \underset{\sim}{Y}_{S,S} & \cdots & \underset{\sim}{0} \\ \vdots & \vdots & & \vdots & & \vdots & & \vdots \\ \underset{\sim}{Y}_{P,1} & \underset{\sim}{Y}_{P,2} & \cdots & \underset{\sim}{Y}_{P,R} & \cdots & \underset{\sim}{Y}_{P,S} & \cdots & \underset{\sim}{Y}_{P,P} \end{bmatrix}$$

Fig 4.2 Partitioning of the pth order admittance matrix $\underset{\sim}{Y}$ into a number of sub-matrices of orders less than p

Corresponding partitioning of the voltage vector $\underset{\sim}{V}$ and the excitation vector $\underset{\sim}{A}$ defined by Eqs (4.6) and (4.7), respectively, gives

$$\underset{\sim}{V} = \begin{bmatrix} \underset{\sim}{V}_1 \\ \underset{\sim}{V}_2 \\ \vdots \\ \underset{\sim}{V}_S \\ \vdots \\ \underset{\sim}{V}_P \end{bmatrix} \qquad \underset{\sim}{A} = \begin{bmatrix} \underset{\sim}{A}_1 \\ \underset{\sim}{0} \\ \vdots \\ \underset{\sim}{0} \end{bmatrix} \tag{4.10}$$

Expressing the matrices $\underset{\sim}{Y}$, $\underset{\sim}{V}$ and $\underset{\sim}{A}$ in terms of their sub-matrices and performing the matrix multiplication (4.4), we obtain the following set of linear matrix equations:

$$\begin{aligned} &\underset{\sim}{Y}_{1,1}\,\underset{\sim}{V}_1 = \underset{\sim}{A}_1 \\ &\underset{\sim}{Y}_{2,1}\,\underset{\sim}{V}_1 + \underset{\sim}{Y}_{2,2}\,\underset{\sim}{V}_2 = 0 \\ &\underset{\sim}{Y}_{3,1}\,\underset{\sim}{V}_1 + \underset{\sim}{Y}_{3,2}\,\underset{\sim}{V}_2 + \underset{\sim}{Y}_{3,3}\,\underset{\sim}{V}_3 = 0 \\ &\text{----------} \\ &\underset{\sim}{Y}_{P,1}\,\underset{\sim}{V}_1 + \underset{\sim}{Y}_{P,2}\,\underset{\sim}{V}_2 + \text{---} + \underset{\sim}{Y}_{P,P}\,\underset{\sim}{V}_P = 0 \end{aligned} \tag{4.11}$$

This set is a generalized form of the set (4.3), to which it reduces if all the matrices are of order unity.

The general solution of Eq (4.11) obviously is identical to the solution (4.9) of Eq (4.3), if the elements in the determinant are replaced by the appropriate matrix elements. Therefore, the voltage vector $\underset{\sim}{V}_P$ of the Pth cavity group is given by the following determinant of matrices:

$$\underset{\sim}{V}_P = \begin{vmatrix} \underset{\sim}{1} & \underset{\sim}{0} & \underset{\sim}{0} \text{----------} & \underset{\sim}{V}_1 \\ -\underset{\sim}{\eta}_{2,1} & \underset{\sim}{1} & \underset{\sim}{0} \text{----------} & \underset{\sim}{0} \\ -\underset{\sim}{\eta}_{3,1} & -\underset{\sim}{\eta}_{3,2} & \underset{\sim}{1} \text{----------} & \underset{\sim}{0} \\ \text{----------} & & \underset{\sim}{1} & \underset{\sim}{0} \\ -\underset{\sim}{\eta}_{P,1} & -\underset{\sim}{\eta}_{P,2} \text{---------} & -\underset{\sim}{\eta}_{P,P-1} & \underset{\sim}{0} \end{vmatrix} \tag{4.12}$$

where the matrix

$$\underset{\sim}{\eta}_{S,R} = -\,\underset{\sim}{Y}^{-1}_{S,S}\,\underset{\sim}{Y}_{S,R} \tag{4.13}$$

represents the cascade gain matrix between group R and group S. This is the generalized form of Eq (3.12) in the single-gap klystron theory. In expanding the matrix determinant (4.12), care must be observed in multiplying the matrices together in the correct order such that terms with highest indices appear first. In analogy with Eq (3.13) we find by expansion

$$\underset{\sim}{V}_P = \sum_{S_1=2}^{P} \sum_{S_2=S_1+1}^{P} \cdots \sum_{\substack{S_{P-2}= \\ S_{P-3}+1}}^{P} \underset{\sim}{\eta}_{P,S_{P-2}} \underset{\sim}{\eta}_{S_{P-2},S_{P-3}} \cdots \underset{\sim}{\eta}_{S_2,S_1} \underset{\sim}{\eta}_{S_1,1} \underset{\sim}{V}_1 \qquad (4.14)$$

As examples, the voltage vectors of the four first groups are given below. The first one follows from Eq (4.8) rather than Eq (4.14).

$$\begin{aligned}
\underset{\sim}{V}_1 &= \underset{\sim}{Y}_{1,1}^{-1} \underset{\sim}{A}_1 \\
\underset{\sim}{V}_2 &= \underset{\sim}{\eta}_{2,1} \underset{\sim}{V}_1 \\
\underset{\sim}{V}_3 &= (\underset{\sim}{\eta}_{3,2} \underset{\sim}{\eta}_{2,1} + \underset{\sim}{\eta}_{3,1}) \underset{\sim}{V}_1 \\
\underset{\sim}{V}_4 &= (\underset{\sim}{\eta}_{4,3} \underset{\sim}{\eta}_{3,2} \underset{\sim}{\eta}_{2,1} + \underset{\sim}{\eta}_{4,3} \underset{\sim}{\eta}_{3,1} + \underset{\sim}{\eta}_{4,2} \underset{\sim}{\eta}_{2,1} + \underset{\sim}{\eta}_{4,1}) \underset{\sim}{V}_1
\end{aligned} \qquad (4.15)$$

This procedure can be continued in an obvious way for P larger than four.

Before proceeding with a further study of the various admittance matrices entering into Eqs (4.13) to (4.15) we shall state the matrix equivalents of the electronic equation (2.71) and the circuit equation (3.1).

4.3 Electronic matrix equation and circuit matrix equation for groups of cavities

4.3.1 The electronic equation

In the matrix formulation the equivalent of the electronic equation (2.71), relating the complex power $\mathcal{P}_p$ extracted by the beam in the pth interaction gap and the RF voltages V_1, V_2, --- V_p of all the preceding gaps, is given by the following expression, which we shall speak of as the electronic equation of group P:

$$\mathcal{P}_P = \frac{1}{2} \sum_{R=1}^{P-1} \tilde{V}_P^* \underset{\sim}{Y}_{P,R} \underset{\sim}{V}_R + \frac{1}{2} \tilde{V}_p^* \underset{\sim}{Y}_{e,P} \underset{\sim}{V}_P \qquad (4.16)$$

where $\tilde{V}_P^*$ is the Hermitian conjugate of $\underset{\sim}{V}_P$. The quantity $\mathcal{P}_P$ is the complex power extracted by the beam in all the interaction gaps belonging to the Pth group.

The last matrix product in Eq (4.16) does not depend on any voltage column vectors other than the vector $\underset{\sim}{V}_P$ of the Pth group itself. The matrix $\underset{\sim}{Y}_{e,P}$, therefore, can be interpreted as the electronic admittance matrix of the Pth group of

gaps. The quantity

$$\mathcal{P}_{e_P} = \tfrac{1}{2} \tilde{\underset{\sim}{V}}^{*}_{P} \underset{\sim}{Y}_{e,P} \underset{\sim}{V}_{P} \qquad , (4.17)$$

represents the complex beam loading power of the Pth group of gaps. By performing the matrix multiplication in Eq (4.17) it is found that $\mathcal{P}_{e,P}$ is the sum of terms proportional to the square of the gap voltages (ordinary beam loading terms of the gaps), and terms proportional to cross-products of gap voltages within the group P (transfer loading terms). In the matrix formulation all these contribute to the overall complex beam loading of the Pth group of gaps.

As shown later, the real and imaginary parts of $\mathcal{P}_{e,P}$ are determined by splitting the matrix $\underset{\sim}{Y}_{e,P}$ into the electronic conductance matrix $\underset{\sim}{G}_{e,P}$ and the electronic susceptance matrix $\underset{\sim}{B}_{e,P}$.

Returning to Eq (4.16), the remaining terms on the right-hand side are transfer terms containing matrix cross-products of voltage vectors $\underset{\sim}{V}_{R}$ and $\underset{\sim}{V}_{P}$. The matrix $\underset{\sim}{Y}_{P,R}$, conveniently referred to as the transfer admittance matrix, will be studied in more detail later.

4.3.2 The circuit equation

In the matrix formulation the equivalent of the circuit equation (3.1) is given by

$$\mathcal{P}_{P} = -\tfrac{1}{2} \tilde{\underset{\sim}{V}}^{*}_{P} \underset{\sim}{Y}_{c,P} \underset{\sim}{V}_{P} \qquad (4.18)$$

where $\mathcal{P}_{P}$ is the complex power extracted by the beam (the same as in Eq (4.16)), and the circuit admittance matrix $\underset{\sim}{Y}_{c,P}$ is a diagonal matrix in which the diagonal elements are the circuit admittances $Y_{c,p}$, $Y_{c,p+1}$, --- of the gaps forming the pth group.

Combination of the electronic equation (4.16) and the circuit equation (4.18) results in the set of matrix equations (4.11), which were already derived directly from Eq (4.4) through partitioning of the admittance matrix $\underset{\sim}{Y}$.

4.4 Definitions of characteristic matrix parameters of cavity groups

The general matrix formulation developed in this chapter is formally similar to the theory of multi-cavity klystrons of Chapter 3 in the sense that the expressions for the gap voltages V_1, V_2, --- V_p (Eq (3.13)) formally are the same as those for the group voltage vectors $\underset{\sim}{V}_1$, $\underset{\sim}{V}_2$, --- $\underset{\sim}{V}_p$ (Eq (4.14)). From the subsequent evaluation of the appropriate matrix parameters of each cavity group it appears that the similarity goes beyond these relations. We shall find that the equations specifying self-admittance, electronic admittance, circuit admittance and transfer admittance in the multi-cavity klystron theory of Chapter 3 all are applicable in generalized form in the present matrix formulation of klystron theory.

4.4.1 Self-admittance matrix

Referring again to Fig 4.2, the Sth group of cavities is represented by the square matrix $\underset{\sim}{Y}_{S,S}$ located on the main diagonal of the $\underset{\sim}{Y}$-matrix. If the Sth group consists of $q+1$ consecutive cavities beginning with the sth cavity, we find from Eq (4.5) that the <u>self-admittance matrix</u> $\underset{\sim}{Y}_{S,S}$ is a triangular matrix given by

$$\underset{\sim}{Y}_{S,S} = \begin{bmatrix} Y_{s,s} & 0 & 0 & \cdots & 0 \\ Y_{s+1,s} & Y_{s+1,s+1} & 0 & \cdots & 0 \\ & & & & \\ Y_{s+q,s} & Y_{s+q,s+1} & \cdots & & Y_{s+q,s+q} \end{bmatrix} \tag{4.19}$$

The diagonal elements are the self-admittances of the cavities constituting the Sth group ; the off-diagonal elements are the transfer admittances between the various gaps of the same group.

4.4.2 Circuit admittance and electronic admittance matrices

Exactly as done in Eq (3.6), the self-admittance matrix $\underset{\sim}{Y}_{S,S}$ can be split into a <u>circuit admittance matrix</u> $\underset{\sim}{Y}_{c,S}$ and an <u>electronic admittance matrix</u> $\underset{\sim}{Y}_{e,S}$

$$\underset{\sim}{Y}_{S,S} = \underset{\sim}{Y}_{c,S} + \underset{\sim}{Y}_{e,S} \tag{4.20}$$

where $\underset{\sim}{Y}_{c,S}$ and $\underset{\sim}{Y}_{e,S}$ are given by

$$\underset{\sim}{Y}_{c,S} = \begin{bmatrix} Y_{c,s} & 0 & \cdots & 0 & 0 \\ 0 & Y_{c,s+1} & \cdots & 0 & 0 \\ & & & & \\ 0 & \cdots & 0 & & Y_{c,s+q} \end{bmatrix} \tag{4.21}$$

and

$$\underset{\sim}{Y}_{e,S} = \begin{bmatrix} Y_{e,s} & 0 & \cdots & 0 \\ Y_{s+1,s} & Y_{e,s+1} & \cdots & 0 \\ & & & \\ Y_{s+q,s} & \cdots & & Y_{e,s+q} \end{bmatrix} \tag{4.22}$$

The elements of the diagonal circuit admittance matrix $\underset{\sim}{Y}_{c,S}$ are the circuit admittances of the q+1 cavities constituting the Sth group. The diagonal elements of the electronic admittance matrix $\underset{\sim}{Y}_{e,s}$ are the electronic admittances of the same cavities; the off-diagonal elements are the transfer admittances between the same cavities.

The electronic admittance matrix $\underset{\sim}{Y}_{e,S}$ can be split further into the electronic conductance matrix $\underset{\sim}{G}_{e,S}$ and the electronic susceptance matrix $\underset{\sim}{B}_{e,S}$ by observing that $\underset{\sim}{Y}_{e,S}$, like any square matrix, can be written as a sum of a Hermitian matrix and a skew Hermitian matrix.

$$\underset{\sim}{Y}_{e,S} = \frac{1}{2}(\underset{\sim}{Y}_{e,S} + \tilde{\underset{\sim}{Y}}^{*}_{e,S}) + \frac{1}{2}(\underset{\sim}{Y}_{e,S} - \tilde{\underset{\sim}{Y}}^{*}_{e,S}) = \underset{\sim}{G}_{e,S} + j\,\underset{\sim}{B}_{e,S} \tag{4.23}$$

where $\tilde{\underset{\sim}{Y}}^{*}_{e,S}$ is the transposed conjugate matrix or the Hermitian conjugate of $\underset{\sim}{Y}_{e,S}$.

The Hermitian part of $\underset{\sim}{Y}_{e,S}$ is the beam loading matrix $\underset{\sim}{G}_{e,S}$, given by

$$\underset{\sim}{G}_{e,S} = \frac{1}{2}(\underset{\sim}{Y}_{e,S} + \tilde{\underset{\sim}{Y}}^{*}_{e,S}) = \begin{bmatrix} G_{e,s} & \frac{Y^{*}_{s+1,s}}{2} & \frac{Y^{*}_{s+2,s}}{2} & \cdots & \frac{Y^{*}_{s+q,s}}{2} \\ \frac{Y_{s+1,s}}{2} & G_{e,s+1} & \frac{Y^{*}_{s+2,s+1}}{2} & \cdots & \\ \frac{Y_{s+2,s}}{2} & \frac{Y_{s+2,s+1}}{2} & G_{e,s+2} & \cdots & \\ & & & & \\ \frac{Y_{s+q,s}}{2} & \frac{Y_{s+q,s+1}}{2} & \cdots & & G_{e,s+q} \end{bmatrix} \tag{4.24}$$

The skew Hermitian part of $\underset{\sim}{Y}_{e,S}$ divided by j is the electronic susceptance matrix $\underset{\sim}{B}_{e,S}$, given by

$$\underset{\sim}{B}_{e,S} = \frac{1}{2j}(\underset{\sim}{Y}_{e,S} - \tilde{\underset{\sim}{Y}}^{*}_{e,S}) = \begin{bmatrix} B_{e,s} & -\frac{Y^{*}_{s+1,s}}{2j} & -\frac{Y^{*}_{s+2,s}}{2j} & \cdots & -\frac{Y^{*}_{s+q,s}}{2j} \\ \frac{Y_{s+1,s}}{2j} & B_{e,s+1} & -\frac{Y^{*}_{s+2,s+1}}{2j} & \cdots & \\ \frac{Y_{s+2,s}}{2j} & \frac{Y_{s+2,s+1}}{2j} & B_{e,s+2} & \cdots & \\ & & & & \\ \frac{Y_{s+q,s}}{2j} & \frac{Y_{s+q,s+1}}{2j} & \cdots & & B_{e,s+q} \end{bmatrix}. \tag{4.25}$$

Note that $\underset{\sim}{G}_{e,S}$ and $\underset{\sim}{B}_{e,S}$ are not real matrices. Their significance will be clearer if the following matrix products are formed:

$$P_{e,S} = \tfrac{1}{2} \tilde{V}_S^* \, \underset{\sim}{G}_{e,S} \, \underset{\sim}{V}_S \tag{4.26}$$

$$P'_{e,S} = \tfrac{1}{2} \tilde{V}_S^* \, \underset{\sim}{B}_{e,S} \, \underset{\sim}{V}_S \tag{4.27}$$

where $\underset{\sim}{V}_S$ is the voltage vector of group S. It is then found that the real numbers $P_{e,S}$ and $P'_{e,S}$ are the real and imaginary components of the complex beam loading power $\wp_{e,S}$ of the Sth group of gaps. Thus

$$\wp_{e,S} = P_{e,S} + jP'_{e,S} = \tfrac{1}{2} \tilde{V}_S^* \, \underset{\sim}{Y}_{e,S} \, \underset{\sim}{V}_S \tag{4.28}$$

which is in accordance with Eq (4.17).

In the same way, the product

$$\wp_{c,S} = \tfrac{1}{2} \tilde{V}_S^* \, \underset{\sim}{Y}_{c,S} \, \underset{\sim}{V}_S \tag{4.29}$$

is the complex circuit power extracted by the q+1 cavities forming the Sth group. Hence

$$\wp_{S,S} = \wp_{e,S} + \wp_{c,S} = \tfrac{1}{2} \tilde{V}_S^* \, \underset{\sim}{Y}_{S,S} \, \underset{\sim}{V}_S \tag{4.30}$$

is the sum of the complex circuit power and the complex beam loading power for the Sth group.

In exactly the same way as the beam loading G_e of a single interaction gap previously was expressed in terms of the coupling coefficients of the slow and fast space-charge waves (see Eq (2.70)), the beam loading matrix $\underset{\sim}{G}_{e,S}$ can be expressed in terms of appropriately defined coupling coefficient matrices $\underset{\sim}{M}_S^+$ and $\underset{\sim}{M}_S^-$, characteristic for the Sth group of cavities. It will be convenient to define these as line vectors, rather than column vectors

$$\underset{\sim}{M}_S^+ = \left[M_s^+ \;\; M_{s+1}^+ \;\; \text{-----} \;\; M_{s+q}^+ \right] \tag{4.31}$$

$$\underset{\sim}{M}_S^- = \left[M_s^- \;\; M_{s+1}^- \;\; \text{-----} \;\; M_{s+q}^- \right] \tag{4.32}$$

Further, we shall need to define a diagonal position matrix $\underset{\sim}{L}_S$ specifying the positions of the gaps of the Sth group

$$\underset{\sim}{L}_S = \begin{bmatrix} \ell_{s,1} & 0 & 0 \text{ ----- } 0 \\ 0 & \ell_{s+1,1} & 0 \text{ ----- } 0 \\ \text{----------} & & \\ 0 & 0 \text{ ------- } & \ell_{s+q,1} \end{bmatrix} \tag{4.33}$$

where the diagonal elements are the spacings between the centers of the interaction gaps of group S and some arbitrary reference point, here chosen as the center of the input gap (see Fig 4.1).

Using the definitions (4.31) to (4.33) and the definition (2.67) of transfer admittance, we find that the beam loading matrix $\underset{\sim}{G}_{e,S}$ defined in Eq (4.24) takes the simple form

$$\underset{\sim}{G}_{e,S} = -\frac{1}{2W}\,\Delta\left(e^{-j\beta_e \underset{\sim}{L}_S}\ \underset{\sim}{\tilde{M}}^{*}_{S}\ \underset{\sim}{M}_S\ e^{j\beta_e \underset{\sim}{L}_S}\right) \tag{4.34}$$

which is analogous to Eq (2.70) in the single-gap theory.

From standard theory on matrix functions, the exponential function of the position matrix $\underset{\sim}{L}_S$ appearing in Eq (4.34) is equal to a matrix of the same order having eigenvectors that are the same as those of $\underset{\sim}{L}_S$, and eigenvalues that are related to the eigenvalues of $\underset{\sim}{L}_S$ by the same exponential function.

Hence

$$e^{j\beta_e \underset{\sim}{L}_S} = \begin{bmatrix} e^{j\beta_e \ell_{s,1}} & 0 & 0 & \cdots & 0 \\ 0 & e^{j\beta_e \ell_{s+1,1}} & 0 & \cdots & 0 \\ \multicolumn{5}{c}{\cdots\cdots\cdots\cdots\cdots\cdots\cdots\cdots\cdots\cdots} \\ 0 & \cdots & \cdots & \cdots & e^{j\beta_e \ell_{s+q,1}} \end{bmatrix} \tag{4.35}$$

As in single-gap theory, it does not seem possible to express the electronic susceptance matrix $\underset{\sim}{B}_{e,S}$ as a simple function of the matrices $\underset{\sim}{M}^{+}_{S}$ and $\underset{\sim}{M}^{-}_{S}$.

4.4.3 Transfer admittance matrix

We shall next consider the transfer admittance matrices represented by the off-diagonal matrix elements in the $\underset{\sim}{Y}$-matrix in Fig 4.2. In contrast to the self-admittance matrices, these are not necessarily square matrices, except in the special case that all the groups 1, 2 --- S, --- P have the same number of cavities. If, as before, the Sth group consists of q+1 cavities, and the Rth group of k+1 cavities, the transfer admittance matrix $\underset{\sim}{Y}_{S,R}$ evidently is given by

$$\underset{\sim}{Y}_{S,R} = \begin{bmatrix} Y_{s,r} & Y_{s,r+1} & \cdots\cdots\cdots & Y_{s,r+k} \\ Y_{s+1,r} & Y_{s+1,r+1} & \cdots\cdots\cdots & Y_{s+1,r+k} \\ Y_{s+2,r} & Y_{s+2,r+1} & \cdots\cdots\cdots & Y_{s+2,r+k} \\ \cdots & \cdots & \cdots & \cdots \\ Y_{s+q,r} & Y_{s+q,r+1} & \cdots\cdots\cdots & Y_{s+q,r+k} \end{bmatrix} \tag{4.36}$$

The matrix elements of $\underset{\sim}{Y}_{S,R}$ are the various transfer admittances between the gaps belonging to the Rth and the Sth group. The transfer admittances between gaps belonging to the same group are contained in the electronic admittance matrix (4.22) of that same group. Again using Eqs (2.67) and (4.31) through (4.33), we find that $\underset{\sim}{Y}_{S,R}$ can be expressed as the following matrix product:

$$\underset{\sim}{Y}_{S,R} = -\frac{1}{W}\,\Delta\left(e^{-j\beta_e \underset{\sim}{L}_S}\ \underset{\sim}{\tilde{M}}^*_S\ \underset{\sim}{M}_R\ e^{j\beta_e \underset{\sim}{L}_R} \right) \tag{4.37}$$

The relation expressed in Eq (4.37) is the matrix equivalent of Eq (2.67) in the single-gap theory.

4.5 Gain and optimum spacing of two cascaded identical multi-cavity klystrons with common beam

As an example of the type of problems that lend themselves to solutions by the matrix formalism, we shall study in some detail a relatively simple cavity configuration, namely that of two cascaded identical groups of cavities, as illustrated in Fig 4.3. The identical groups, each consisting of q arbitrarily tuned and spaced cavities, are located a distance L apart and the gaps traversed by the same beam. As before, let $\underset{\sim}{V}_1$ and $\underset{\sim}{V}_2$ be the voltage column vectors of groups 1 and 2, respectively. Noting that the self-admittance matrices $\underset{\sim}{Y}_{1,1} = \underset{\sim}{Y}_{2,2} = \underset{\sim}{Y}$, we obtain from the first two equations of the set (4.11)

$$\underset{\sim}{V}_1 = \underset{\sim}{Y}^{-1}\,\underset{\sim}{A}_1 \tag{4.38}$$

$$\underset{\sim}{V}_2 = -\underset{\sim}{Y}^{-1}\,\underset{\sim}{Y}_{2,1}\,\underset{\sim}{V}_1 = -\underset{\sim}{Y}^{-1}\,\underset{\sim}{Y}_{2,1}\,\underset{\sim}{Y}^{-1}\,\underset{\sim}{A}_1 \tag{4.39}$$

where the self-admittance matrix $\underset{\sim}{Y}$ is given by Eq (4.19), the transfer admittance matrix $\underset{\sim}{Y}_{2,1}$ by Eq (4.36) or (4.37), and the excitation vector $\underset{\sim}{A}_1$ by Eq (4.7), i e

$$\underset{\sim}{A}_1 = \begin{bmatrix} a \\ 0 \\ 0 \\ \vdots \\ 0 \end{bmatrix} = a \begin{bmatrix} 1 \\ 0 \\ 0 \\ \vdots \\ 0 \end{bmatrix} \tag{4.40}$$

In Eq (4.40) the absolute value of the only non-zero element a, defined in Eq (4.2), is proportional to the square root of the input power P_i.

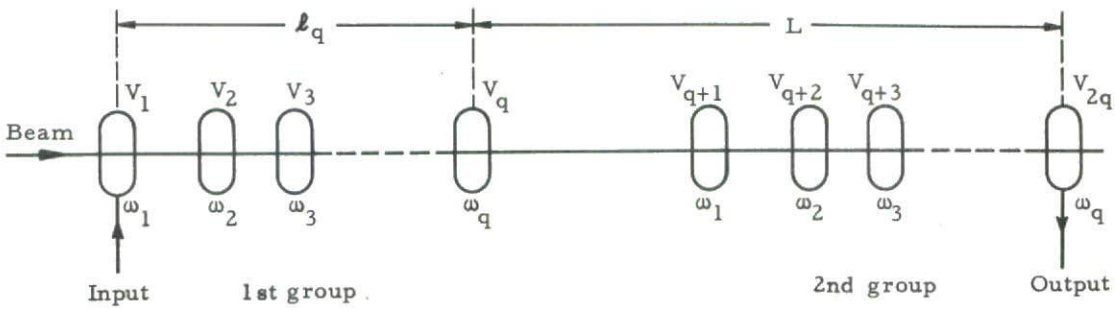

Fig 4.3 Sketch showing the configuration studied in the text, consisting of two identical cascaded groups of cavities spaced a distance L apart

The matrix equations (4.38) and (4.39) express the various voltage components of the vectors $\underset{\sim}{V}_1$ and $\underset{\sim}{V}_2$ in terms of the quantity a, i e the square root of the input power P_i. In particular, the relations between the gap voltages V_{2q} and V_q of the last cavity in each group can be established in an obvious way by evaluation of the matrices $\underset{\sim}{Y}^{-1}$ and $\underset{\sim}{Y}^{-1} Y_{2,1} \underset{\sim}{Y}^{-1}$ (for calculation of the ratio V_{2q}/V_q it suffices to know the first element in the last line of each of these matrices)

We shall next proceed to evaluate the optimum spacing L between the two groups, defined as the spacing that maximizes the gain of the composite structure. During this optimization the configuration of each group, including gap spacing, tuning, etc, is not changed.

If we define a column vector $\underset{\sim}{S}$ by

$$\underset{\sim}{S} = \begin{bmatrix} 0 \\ 0 \\ \vdots \\ \vdots \\ 1 \end{bmatrix} , \tag{4.41}$$

the gap voltage V_{2q} of the last cavity is given by the matrix product

$$V_{2q} = \tilde{S}\, \underset{\sim}{V}_2 \tag{4.42}$$

where $\tilde{S}$ is the transpose of $\underset{\sim}{S}$. Using Eq (4.39) we find

$$V_{2q} = -\tilde{S}\, \underset{\sim}{Y}^{-1} \underset{\sim}{Y}_{2,1}\, \underset{\sim}{V}_1 \tag{4.43}$$

In this equation the transfer matrix $\underset{\sim}{Y}_{2,1}$ is the only matrix depending on the group

spacing L. Since maximization of V_{2q} with respect to L thus involves only this matrix, it is convenient to introduce a new line vector $\underset{\sim}{R}$ by the equation

$$\underset{\sim}{R} = -\tilde{S}\ \underset{\sim}{Y}^{-1} \tag{4.44}$$

whereby

$$\underset{\sim}{V}_{2q} = \underset{\sim}{R}\ \underset{\sim}{Y}_{2,1}\ \underset{\sim}{V}_1 \tag{4.45}$$

Evaluation of $\underset{\sim}{Y}_{2,1}$ from the general formula (4.37) yields

$$\underset{\sim}{Y}_{2,1} = -\frac{1}{W}\ \Delta\left(e^{-j\beta_e \underset{\sim}{L}_2}\ \tilde{M}_2^*\ M_1\ e^{j\beta_e \underset{\sim}{L}_1}\right) \tag{4.46}$$

Noting that $\underset{\sim}{M}_2 = \underset{\sim}{M}_1 = \underset{\sim}{M}$ and $\underset{\sim}{L}_2 = \underset{\sim}{L}_1 + L\,\underset{\sim}{1}$, where $\underset{\sim}{1}$ is the unit matrix, we find

$$\underset{\sim}{Y}_{2,1} = -\frac{1}{W}\ \Delta\left(e^{-j\beta_e L}\ e^{-j\beta_e \underset{\sim}{L}_1}\ \tilde{M}^*\underset{\sim}{M}\ e^{-j\beta_e \underset{\sim}{L}_1}\right) \tag{4.47}$$

Expansion of the expression in the parenthesis by means of the difference operator Δ yields

$$\underset{\sim}{Y}_{2,1} = e^{-j\beta_e L}\left[-\frac{1}{W}\cos\beta_q L\ \Delta\left(e^{-j\beta_e \underset{\sim}{L}_1}\ \tilde{M}^*\underset{\sim}{M}\ e^{j\beta_e \underset{\sim}{L}_1}\right) + \frac{j}{W}\sin\beta_q L\ \mathcal{S}\left(e^{-j\beta_e \underset{\sim}{L}_1}\ \tilde{M}^*\underset{\sim}{M}\ e^{j\beta_e \underset{\sim}{L}_1}\right)\right] \tag{4.48}$$

The first term is recognized as the beam loading matrix $\underset{\sim}{G}_e$ defined in Eq (4.34)

$$\underset{\sim}{G}_e = -\frac{1}{2W}\ \Delta\left(e^{-j\beta_e \underset{\sim}{L}_1}\ \tilde{M}^*\underset{\sim}{M}\ e^{j\beta_e \underset{\sim}{L}_1}\right) \tag{4.49}$$

Furthermore, defining a mean square coupling coefficient matrix by the equation

$$\underset{\sim}{\overline{M}}^2 = \mathcal{S}\left[e^{-j\beta_e \underset{\sim}{L}_1}\ \tilde{M}^*\ \underset{\sim}{M}\ e^{j\beta_e \underset{\sim}{L}_1}\right] \tag{4.50}$$

we find that Eq (4.48) reduces to

$$\underset{\sim}{Y}_{2,1} = e^{-j\beta_e L}\left[2\underset{\sim}{G}_e\cos\beta_q L + \frac{1}{W}\,\underset{\sim}{\overline{M}}^2\sin\beta_q L\right] \tag{4.51}$$

In the single-gap theory Eq (4.51) has its equivalent in Eq (B.9), Appendix B. The matrix $\underset{\sim}{\overline{M}}^2$ is equivalent to the mean square coupling coefficient $\overline{M^2}$ defined in Eq (B.10).

Substitution of Eq (4.51) in Eq (4.45) yields

$$V_{2q} = e^{-j\beta_e L} \underset{\sim}{R}\left[2\underset{\sim}{G}_e \cos\beta_q L + \frac{j}{W}\underset{\sim}{\bar{M}}^2 \sin\beta_q L\right]\underset{\sim}{V}_1 \qquad (4.52)$$

where now $\sin\beta_q L$ and $\cos\beta_q L$ are the only terms that are functions of the group spacing L. Forming the complex conjugate

$$V_{2q}^* = e^{j\beta_e L}\,\tilde{V}_1^*\left[2\tilde{G}_e^* \cos\beta_q L - \frac{j}{W}\left(\underset{\sim}{\bar{M}}^2\right)^* \sin\beta_q L\right]\tilde{R}^* \qquad (4.53)$$

and multiplying V_{2q} by V_{2q}^*, we find

$$|V_{2q}|^2 = \underset{\sim}{R}\left[2\underset{\sim}{G}_e\,\underset{\sim}{V}_1\tilde{V}_1^*\tilde{G}_e^* + \frac{1}{2W^2}\underset{\sim}{\bar{M}}^2\underset{\sim}{V}_1\tilde{V}_1^*\left(\underset{\sim}{\bar{M}}^2\right)^*\right]\tilde{R}^*$$

$$+ \underset{\sim}{R}\left[2\underset{\sim}{G}_e\,\underset{\sim}{V}_1\tilde{V}_1^*\tilde{G}_e^* - \frac{1}{2W^2}\underset{\sim}{\bar{M}}^2\underset{\sim}{V}_1\tilde{V}_1^*\left(\underset{\sim}{\bar{M}}^2\right)^*\right]\tilde{R}^* \cos(2\beta_q L) \qquad (4.54)$$

The optimum value of $\beta_q L$, making $|V_{2q}|^2$ an extremum, is determined by differentiation. We find

$$\frac{d|V_{2q}|^2}{d(\beta_q L)} = -2\sin(2\beta_q L)\,\underset{\sim}{R}\left[2\underset{\sim}{G}_e\,\underset{\sim}{V}_1\tilde{V}_1^*\tilde{G}_e^* - \frac{1}{2W^2}\underset{\sim}{\bar{M}}^2\underset{\sim}{V}_1\tilde{V}_1^*\left(\underset{\sim}{\bar{M}}^2\right)^*\right]\tilde{R}^* = 0 \qquad (4.55)$$

For convenience let us write

$$\frac{d|V_{2q}|^2}{d(\beta_q L)} = -2\sin(2\beta_q L)\,\underset{\sim}{R}\,\underset{\sim}{T}\,\tilde{R}^* = 0 \qquad (4.56)$$

where the Hermitian matrix $\underset{\sim}{T}$ is given by

$$\underset{\sim}{T} = 2\,\underset{\sim}{G}_e\,\underset{\sim}{V}_1\tilde{V}_1^*\tilde{G}_e^* - \frac{1}{2W^2}\underset{\sim}{M}^2\underset{\sim}{V}_1\tilde{V}_1^*\left(\underset{\sim}{\bar{M}}^2\right)^* \qquad (4.57)$$

Equation (4.56) is solved by $\sin(2\beta_q L) = 0$, i e

$$2\beta_q L = n\pi \qquad n = 1, 2, 3 \text{ ---} \qquad (4.58)$$

Whether this condition yields maximum or minimum is determined by forming the second derivative

$$\frac{d^2|V_{2q}|^2}{d(\beta_q L)^2} = -4\cos(2\beta_q L)\,\underset{\sim}{R}\,\underset{\sim}{T}\,\tilde{R}^* = 4(-1)^{n+1}\,\underset{\sim}{R}\,\underset{\sim}{T}\,\tilde{R}^* \qquad (4.59)$$

The sign of the second derivative thus depends on the sign of the matrix product $\underset{\sim}{R}\,\underset{\sim}{T}\,\tilde{R}^*$ and on the even or odd character of the integer n. We shall list the two possible cases without studying the matrix product in detail. The second deriva-

tive is negative, corresponding to a maximum of $|V_{2q}|$, if:

a) $\underset{\sim}{R}\,\underset{\sim}{T}\,\tilde{\bar{R}}^{*} > 0$ and $n = 2k$, $k = 1, 2, 3$ --- (4.60)

Optimum spacing and output voltage are given by

$$\beta_q L = k\pi \tag{4.61}$$

$$|V_{2q}|^2_{max} = 2\,\underset{\sim}{R}\,\underset{\sim}{G}_e\,\underset{\sim}{V}_1\,\tilde{V}_1^{*}\,\tilde{G}_e^{*}\,\tilde{R}^{*} \tag{4.62}$$

b) $\underset{\sim}{R}\,\underset{\sim}{T}\,\tilde{\bar{R}}^{*} < 0$ and $n = 2k+1$, $k = 1, 2, 3$ --- (4.63)

Optimum spacing and output voltage are given by

$$\beta_q L = (2k+1)\frac{\pi}{2} \tag{4.64}$$

$$|V_{2q}|^2_{max} = \frac{1}{W^2}\,\underset{\sim}{R}\,\underset{\sim}{\bar{M}}^2\,\underset{\sim}{V}_1\,\tilde{V}_1^{*}\left(\tilde{\bar{M}}^2\right)^{*}\,\tilde{R}^{*} \tag{4.65}$$

The question whether case a) or b) applies cannot be decided without a closer study of the matrix product $\underset{\sim}{R}\,\underset{\sim}{T}\,\tilde{\bar{R}}^{*}$. In the special case that each of the groups consists of one cavity only, the configuration degenerates to a simple two-cavity klystron, and the matrix product $\underset{\sim}{R}\,\underset{\sim}{T}\,\tilde{\bar{R}}^{*}$ reduces to $V_1 V_1^{*}(\varkappa\varkappa^{*} - \xi\xi^{*})$ where $\varkappa$ and ξ are defined in Eqs (3.38) and (3.39). In view of Eq (3.42) the difference $\varkappa\varkappa^{*} - \xi\xi^{*}$ is always negative and the optimum spacing is therefore equal to $k\pi + \pi/2$ as specified by Eq (4.64). This is in accordance with well-known results from simple klystron theory.

In the general case, however, the matrix product $\underset{\sim}{R}\,\underset{\sim}{T}\,\tilde{\bar{R}}^{*}$ can be either positive or negative. The optimum spacing is therefore either $k\pi$ or $k\pi + \pi/2$ depending on the detailed arrangement within each cavity group.

4.6 Alternate matrix formulation

The matrix formulation used in the theory developed in the preceding sections has been built on the set (4.3) of linear equations in the RF gap voltages $V_1, V_2, \text{---}\ V_p$. It will also be useful to consider an alternate description based on Eq (3.24) which, as we remember, resulted from taking suitable linear combinations of the set (3.10) or the equivalent (4.3). Rewriting Eq (3.24) in terms of RF gap voltages, we obtain the equation

$$\begin{bmatrix} -1 & 0 & 0 & 0 & 0 & \cdots & 0 \\ \eta_{2,1} & -1 & 0 & 0 & 0 & \cdots & 0 \\ \eta_{3,1} & \eta_{3,2} & -1 & 0 & 0 & \cdots & 0 \\ 0 & S_4 & T_4 & -1 & 0 & \cdots & 0 \\ 0 & 0 & S_5 & T_5 & -1 & \cdots & 0 \\ & & & & & & \\ 0 & \cdots & 0 & S_p & T_p & & -1 \end{bmatrix} \begin{bmatrix} V_1 \\ V_2 \\ \cdot \\ \cdot \\ \cdot \\ \cdot \\ \cdot \\ \cdot \\ \cdot \\ V_p \end{bmatrix} = - \begin{bmatrix} V_1 \\ 0 \\ \cdot \\ \cdot \\ \cdot \\ \cdot \\ \cdot \\ \cdot \\ \cdot \\ 0 \end{bmatrix} \tag{4.66}$$

which can be written

$$\underset{\sim}{U}\ \underset{\sim}{V} = - \frac{1}{Y_{1,1}}\ \underset{\sim}{A} \tag{4.67}$$

where the column vectors $\underset{\sim}{V}$ and $\underset{\sim}{A}$ are the same as those in Eq (4.6) and (4.7), and $\underset{\sim}{U}$ is the triangular matrix on the left. Exactly in the same way as done previously, the matrices $\underset{\sim}{U}$, $\underset{\sim}{V}$ and $\underset{\sim}{A}$ can be partitioned in the manner indicated by Eq (4.68).

$$\begin{bmatrix} \underset{\sim}{U}_{1,1} & \underset{\sim}{0} & \underset{\sim}{0} & \underset{\sim}{0} & \cdots & \underset{\sim}{0} \\ \underset{\sim}{U}_{2,1} & \underset{\sim}{U}_{2,2} & \underset{\sim}{0} & \underset{\sim}{0} & \cdots & \underset{\sim}{0} \\ \underset{\sim}{0} & \underset{\sim}{U}_{3,2} & \underset{\sim}{U}_{3,3} & \underset{\sim}{0} & \cdots & \underset{\sim}{0} \\ \underset{\sim}{0} & \underset{\sim}{0} & \underset{\sim}{U}_{4,3} & \underset{\sim}{U}_{4,4} & \cdots & \underset{\sim}{0} \\ & & & & & \\ & & & & & \\ & & & & & \\ \underset{\sim}{0} & \underset{\sim}{0} & \underset{\sim}{0} & & \underset{\sim}{U}_{P,P-1} & \underset{\sim}{U}_{P,P} \end{bmatrix} \begin{bmatrix} \underset{\sim}{V}_1 \\ \underset{\sim}{V}_2 \\ \underset{\sim}{V}_3 \\ \underset{\sim}{V}_4 \\ \\ \\ \\ \underset{\sim}{V}_P \end{bmatrix} = - \frac{1}{Y_{1,1}} \begin{bmatrix} \underset{\sim}{A}_1 \\ \underset{\sim}{0} \\ \underset{\sim}{0} \\ \underset{\sim}{0} \\ \\ \\ \\ \underset{\sim}{0} \end{bmatrix} \tag{4.68}$$

The partitioning shown in Eq (4.68), in which the only non-zero off-diagonal elements are of the form $\underset{\sim}{U}_{S,S-1}$, is possible only if each group contains two or more cavities. The trivial case of one cavity in each group is of course represented by the original Eq (4.66).

Of the sub-matrices in Eq (4.68) the matrices along the diagonal are all square matrices of orders corresponding to the number of cavities in the associated cavity group. The off-diagonal matrices are in general rectangular, but reduce

to square matrices if all the groups contain the same number of cavities.

Performing the matrix multiplication in Eq (4.68) we obtain the following set of matrix equations:

$$\begin{aligned}
\underset{\sim}{U}_{1,1}\,\underset{\sim}{V}_1 &= -\frac{1}{Y_{1,1}}\,\underset{\sim}{A}_1 \\
\underset{\sim}{U}_{2,1}\,\underset{\sim}{V}_1 + \underset{\sim}{U}_{2,2}\,\underset{\sim}{V}_2 &= 0 \\
\underset{\sim}{U}_{3,2}\,\underset{\sim}{V}_2 + \underset{\sim}{U}_{3,3}\,\underset{\sim}{V}_3 &= 0 \\
\underset{\sim}{U}_{4,3}\,\underset{\sim}{V}_3 + \underset{\sim}{U}_{4,4}\,\underset{\sim}{V}_4 &= 0 \\
&\cdots\cdots\cdots\cdots\cdots \\
\underset{\sim}{U}_{P,P-1}\,\underset{\sim}{V}_{P-1} + \underset{\sim}{U}_{P,P}\,\underset{\sim}{V}_P &= 0
\end{aligned} \tag{4.69}$$

We see from this that any two consecutive voltage vectors $\underset{\sim}{V}_{S-1}$ and $\underset{\sim}{V}_S$ are related through the following first order matrix difference equation, or recurrence formula:

$$\underset{\sim}{U}_{S,S-1}\,\underset{\sim}{V}_{S-1} + \underset{\sim}{U}_{S,S}\,\underset{\sim}{V}_S = 0 \qquad s \geq 2 \tag{4.70}$$

Or

$$\underset{\sim}{V}_S = \underset{\sim}{\alpha}_S\,\underset{\sim}{V}_{S-1} \tag{4.71}$$

where the group gain matrix $\underset{\sim}{\alpha}_S$ is given by

$$\underset{\sim}{\alpha}_S = -\,\underset{\sim}{U}_{S,S}^{-1}\,\underset{\sim}{U}_{S,S-1} \qquad s \geq 2 \tag{4.72}$$

$$\underset{\sim}{\alpha}_1 = \underset{\sim}{V}_1 = -\frac{1}{Y_{1,1}}\,\underset{\sim}{U}_{1,1}^{-1}\,\underset{\sim}{A}_1 \tag{4.73}$$

The difference equation (4.71) evidently is solved by the matrix product

$$\underset{\sim}{V}_P = \underset{\sim}{\alpha}_P\,\underset{\sim}{\alpha}_{P-1} \cdots \underset{\sim}{\alpha}_S \cdots \underset{\sim}{\alpha}_3\,\underset{\sim}{\alpha}_2\,\underset{\sim}{V}_1 \tag{4.74}$$

This formula is useful in that it is in cascade form, i e the overall gain is expressed as a matrix product of the "group gains". We shall later take advantage of this property for evaluation of the gain of periodically stagger-tuned multicavity klystrons.

4.7 Matrix parameters in the alternate formulation

The partition matrices $\underset{\sim}{U}_{S,S}$ and $\underset{\sim}{U}_{S,S-1}$ of the matrix $\underset{\sim}{U}$ in Eq (4.68) are given by the expressions below. Again we assume that the Sth group contains q+1 cavities, of which the first is the sth cavity.

$$\underset{\sim}{U}_{S,S} = \begin{bmatrix} -1 & 0 & 0 & 0 \text{ ---------- } 0 \\ T_{s+1} & -1 & 0 & 0 \text{ ---------- } 0 \\ S_{s+2} & T_{s+2} & -1 & 0 \text{ ---------- } 0 \\ 0 & S_{s+3} & T_{s+3} & -1 \text{ ---------- } 0 \\ \text{----------} & & & \\ 0 & 0 \text{ ------ } S_{s+q} & T_{s+q} & -1 \end{bmatrix} \tag{4.75}$$

where the elements S_s and T_s are given by Eqs (3.21) and (3.22) for values of s equal to or larger than four. For s smaller than four the corresponding elements are obtained directly from Eq (4.66).

$$\begin{aligned} S_3 &= \eta_{3,1} \\ T_3 &= \eta_{3,2} \\ T_2 &= \eta_{2,1} \end{aligned} \tag{4.76}$$

If the groups S and S-1 consist of q+1 and r+1 cavities, respectively, $\underset{\sim}{U}_{S,S-1}$ is an r+1 by q+1 rectangular matrix given by

$$\underset{\sim}{U}_{S,S-1} = \begin{bmatrix} 0 & 0 & 0 \text{ ------- } S_s & T_s \\ 0 & 0 & 0 \text{ ------- } 0 & S_{s+1} \\ 0 & 0 & 0 \text{ ------- } 0 & 0 \\ \text{----------} & & & \\ 0 & 0 & 0 \text{ ------- } 0 & 0 \end{bmatrix} \tag{4.77}$$

4.8 Periodic stagger-tuning

If we take advantage of the mathematical apparatus developed in this chapter, the analysis of periodic stagger-tuning is straight forward. Although this problem can be analyzed using the scalar difference equation (3.34), noting that the coefficients in this case are periodic with respect to the variable p, the matrix formulation derived in this chapter simplifies the analysis considerably. It turns out that the periodic stagger-tuning is represented by a matrix difference equation with constant coefficients, the solution of which is a linear combination of one growing wave and one attenuated wave, quite analogous to the results obtained in Chapter 3 for the case of synchronously tuned cavities. If the periodic tuning pattern is repeated sufficiently many times, the attenuated wave obviously can be neglected

and the increase in voltage gain per period will be constant. We shall analyze the problem using several slightly different approaches which lead to solutions that are all equivalent but differ in their mathematical form.

The situation which we shall study is shown schematically in Fig 4.4. Each of the P identical groups consisting of q+1 cavities has the same stagger-tuning pattern characterized by the resonant frequencies $\omega_1, \omega_2, \cdots \omega_{q+1}$.

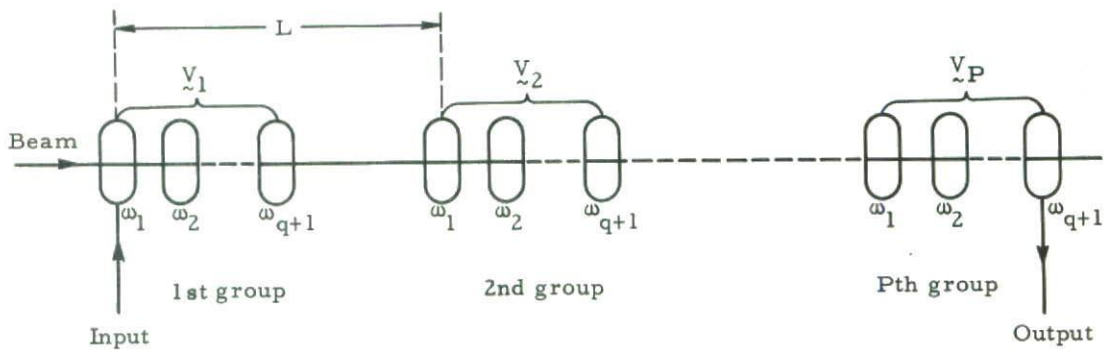

Fig 4.4 Details of the periodic stagger-tuning analyzed in the text

4.8.1 Matrix cascade gain formula

Using the approach shown in Section 4.6 for the special case of identical groups, i e periodic stagger-tuning, we have that the group gain matrix $\underset{\sim}{\alpha}_S$ defined in Eq (4.72) is independent of S.

$$\underset{\sim}{\alpha}_3 = \underset{\sim}{\alpha}_4 = \cdots \underset{\sim}{\alpha}_{P-1} = \underset{\sim}{\alpha}_P = \underset{\sim}{\alpha} \tag{4.78}$$

It should be noted that $\underset{\sim}{\alpha}_2$ is different from the other α's if there are only two cavities in each group. This is a minor detail, and if we assume $q \geq 2$, we also have $\underset{\sim}{\alpha}_2 = \underset{\sim}{\alpha}$. Hence, Eq (4.74) reduces to

$$\underset{\sim}{V}_P = \underset{\sim}{\alpha}^{P-1} \underset{\sim}{V}_1 \tag{4.79}$$

where $\underset{\sim}{\alpha}$ is a square matrix given by the matrix product in Eq (4.72). In Eq (4.79) each of the RF gap voltages within the Pth group is expressed as a linear combination of all the RF gap voltages in the first group.

We shall next present an alternate formula, in which the gain per group is given by a scalar rather than a matrix.

4.8.2 Gain in terms of growing and attenuated waves

Let us consider the first-order matrix difference equation (4.71). We shall show that the difference equation has particular solutions of the form

$$\underset{\sim}{V}_S = k\,\underset{\sim}{V}_{S-1} \qquad S \geq 2 \tag{4.80}$$

where k is some scalar constant independent of S. Equation (4.80) can also be expressed in a different, but equivalent way

$$\underset{\sim}{V}_P = k^{P-1}\,\underset{\sim}{\phi} \qquad P \geq 1 \tag{4.81}$$

where $\underset{\sim}{\phi}$ is some constant column vector independent of P.

Substitution of Eq (4.80) in Eq (4.71) yields

$$\underset{\sim}{\alpha}\ \underset{\sim}{V}_S = k\,\underset{\sim}{V}_S \tag{4.82}$$

which is an eigenvalue equation, k representing one of the q+1 eigenvalues, and $\underset{\sim}{V}_S$ the associated eigenvectors. The equation can also be written

$$(\underset{\sim}{\alpha} - k\,\underset{\sim}{1})\ \underset{\sim}{V}_S = 0 \tag{4.83}$$

where $\underset{\sim}{1}$ is the unit matrix. This homogeneous system of equations has non-trivial solutions only if

$$\text{Det}\,(\underset{\sim}{\alpha} - k\,\underset{\sim}{1}) = 0 \tag{4.84}$$

The q+1 eigenvalues k are determined by this algebraic equation of order q+1. It turns out that the equation is degenerate because only two of the k's are different. This is most easily shown by expressing Eq (4.84) in a slightly different form, obtained by premultiplication of Eq (4.83) by the square matrix $\underset{\sim}{U}_{S,S}$ defined in Eq (4.75). Instead of Eq (4.84) the following equivalent determinantal equation is obtained:

$$\text{Det}\,(k^{-1}\,\underset{\sim}{U}_{S,S-1} + \underset{\sim}{U}_{S,S}) = 0 \tag{4.85}$$

By means of Eqs (4.75) and (4.77) this determinantal equation can be written in the form

$$\begin{vmatrix} T_s & -1 & 0 & 0 & 0 \text{ ------- } & k^{-1}S_s \\ S_{s+1} & T_{s+1} & -1 & 0 & 0 \text{ ------- } & 0 \\ 0 & S_{s+2} & T_{s+2} & -1 & 0 \text{ ------- } & 0 \\ \multicolumn{6}{c}{\text{----------}} \\ 0 \text{ ---------- } & 0 & S_{s+q-1} & T_{s+q-1} & -1 & \\ -k & 0 \text{ ---------- } & 0 & S_{s+q} & T_{s+q} & \end{vmatrix} = 0 \tag{4.86}$$

Because of the degeneracy the factor k appears only in two of the elements. A little consideration shows that the expansion results in the following second-order equation for k:

$$k + k^{-1} \prod_{i=s}^{s+q} (-S_i) - D = 0 \tag{4.87}$$

where D is a determinant obtained from Eq (4.86), replacing by zero the two elements containing k.

$$D = \begin{vmatrix} T_s & -1 & 0 & 0 \text{ ---------- } 0 \\ S_{s+1} & T_{s+1} & -1 & 0 \text{ ---------- } 0 \\ 0 & S_{s+2} & T_{s+2} & -1 \text{ ---------- } 0 \\ \text{---------- } & & & \\ 0 \text{ ---------- } & S_{s+q-1} & T_{s+q-1} & -1 \\ 0 & 0 \text{ -------- } 0 & S_{s+q} & T_{s+q} \end{vmatrix} \tag{4.88}$$

Solving Eq (4.87) with respect to k, we obtain the two values k_1 and k_2 satisfying Eq (4.80)

$$\left.\begin{matrix} k_1 \\ k_2 \end{matrix}\right\} = \frac{D}{2} \mp \left[\left(\frac{D}{2}\right)^2 - \prod_{i=s}^{s+q} (-S_i) \right]^{\frac{1}{2}} \tag{4.89}$$

The general solution of the difference equation (4.71) is a linear combination of the two particular solutions:

$$\underset{\sim}{V}_P = k_1^{P-1} \underset{\sim}{\Phi}_1 + k_2^{P-1} \underset{\sim}{\Phi}_2 \qquad P \geq 1 \tag{4.90}$$

where the unknown column vectors $\underset{\sim}{\Phi}_1$ and $\underset{\sim}{\Phi}_2$ must be chosen such that Eq (4.90) satisfies the initial conditions. Substitution of $\underset{\sim}{V}_1$ at P = 1 and $\underset{\sim}{V}_2$ at P = 2 in the equation gives two linear equations in $\underset{\sim}{\Phi}_1$ and $\underset{\sim}{\Phi}_2$. Expressing these vectors in terms of $\underset{\sim}{V}_1$ and $\underset{\sim}{V}_2$ and substituting in Eq (4.90), we obtain

$$\underset{\sim}{V}_P = \frac{1}{k_1 - k_2} \left[(\underset{\sim}{V}_2 - k_2 \underset{\sim}{V}_1) k_1^{P-1} - (\underset{\sim}{V}_2 - k_1 \underset{\sim}{V}_1) k_2^{P-1} \right] \qquad P \geq 1 \tag{4.91}$$

The analysis done here serves as a simple proof of the equivalent of Floquet's theorem (25) known from the theory of differential equations with periodic coefficients. Equation (4.80) or the equivalent (4.81) is Floquet's theorem in matrix form for difference equations with periodic coefficients, stating that particular solutions can be found with the property that two values of the dependent variable taken one period apart differ by a constant factor only. In the theory of differential equations the determinantal equation has an infinite number of terms (Hill's determinant). The present theory shows that for difference equations the order of the determinant is equal to the number of terms in the period, and its evaluation is therefore correspondingly simpler.

The matrix equation (4.91) holds for any of the corresponding q+1 scalar components of $\underset{\sim}{V}_P$, $\underset{\sim}{V}_2$ and $\underset{\sim}{V}_1$. The analysis of synchronous tuning in Chapter 3 resulted in the analogous equation (3.47) which expressed the solution as a sum of one attenuated and one growing gap voltage wave with gain per stage equal to α_1 and α_2 for the two waves, respectively (see Eq (3.46)). In the present analysis of periodic stagger-tuning, the solution (4.91) is also expressed as a sum of two waves with gain per period equal to k_1 and k_2. It will be shown below that also in this case one wave is attenuated and the other growing. We have from Eq (4.87)

$$k_1 k_2 = \prod_{i=s}^{s+q} (-S_i) \tag{4.92}$$

In evaluating the product on the right-hand side we shall assume, for simplicity, that the coupling coefficients for all the gaps are the same, i e $M_1^+ = M_2^+$ --- and $M_1^- = M_2^-$ ---. This assumption also implies that the beam loading is the same in all the gaps. In this case the coefficients S_i and T_i are obtained by comparison of Eq (3.23) with Eq (B.11), Appendix B. We find

$$S_i = -e^{-j\beta_e \ell_{i,i-2}} \frac{\sin \beta_q \ell_{i,i-1}}{\sin \beta_q \ell_{i-1,i-2}} \frac{Y_{i-2,i-2}}{Y_{i,i}} \left(1 - \frac{2G_e}{Y_{i-2,i-2}} \right) \tag{4.93}$$

$$T_i = 2 e^{-j\beta_e \ell_{i,i-1}} \left(\frac{1}{2} \frac{\sin \beta_q \ell_{i,i-2}}{\sin \beta_q \ell_{i-1,i-2}} \frac{Y_{i-1,i-1}}{Y_{i,i}} - \frac{G_e}{Y_{i,i}} \cos \beta_q \ell_{i,i-1} - j \frac{\bar{M}^2}{2WY_{i,i}} \sin \beta_q \ell_{i,i-1} \right) \tag{4.94}$$

Evaluation of the product in Eq (4.92) by means of Eq (4.93) yields

$$k_1 k_2 = e^{-j\beta_e 2L} \prod_{i=s}^{s+q} \left(1 - \frac{2G_e}{Y_{i-2,i-2}} \right) \tag{4.95}$$

where L is the periodic length. For zero beam loading, $G_e = 0$, and the expression simplifies to

$$|k_1| \, |k_2| = 1 \tag{4.96}$$

Even with G_e slightly different from zero, the product of the absolute values of k_1 and k_2 is of the order of unity. Since k_2 is the larger of the two, and the overall gain per period is large if the period includes several stages, we must have

$$|k_2| \gg 1 , \qquad |k_1| \ll 1 \tag{4.97}$$

It is therefore entirely justified to neglect the attenuated wave compared to the

growing wave. For $P \geq 2$ the gain is thus given by the growing wave in Eq (4.91).

$$\underset{\sim}{V}_P = \frac{1}{k_2 - k_1} (\underset{\sim}{V}_2 - k_1 \underset{\sim}{V}_1) k_2^{P-1} , \qquad P \geq 2 \tag{4.98}$$

Since the gain per period presumably is considerably larger than unity, we must have that $\underset{\sim}{V}_2 \gg \underset{\sim}{V}_1$, and in view of Eq (4.97), $|k_1| \ll 1$ and $|k_2| \gg 1$. Therefore, Eq (4.98) can be simplified further by introducing the approximations

$$\begin{aligned} \underset{\sim}{V}_2 - k_1 \underset{\sim}{V}_1 &\approx \underset{\sim}{V}_2 \\ k_2 - k_1 &\approx k_2 \end{aligned} \tag{4.99}$$

yielding

$$\underset{\sim}{V}_P = \underset{\sim}{V}_2 k_2^{P-2} , \qquad P \geq 2 \tag{4.100}$$

Thus, the increase in gain per period of a periodically stagger-tuned multi-cavity klystron is constant and equal to k_2, which can be found from Eqs (4.88) and (4.89). For a klystron with several stages in one period, k_2 necessarily must be relatively large, permitting the following approximation of Eq (4.89)

$$\begin{aligned} k_1 &= 0 \\ k_2 &= D \end{aligned} \tag{4.101}$$

where D is the determinant (4.88), whose elements are given by Eqs (4.93) and (4.94) for arbitrary resonant frequencies of the $q+1$ cavities in the period.

It must be expected that the formulae derived here for periodic stagger-tuning reduces to those derived in Chapter 3 for synchronous tuning, if in Eq (4.88) we put $T_s = T_{s+1} = \text{---} T_{s+q} = T$ and $S_{s+1} = S_{s+2} = \text{---} S_{s+q} = S$. Since each period has $q+1$ cavities or q stages, the quantities appearing in Eqs (4.90) and (3.47) must in this special case be related by the following equations:

$$k_1 = e^{-j\vartheta q} \alpha_1^q \tag{4.102}$$

$$k_2 = e^{-j\vartheta q} \alpha_2^q \tag{4.103}$$

Rather than proving these relations rigorously, we shall only show that the last relation is satisfied if the gain per period is large. In this case we found that $k_2 \approx D \gg 1$. Furthermore, for the synchronous case the determinant D in Eq (4.88) evidently satisfies the following recurrence formula

$$D_{q+1} - TD_q - SD_{q-1} = 0 \tag{4.104}$$

which is identical with the difference equation (3.23), or rather (3.43). Under the assumption stated above, $k_2 \approx D \gg 1$, the complete solutions of either equations are approximated by the larger of the two particular solutions. Since Eq (3.43) is solved by Eq (3.44), the relation (4.103) is proved.

5 GENERAL GAP THEORY OF EXTENDED INTERACTION REGIONS

5.1 Introduction

The small-signal multi-cavity klystron theory developed in Chapters 3 and 4 is based on a formalism in which the RF current and velocity modulations on the beam are not appearing explicitly in the various expressions for klystron gain. Instead, the propagation of the signal from gap to gap is expressed in terms of appropriately defined self-admittances and transfer admittances representing the beam coupling between the various gaps. Mathematically this formalism is simpler than the more direct approach based on a description in terms of the beam modulations. For a thorough physical understanding, however, it is also useful to study the modulation phenomena taking place in input and output regions of the general types considered in this report.

The analysis carried out in the present chapter will be concerned mainly with the two following subjects:

a) The small-signal RF current and velocity modulations imposed on a beam traversing an extended modulation region of the general type considered in this report

b) The excitation of a general cavity gap by a beam with specified current and velocity modulations

Both of these subjects can be analyzed by means of some of the results derived in Chapters 2 and 3. The results arrived at in this chapter serve as a further illustration of the previously discussed differences between the present theory and the less complete conventional narrow-gap klystron theory, arising from the neglect of space-charge forces and density modulation in the gaps.

We shall find in the general case that the interaction region can be represented as a non-reciprocal two-port, in which the terminal excitations are the beam currents and kinetic voltages at the input and output cross-sections of the gaps. Furthermore, we shall find that the two-port is reciprocal only if the beam loading G_e vanishes, in which case the two-port can be represented by a passive, reciprocal network consisting of transmission-line sections and lumped resonant circuits.

5.2 Launching of space-charge waves by extended modulation gaps

The situation which we shall first study is shown schematically in Fig 5.1, and applies for instance to the input gap of a klystron. An interaction gap of arbitrary length and with arbitrary longitudinal RF field distribution is traversed by a beam having zero initial kinetic voltage and current modulations at the input cross-section of the gap, i e at the position $x = -\ell/2$.

The modulation imposed on the beam due to the longitudinal RF gap field can be found from Eqs (2.54) and (2.55), setting $p=1$ and $I(0) = U(0) = 0$. The modulations at some position beyond the gap region, $x \geq \ell/2$, are given by

$$U(x) = V \not{S}\left[e^{-j\beta_e x} M(\beta_e)\right] \tag{5.1}$$

$$I(x) = -\frac{V}{W} \Delta\left[e^{-j\beta_e x} M(\beta_e)\right] \tag{5.2}$$

where V is the RF gap voltage defined by Eq (2.50) or (2.52), and $M(\beta_e)$ is the gap coupling coefficient defined by Eq (2.53).

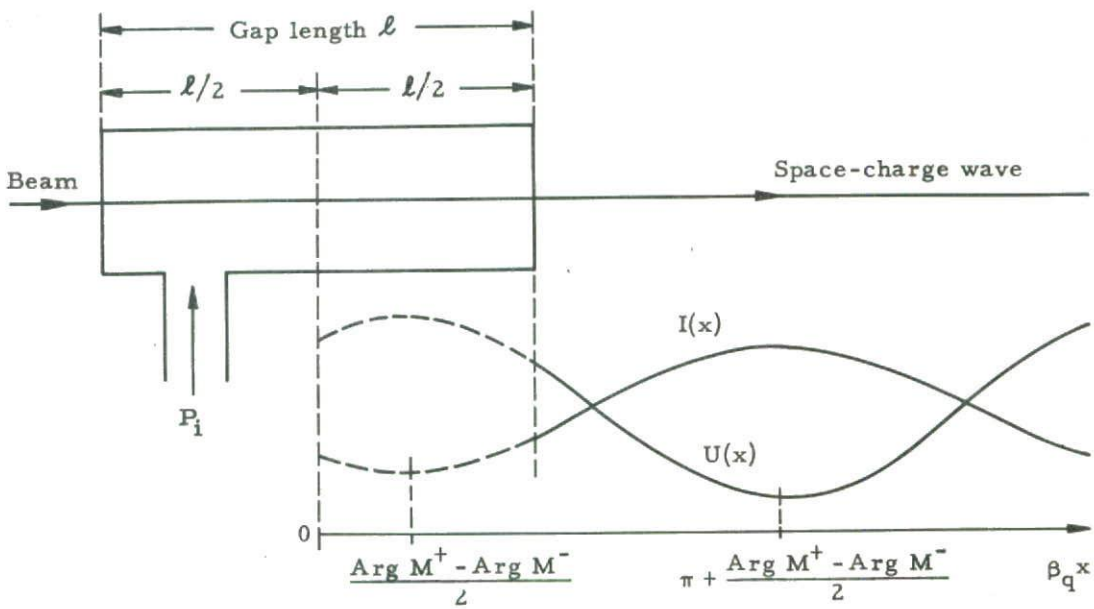

Fig 5.1 Modulation of a beam in a single extended interaction gap

If we rewrite Eqs (5.1) and (5.2) using the definitions (2.38) and (2.39) of the sum and the difference operators $\not{S}$ and Δ, we obtain

$$U(x) = \frac{V}{2} e^{-j\beta_e x}\left(M^- e^{j\beta_q x} + M^+ e^{-j\beta_q x}\right) \tag{5.3}$$

$$I(x) = \frac{V}{2W} e^{-j\beta_e x}\left(M^- e^{j\beta_q x} - M^+ e^{-j\beta_q x}\right) \tag{5.4}$$

where M^+ and M^- are the coupling coefficients of the slow and the fast space-charge waves defined in Eq (2.58). In general, the coupling coefficients are complex, and if we write

$$M^+ = M_o^+ e^{jArgM^+}, \tag{5.5}$$

$$M^- = M_o^- e^{jArgM^-}, \tag{5.6}$$

where M_o^+ and M_o^- are absolute values, we find

$$U(x)\,U(x)^* = \frac{VV^*}{2}\left[\frac{(M_o^+)^2 + (M_o^-)^2}{2} + M_o^+ M_o^- \cos(2\beta_q x - \mathrm{Arg}\,M^+ + \mathrm{Arg}\,M^-)\right] \tag{5.7}$$

$$I(x)\,I(x)^* = \frac{VV^*}{2W^2}\left[\frac{(M_o^+)^2 + (M_o^-)^2}{2} - M_o^+ M_o^- \cos(2\beta_q x - \mathrm{Arg}\,M^+ + \mathrm{Arg}\,M^-)\right] \tag{5.8}$$

As shown in Fig 5.1, the periodically repeated maxima of $|U(x)|$ and minima of $|I(x)|$ occur at the positions for which the cosine term in Eqs (5.7) and (5.8) is equal to plus one.

$$\beta_q x = k\pi + \frac{\mathrm{Arg}\,M^+ - \mathrm{Arg}\,M^-}{2}\,, \qquad k = 0, 1, 2, 3 \text{ ---} \tag{5.9}$$

The minima of $|U(x)|$ and maxima of $|I(x)|$ are shifted $\pi/2$, occurring at

$$\beta_q x = (k+\tfrac{1}{2})\pi + \frac{\mathrm{Arg}\,M^+ - \mathrm{Arg}\,M^-}{2}\,, \qquad k = 0, 1, 2, 3 \text{ ---} \tag{5.10}$$

The maxima and minima are given by

$$|U(x)|_{max} = |V|\,\frac{M_o^+ + M_o^-}{2} \tag{5.11}$$

$$|U(x)|_{min} = |V|\left|\frac{M_o^+ - M_o^-}{2}\right| \tag{5.12}$$

$$|I(x)|_{max} = \frac{|V|}{W}\,\frac{M_o^+ + M_o^-}{2} \tag{5.13}$$

$$|I(x)|_{min} = \frac{|V|}{W}\left|\frac{M_o^+ - M_o^-}{2}\right| \tag{5.14}$$

The launching of the fundamental pair of space-charge waves on a stream by a single modulation gap is fully described by Eqs (5.1) through (5.14). Comparison of the general results derived in this analysis with conventional narrow-gap klystron theory brings out some important differences which are due to the fact that the latter operates with only one coupling coefficient. Unless $M^+ = M^-$, corresponding to zero beam loading (see Eq (2.70)), the two space-charge waves are excited with different amplitudes, and the space-charge standing-wave pattern behind the modulation gap is characterized by the fact that the velocity modulations or the current modulations of the two waves never cancel completely, but leave resulting minimum modulations proportional to the difference between the coupling coefficients. This, of course, is in accordance with power conservation principles for longitudinal beams, discussed in Section 2.7. It should also be noted that two different modulation gaps, one with positive beam loading, $M_o^- > M_o^+$, and the other with negative beam loading, $M_o^+ > M_o^-$, can launch space-charge waves having

identical space-charge standing-wave patterns. In the first case the net kinetic energy flow is positive, in the second case negative. A knowledge of the standing-wave patterns of I(x) and U(x) is therefore not sufficient for a complete specification of the space-charge waves. In addition, the sign of the net energy flow must be known.

If we imagine that the standing-wave pattern is extrapolated back into the modulation region, a correct representation is obtained by assuming an infinitely narrow hypothetical gap located near the center at the position corresponding to $k = 0$ in Eq (5.9). This hypothetical gap, then, imposes a velocity modulation given by Eq (5.11) and, in addition, a small current modulation given by Eq (5.14). The current modulation is neglected in the conventional narrow-gap klystron theory. For narrow gaps the approximation involved is, of course, quite small, because the two coupling coefficients are approximately equal.

Nevertheless, the fact that for non-zero beam loading the periodic minima of the fundamental space-charge modulation are never zero is worth while noticing in some types of experimental work involving exploration of space-charge waves by sliding a cavity along the electron beam for measurement of the standing-wave pattern. Obviously, great care should be observed in drawing any conclusion as to the cause of observed non-vanishing minima, because these may be due partly to the effect described above arising from non-zero beam loading of the modulation gap, and partly to higher-order space-charge modes launched on the beam in addition to the pair of fundamental space-charge waves discussed in this report.

5.3 Characteristics of modulation gaps with coupling to one of the space-charge waves. Fast-wave cavity couplers

We shall here discuss the special situations arising when one of the two coupling coefficients M^+ or M^- vanishes. If M^+ is zero and M^- different from zero we obtain a case of considerable practical interest in connection with low-noise beam parametric amplifiers based on fast space-charge wave interaction (24). The modulation gap then serves as a fast-wave coupler, exciting only the fast space-charge wave. From Eqs (5.3) and (5.4) the kinetic voltage $U(x)$ and the current $I(x)$ excited by a fast-wave coupler are given by

$$U(x)^- = \frac{V}{2} M^- e^{-j(\beta_e - \beta_q)x} \tag{5.15}$$

$$I(x)^- = \frac{V}{2W} M^- e^{-j(\beta_e - \beta_q)x} \tag{5.16}$$

or

$$U(x)^- = W\, I(x)^- \tag{5.17}$$

which has the characteristics of a pure traveling wave in which the current and the kinetic voltage are in phase everywhere. The positive beam loading of the

gap launching the fast wave equals the positive RF kinetic power P^- carried in the forward direction by the fast wave.

$$P^- = \frac{1}{2} W I^- I^{-*} = \frac{1}{8W} M^- M^{-*} V V^* \tag{5.18}$$

Conversely, if M^- is zero and M^+ different from zero, the gap is a slow-wave coupler exciting the slow wave only. In this case the modulations are given by

$$U(x)^+ = \frac{V}{2} M^+ e^{-j(\beta_e + \beta_q)x} \tag{5.19}$$

$$I(x)^+ = \frac{-V}{2W} M^+ e^{-j(\beta_e + \beta_q)x} \tag{5.20}$$

or

$$U(x)^+ = - W I(x)^+ \tag{5.21}$$

The wave launched by this slow-wave coupler also is a pure traveling wave in which the current and the kinetic voltage are in opposite phase everywhere. The negative beam loading of the gap equals the negative RF kinetic power P^+ carried in the forward direction by the slow wave.

$$P^+ = - \frac{1}{2} W I^+ I^{+*} = - \frac{1}{8W} M^+ M^{+*} V V^* \tag{5.22}$$

Evidently both fast and slow-wave couplers can be realized using extended-interaction cavities for which either M^+ or M^- in general can be made zero by proper choice of DC beam voltage. In order to see this, let us assume that the Fourier transform of the longitudinal electric field, i e the gap coupling coefficient $M(\beta_e)$ defined by Eq (2.53), is zero at $\beta_e = \beta_{e,o}$. By a slight increase in beam velocity, as specified below, we obtain:

$$\begin{aligned} M^+ &= M(\beta_e + \beta_q) = 0 \\ M^- &= M(\beta_e - \beta_q) \neq 0 \end{aligned} \qquad \text{for } \beta_e = \beta_{e,o} - \beta_q \tag{5.23}$$

In this case the gap acts as a fast-wave coupler. On the other hand, a slight decrease in beam velocity, as specified below, leads to the following relations:

$$\begin{aligned} M^- &= M(\beta_e - \beta_q) = 0 \\ M^+ &= M(\beta_e + \beta_q) \neq 0 \end{aligned} \qquad \text{for } \beta_e = \beta_{e,o} + \beta_q \tag{5.24}$$

In this case the same gap acts as a slow-wave coupler. Examples of such couplers with sinusoidal RF field distributions are given in Section 5.12.2.

For efficient operation of a fast-wave coupler of the cavity-type discussed here, the signal generator would have to be appropriately matched to the coupler such that reflections would not occur. If this matching condition is satisfied, the input

cavity serves as a perfect coupler between the generator and the beam. In the ideal coupler all the input power P_i is transferred to the fast space-charge wave on the beam as shown schematically in Fig 5.2. In a practical coupler some small fraction of the power would be dissipated as losses in the coupler itself. The required optimum coupling is readily determined using the general equations derived in Section 3.11, relating the unloaded cavity Q, the external Q, the characteristic impedance R_{sh}/Q, and the electronic conductance G_e. For a coupler with loss, the optimum coupling for perfect match between the generator and coupler is specified by the following relation derived from Eq(3.82):

$$\left(\frac{R_{sh}}{Q}\right) G_e = \frac{1}{Q_{ext}} - \frac{1}{Q} \tag{5.25}$$

The input power P_i is divided between circuit loss P_c and beam loading power P^- transferred to the fast space-charge wave. The ratio between these is given by

$$\frac{P_c}{P^-} = \frac{Q_{ext}}{Q - Q_{ext}} = \frac{1}{R_{sh} G_e} \tag{5.26}$$

For an ideal lossless coupler the ratio P_c/P^- is zero. This situation evidently is approached if the beam loading conductance G_e is considerably higher than the unloaded circuit conductance $1/R_{sh}$. In this case $P_i \approx P^-$ if the external Q is adjusted to its optimum value given by

$$Q_{ext} \approx Q_L = \frac{1}{G_e (R_{sh}/Q)} \tag{5.27}$$

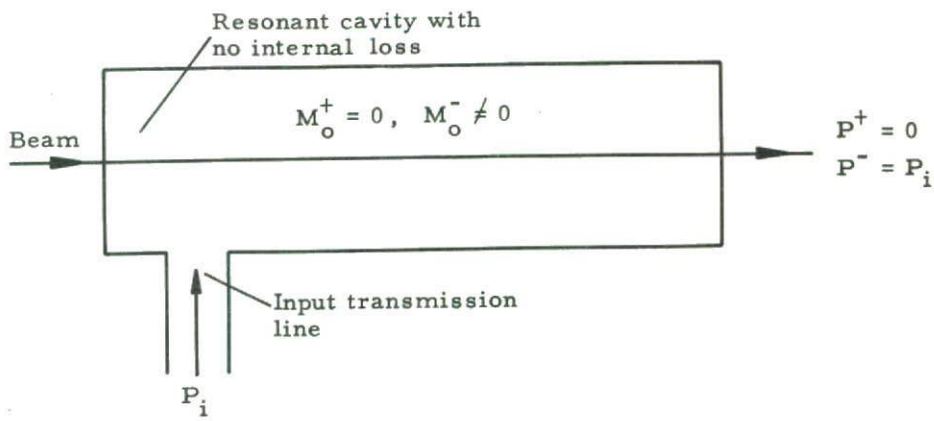

Fig 5.2 Schematic diagram of the power relationship in an ideal fast-wave coupler of the cavity-type characterized by $M_o^+ = 0$, $M_o^- \neq 0$

All the input power P_i is transferred to positive kinetic power P^- associated with the fast space-charge wave propagating on the beam:

$$P^- \approx P_i = \frac{1}{8W} M^- M^{-*} V V^* \tag{5.28}$$

The kinetic voltage $U(x)$ and the current $I(x)$ of the fast wave excited by the coupler are given by Eqs (5.15) and (5.16), respectively.

5.4 Excitation of an extended-interaction cavity by a modulated beam

We shall here study the converse problem, namely the small-signal excitation of a cavity by an electron beam modulated in the fundamental space-charge mode. The configuration to be studied is shown schematically in Fig 5.3 and may, for instance, refer to the output cavity of a klystron.

The RF kinetic voltage and current modulations at the input and output cross-sections of the gap are U_1, I_1 and U_2, I_2, respectively.

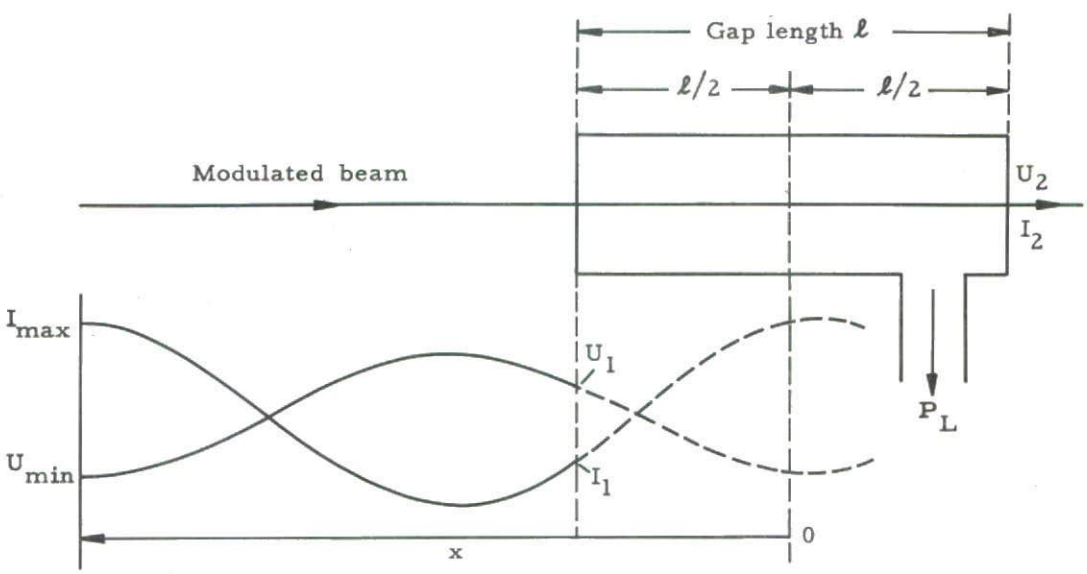

Fig 5.3 Excitation of an extended interaction cavity by a modulated beam

Again using some of the results from Chapters 2 and 3 we shall determine:

a) The induced RF gap voltage V in terms of the input modulations U_1 and I_1 or some suitable linear combinations of these

b) The output modulations U_2, I_2 in terms of the input modulations U_1 and I_1

The last relation determines the two-port matrix of an interaction gap of the general type analyzed here.

From Eqs (2.71) and (3.1), setting p = 1, we obtain the following relation between the induced gap voltage V and the input modulations U_1 and I_1:

$$V = -\frac{1}{Y}\left[I_1 \not{S}\left(M^* e^{-j\beta_e \ell/2}\right) - \frac{U_1}{W}\Delta\left(M^* e^{-j\beta_e \ell/2}\right)\right] \tag{5.29}$$

Rather than expressing V in terms of the input modulations I_1 and U_1 we shall rewrite V in terms of the modulations I(x) and U(x) at the arbitrary position x. This reference position can be chosen either outside or within the interaction region, if in the last case I(x) and U(x) are the original modulations that would exist on the beam if the interaction region were removed. The transformations from I_1 and U_1 to I(x) and U(x) are simply affected by means of the relations expressed in Eq (2.54) and (2.55) for the special case that p=0 (pure drift action). We obtain

$$V = -\frac{1}{Y}\left[I(x) \not{S}\left(M^* e^{j\beta_e x}\right) - \frac{U(x)}{W}\Delta\left(M^* e^{j\beta_e x}\right)\right] \tag{5.30}$$

where x as before is measured from the center of the gap. In Eqs (5.29) and (5.30) Y is the self-admittance of the cavity, i e the sum of the circuit admittance Y_c and the electronic admittance Y_e.

If the cavity is moved axially along the beam, the induced gap voltage V will vary periodically with x in accordance with the periodic modulation U(x) and I(x) on the beam. The fact that the induced gap voltage V is a linear combination of both the current I(x) and the kinetic voltage U(x), rather than being a function of the current alone, has some important implications, which we shall discuss in the following. In this discussion it will be convenient to let x refer to one of the positions for which the current is maximum (or the kinetic voltage is minimum) as shown in Fig 5.3. We shall then have to put $I(x) = I_{max}$ and $U(x) = U_{min}$ in Eq (5.30). For evaluation of the induced voltage V it will be useful to state some relations between I_{max}, I_{min}, U_{max} and U_{min} that follow immediately from Eqs (5.3) through (5.14)

$$|U|_{max} = W\,|I|_{max} \tag{5.31}$$

$$|U|_{min} = W\,|I|_{min} \tag{5.32}$$

If the amplitude of the fast space-charge wave exceeds that of the slow wave, we have

$$\mathrm{Re}\,(I_{max}\,U^*_{min}) = W\,|I|_{max}\,|I|_{min} \tag{5.33}$$

In the opposite case, if the slow wave dominates,

$$\mathrm{Re}\,(I_{max}\,U^*_{min}) = -W\,|I|_{max}\,|I|_{min} \tag{5.34}$$

In both cases

$$\mathrm{Im}\,(I_{max}\,U^*_{min}) = \mathrm{Im}\,(I_{min}\,U^*_{max}) = 0 \tag{5.35}$$

Multiplying Eq (5.30) by its complex conjugate and using the relations above, we find after performing some algebraic manipulations

$$VV^* = \frac{I}{YY^*}\left\{\left[|I|_{max}\frac{M_o^+ + M_o^-}{2} \mp |I|_{min}\frac{M_o^+ - M_o^-}{2}\right]^2 - \left[|I|_{max}^2 - |I|_{min}^2\right] M_o^+ M_o^- \sin^2\left(\beta_q x - \frac{\text{Arg}\, M^+ - \text{Arg}\, M^-}{2}\right)\right\} \qquad (5.36)$$

where the upper and lower signs apply when the net energy flow on the beam is positive or negative, respectively. In this equation the square of the induced gap voltage is expressed in terms of the two modulation variables represented by the current maximum and the current minimum rather than the current and the kinetic voltage. Again, it is important to notice that the space-charge waves are not fully determined by $|I|_{max}$ and $|I|_{min}$ and their positions, i e the standing-wave pattern of the current. The sign of the energy flow must also be specified.

The exploration of space-charge standing-wave pattern on a longitudinal beam by means of a cavity that can be moved along the beam can now be discussed using Eq (5.36). The periodic maxima and minima of the observed power (proportional to VV^*) occur at the positions x_1 and x_2 given by

$$\beta_q x_1 = k\pi + \frac{\text{Arg}\, M^+ - \text{Arg}\, M^-}{2}, \qquad k = 0, \pm 1, \pm 2 \text{ ---} \qquad (5.37)$$

$$\beta_q x_2 = (k+\tfrac{1}{2})\pi + \frac{\text{Arg}\, M^+ - \text{Arg}\, M^-}{2}, \qquad k = 0, \pm 1, \pm 2 \text{ ---} \qquad (5.38)$$

for the maxima and minima, respectively. The periodic maxima and minima are obtained from Eq (5.36) by substitution of x_1 and x_2 from Eqs (5.37) and (5.38), and taking the square roots of the resulting expressions. We find

$$|V|_{max} = \frac{1}{|Y|}\left(|I|_{max}\frac{M_o^+ + M_o^-}{2} \mp |I|_{min}\frac{M_o^+ - M_o^-}{2}\right) \qquad (5.39)$$

$$|V|_{min} = \frac{1}{|Y|}\left|\,|I|_{max}\frac{M_o^+ - M_o^-}{2} \mp |I|_{min}\frac{M_o^+ + M_o^-}{2}\,\right| \qquad (5.40)$$

In the expression for $|V|_{min}$ we shall have to use the absolute value of the right-hand side because the expression may become negative when M_o^- is larger than M_o^+, i e by positive beam loading in the gap.

Again, the upper and lower signs in Eqs (5.39) and (5.40) refer to the cases for which the net energy flow on the beam is positive and negative, respectively.

The conclusions that can be drawn from examining Eqs (5.39) and (5.40) are the following:

a) For the general case in which M_o^+ and M_o^- are different, the induced maximum and minimum voltage $|V|_{max}$ and $|V|_{min}$ are linear combinations of the maximum and minimum RF beam current $|I|_{max}$ and $|I|_{min}$, and depend, furthermore, on the sign of the net energy flow on the beam.

b) Only in the special case for which the beam loading is zero ($M_o^+ = M_o^- = M_o$) are the beam current maxima and minima simply related to the observed gap voltage maxima and minima, respectively. Because in this case $Y_e = 0$, $Y = Y_c$, we have

$$|V|_{max} = \frac{1}{|Y_c|} M_o |I|_{max} \tag{5.41}$$

$$|V|_{min} = \frac{1}{|Y_c|} M_o |I|_{min} \tag{5.42}$$

This is a situation approximated to a fair degree by a narrow-gap re-entrant cavity often used for experimental exploration of space-charge waves on linear beams.

From the above analysis it also follows that the converse problem of determining the beam current maxima and minima from information obtained by measuring gap voltage maxima and minima, as the cavity is moved along the electron beam, has no unique solution in all the cases that can occur. This conclusion follows immediately if Eqs (5.39) and (5.40) are solved with respect to $|I|_{max}$ and $|I|_{min}$, proper care being taken of the various combinations of signs that can occur. The final results are conveniently listed in the following table. Here, the quantity χ characterizes the type of gap used in the observation of the space-charge wave pattern. By definition

$$\chi = \frac{M_o^- - M_o^+}{M_o^- + M_o^+} \tag{5.43}$$

For a gap with positive beam loading, χ is positive, and vice versa.

Case	Observed gap voltage ratio $\lvert V\rvert_{min}/\lvert V\rvert_{max}$	Characteristics of the space-charge waves	
		Sign of beam energy flow	Appropriate formulae for beam current standing-wave ratio expressed in terms of the observed gap voltage ratio
I	$0 \leq \frac{\lvert V\rvert_{min}}{\lvert V\rvert_{max}} \leq 1$	Sign $(-\chi)$	$\frac{\lvert I\rvert_{min}}{\lvert I\rvert_{max}} = \frac{\lvert\chi\rvert + \lvert V\rvert_{min}/\lvert V\rvert_{max}}{1 + \lvert\chi\rvert\lvert V\rvert_{min}/\lvert V\rvert_{max}}$
II	$0 \leq \frac{\lvert V\rvert_{min}}{\lvert V\rvert_{max}} \leq \lvert\chi\rvert$	Sign $(-\chi)$	$\frac{\lvert I\rvert_{min}}{\lvert I\rvert_{max}} = \frac{\lvert\chi\rvert - \lvert V\rvert_{min}/\lvert V\rvert_{max}}{1 - \lvert\chi\rvert\lvert V\rvert_{min}/\lvert V\rvert_{max}}$
III	$\lvert\chi\rvert \leq \frac{\lvert V\rvert_{min}}{\lvert V\rvert_{max}} \leq 1$	Sign $(+\chi)$	$\frac{\lvert I\rvert_{min}}{\lvert I\rvert_{max}} = \frac{\lvert V\rvert_{min}/\lvert V\rvert_{max} - \lvert\chi\rvert}{1 - \lvert\chi\rvert\lvert V\rvert_{min}/\lvert V\rvert_{max}}$

Table 5.1 Possible space-charge waves associated with the gap voltage ratio $|V|_{min}/|V|_{max}$ as observed with a gap specified by the gap parameter $\chi = (M_o^- - M_o^+)/(M_o^- + M_o^+)$

The use of the table is quite simple. The first column lists the three possible cases that can occur, determined by the relative magnitudes of the observed gap voltage ratio and the presumably known absolute value of the gap parameter χ, as indicated by the second column. The third and fourth columns give the sign of the beam energy flow and the appropriate formulae for evaluation of the current standing-wave ratio.

The conclusions which can be drawn from a study of Table 5.1 are the following:

a) Unambiguous determination of the beam current standing-wave ratio from the observed gap voltage ratio $|V|_{min}/|V|_{max}$ is not possible in the general case with χ different from zero. For a given gap (χ given) there exist in general two different space-charge waves with different current standing-wave ratios giving rise to the same gap voltage ratio $|V|_{min}/|V|_{max}$. The first of these is always the wave listed in Table 5.1 as case I; the second is one of the two waves listed as case II or case III depending on the relative magnitudes of the observed $|V|_{min}/|V|_{max}$ and the presumably known absolute value of χ.

b) If we have a priori knowledge of the sign of the beam energy flow, unambiguous determination of the current standing-wave ratio from the observed gap voltage ratio is possible by proper choice of gap. By arranging matters such that the gap parameter χ and the energy flow have the same sign, the wave listed as case III in Table 5.1 evidently represents the only possible space-charge wave associated with a given gap voltage ratio. Therefore, we may conclude that in order to avoid ambiguous results, a beam having positive energy flow should be explored with a gap having positive χ, i e positive beam loading, and vice versa.

c) Unambiguous determination of beam current standing-wave pattern is always possible by choosing a gap having zero beam loading, i e $\chi = 0$. This, however, seems very difficult to achieve in practice. In this connection it should be pointed out that the neglect of beam loading in narrow-gap conventional klystron cavities, which probably are the types of cavities that have been used most extensively for exploration of current standing-wave pattern on linear beams, in many cases leads to entirely incorrect results as shown in the example below. The results of such measurements should therefore be interpreted with great care.

A numerical example will serve to illustrate the statement given above. Assume a conventional klystron cavity for which the gap coupling coefficient is given by $M = \sin(\theta/2)/(\theta/2)$ where $\theta = \beta_e \ell$ is the gap transit angle. Evaluation of the parameter χ from the defining equation (5.43) yields the curve shown in Fig 5.4, where the calculated ratio $\chi/(\omega_q/\omega)$ is plotted vs the gap transit angle θ. If we choose θ equal to π, which is a reasonable value, χ will be exactly equal to the space-charge parameter ω_q/ω, whose magnitude is far from negligible. Let us assume that $\omega_q/\omega = \chi = 0.1$, and that the gap voltage ratio observed by sliding the cavity along the modulated beam is $|V|_{min}/|V|_{max} = 0.1$. From Table 5.1 the space-charge wave giving rise to this gap voltage ratio may be either one of the following:

i) A wave carrying negative energy listed as Case I in the table, with current standing wave ratio

$$\frac{|I|_{min}}{|I|_{max}} = 0.198 \qquad (5.44)$$

ii) A wave carrying zero energy with current standing wave ratio

$$\frac{|I|_{min}}{|I|_{max}} = 0 \qquad (5.45)$$

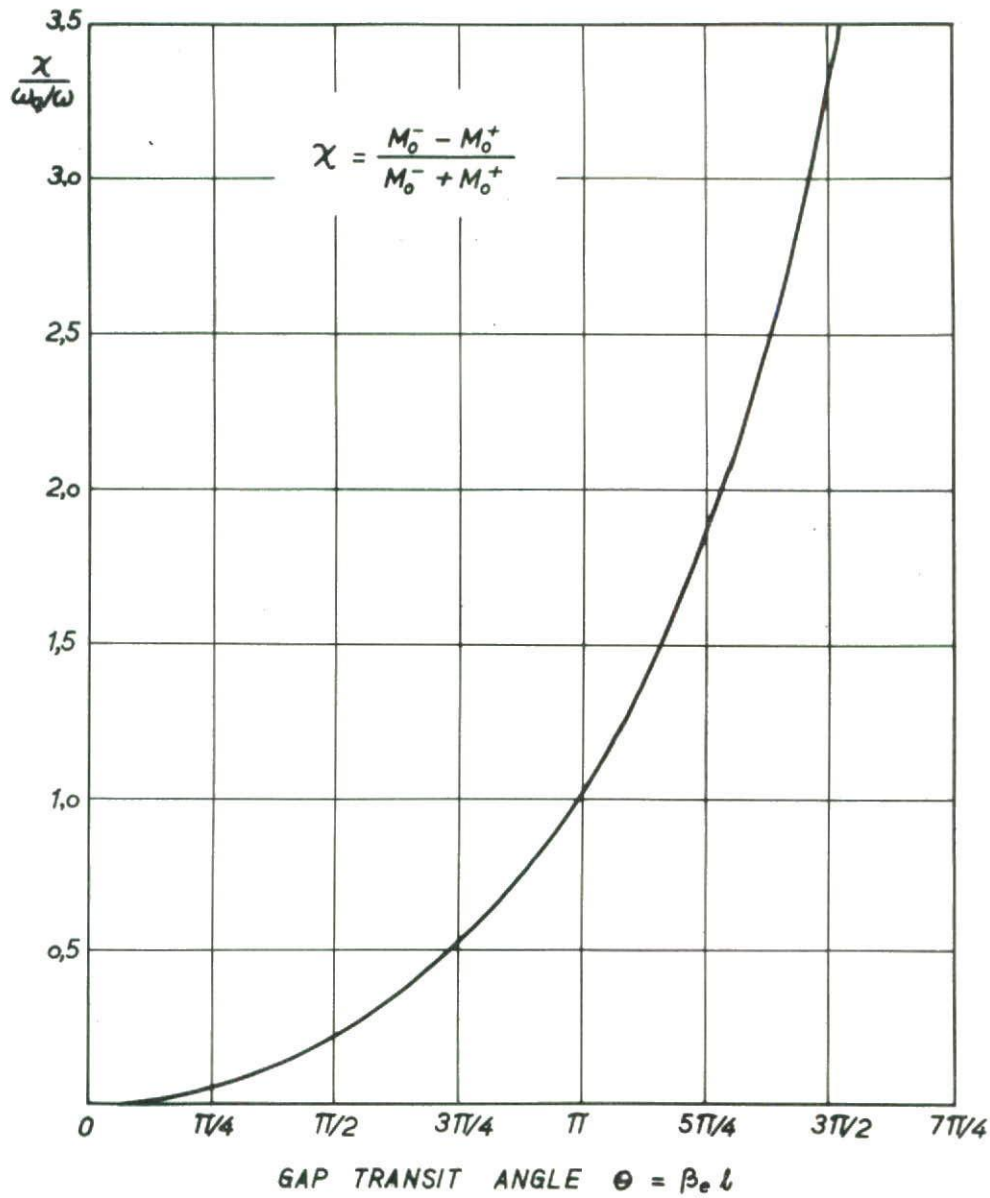

Fig 5.4 Curve showing the parameter $\chi/(\omega_q/\omega)$ for a conventional narrow-gap cavity plotted vs the gap transit angle θ

The actual space-charge wave on the beam may be either one of the waves i) and ii). For neither of these does the current standing-wave pattern correspond to the observed gap voltage ratio. The discrepancy is particularly large if the magnitudes of χ and $|V|_{min}/|V|_{max}$ are approximately the same as in this example.

The discussion clearly shows that great care should be observed in interpreting data from such measurements. The simple conventional theory is quite insufficient and may lead to appreciable errors even if conventional narrow gap cavities are used. Reported discrepancies between theoretically predicted noise standing-wave pattern on a drifting beam, subject to transformations by passive beam transducers, and experimental measurements are often ascribed to higher order space-charge modes not accounted for in the one-dimensional model of the beam (26.27). It appears possible that the observed discrepancies, which are particularly pronounced for small values of $|I|_{min}/|I|_{max}$, at least in part may be due to misinterpretation of experimental data caused by the effect discussed above.

5.5 Excitation of fast-wave cavity couplers by a modulated beam

In supplement to the study made in Section 5.3 of beam modulation by fast-wave cavity couplers, we shall here deal with excitation of a fast-wave coupler by a modulated beam, as shown schematically in Fig 5.5. The fast-wave coupler is characterized by having $M_o^+ = 0$ and $M_o^- \neq 0$. Thus, a possible slow-wave component on the beam propagates through the coupler without contributing to the induced voltage, as is easily verified using Eqs (5.30) and (5.21). We need therefore consider only the fast-wave modulations $U(x)^-$ and $I(x)^-$ given by Eqs (5.15) and (5.16).

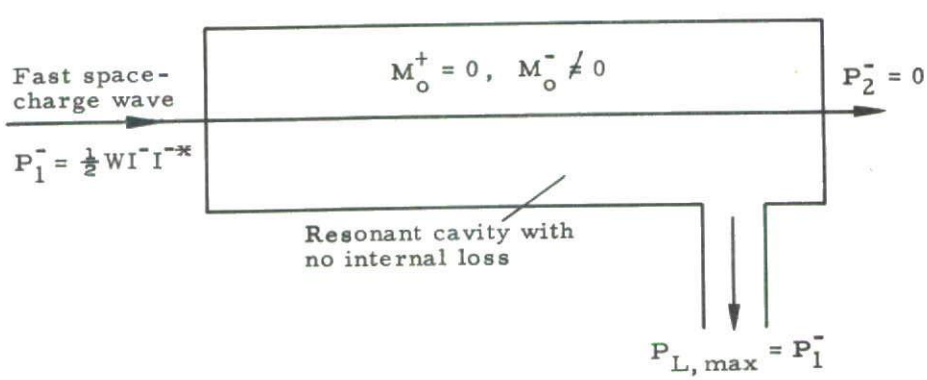

Fig 5.5 Schematic diagram of the power relations in an ideal fast-wave output cavity coupler for which $M_o^+ = 0$, $M_o^- \neq 0$

The induced gap voltage, evaluated from Eq (5.30) for the special case at hand, is given by

$$V = -\frac{1}{Y} M^{*-} I(x)^{-} e^{j(\beta_e - \beta_q)x} \tag{5.46}$$

The useful power output dissipated in the external load is related to the gap voltage V through Eq (3.85)

$$P_L = \frac{1}{2} VV^* \left(\frac{Q}{R_{sh}}\right) \frac{1}{Q_{ext}} \tag{5.47}$$

where R_{sh}/Q is the characteristic impedance of the cavity and Q_{ext} is the external Q. Substitution of V from Eq (5.46) yields

$$P_L = \frac{1}{2} \left| \frac{M^{-} I(x)^{-}}{Y} \right|^2 \left(\frac{Q}{R_{sh}}\right) \frac{1}{Q_{ext}} \tag{5.48}$$

Remembering that Y is the sum of the circuit admittance Y_c and the electronic admittance Y_e, the optimum value of Q_{ext} maximizing the output power P_L is readily determined. We find that the optimum coupling at resonance for maximum output power is the same as the optimum coupling (5.25) for maximum transfer of power from the generator to the beam for the input fast-wave coupler:

$$\left(\frac{R_{sh}}{Q}\right) G_e = \left(\frac{1}{Q_{ext}}\right)_{opt} - \frac{1}{Q} \tag{5.49}$$

Substitution in Eq (5.48) yields the maximum power in the external load expressed in terms of the initial kinetic beam power P_1^{-}.

$$(P_L)_{max} = P_1^{-} \left[1 - \frac{(Q_{ext})_{opt}}{Q}\right] \tag{5.50}$$

A small fraction P_2^{-} of the initial kinetic beam power P_1^{-} remains as a small fast-wave modulation on the beam after the output coupler. Using Eqs (5.46) and (5.57) we find

$$P_2^{-} = P_1^{-} \left[\frac{(Q_{ext})_{opt}}{Q}\right]^2 \tag{5.51}$$

Another small fraction P_c of the initial kinetic power is dissipated in the coupler itself due to its internal losses:

$$P_c = P_1^{-} \left[\frac{(Q_{ext})_{opt}}{Q} - \frac{(Q_{ext})_{opt}}{Q}\right]^2 \tag{5.52}$$

It is noted that the relation $P_1^{-} + P_L + P_c = P_2^{-}$, required by the small-signal power theorem (2.84), is satisfied by these expressions. If the product $G_e R_{sh}/Q$ is suf-

ficiently large, the optimum condition (5.49) shows that $Q_{ext}/Q \ll 1$. In this case a practical coupler approaches the ideal coupler shown in Fig 5.5 in which the entire kinetic power P_1^- is transferred to the external load, the remaining kinetic power P_2^- after the coupler being zero. Returning again to the general case with lossy couplers, we note that although the maximum output power is transferred to the external load if Q_{ext} satisfies the condition stated in Eq (5.49), a slightly different load will maximize the total power dissipated in the external load plus the coupler itself. In this case the beam will be matched completely to the coupler, and the initial fast-wave kinetic power in its entirety is transferred to the circuit. This situation arises if

$$\frac{R_{sh}}{Q} G_e = \frac{1}{Q_L} \tag{5.53}$$

Then we have

$$P_L + P_c = P_1^- \tag{5.54}$$

$$P_2^- = 0 \tag{5.55}$$

Obviously, an amplifier based on fast-wave interaction consisting for instance of the input coupler shown in Fig 5.2 and the output coupler shown in Fig 5.5 has a power gain that never exceeds unity. Otherwise the small-signal power theorem would be violated. The results of the detailed calculations done in Sections 5.3 and 5.5 are in agreement with this requirement. Gain larger than unity can be achieved through parametric amplification of the fast space-charge wave in the region between the input and output coupler (24). The additional power required for amplification is then supplied by an external RF generator, the "pump". For low-noise amplification the input fast-wave coupler serves the double purpose of simultaneously modulating the beam and removing the fast-wave noise power that exists on the beam before the input coupler. The equations derived in sections 5.3 and 5.5 show that complete removal of fast-wave noise can be achieved by a cavity-type input coupler having its loaded Q adjusted according to the relation (5.53).

For a general discussion of parametric amplifiers and fast-wave couplers different from the cavity types discussed here, such as traveling-wave couplers, the reader is referred to the literature on the subject (24, 28).

5.6 General two-port representation of extended interaction gaps

The linear relations between the beam current and the kinetic voltage modulations I_1 and U_1, I_2 and U_2 referred to the input and output cross-sections of a gap associated with a "floating" cavity can be found using Eqs (5.29), (2.54) and (2.55), setting $p = 1$ in the last two equations. We obtain

$$V = -\frac{1}{Y}\left[I_1 \, \mathcal{S}\left(M^* e^{-j\beta_e \ell/2} \right) - \frac{U_1}{W} \, \Delta\left(M^* e^{-j\beta_e \ell/2} \right) \right] \tag{5.56}$$

$$U_2 = U_1 \, \mathcal{S}\left(e^{-j\beta_e \ell}\right) - I_1 W \, \Delta\left(e^{-j\beta_e \ell}\right) + V \, \mathcal{S}\left(M\, e^{-j\beta_e \ell/2}\right) \tag{5.57}$$

$$I_2 = I_1 \, \mathcal{S}\left(e^{-j\beta_e \ell}\right) - \frac{U_1}{W} \, \Delta\left(e^{-j\beta_e \ell}\right) - \frac{V}{W} \, \Delta\left(M\, e^{-j\beta_e \ell/2}\right) \tag{5.58}$$

Substitution of the gap voltage V from Eq (5.56) in the other two equations yields two linear relations between the input and output modulations. These linear transformations of the kinetic voltage and current, taking place when the beam traverses the interaction region, can be represented by a linear two-port whose matrix relates the output and input quantities

$$\begin{bmatrix} U_2 \\ I_2 \end{bmatrix} = \begin{bmatrix} A & B \\ C & D \end{bmatrix} \begin{bmatrix} U_1 \\ I_1 \end{bmatrix} = \underset{\sim}{K} \begin{bmatrix} U_1 \\ I_1 \end{bmatrix} \tag{5.59}$$

The elements of the matrix $\underset{\sim}{K}$ follow very simply from Eqs (5.56) through (5.58). We find

$$A = \mathcal{S}\left(e^{-j\beta_e \ell}\right) + \frac{1}{WY} \, \Delta\left(M^* e^{-j\beta_e \ell/2}\right) \mathcal{S}\left(M\, e^{-j\beta_e \ell/2}\right) \tag{5.60}$$

$$B = -W \, \Delta\left(e^{-j\beta_e \ell}\right) - \frac{1}{Y} \, \mathcal{S}\left(M^* e^{-j\beta_e \ell/2}\right) \mathcal{S}\left(M\, e^{-j\beta_e \ell/2}\right) \tag{5.61}$$

$$C = -\frac{1}{W} \, \Delta\left(e^{-j\beta_e \ell}\right) - \frac{1}{W^2 Y} \, \Delta\left(M^* e^{-j\beta_e \ell/2}\right) \Delta\left(M\, e^{-j\beta_e \ell/2}\right) \tag{5.62}$$

$$D = \mathcal{S}\left(e^{-j\beta_e \ell}\right) + \frac{1}{WY} \, \Delta\left(M\, e^{-j\beta_e \ell/2}\right) \mathcal{S}\left(M^* e^{-j\beta_e \ell/2}\right) \tag{5.63}$$

For the special case of narrow symmetric gaps, similar relations have been obtained by A Bers (29) using a different approach. His results agree with the more general results of this section if we set $M^* = M$, a relation which holds for gaps having symmetric RF field distributions.

The matrix elements (5.60) through (5.63) can be interpreted in several ways as done by Bers for the case of symmetric narrow gaps. The first terms in all the elements are independent of the specific nature of the interaction gap and are the result of pure drift action between the input and output cross-sections. This drift action is equivalent to that taking place in a drift tube with metallic walls or in free space. The drift matrix is given by

$$\underset{\sim}{D} = \begin{bmatrix} A_d & B_d \\ C_d & D_d \end{bmatrix} = \begin{bmatrix} \cos \beta_q \ell & j\, W \sin \beta_q \ell \\ j \frac{1}{W} \sin \beta_q \ell & \cos \beta_q \ell \end{bmatrix} e^{-j\beta_e \ell} \tag{5.64}$$

where the drift matrix elements are determined from the identities

$$A_d = \mathcal{S}\left(e^{-j\beta_e \ell}\right) = \cos \beta_q \ell \, e^{-j\beta_e \ell} \tag{5.65}$$

$$B_d = -W \, \Delta\left(e^{-j\beta_e \ell}\right) = j W \sin \beta_q \ell \, e^{-j\beta_e \ell} \tag{5.66}$$

$$C_d = -\frac{1}{W} \Delta\left(e^{-j\beta_e \ell}\right) = j \frac{1}{W} \sin \beta_q \ell \, e^{-j\beta_e \ell} \tag{5.67}$$

$$D_d = \mathcal{S}\left(e^{-j\beta_e \ell}\right) = \cos \beta_q \ell \, e^{-j\beta_e \ell} \tag{5.68}$$

One particularly interesting representation of a general extended interaction gap is obtained by writing the gap matrix $\underset{\sim}{K}$ as a product of matrices that may be identified with drift and gap parameters, respectively. We shall assume, as shown schematically in Fig 5.6, that the drift matrices $\underset{\sim}{D}_1$ and $\underset{\sim}{D}_2$ are associated with the lengths ℓ_1 and ℓ_2 of the interaction gap $(\ell_1 + \ell_2 = \ell)$, and the matrix $\underset{\sim}{C}$ with the circuit itself.

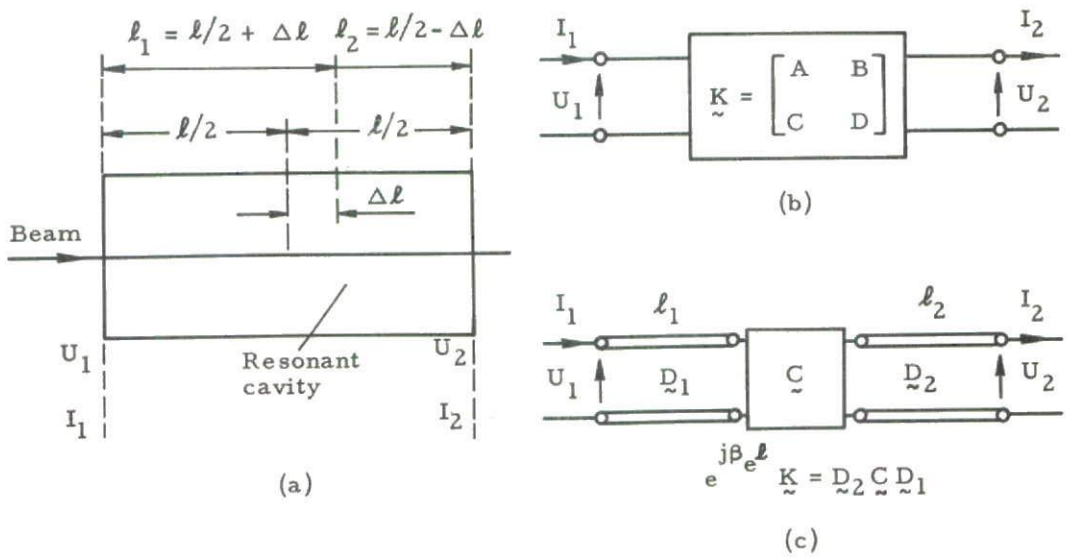

Fig 5.6 Representation of interaction gaps by linear two-ports

(a) General interaction gap of length ℓ

(b) Representation by a linear two-port with matrix $\underset{\sim}{K}$

(c) Representation by cascaded two-ports associated with drift and gap parameters

For convenience, the factor $\exp(-j\beta_e \ell)$ is taken outside the matrix product. Then, by definition

$$\underset{\sim}{K} = \underset{\sim}{D}_2 \underset{\sim}{C} \underset{\sim}{D}_1 e^{-j\beta_e \ell} \tag{5.69}$$

where, in general, $\underset{\sim}{D}_2$ and $\underset{\sim}{D}_1$ are different. They are equal only for gaps characterized by symmetric or antisymmetric field distributions. The matrices $\underset{\sim}{D}_1$ and $\underset{\sim}{D}_2$ are given by Eq (5.64) by insertion of the proper drift lengths.

$$\underset{\sim}{D}_1 = \begin{bmatrix} \cos \beta_q \ell_1 & j\, W \sin \beta_q \ell_1 \\ j \frac{1}{W} \sin \beta_q \ell_1 & \cos \beta_q \ell_1 \end{bmatrix} \tag{5.70}$$

$$\underset{\sim}{D}_2 = \begin{bmatrix} \cos \beta_q \ell_2 & j\, W \sin \beta_q \ell_2 \\ j \frac{1}{W} \sin \beta_q \ell_2 & \cos \beta_q \ell_2 \end{bmatrix} \tag{5.71}$$

where the drift lengths ℓ_1 and ℓ_2 are determined from the requirement that the gap matrix $\underset{\sim}{C}$ be independent of drift lengths. The matrix $\underset{\sim}{C}$ is obtained by premultiplication and postmultiplication of Eq (5.69) by the inverse of the drift matrices $\underset{\sim}{D}_2$ and $\underset{\sim}{D}_1$, respectively:

$$\underset{\sim}{C} = \underset{\sim}{D}_2^{-1} \underset{\sim}{K} \underset{\sim}{D}_1^{-1} e^{j\beta_e \ell} \tag{5.72}$$

If

$$\underset{\sim}{C} = \begin{bmatrix} C_{1,1} & C_{1,2} \\ C_{2,1} & C_{2,2} \end{bmatrix}, \tag{5.73}$$

equation (5.72) yields

$$C_{1,1} = 1 - \frac{1}{Y} G_e + \frac{j}{2WY} \operatorname{Im}\left(M^- M^{+*} e^{j\beta_q (\ell_1 - \ell_2)} \right) \tag{5.74}$$

$$C_{1,2} = -\frac{1}{4Y} \left[M^+ M^{+*} + M^- M^{-*} + 2 \operatorname{Re}\left(M^- M^{+*} e^{j\beta_q (\ell_1 - \ell_2)} \right) \right] \tag{5.75}$$

$$C_{2,1} = -\frac{1}{4YW^2} \left[M^+ M^{+*} + M^- M^{-*} - 2 \operatorname{Re}\left(M^- M^{+*} e^{j\beta_q (\ell_1 - \ell_2)} \right) \right] \tag{5.76}$$

$$C_{2,2} = 1 - \frac{1}{Y} G_e - \frac{j}{2WY} \operatorname{Im}\left(M^- M^{+*} e^{j\beta_q (\ell_1 - \ell_2)} \right) \tag{5.77}$$

The gap coupling coefficients M^- and M^+ appearing in these equations are, in general, complex. Let

$$M^- = M_o^- e^{j \operatorname{Arg} M^-} \tag{5.78}$$

$$M^+ = M_o^+ e^{j \operatorname{Arg} M^+} \tag{5.79}$$

where M_o^- and M_o^+ are the absolute values of M^- and M^+. Using these relations, we find that the elements of the matrix $\underset{\sim}{C}$ are independent of the lengths ℓ_1 and ℓ_2 if these are chosen in accordance with the relation

$$\beta_q(\ell_1 - \ell_2) = \operatorname{Arg} M^+ - \operatorname{Arg} M^- \tag{5.80}$$

Then

$$C_{1,1} = C_{2,2} = 1 - \frac{1}{Y} G_e \tag{5.81}$$

$$C_{1,2} = -\frac{1}{Y}\left(\frac{M_o^+ + M_o^-}{2}\right)^2 = -\frac{1}{Y}\bar{M}^2 \tag{5.82}$$

$$C_{2,1} = \frac{1}{YW^2}\left(\frac{M_o^+ - M_o^-}{2}\right)^2 = -\frac{1}{Y}\frac{G_e^2}{\bar{M}^2} \tag{5.83}$$

where $\bar{M}$ is the arithmetic mean of the coupling coefficients M_o^+ and M_o^-, and G_e is the beam loading. Hence, the two-port in Fig 5.6c representing the gap parameters has the matrix

$$\underset{\sim}{C} = \begin{bmatrix} 1 - \frac{1}{Y} G_e & -\frac{1}{Y}\bar{M}^2 \\ -\frac{1}{Y}\frac{G_e^2}{\bar{M}^2} & 1 - \frac{1}{Y} G_e \end{bmatrix} \tag{5.84}$$

which is identical with the result obtained by Bers (29) for a symmetric, narrow gap, for which both M^+ and M^- are real, and therefore $\ell_1 = \ell_2$.

The analysis done in this section shows that also an arbitrary, extended interaction gap can be represented by the chain of two-ports shown in Fig 5.6c. The two-ports represented by the drift matrices $\underset{\sim}{D}_1$ and $\underset{\sim}{D}_2$ are associated with pure drift action through the drift lengths ℓ_1 and ℓ_2, the sum of which is equal to the length ℓ of the interaction gap. These matrices, except for opposite signs in the off-diagonal elements, are analogous to the matrices relating the line voltage and line current of lossless transmission lines. In fact, by a trivial sign transformation of the variable U they become identical.

The gap matrix $\underset{\sim}{C}$ is specified entirely by the circuit parameters $Y = Y_c + Y_e$, $\bar{M}^2$, and G_e, representing the self-admittance, the square of the mean coupling coefficient, and the beam loading, respectively.

5.7 Representation of interaction gaps by passive networks

The question whether the cascaded two-ports associated with the general interaction gap shown in Fig 5.6 can be represented by passive, reciprocal networks cannot be answered without a closer investigation. It turns out that such a repre-

sentation is possible for the drift matrices $\underset{\sim}{D}_1$ and $\underset{\sim}{D}_2$ but not for the gap matrix $\underset{\sim}{C}$ except in the special case for which the beam loading is zero. If we consider reciprocity first, obviously the two-ports representing the drift-matrices $\underset{\sim}{D}_1$ and $\underset{\sim}{D}_2$ satisfy the requirement for reciprocity, namely that the determinants of the matrices are equal to unity. Furthermore, it is noted from Eqs (5.70) and (5.71) that the two-ports associated with the drift matrices $\underset{\sim}{D}_1$ and $\underset{\sim}{D}_2$ cannot be represented directly by simple transmission lines, without redefining either U or I with opposite sign. An equivalent method achieving essentially the same result is to consider the inverse drift matrices

$$\underset{\sim}{D}_1^{-1} = \begin{bmatrix} \cos \beta_q \ell_1 & -j\, W \sin \beta_q \ell_1 \\ -j \frac{1}{W} \sin \beta_q \ell_1 & \cos \beta_q \ell_1 \end{bmatrix} \tag{5.85}$$

with a similar expression for $\underset{\sim}{D}_2^{-1}$. Evidently the inverse drift matrices are equivalent to transmission-line matrices.

For a beam in a drift tube or in free space the following relation holds:

$$\begin{bmatrix} U_1 \\ I_1 \end{bmatrix} = \underset{\sim}{D}_1^{-1} \begin{bmatrix} U_2 \\ I_2 \end{bmatrix} e^{j\beta_e \ell_1} \tag{5.86}$$

where the matrix $\underset{\sim}{D}_1^{-1}$ according to the discussion above can be represented as shown in Fig 5.7 by a two-port consisting of a section of a transmission line having the characteristic impedance W and the same phase shift $\beta_q \ell_1$ between input and output. Although the plasma phase shift in the drift tube and the phase shift in the equivalent transmission line are different functions of frequencies, the variations with frequency are very small over the relatively narrow band of the cavity. It is therefore entirely justified to neglect these variations and consider the transmission-line representation of a beam in a drift tube correct for all the frequencies within the band.

Except for the trivial factor $\exp(j\beta_e \ell)$ there is one-to-one correspondence between the beam kinetic voltage and current of the space-charge wave propagating on the beam and the line voltage and line current of the electromagnetic wave propagating on the equivalent transmission line. The positive or negative energy flow on the beam is always in the positive direction, i e in the direction of the beam. Since the inverse of $\underset{\sim}{D}_1$ rather than $\underset{\sim}{D}_1$ represents the transmission-line matrix, it follows from Eq (5.86) that flow of energy on the equivalent transmission line is in the negative direction if the beam energy flow is positive, and vice versa.

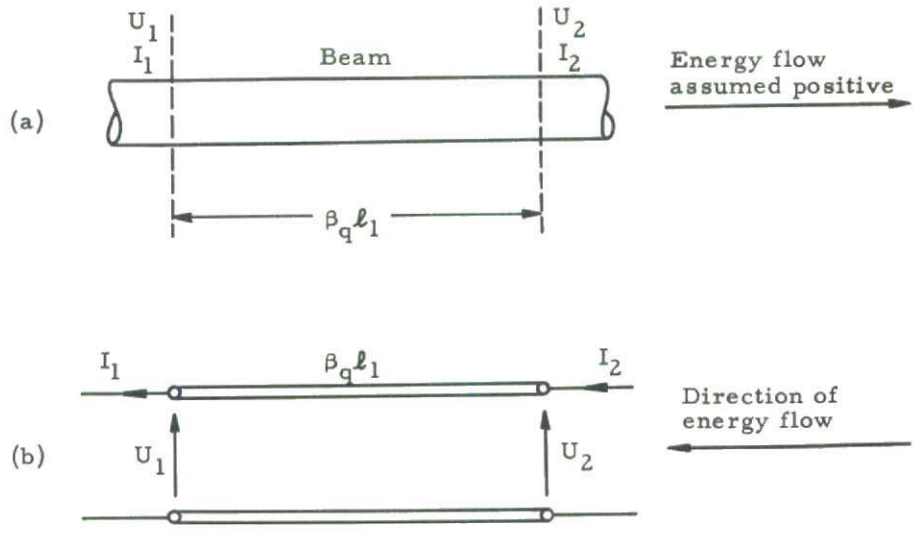

Fig 5.7 Representation of a drifting beam by transmission lines

(a) Drifting beam in a drift tube or in free space. The beam energy flow is assumed positive.

(b) Equivalent transmission line representing the drifting beam. The energy flow is in the negative direction if the beam energy flow is positive, and vice versa.

The reciprocity relations of the gap matrix $\underset{\sim}{C}$ given by Eq (5.73) can be investigated by forming the determinant of $\underset{\sim}{C}$ by means of Eqs (5.74) through (5.77). We obtain

$$\text{Det } \underset{\sim}{C} = C_{1,1} C_{2,2} - C_{2,1} C_{1,2} = 1 - 2 \frac{G_e}{Y} \tag{5.87}$$

The requirement for reciprocity, a determinant equal to unity, is satisfied only if the beam loading vanishes. Therefore, representation of the gap by passive, reciprocal networks, if at all possible, requires zero beam loading. In this case the gap matrix C reduces to

$$\underset{\sim}{C} = \begin{bmatrix} 1 & -\frac{1}{Y_c} \bar{M}^2 \\ 0 & 1 \end{bmatrix} \tag{5.88}$$

which evidently can be represented by the simple passive, reciprocal network shown in Fig 5.8. Here, the direction of energy flow in the equivalent two-port is positive if the beam energy flow is positive, and vice versa, while the opposite was true for the transmission-line two-port representing the drift matrices.

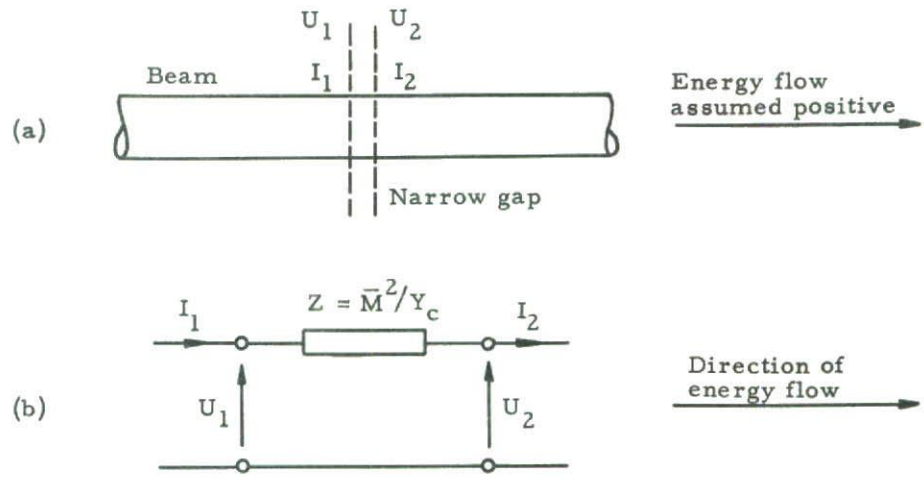

Fig 5.8 Representation of a narrow gap by a passive network

(a) Infinitely narrow gap excited by a beam. The beam energy flow is assumed positive.

(b) Network representation of the gap matrix $\underset{\sim}{C}$ of a gap having zero beam loading. The energy flow is in the positive direction if the beam energy flow is positive, and vice versa.

After having discussed reciprocity and energy flow relations of the separate two-ports and their network representations, we shall next consider the chain of cascaded two-ports representing the general interaction gap. The matrix equation relating the input and output modulations of the general gap in Fig 5.6a is given by

$$\begin{bmatrix} U_2 \\ \\ I_2 \end{bmatrix} = e^{-j\beta_e \ell} \, \underset{\sim}{D}_2 \, \underset{\sim}{C} \, \underset{\sim}{D}_1 \begin{bmatrix} U_1 \\ \\ I_1 \end{bmatrix} \tag{5.89}$$

From a study of this equation we are led to the conclusion that although the drift matrices $\underset{\sim}{D}_1$ and $\underset{\sim}{D}_2$ and the gap matrix $\underset{\sim}{C}$ are represented by passive networks if considered separately, representation of the matrix product $\underset{\sim}{D}_2 \, \underset{\sim}{C} \, \underset{\sim}{D}_1$ by the cascaded networks associated with $\underset{\sim}{D}_2$, $\underset{\sim}{C}$ and $\underset{\sim}{D}_1$ is not possible because the energy flows are in opposite directions in the networks representing gap and drift matrices.

However, even if representation of a general gap is not possible by means of transmission lines having the same total phase shift as the phase shift of the drifting beam across the interaction gap, a little consideration shows that representation certainly is possible with transmission lines of different phase shifts $\beta_q \ell'_1$ and $\beta_q \ell'_2$ if these are chosen according to the following relation:

$$\beta_q \ell_1' = n\pi - \beta_q \ell_1 \qquad n = 1, 2, \text{---} \tag{5.90}$$

$$\beta_q \ell_2' = n\pi - \beta_q \ell_2 \qquad n = 1, 2, \text{---} \tag{5.91}$$

By substitution in Eqs (5.70) and (5.71) we find that the associated drift matrices $\underset{\sim}{D}_1'$ and $\underset{\sim}{D}_2'$ are related to the original ones by the relations

$$\underset{\sim}{D}_1 = (-1)^n (\underset{\sim}{D}_1')^{-1} \tag{5.92}$$

$$\underset{\sim}{D}_2 = (-1)^n (\underset{\sim}{D}_2')^{-1} \tag{5.93}$$

Substitution in Eq (5.89) yields

$$\begin{bmatrix} U_2 \\ \\ I_2 \end{bmatrix} = e^{-j\beta_e \ell} (\underset{\sim}{D}_2')^{-1} \underset{\sim}{C} (\underset{\sim}{D}_1')^{-1} \begin{bmatrix} U_1 \\ \\ I_1 \end{bmatrix} \tag{5.94}$$

By modifying the lengths of the transmission-line sections we have been able to express the matrix product in terms of inverted drift matrices. Since inversion of a drift matrix corresponds to switching the direction of energy flow in the two-port representing the matrix, the matrix product in Eq (5.94), according to the preceding discussion, can be represented by the cascaded networks shown in Fig 5.9 where we have chosen n=1. In this equivalent of a gap with zero beam loading, the direction of energy flow is positive if the beam energy flow is positive, and vice versa.

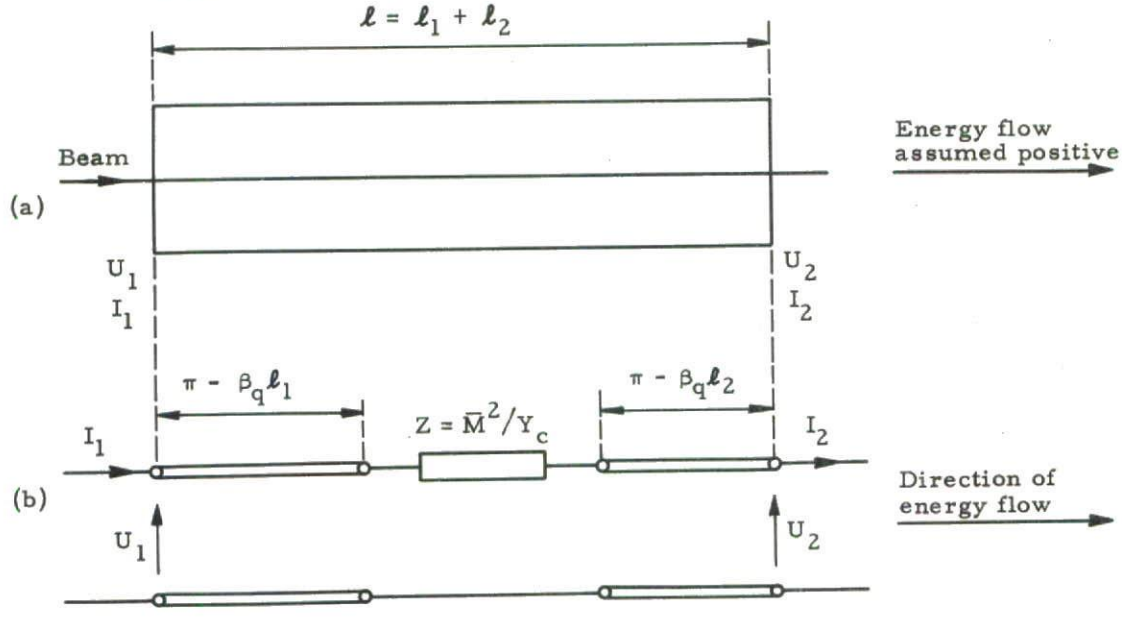

Fig 5.9 Representation of a general gap by passive networks

(a) General gap having zero beam loading.

(b) Representation by passive networks. The direction of energy flow corresponds to the sign of beam energy flow.

An alternate gap representation by active networks is obtained if Eq (5.89) is solved for the input modulations in terms of the output modulations by inversion of the matrix product.

$$\begin{bmatrix} U_1 \\ I_1 \end{bmatrix} = e^{j\beta_e \ell} \underset{\sim}{D}_1^{-1} \underset{\sim}{C}^{-1} \underset{\sim}{D}_2^{-1} \begin{bmatrix} U_2 \\ I_2 \end{bmatrix} \tag{5.95}$$

In the two-port representation the inversion corresponds to switching the direction of energy flow. In this case the matrices $\underset{\sim}{D}_1^{-1}$ and $\underset{\sim}{D}_2^{-1}$ can be represented by the transmission lines in Fig 5.7 with the original drift lengths ℓ_1 and ℓ_2, but the matrix $\underset{\sim}{C}^{-1}$ is no longer represented by the passive network shown in Fig 5.8, but by a similar active network with a negative series impedance Z, i e an impedance whose real part is negative. This leads to the active network representation of a gap shown in Fig 5.10. Here, the direction of the energy flow is opposite that of the sign of the beam energy flow.

To summarize the results, we have shown:

a) Interaction gaps of the general type discussed can be represented by reciprocal networks only if the beam loading is zero.

b) For gaps with zero beam loading two network representations are suggested, of which one is passive and one active. The passive network shown in Fig (5.9) involves a cascade of a transmission-line section of length $\pi - \beta_q \ell_1$, a lumped series impedance $\bar{M}^2/Y_c$ having positive real part, and a transmission-line section of length $\pi - \beta_q \ell_2$, the relative magnitudes of ℓ_1 and ℓ_2 being such that Eq (5.80) is satisfied. The direction of energy flow through the cascade is the same as the sign of beam energy flow.

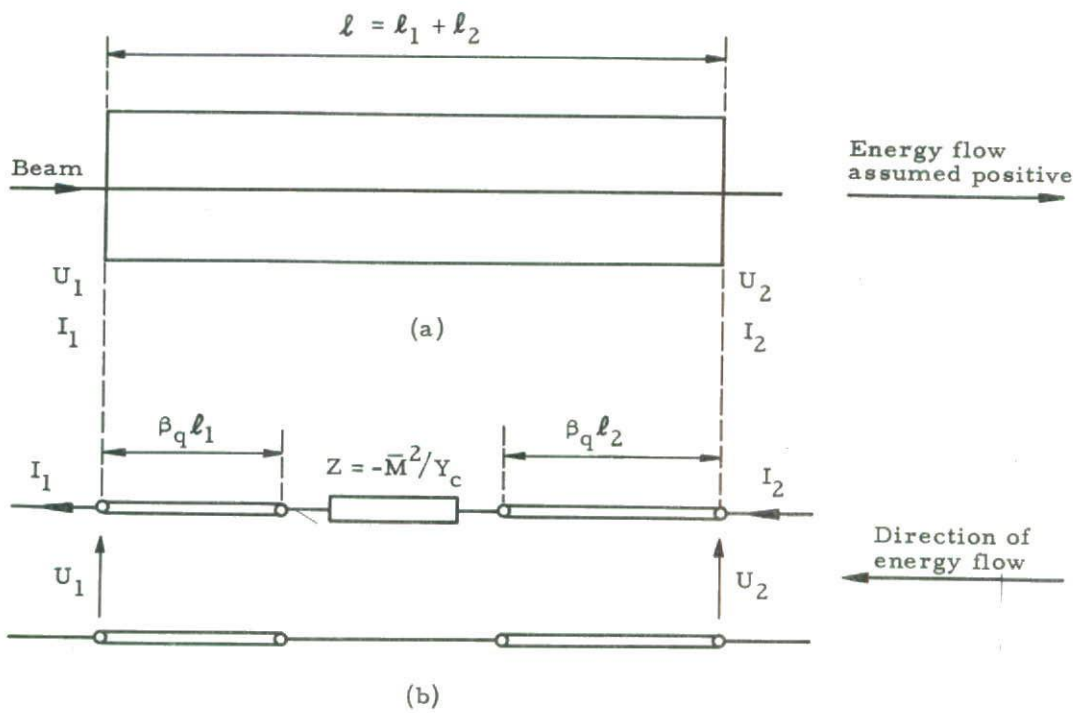

Fig 5.10 Representation of a general gap by active networks

(a) General gap having zero beam loading.

(b) Representation by active networks. Direction of energy flow is opposite that of the sign of beam energy flow.

The active network representation shown in Fig 5.10 is a cascade of a transmission-line section of length $\beta_q \ell_1$, a lumped series impedance $-\bar{M}^2/Y_c$ having negative real part, and a transmission-line section of length $\beta_q \ell_2$. The direction of energy flow through the cascade is opposite the sign of beam energy flow.

5.8 Loaded transmission-line analog of multi-cavity klystrons with extended interaction regions

The passive network representation shown in Fig 5.9 is the basis of a transmission-line analog of multi-cavity klystrons (16) that exactly simulates the actual small-signal klystron performance with the following restrictions that are immediately understood from the preceding discussion:

a) The beam loading of all the cavities must be zero. This is a rather severe restriction which is not satisfied in actual klystrons except under special circumstances. The errors introduced by non-zero beam loading, however, are not expected to be significant in most practical cases for which normally the ratio $G_e/Y_c \ll 1$ (see Eq (5.84)). If this condition is satisfied, the network analog will probably be sufficiently accurate for practical purposes.

b) The frequency dependence of the phase shifts of the transmission-line sections are disregarded compared to the more rapid frequency dependence of the cavity admittance Y_c. This assumption is well satisfied in practice, the approximation being of the same order as the approximation involved by neglecting the frequency dependence of the plasma drift angles in the actual klystrons.

c) It is assumed that Eq (5.80) is satisfied, at least approximately, over the frequency band of the klystron. It is noted, in particular, that the equation is always satisfied for gaps with symmetric or anti-symmetric RF field distributions, in which cases $\text{Arg } M^+ = \text{Arg } M^-$ for all frequencies, i e $\ell_1 = \ell_2$.

With the restrictions mentioned above under a), b) and c), the transmission-line analog shown in Fig 5.11 simulates accurately the small-signal behavior of multi-cavity klystrons with arbitrary, extended interaction regions. The analog shown in Fig 5.11b is obtained directly by cascading a series of gap representations of the type shown in Fig 5.9. In the analog the beam modulations U and I are represented directly by the line voltage and line current except for a trivial exponential factor $\exp(j\beta_e z)$. The proper boundary conditions are established by open-circuiting the transmission line at the position corresponding to the input cavity, thus forcing the current to be zero, as required. The RF power is fed from a generator into the line at the opposite end. Since the beam energy flow in the klystron is always negative, the energy on the line will flow in the correct direction from the right to the left, according to the discussion in connection with Fig 5.9. In the analog the characteristic impedance of the transmission-line sections corresponds to the characteristic impedance of the beam, and the lumped series impedances correspond to the cavity impedances, i e they are parallel LC circuits.

The analog shown in Fig 5.11c refers to the special situation for which all the plasma drift angles are equal to $\pi/2$. In this case the transmission-line sections can be eliminated altogether by successive simple transformations of the two-ports consisting of two quarter-wave sections and one parallel resonant circuit in series

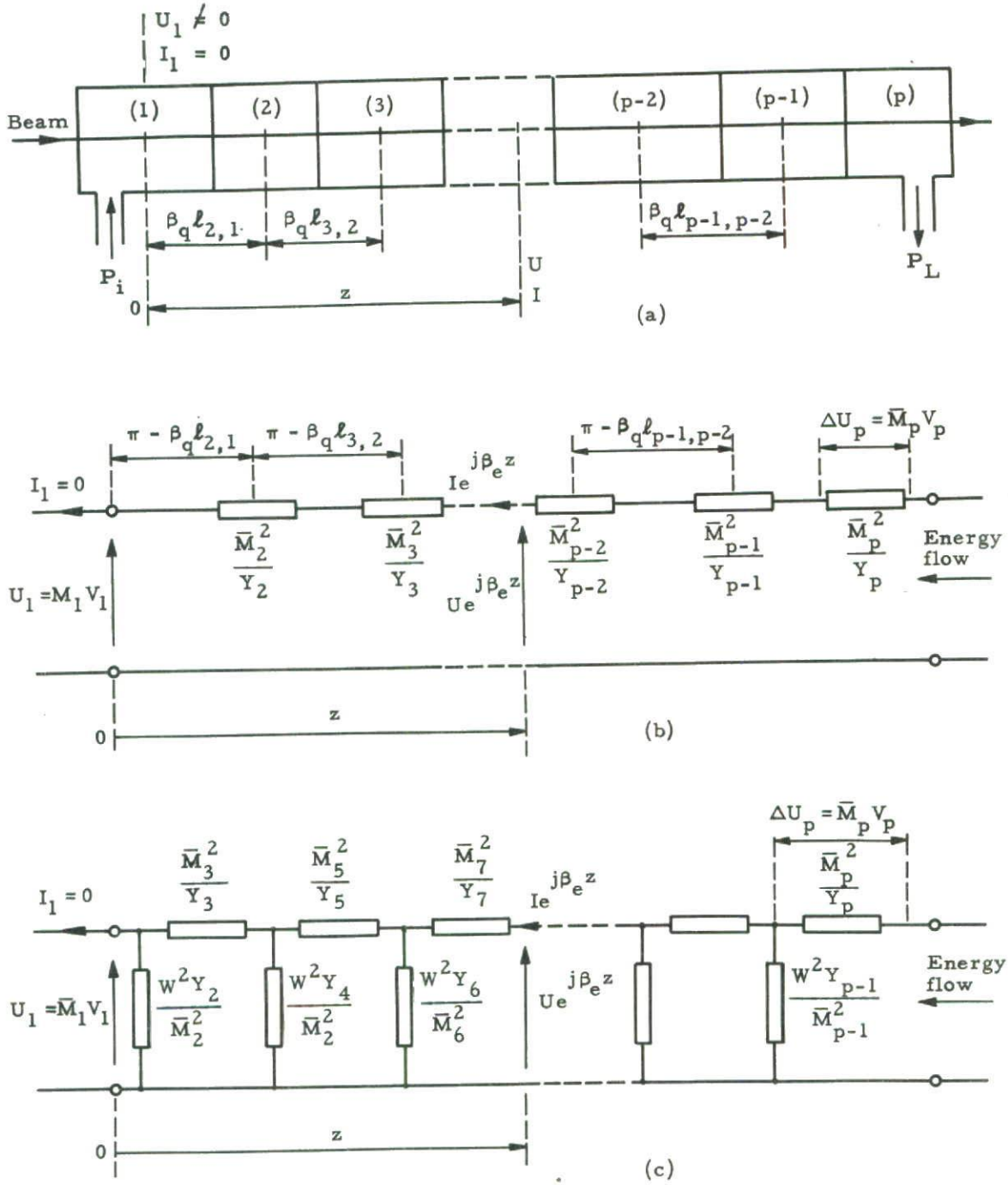

Fig 5.11 Transmission-line analog of multi-cavity klystrons with arbitrary gaps having zero or negligible beam loading

(a) Multi-cavity klystron structure with RF beam modulations given by U and I.

(b) Transmission-line analog based on representation of the interaction gaps by the networks shown in Fig 5.9. The line voltage and line current correspond to the beam modulations U and I multiplied by $\exp(j\beta_e z)$.

(c) Ladder-network analog in the special case for which all the plasma drift angles between centers of consecutive gaps are $\pi/2$. In this case no transmission lines are required.

between these into one single series resonant circuit in parallel. The resulting ladder-network analog is a stop-band filter, the stop-band corresponding to the pass-band of the klystron.

Although it is not immediately obvious, it can be shown, using the general relations for arbitrary extended gaps developed in this chapter, that the RF gap voltages of the various extended interaction gaps along the electron stream are represented in the analog by the voltage drops across the lumped series impedances, modified by the coupling coefficients. Referring to Fig 5.11b, the pth gap voltage is given by the relation

$$V_p = \frac{1}{\bar{M}_p} (U_{p,2} - U_{p,1}) = \frac{1}{\bar{M}_p} \Delta U_p \tag{5.96}$$

where $U_{p,1}$ and $U_{p,2}$ are the transmission-line voltages immediately before and after the series impedance $\bar{M}^2/Y_p$. Therefore, the voltage gain of the klystron is represented by

$$\eta_p = \frac{V_p}{V_1} = \frac{\Delta U_p}{U_1} \frac{\bar{M}_1}{\bar{M}_p} \tag{5.97}$$

where ΔU_p is the voltage drop across the series impedance representing the output cavity, and U_1 is the line voltage at the open-circuit position corresponding to the position of the input cavity.

The duals of the networks shown in Fig 5.11 are also possible analogs of multicavity klystrons, but will not be considered here.

The suggested simple network analogs may have potential uses for optimization of stagger-tuning pattern, particularly for klystrons having a large number of cavities, because in these cases analytical and numerical synthesizing methods are exceedingly difficult to handle. In a practical analog one would scale the klystron parameters to a convenient lower frequency for which full advantage can be taken of simple LC resonant circuits and low-frequency measuring technique.

5.9 Some general properties of the coupling coefficient

In the next sections a relatively detailed study will be made of the relevant gap parameters that characterize small-signal interaction with longitudinal beams. These parameters are the gap coupling coefficient $M(\beta_e)$ and the gap electronic admittance Y_e, defined by Eqs (2.53) and (2.68), respectively. Actually, the gap is characterized by two coupling coefficients M^- and M^+, associated with the fast and the slow space-charge waves. However, since these are derived from the zero space-charge coupling coefficient $M(\beta_e)$, a study of $M(\beta_e)$ suffices.

We shall prove some general properties satisfied by the coupling coefficient of any gap having arbitrary longitudinal RF field distribution:

a) The absolute value of the coupling coefficient of any gap is always less than unity

b) The coupling coefficient of a gap having symmetric RF field distribution is real

c) The coupling coefficient of a gap having anti-symmetric RF field distribution is imaginary

In order to prove the first statement let us consider the expression for the coupling coefficient

$$M = \int_{-\ell/2}^{\ell/2} F(x)\, e^{j\beta_e x}\, dx \tag{5.98}$$

We shall allow complex values of the normalized longitudinal RF field distribution $F(x)$. Using Schwarz' inequality and the normalization condition (2.51) we find

$$MM^* \leq \int_{-\ell/2}^{\ell/2} F(x)\,F(x)^* dx \int_{-\ell/2}^{\ell/2} e^{j\beta_e x}\, e^{-j\beta_e x}\, dx = \ell \int_{-\ell/2}^{\ell/2} F(x)\,F(x)^* dx = 1 \tag{5.99}$$

or

$$|M| \leq 1$$

which proves the property listed above under a).

The properties listed under b) and c) follow immediately from the reciprocity theorem a) derived in Section 3.14, stating that the gap coupling coefficient transfers to its complex conjugate if the electron flow through the gap is reversed. Hence, for a symmetric RF field:

$$M = M^* \qquad \text{i e} \quad M \text{ is real} \tag{5.100}$$

For an anti-symmetric RF field:

$$M = -M^* \qquad \text{i e} \quad M \text{ is imaginary} \tag{5.101}$$

The coupling coefficient of a gap whose RF field distribution is neither symmetric nor anti-symmetric is, in general, complex.

5.10 Series expansion of the coupling coefficient in terms of sinusoidal field components

For a gap with arbitrary longitudinal RF field distribution, series expansion of the coupling coefficient M in terms of the Fourier components of the gap field is useful in that it shows explicitly the relative contributions to M from the various Fourier components. The problems arising in connection with the realization of a specified RF field distribution by practical structures are irrelevant to the present discussion. We shall assume, however, that the RF field has the character of a pure standing wave, i e that $F(x)$ is in phase everywhere, and that the derivatives dF/dx at the two cross-sections corresponding to $x = -\ell/2$ and $x = \ell/2$ are both zero. These restrictions mean that the types of interaction gaps analyzed

here are those which are typical for high-Q cavities having conducting metal boundaries at the cross-sections $x = -\ell/2$ and $x = \ell/2$.

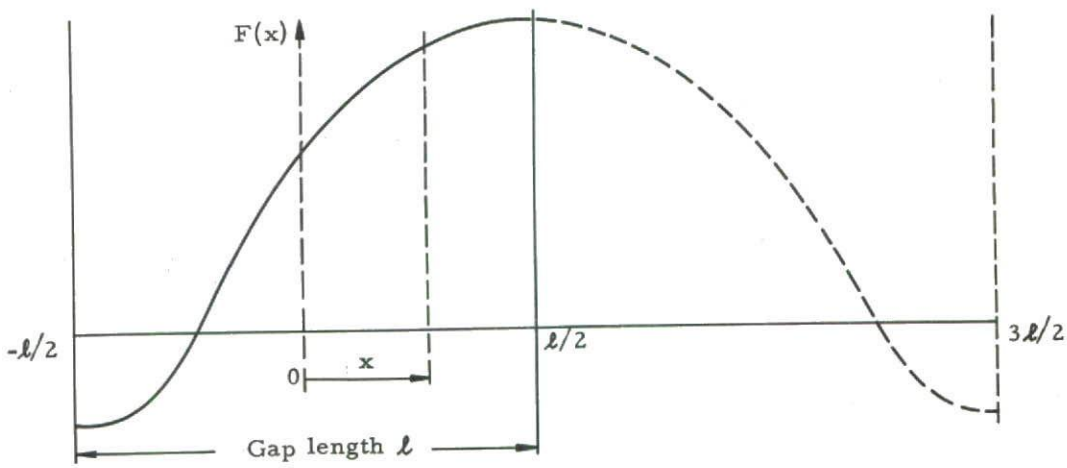

Fig 5.12 Sketch showing the gap boundary conditions: $dF/dx = 0$ at $x = -\ell/2$ and $x = \ell/2$

The Fourier expansion of $F(x)$ is based on a fundamental period of twice the gap length for reasons that are obvious if we consider the periodic gap field in a resonated section of some slow-wave structure. These structures resonate at a set of frequencies for which the periodic RF field distributions comprise a whole number of half periods.

Referring to Fig 5.12, the mathematical extension of $F(x)$ in the region $\ell/2 < x < 3\ell/2$ will be chosen such that

$$F(x) = F(\ell - x) \qquad (5.102)$$

or

$$F(-x) = F(\ell + x)$$

The Fourier expansion, valid in the interval $-\ell/2 < x < 3\ell/2$ and therefore, in particular, over the gap itself, is given by the cosine series

$$F(x) = F_o + \sum_{1}^{\infty} F_n \cos[n\pi(x/\ell - 1/2)] \qquad (5.103)$$

where the coefficients are obtained from

$$F_n = \frac{1}{\ell} \int_{-\ell/2}^{3\ell/2} F(x) \cos[n\pi(x/\ell - 1/2)]\, dx = \frac{2}{\ell} \int_{-\ell/2}^{\ell/2} F(x) \cos[n\pi(x/\ell - 1/2)]\, dx \qquad (5.104)$$

$$F_o = \frac{1}{2\ell} \int_{-\ell/2}^{3\ell/2} F(x)\, dx = \frac{1}{\ell} \int_{-\ell/2}^{\ell/2} F(x)\, dx \qquad (5.105)$$

The Fourier components satisfy the following relation derived from the normalization condition (2.51):

$$\ell \int_{-\ell/2}^{\ell/2} F(x)^2 \, dx = \ell^2 F_o^2 + \frac{1}{2} \ell^2 \sum_{n=1}^{\infty} F_n^2 = 1 \tag{5.106}$$

The Fourier components F_n for $n \geq 1$ represent a set of standing waves each of which can be considered the superposition of two waves traveling in opposite directions. The propagation constant β_n of these waves is

$$\beta_n = \pi n / \ell \tag{5.107}$$

The integer n therefore represents the number of half waves over the interaction length ℓ. For evaluation of the coupling coefficient M in terms of the Fourier components it is convenient to introduce a velocity parameter ϵ_n defined by

$$\epsilon_n = 1 - \frac{\beta_e}{\beta_n} = 1 - \frac{v_n}{u_o} \tag{5.108}$$

where $\beta_e = \omega / u_o$ is the propagation factor associated with the DC electron velocity u_o, and v_n the phase velocity of the wave constituting the nth Fourier component. The parameter ϵ_n is a measure of the deviation of the beam velocity from synchronism with the nth Fourier component.

Substituting the series expansion of F(x) in the expression for the coupling coefficient and using Eq (5.108), we obtain

$$M = \ell F_o \frac{\sin(\beta_e \ell/2)}{\beta_e \ell/2} + \frac{1}{2} \ell \sum_{n=1}^{\infty} F_n \, e^{j\pi n/2} \, \frac{1 - \epsilon_n}{1 - \epsilon_n/2} \, \frac{\sin(n\pi\epsilon_n/2)}{n\pi\epsilon_n/2} \tag{5.109}$$

The first term in the equation, recognized as the coupling coefficient of a gridded gap with constant field, multiplied by ℓF_o, represents the contribution to the coupling coefficient from the average RF field component F_o. The remaining terms represent contributions from the various sinusoidal components of the field.

As expected, interaction with a given component is strong only if the beam is nearly synchronized with the same component. Under these circumstances the small interaction with the remaining components can often be neglected. In particular, this is true for resonated sections of slow-wave structures in which normally one of the Fourier components of the longitudinal RF field is dominating. Thus, if all the components except the nth component are zero or negligible, i e if the RF field is sinusoidal, the coupling coefficient is given by

$$M = \frac{1}{\sqrt{2}} \, \frac{1 - \epsilon_n}{1 - \epsilon_n/2} \, \frac{\sin(n\pi\epsilon_n/2)}{n\pi\epsilon_n/2} \, e^{jn\pi/2} \, . \tag{5.110}$$

or

$$M_o = |M| = \frac{1}{\sqrt{2}} \frac{1 - \epsilon_n}{1 - \epsilon_n/2} \frac{\sin(n\pi\epsilon_n/2)}{n\pi\epsilon_n/2} \tag{5.111}$$

The factor $\sqrt{2}$ in these equations is due to the normalization condition (5.106). The absolute value of M^2, calculated from Eq (5.111), is plotted in Fig 5.14 (appearing at the end of the chapter) as a function of the velocity parameter ϵ and the number of half waves n. The non-symmetry of the curves, which is particularly pronounced for small n-values, can be shown to be due to interaction with the reflected wave. This interaction becomes negligible for large values of n; the maximum of M_o^2 is then equal to 0.5 for all values of n and occurs at synchronism. This fact is significant because it shows that for sinusoidal field distributions the lengths of the interaction gaps are not limited by transit time considerations, as are conventional klystron gaps. Since the characteristic impedance of a resonator generally increases with the length of the gap, the use of resonators and gaps with sinusoidal field distributions evidently provided a possibility for enhancing the gain or bandwidth of multi-cavity klystrons. Results from experimental tubes using such resonators tend to confirm these theoretical considerations (9).

5.11 Some general properties of the small-signal electronic admittance

The general expression for the small-signal electronic admittance of an arbitrary gap characterized by the longitudinal RF field distribution $F(x)$ is given by Eq (2.69), for convenience repeated here

$$Y_e = -\frac{1}{W} \Delta\left\{\frac{1}{2}M_o^2 + j \int_{-\ell/2}^{\ell/2} \int_{-\ell/2}^{x} F(x)F(y) \sin[\beta_e(y-x)]\, dx\, dy\right\} \tag{5.112}$$

In this equation W is the RF characteristic impedance of the beam, given by Eq (2.30), and Δ is the difference operator defined in Eq (2.38).

The zero space-charge approximation of the electronic admittance is derived by making the observation that if the space-charge density in the beam is negligible, such that β_q/β_e is much less than unity, Eq (5.112) reduces to the following expression obtained by simple application of the transformation rule (2.45) and the definition of W:

$$Y_e = -\frac{1}{4} G_o \beta_e \frac{d}{d\beta_e} \left\{M_o^2 + 2j \int_{-\ell/2}^{\ell/2} \int_{-\ell/2}^{x} F(x)F(y) \sin[\beta_e(y-x)]\, dx\, dy\right\} \tag{5.113}$$

where $G_o = I_o/V_o$. Equation (5.113) is in agreement with results obtained using purely kinematic analyses neglecting space-charge (10).

For arbitrary space-charge, the real and imaginary components of the electronic admittance of a gap with specified longitudinal RF field distribution $F(x)$ can be evaluated either analytically from Eq (5.112), or by a graphical method suggested

by the form of this equation and described in the following: If Eq (5.112) is re-written in terms of G_o rather than W, we obtain

$$y_e = \frac{Y_e}{G_o} = -\frac{1}{4}\beta_e \frac{1}{\beta_q} \Delta\left\{M_o^2 + 2j \int_{-\ell/2}^{\ell/2} \int_{-\ell/2}^{x} F(x)F(y) \sin[\beta_e(y-x)]\, dx\, dy\right\} \qquad (5.114)$$

where y_e is the electronic admittance normalized with respect to G_o. If we limit our attention to the real part of the expression, i e the beam loading, we obtain

$$\text{Re } y_e = g_e = \frac{G_e}{G_o} = -\frac{1}{4}\beta_e \frac{1}{\beta_q} \Delta(M_o^2) = -\frac{1}{4}\beta_e \frac{M_o^2(\beta_e+\beta_q) - M_o^2(\beta_e-\beta_q)}{2\beta_q} \qquad (5.115)$$

The form of this expression suggests the graphical method shown in Fig 5.13 for evaluation of g_e for any value of the space-charge parameter β_q, if a plot of M_o^2 vs β_e is available for the particular gap considered.

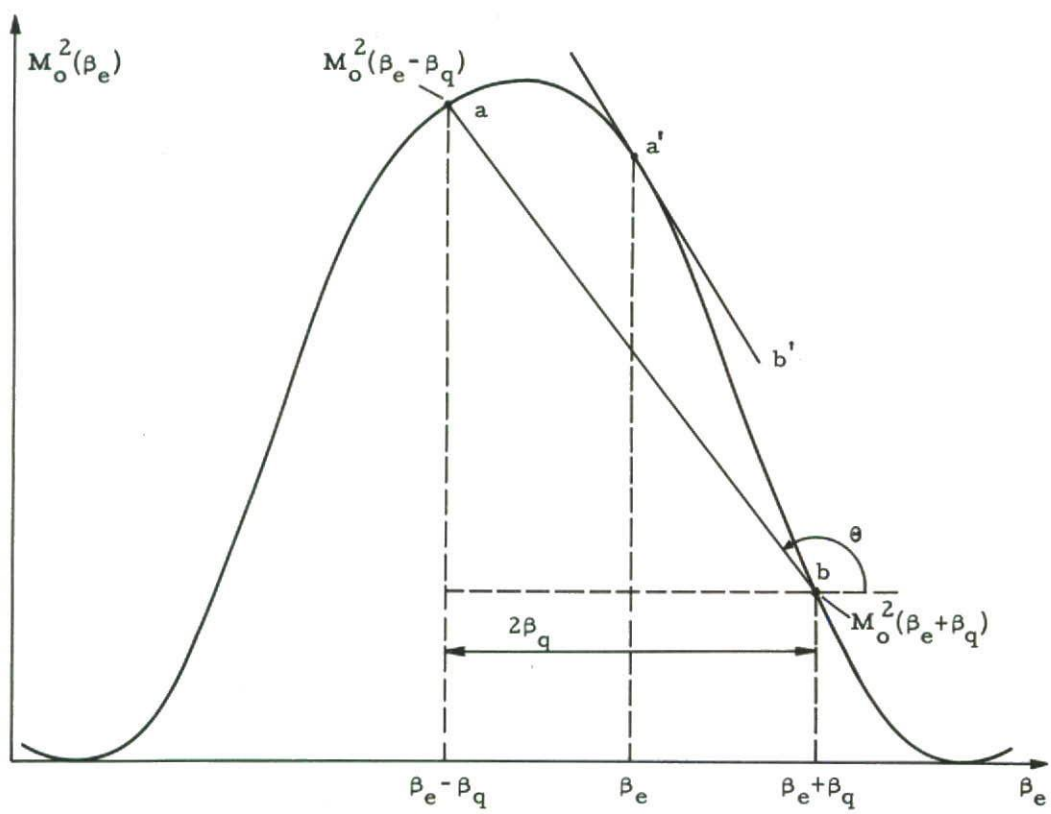

Fig 5.13 Graphical method for evaluation of electronic conductance from a plot of the square of the coupling coefficient

From a comparison of Eq (5.115) and the geometrical relations in Fig 5.13 it is observed that the beam loading is proportional to the slope of the straight line

labeled ab. For negligible space-charge this line approaches the tangent $a' b'$, in which case g_e is proportional to the derivative of M_o^2 with respect to β_e (compare Eqs (5.113) and (5.114). In general, if θ is the angle between the horizontal axis and the line ab, the beam loading is given by

$$g_e = \frac{G_e}{G_o} = -\frac{1}{4}\beta_e \tan\theta \qquad (5.116)$$

The imaginary part of Eq (5.114) can be determined by essentially the same graphical method as shown in Fig 5.13 if M_o^2 is replaced by the appropriate function, which is twice the double integral in Eq (5.114).

For a given gap with specified DC beam velocity (β_e fixed), the question whether the electronic conductance and susceptance always decrease with increasing space-charge is a very interesting one. It turns out that although this is true in many cases, it is not generally true for any RF field distribution and beam velocity, as is readily observed from a study of the graphical method shown in Fig 5.13, or perhaps better from the subsequent analytical method. Let g_e and $(g_e)_o$ be the normalized electronic conductance with and without space-charge, respectively. Taylor series expansion of Eq (5.115) in terms of β_q yields

$$g_e - (g_e)_o = -\frac{1}{4}\beta_e\left[\frac{\beta_q^2}{3!}\frac{\partial^3(M_o^2)}{\partial\beta_e^3} + \frac{\beta_q^4}{5!}\frac{\partial^5(M_o^2)}{\partial\beta_e^5} + \text{-----}\right] \qquad (5.117)$$

and similarly for the electronic susceptance, if M_o^2 is replaced by the appropriate function.

The conclusions that can be drawn from Eq (5.117) concerning the effect of space-charge on the small-signal electronic conductance in a general interaction gap are the following:

a) Space-charge effects are of second order in the space-charge parameter β_q.

b) As the space-charge parameter β_q is increased from zero, the sign of the first derivative of g_e with respect to β_q is determined by the sign of the third derivative of M_o^2 with respect to β_e. If $\partial^3(M_o^2)/\partial\beta_e^3 > 0$, the electronic conductance becomes smaller as the space-charge increases from zero, and vice versa.

c) The rate of change of g_e with increasing space-charge is determined by the odd derivatives of M_o^2 with respect to β_e. It is a general characteristic of a Fourier transform that the rate of change with β_e increases with the length ℓ of the interaction region, regardless of the details of the RF field distribution. Therefore, it is anticipated that space-charge effects are relatively more pronounced in long gaps. For most practical gaps of moderate lengths the following discussion indicates, however, that the zero space-charge approximation is sufficiently accurate if the space-charge density is not excessive.

5.12 Electronic admittance of gaps with sinusoidal RF field distributions

As previously stated, a more detailed knowledge of the gap parameters of resonated slow-wave structures is of considerable practical interest. The longitudinal RF field distributions in such structures are essentially sinusoidal standing waves. In this section the electronic admittance of such fields will be evaluated for relatively wide ranges of the relevant parameters which are the velocity parameter ϵ defined in Eq (5.108), the space-charge parameter β_q/β where β is defined in Eq (5.107), and the number of half standing waves n. In order to evaluate Eq (5.114) for a pure sinusoidal field it is convenient to define two functions $\phi_n(\epsilon)$ and $\psi_n(\epsilon)$ by the following expressions:

$$\phi_n(\epsilon) = M_o^2 = \frac{1}{2}\left[\frac{1-\epsilon}{1-\epsilon/2}\right]^2\left[\frac{\sin(n\pi\epsilon/2)}{n\pi\epsilon/2}\right]^2 \tag{5.118}$$

$$\psi_n(\epsilon) = 2\int_{-\ell/2}^{\ell/2}\int_{-\ell/2}^{x} F(x)F(y)\sin[\beta_e(y-x)]\,dx\,dy$$

$$= \frac{1}{n\pi\epsilon}\frac{1-\epsilon}{1-\epsilon/2}\left[1 - \frac{1-\epsilon}{1-\epsilon/2}\frac{\sin n\pi\epsilon}{n\pi\epsilon}\right] \tag{5.119}$$

It is noted that $\phi_n(\epsilon)$ is equal to the square of the coupling coefficient M_o.

Making the proper substitutions of ϵ and β_q/β in Eq (5.114), we obtain the normalized electronic conductance and susceptance expressed in terms of the two functions $\phi_n(\epsilon)$ and $\psi_n(\epsilon)$.

$$g_e = \frac{1}{8}(1-\epsilon)\frac{\phi_n(\epsilon+\Omega)-\phi_n(\epsilon-\Omega)}{\Omega} \tag{5.120}$$

$$b_e = \frac{1}{8}(1-\epsilon)\frac{\psi_n(\epsilon+\Omega)-\psi_n(\epsilon-\Omega)}{\Omega} \tag{5.121}$$

where Ω is a space-charge parameter defined by

$$\Omega = \frac{\beta_q}{\beta} \tag{5.122}$$

It should be noted that the quantities $\phi_n(\epsilon+\Omega)$ and $\psi_n(\epsilon\pm\Omega)$ are functional symbols indicating that the independent variable is $(\epsilon\pm\Omega)$. These functions can be interpreted as determining the coupling between the circuit field and the fast space-charge wave (upper signs), and the slow space-charge wave (lower signs). In discussing Eqs (5.120) and (5.121), two significantly different cases may occur:

a) The gap field couples to both space-charge waves simultaneously, i e all the four functions $\phi_n(\epsilon\pm\Omega)$ and $\psi_n(\epsilon\pm\Omega)$ are different from zero

b) The gap field couples only to one of the waves, in which case either $\phi_n(\epsilon+\Omega)$ or $\phi_n(\epsilon-\Omega)$ is zero

A study of the function $\Phi_n(\epsilon)$ in Fig 5.14 reveals that the question whether case a) or b) applies depends essentially on the product of n and Ω only. We find that if the following inequality is satisfied, the circuit cannot couple to both space-charge waves simultaneously:

$$n\Omega \geq 2 \tag{5.123}$$

This result is obtained from Eq (5.111) or Fig 5.14 by observing that the width of the main peak of the function $M_o^2(\epsilon)$ is given approximately by $\Delta\epsilon = 4/n$ (asymptotically correct for large n). Therefore, if the inequality (5.123) is satisfied, either $\epsilon+\Omega$ or $\epsilon-\Omega$ will fall outside this interval, meaning that the main peaks of the functions $\Phi_n(\epsilon+\Omega)$ and $\Phi_n(\epsilon-\Omega)$ do not overlap. Thus, if the small secondary peaks of $\Phi_n(\epsilon)$ are neglected, the statement above is shown to be correct. Even if the inequality (5.123) is a sufficient condition for coupling to one wave only, it is by no means a necessary condition, since by proper adjustment of DC beam velocity either $\Phi_n(\epsilon+\Omega)$ or $\Phi_n(\epsilon-\Omega)$ can always be made equal to zero.

We shall study the two cases a) and b) separately.

5.12.1 Gaps with simultaneous coupling to both space-charge waves

This case is typical for moderate values of n and Ω, and is probably of most interest since the condition $n\Omega < 2$ is likely to be satisfied in practical resonators for possible use in klystrons (9). For the purpose of evaluation of the functions (5.120) and (5.121) by graphical methods essentially similar to the methods shown in Fig 5.13, curves have been prepared of the functions $\Phi_n(\epsilon) = M_o^2(\epsilon)$ and $\Psi_n(\epsilon)$, shown in Figs 5.14 and 5.15 for values of n ranging from one to six. The additional curves for n = 50 illustrate how the functions become sharply peaked for large n.

The graphical method is quite illuminating in the sense that it clearly brings out the physical interpretation of the terms $\Phi_n(\epsilon+\Omega)$ and $\Phi_n(\epsilon-\Omega)$ etc as representing coupling between the circuit field and the fast and the slow space-charge waves, respectively. Of course the graphical method suffers from being less accurate than numerical methods. The set of curves shown in Figs 5.16 to 5.20 at the end of the chapter are obtained from an electronic computer. Here, the normalized electronic conductance g_e and susceptance b_e are plotted vs the velocity parameter ϵ for values of n from one to six and for Ω equal to 0, 0.1 and 0.2.

Around synchronism, where the interaction is strongest, the general behavior of the electronic conductance is such that it changes from a positive maximum below synchronism to a negative maximum above synchronism, the maxima increasing with the number of half waves n. The preceding qualitative discussion concerning the reduction of the maxima of g_e due to space-charge is confirmed by these curves: the reduction becomes more predominant as Ω increases, especially at the higher n-values, but is nevertheless negligible for moderate values of Ω and n ($n < 6$ and $\Omega < 0.1$).

The electronic susceptance b_e is maximum at or near synchronism; otherwise the general comments made above concerning the dependence of the electronic conductance on n and Ω apply equally well to the electronic susceptance.

5.12.2 Gaps with coupling to one space-charge wave only

If the inequality $n\Omega \geq 2$ is satisfied, it is not possible to have appreciable coupling to both space-charge waves simultaneously. Obviously this inequality is a sufficient condition but not a necessary one. Practical fast-wave couplers for possible use in parametric amplifiers should be designed such that the coupling to the slow wave is zero and the coupling to the fast wave is maximum. Expressed mathematically

$$\phi_n(\epsilon - \Omega) = 0 \tag{5.124}$$

$$\phi_n(\epsilon + \Omega) = \max \tag{5.125}$$

From the curves in Fig (5.14) it is found that these equations are approximately satisfied for

$$n\epsilon = -1 \tag{5.126}$$

$$n\Omega = 1 \tag{5.127}$$

Thus, the beam velocity for a fast-wave coupler of this type must satisfy the requirement $\epsilon = -\Omega$. The corresponding relations for a slow-wave coupler are $n\epsilon = 1$ and $\epsilon = \Omega$.

In evaluating the electronic admittance of a gap with coupling to only one of the space-charge waves it is convenient to write

$$\epsilon' = \epsilon \pm \Omega \tag{5.128}$$

where ϵ' is zero for maximum coupling. Noting that $(1 - \epsilon)/\Omega$ is identical to $\beta_e/\beta_q = \omega/\omega_q$, Eqs (5.118) and (5.119) yield the following expressions for g_e and b_e valid in a small velocity interval around the points of maximum interaction:

$$g_e = \pm \frac{1}{16} \frac{\beta_e}{\beta_q} \left[\frac{\sin(n\pi\epsilon'/2)}{n\pi\epsilon'/2} \right]^2 \tag{5.129}$$

$$b_e = \pm \frac{1}{8} \frac{\beta_e}{\beta_q} \frac{1}{n\pi\epsilon'} \left[1 - \frac{\sin n\pi\epsilon'}{n\pi\epsilon'} \right] \tag{5.130}$$

where the upper and lower signs refer to the situations for which the gap couples to the fast and the slow waves, respectively.

The maxima of g_e and b_e are readily evaluated from Eqs (5.129) and (5.130). We find

$$(g_e)_{max} = 0.0625 \frac{\beta_e}{\beta_q} \tag{5.131}$$

$$(b_e)_{max} = 0.08 \frac{\beta_e}{\beta_q} \quad \text{(peak to peak)} \tag{5.132}$$

Thus, the maxima of g_e and b_e are inversely proportional to β_q/β_e or ω_q/ω regardless of the value of n if the conditions stated previously for coupling to only one wave are satisfied.

The sketch shown in Fig 5.22 of the functions g_e and b_e evaluated from Eqs (5.129) and (5.130) serves as a further illustration of the points stated in the above discussion.

To conclude this section, we have established that the electronic conductance and susceptance of an interaction gap with sinusoidal RF field distribution varies with the number of half standing waves n in the following way. For small n and Ω ($n\Omega \ll 2$), the field couples simultaneously to both space-charge waves, and the maxima of g_e and b_e are roughly proportional to n. As n is increased towards $n\Omega = 2$ the field couples predominantly to one of the space-charge waves, yielding the maxima of g_e and b_e substantially independent of n.

For practical klystrons based on extended-interaction cavities consisting of resonated slow-wave structures with essentially sinusoidal RF field distribution, operational stability requires that the magnitude of the negative electronic conductance is smaller than the value causing self-oscillations, as specified by the stability criterion (3.28). From the numerical data and discussion presented in this section these considerations determine the maximum safe value of n and thus the maximum characteristic impedance R_{sh}/Q. The requirement of stable operation, therefore, puts a restriction on the enhancement of gain and bandwidth that can be expected from the use of extended interaction gaps rather than narrow gaps.

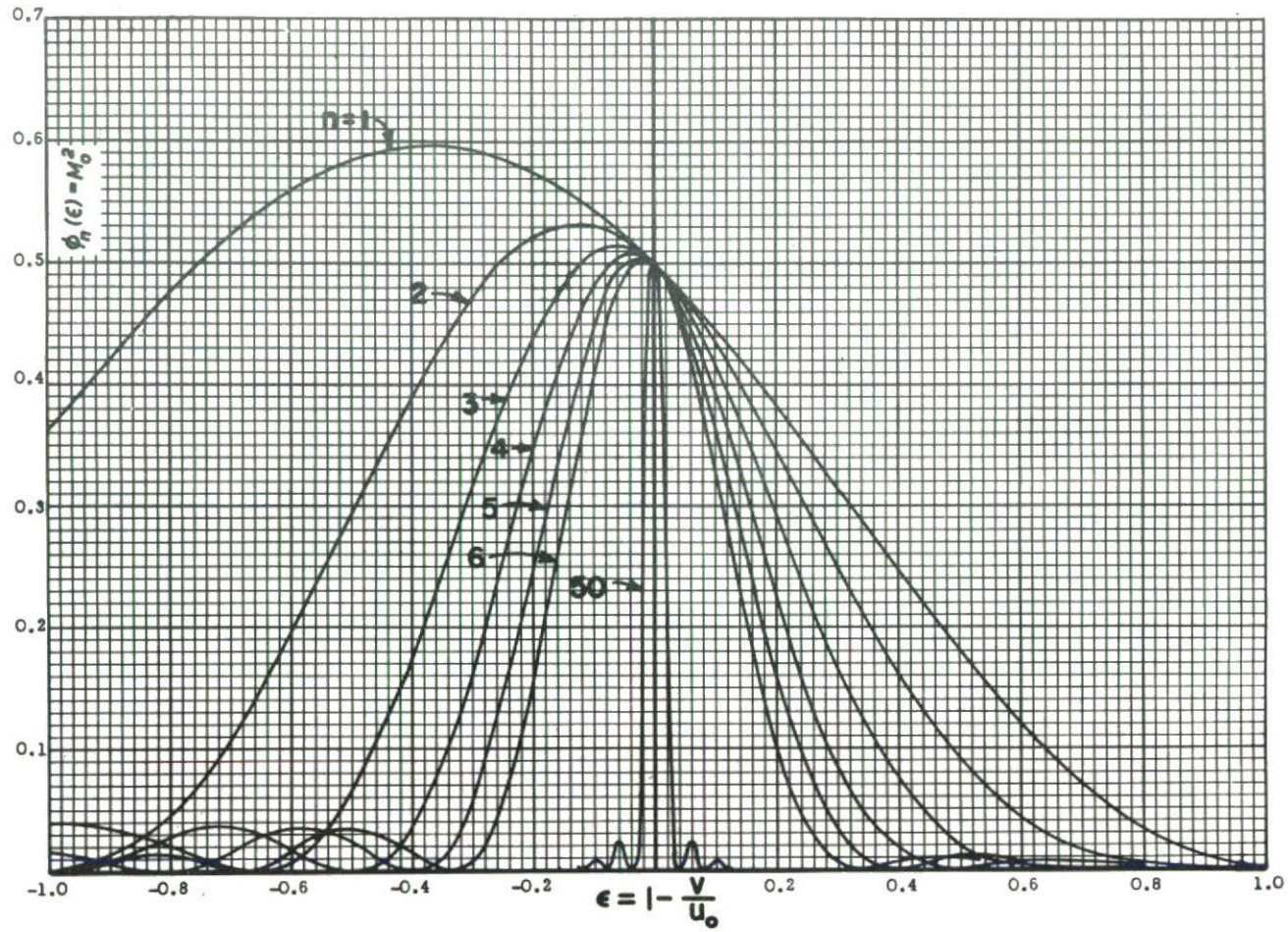

Fig 5.14 Graphs of the function $\phi_n(\epsilon) = M_o^2$ from which the small-signal electronic conductance of a gap with sinusoidal RF field distribution can be determined by the graphical method suggested in Fig 5.13

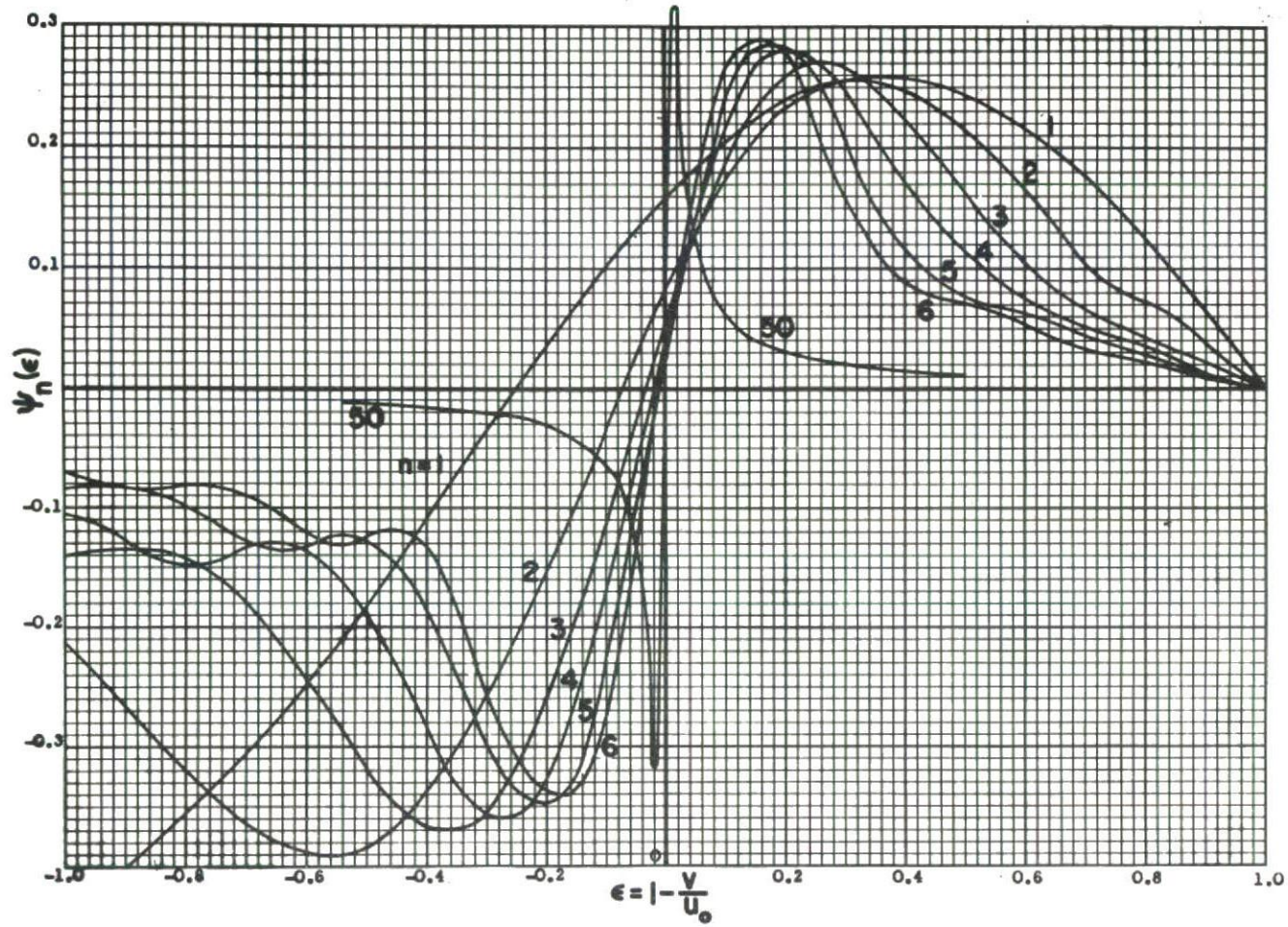

Fig 5.15 Graphs of the function $\psi_n(\epsilon)$ from which the small-signal electronic susceptance of a gap with sinusoidal RF field distribution can be determined by the graphical method suggested in Fig 5.13

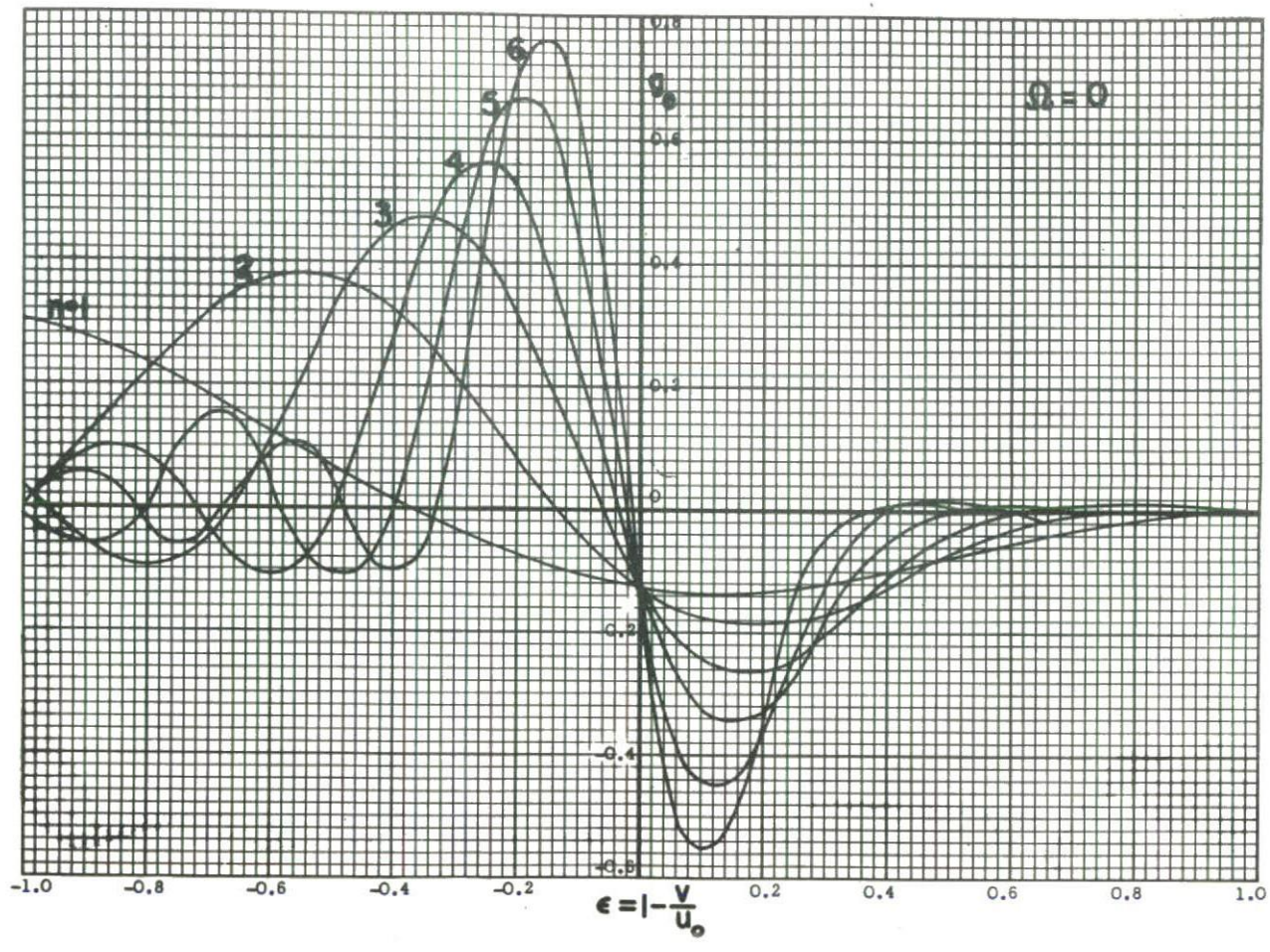

Fig 5.16 Normalized small-signal electronic conductance of a gap having sinusoidal RF field distribution. The space-charge parameter $\Omega = 0$

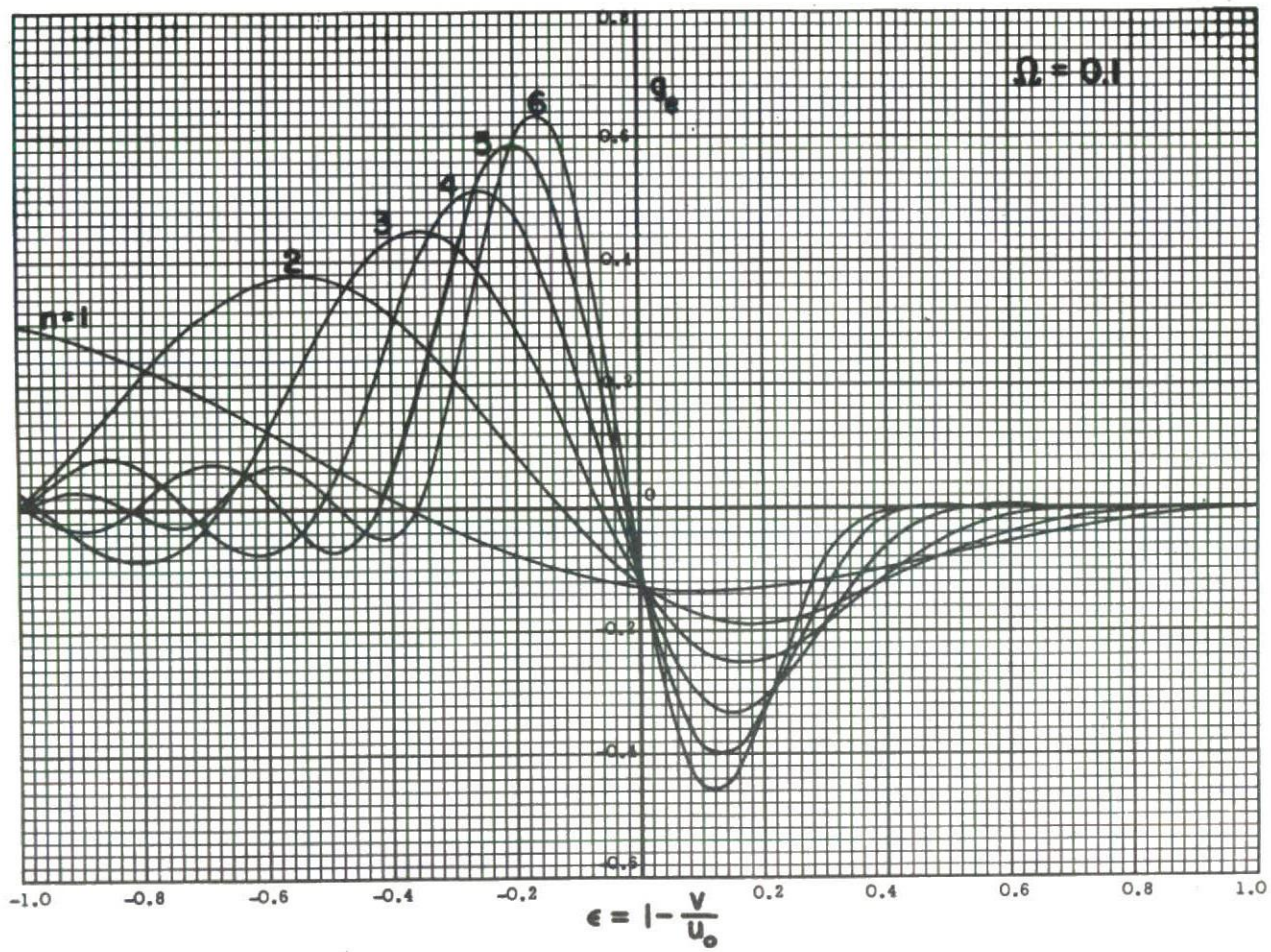

Fig 5.17 Normalized small-signal electronic conductance of a gap having sinusoidal RF field distribution. The space-charge parameter $\Omega = 0.1$

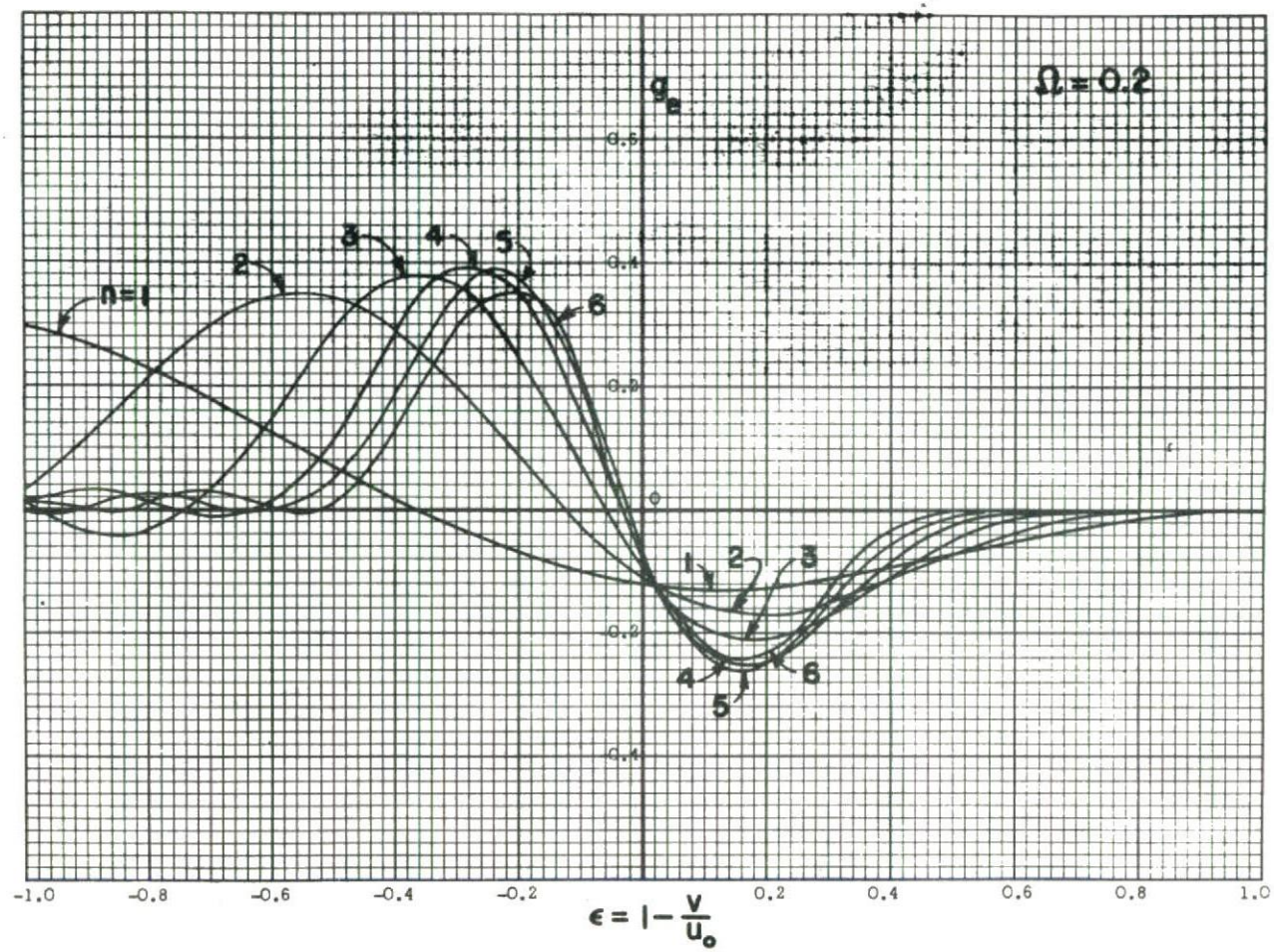

Fig 5.18 Normalized small-signal electronic conductance of a gap having sinusoidal RF field distribution. The space-charge parameter $\Omega = 0.2$

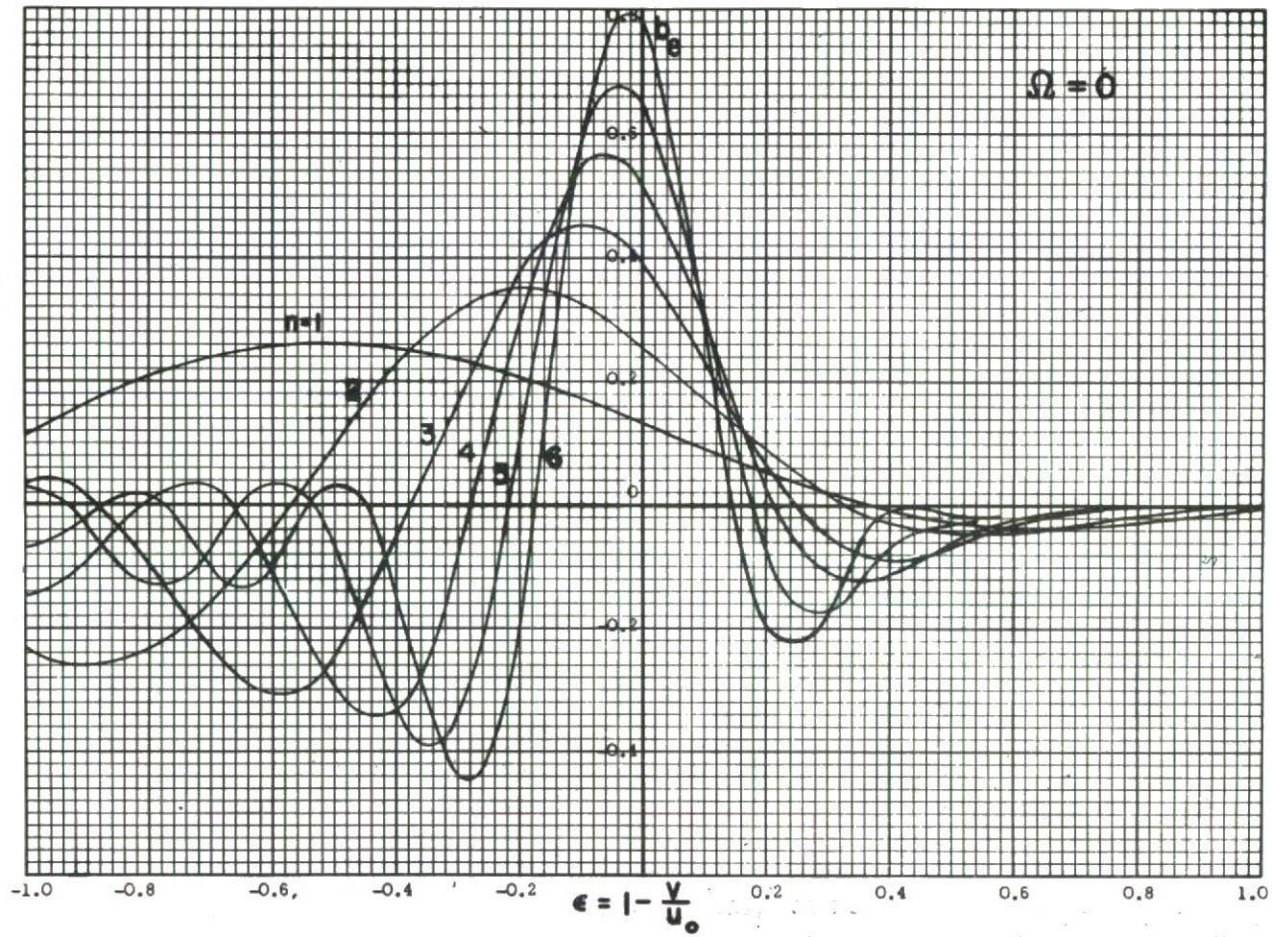

Fig 5.19 Normalized small-signal electronic susceptance of a gap having sinusoidal RF field distribution. The space-charge parameter $\Omega = 0$

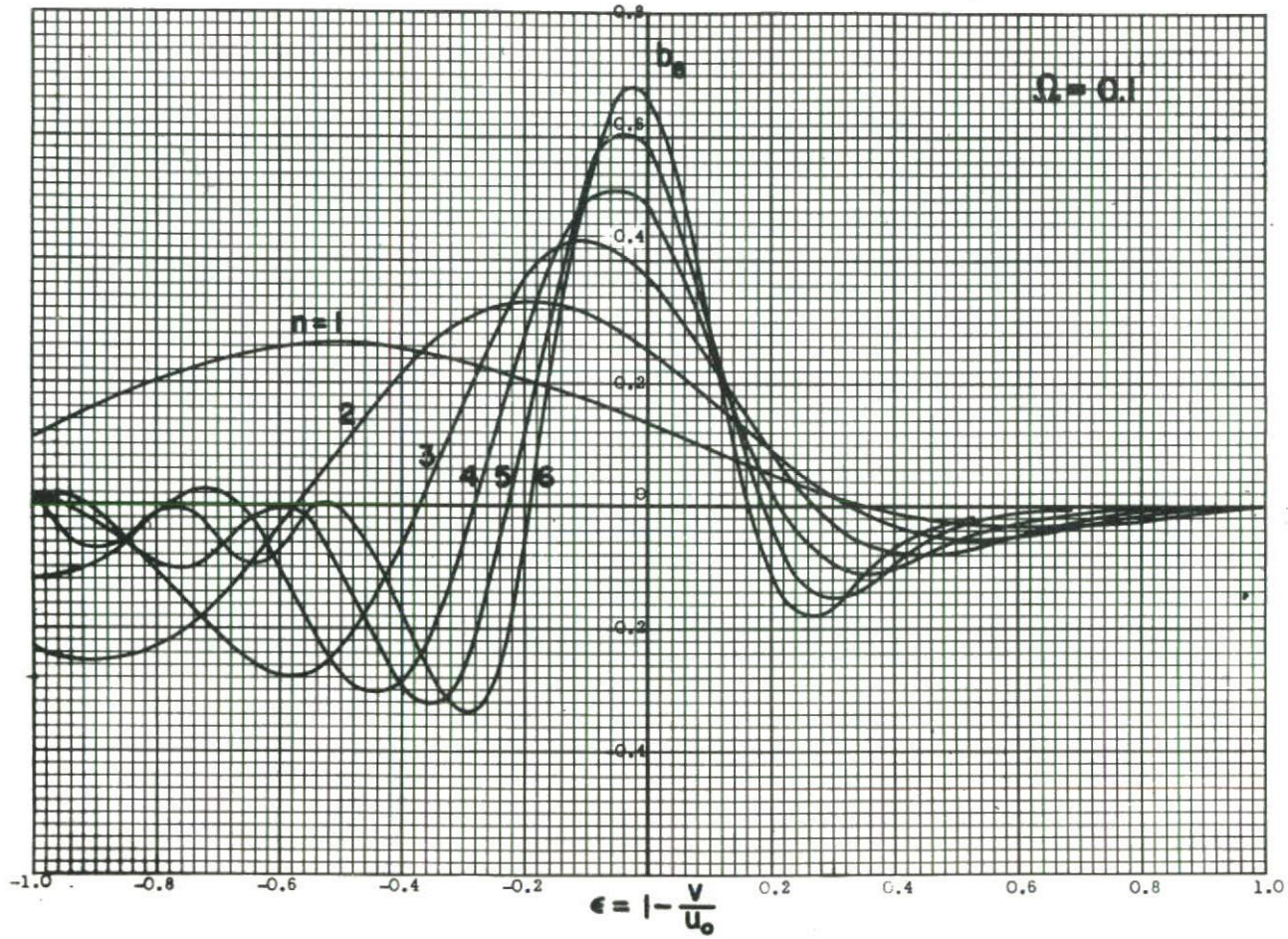

Fig 5.20 Normalized small-signal electronic susceptance of a gap having sinusoidal RF field distribution. The space-charge parameter $\Omega = 0.1$

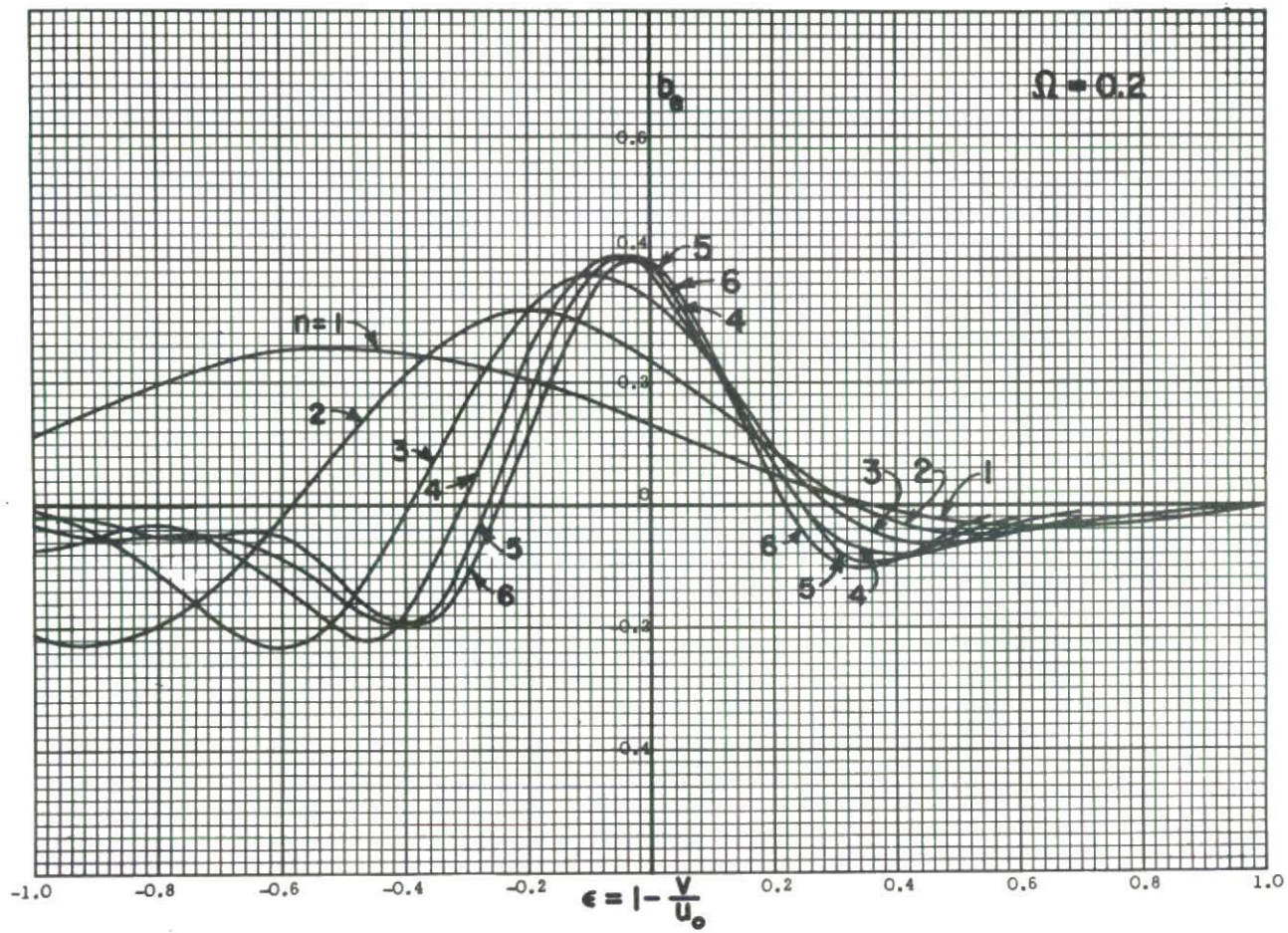

Fig 5.21 Normalized small-signal electronic susceptance of a gap having sinusoidal RF field distribution. The space-charge parameter $\Omega = 0.2$

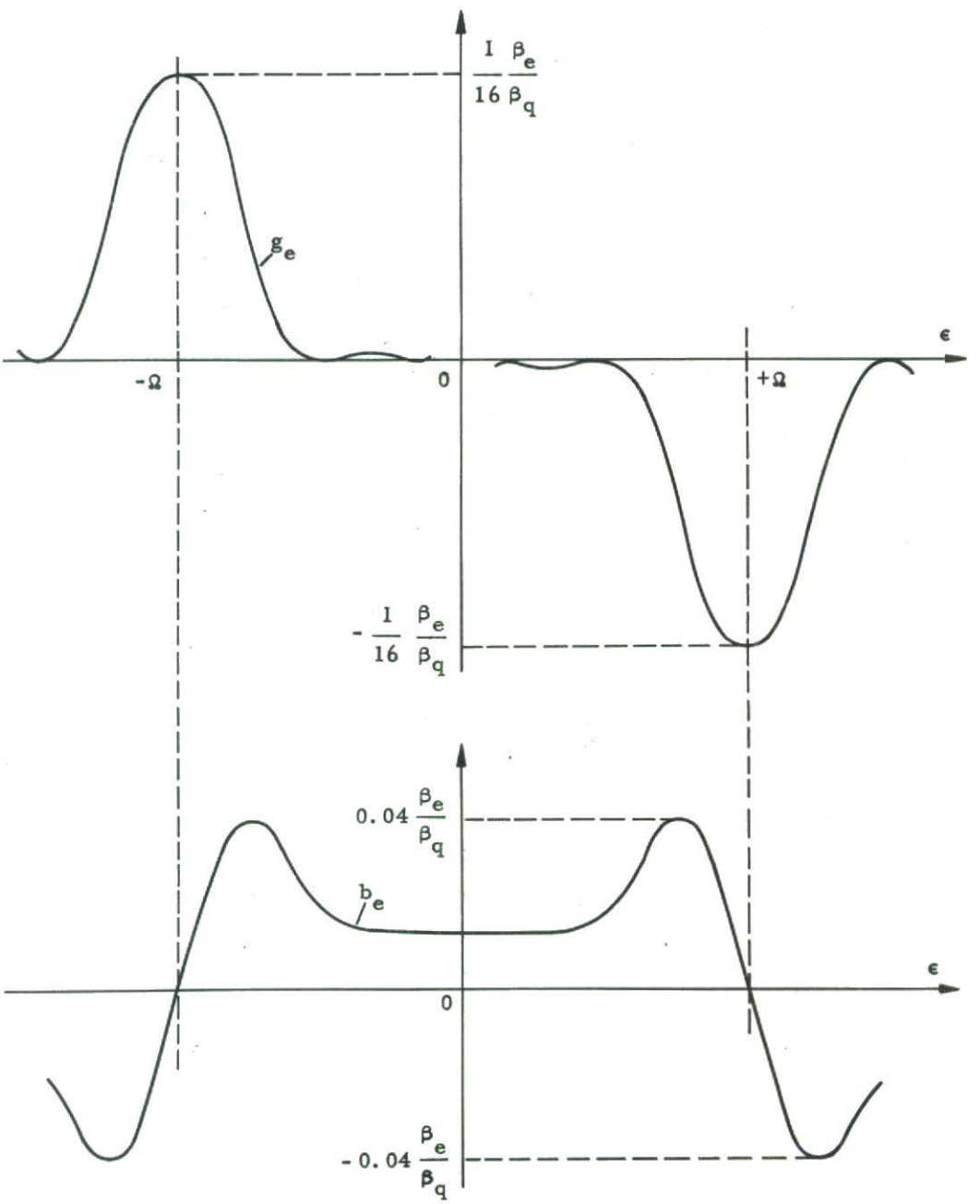

Fig 5.22 Sketch showing the electronic conductance and susceptance of a gap with sinusoidal RF field distribution for the case that $n\Omega \geq 2$

APPENDIX A: GENERAL CIRCUIT EQUATIONS OF CAVITIES WITH EXTENDED INTERACTION GAPS

A general circuit equation for arbitrary resonant cavities interacting with electron beams has been given by Slater in his normal-mode theory of resonant cavities (2). We shall state without proof some of the results from this theory that are useful for the applications that we have in mind, and rewrite the equations in terms of the notations used in the present report.

In principle, the normal-mode theory is applicable to any configurations of the resonant cavity and the electron beam inside its volume, regardless of geometrical details. Slater arrives at his theory by defining two sets of orthogonal vector functions, one of which is solenoidal and the other irrotational. The vector functions satisfy the wave equation inside the cavity with appropriately chosen boundary conditions on the cavity walls. The electromagnetic field quantities in the cavity are then expanded in terms of these orthogonal functions or normal modes. The solenoidal part of any of the vector fields is expanded in terms of the solenoidal normal modes, and the irrotational part of the field in terms of the irrotational normal modes. In particular, the electric field vector $\bar{E}$ is given by

$$\bar{E} = \bar{E}_c + \bar{E}_b \tag{A.1}$$

where the solenoidal part $\bar{E}_c$ and the irrotational part $\bar{E}_b$ can be interpreted physically as the circuit field and the space-charge field, respectively. The solenoidal circuit field $\bar{E}_c$ is given by the solution of Maxwell's equations within the volume bounded by the cavity walls with no free electric charges in the volume. As shown by Slater, the irrotational space-charge field $\bar{E}_b$, which is due to the free distribution of charges in the beam, is derived from a scalar potential satisfying Poisson's equation. The problem of finding $\bar{E}_b$ is essentially an electrostatic problem of determining the field from a known charge distribution, subject to the proper boundary conditions. The space-charge field is thus a local field, which accounts for the fact that it does not contribute to the energy flow from the beam to the surrounding circuit.

It follows from the normal-mode theory that if the internal and possible external cavity losses are negligible (high values of the loaded Q), and the resonant frequencies associated with the normal modes are spaced sufficiently far apart, the excitation of the particular mode that is closest to the operating frequency will be predominant. If this assumption is satisfied, as assumed in the present report, the circuit field $\bar{E}_c$ will simply be given by the particular normal mode that is excited, the contributions to the field from the remaining normal modes being negligible in comparison. For this situation the formulae stated in the following

are those derived by Slater, some of them in the original form and some modified in accordance with the notations used in this report.

Figure A. 1a shows a cavity with an electron beam that enters the interior volume through fine metallic grids in the cavity walls, or alternatively, through short sections of waveguides with cut-off frequencies above the operating frequency. The details of the geometrical configuration of cavity and beam are chosen arbitrarily. The cavity is coupled to the external system through a number of transmission lines of which two are indicated in the figure. The reference planes S_1 and S_2 normal to the transmission lines are the positions to which we shall refer the input admittance when looking into the cavity. These positions, characterized by the fact that the cavity admittance behaves as that of a lumped parallel resonant circuit, are often referred to as "detuned short" positions because the input admittance becomes zero for frequencies far off resonance.

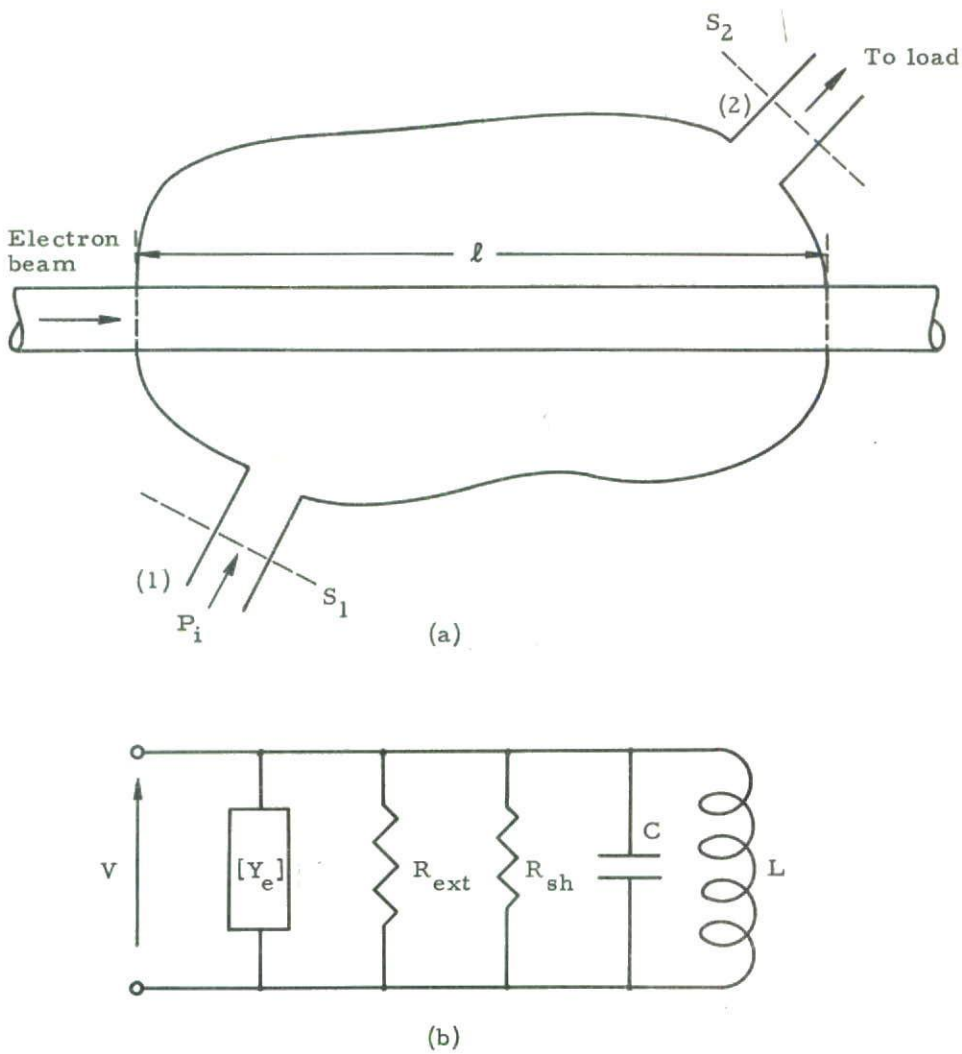

Fig A. 1 Resonant cavity and electron beam configuration

(a) Cavity with arbitrary shape in which the electron beam interacts with the RF electric field over an extended region of length ℓ

(b) Lumped-circuit equivalent for one of the resonant modes

Under the assumption that one single cavity mode is excited, the input admittance y_1 at the reference plane S_1 in the transmission line (1) is given by

$$y_1 = Q_{ext,1}\left[j\left(\frac{\omega}{\omega_o} - \frac{\omega_o}{\omega}\right) + \frac{1}{Q} + \frac{1}{Q_{ext,2}} + \frac{1}{\epsilon_o \omega_o} \frac{\int \bar{i} \cdot \bar{E}_c^* \, dV}{\int \bar{E}_c \cdot \bar{E}_c^* dV} \right] \qquad (A.2)$$

where y_1 is normalized with respect to the characteristic impedance of the transmission line, and the second transmission line is terminated in its characteristic admittance. Of the remaining quantities in the equation, Q is the unloaded Q-value of the cavity; $Q_{ext,1}$ and $Q_{ext,2}$ are the external Q's associated with line (1) and (2), respectively; ω_o is the resonant frequency of the single mode that is excited in the cavity; ω is the signal frequency; ϵ_o is the permittivity of free space; $\bar{i}$ is the complex amplitude of the RF current in the beam; and $\bar{E}_c$ is the complex amplitude of the RF electric field intensity of the solenoidal circuit field. The two integrands on the right are integrated over the volume bounded by the cavity walls and the reference planes S_1 and S_2.

The unloaded Q is defined in the conventional way by

$$Q = \omega_o \frac{W_{em}}{P} \qquad (A.3)$$

where W_{em} is the stored electromagnetic energy in the circuit field, and P is the power dissipated on the surface of the cavity walls due to their finite electrical conductivity. The external Q is also given by Eq (A.3) where in this case P is the power dissipated in the external load.

The stored energy W_{em} alternates periodically between electric and magnetic energy, and is thus given by the maximum electric energy

$$W_{em} = \frac{1}{2} \epsilon_o \int_V \bar{E}_c \cdot \bar{E}_c^* \, dV \qquad (A.4)$$

The last integral in Eq (A.2)

$$\mathcal{P}_e = \frac{1}{2} \int_V \bar{i} \cdot \bar{E}_c^* \, dV \qquad (A.5)$$

is the complex power extracted by the beam in traversing the interior region of the cavity. It is significant that the space-charge field E_b does not contribute to the complex energy flow $\mathcal{P}_e$ except indirectly through its effect on the RF beam current $\bar{i}$ through the modulation processes in the interaction region.

By introducing some additional quantities, which are characteristic for the cavity and beam configuration, we shall give two alternate forms of Eq (A.2). In analogy with the definition (A.3) of the Q-value of a passive circuit, we shall define an electronic Q by the relation

$$Q_e = \omega_o \frac{W_{em}}{\mathrm{Re}\, \mathcal{P}_e} \tag{A.6}$$

Equation (A.2) can then be written

$$y_1 = Q_{ext,1} \left[j(2\delta + \mathrm{Im}\, \mathcal{P}_e) + \frac{1}{Q} + \frac{1}{Q_{ext,2}} + \frac{1}{Q_e} \right] \tag{A.7}$$

where we also have introduced the frequency-tuning parameter δ defined by

$$\delta = \frac{1}{2} \left(\frac{\omega}{\omega_o} - \frac{\omega_o}{\omega} \right) \approx \frac{\omega - \omega_o}{\omega_o} \tag{A.8}$$

Equation (A.7) is quite general in the sense that the concept of an electronic Q representing the effect of the beam is applicable for any beam configuration.

In many practical cases the beam configuration is such that it is possible to define a typical interaction length ℓ and an interaction voltage or gap voltage V. In particular, for a thin linear beam the longitudinal electric field E(x) does not vary appreciably over the beam cross section. In these cases it is natural to rewrite Eq (A.2) in terms of admittances or impedances associated with the cavity and the beam. If V is the gap voltage, to be defined later, the cavity shunt impedance R_{sh} is defined on a power-voltage basis by the relation

$$R_{sh} = \frac{1}{2} \frac{VV^*}{P} \tag{A.9}$$

where P is the power dissipated internally on the cavity walls. The <u>characteristic impedance</u> of the cavity will be defined by

$$\frac{R_{sh}}{Q} = \frac{1}{2} \frac{VV^*}{\omega_o W_{em}} \tag{A.10}$$

The characteristic impedance R_{sh}/Q depends only on the geometrical configuration and the frequency. The theory of multi-cavity klystrons shows that R_{sh}/Q is the deciding circuit parameter as far as ultimate gain and bandwidth are concerned; it seems therefore natural to consider R_{sh}/Q as a "figure of merit" for klystron cavities.

Further, we shall define a total electronic admittance $[Y_e]$ by a similar relation

$$[Y_e] = \frac{2\mathcal{P}_e}{VV^*} \tag{A.11}$$

where $\mathcal{P}_e$ is given by Eq (A.5). The <u>total</u> electronic admittance $[Y_e]$ should not be confused with the electronic admittance Y_e as defined in Eq (2.68). In general $[Y_e]$ is the sum of Y_e, due to modulation by the gap voltage itself, and other terms (transfer admittances) arising from RF modulations imposed on the beam prior to the cavity in question. Only for the case of initial zero beam modulation is $[Y_e]$ equal to Y_e.

Introducing these new notations into Eq (A. 2) we obtain

$$y_1 = Q_{ext,1} \left\{ 2j\delta + \frac{1}{Q} + \frac{1}{Q_{ext,2}} + \frac{R_{sh}}{Q} [Y_e] \right\} \tag{A.12}$$

If also transmission line number (1) is terminated in its characteristic admittance in the same way as line number (2), the admittance looking into the cavity is $-y_1 = -1$, and Eq (A. 12) transfers to

$$\frac{Q}{R_{sh}} \frac{1}{Q_L} (1 + 2jQ_L\delta) + [Y_e] = 0 \tag{A.13}$$

where Q_L is the loaded Q, given by

$$\frac{1}{Q_L} = \frac{1}{Q} + \frac{1}{Q_{ext,1}} + \frac{1}{Q_{ext,2}} \tag{A.14}$$

Equation (A. 13), expressing the complex power balance in a cavity excited in one of its modes by an electron beam, can be considered as the circuit equation for this mode. Its form suggests the lumped-circuit equivalent diagram shown in Fig A. 1b, consisting of the total electronic admittance $[Y_e]$ and the circuit admittance Y_c coupled in parallel. The circuit admittance Y_c is thus given by

$$Y_c = \frac{Q}{R_{sh}} \frac{1}{Q_L} (1 + 2jQ_L\delta) \tag{A.15}$$

According to Eq (A. 13), we have

$$Y_c + [Y_e] = 0 \tag{A.16}$$

The gap voltage V appearing in Eqs (A. 9) and (A. 11) was introduced in a formal way without giving a specific definition of its meaning. Actually, since the gap voltage is not contained in the final equations (A. 12) or (A. 13), its definition is irrelevant. The only restriction on the definition is that it should satisfy the obvious requirement that V must be proportional to the amplitude of the RF electric field intensity. Since the longitudinal RF field distributions of the extended interaction regions considered in this report are quite arbitrary, the conventional definition of gap voltage as the line integral of the electric field intensity across the gap must be rejected. Otherwise a number of RF field distributions such as antisymmetric fields, pure sinusoidal fields, etc, would yield V identically zero regardless of the electric field strength.

The physically most appealing definition of gap voltage seems to be the one that is associated with the maximum absolute value of the Fourier transfer of the longitudinal electric field:

$$V = \left| \int_{-\ell/2}^{\ell/2} E(x)\, e^{j\beta_e x}\, dx \right|_{max} \tag{A.17}$$

where $E(x)$ is the longitudinal electric field and ℓ the length of the interaction gap. In this case V has a definite physical meaning, specifying the maximum kinetic voltage modulation imposed on a beam with negligible space-charge traversing the gap with the appropriate DC beam velocity that maximizes the Fourier transform, (see Eq (5.3)). However, due to the complexity of Eq (A.17) we shall adopt the following simpler definition of V used throughout this paper:

$$VV^* = \ell \int_{-\ell/2}^{\ell/2} E(x)\, E(x)^* \, dx \tag{A.18}$$

This equation can also be written

$$V = \ell \sqrt{\overline{EE^*}} \tag{A.19}$$

where $\overline{EE^*}$ is the mean square of E. The definition (A.18) thus implies that the gap voltage V is an rms (root mean square) voltage in the longitudinal co-ordinate. For the simple configuration of a narrow gap with constant field the general definition (A.18) reduces to the conventional one, namely $V = E\ell$.

APPENDIX B: DERIVATION OF A SECOND-ORDER DIFFERENCE EQUATION FOR THE VOLTAGE GAIN

The system of linear algebraic equations (3.10) can be transformed to a second-order linear homogeneous difference equation by forming a linear combination of the last three equations. Assuming p equal or larger than four, we find

$$\sum_{r=2}^{p-3} (a_p Y_{p-2,r} + b_p Y_{p-1,r} + Y_{p,r})\,\eta_r$$

$$+ (a_p Y_{p-2,p-2} + b_p Y_{p-1,p-2} + Y_{p,p-2})\,\eta_{p-2}$$

$$+ (b_p Y_{p-1,p-1} + Y_{p,p-1})\eta_{p-1} + Y_{p,p}\,\eta_p = 0 \qquad \text{(B.1)}$$

where a_p and b_p are suitable constants which are functions of p but not of r. Evidently this relation reduces to a linear combination of η_p, η_{p-1}, and η_{p-2} if the following relation is identically satisfied:

$$a_p Y_{p-2,r} + b_p Y_{p-1,r} + Y_{p,r} = 0 \quad \text{for} \quad r = 2, \text{---} p-3 \qquad \text{(B.2)}$$

We shall show that a_p and b_p can be chosen such as to satisfy this requirement. Expressing the transfer admittances $Y_{p-2,r}$ $Y_{p-1,r}$ and $Y_{p,r}$ explicitly in terms of the coupling coefficients of the slow and the fast space-charge waves using Eq (2.67), and rearranging terms, we obtain from Eq (B.2)

$$M_r^+ e^{-j\beta_e^+ \ell_{p-2,r}} \left[a_p M_{p-2}^{+*} + b_p M_{p-1}^{+*} e^{-j\beta_e^+ \ell_{p-1,p-2}} + M_p^{+*} e^{-j\beta_e^+ \ell_{p,p-2}} \right]$$

$$- M_r^- e^{-j\beta_e^- \ell_{p-2,r}} \left[a_p M_{p-2}^{-*} + b_p M_{p-1}^{-*} e^{-j\beta_e^- \ell_{p-1,p-2}} + M_p^{-*} e^{-j\beta_e^- \ell_{p,p-2}} \right] = 0$$

$$r = 2, \text{---} p-3 \qquad \text{(B.3)}$$

where $\beta_e^+ = \beta_e + \beta_q$ and $\beta_e^- = \beta_e - \beta_q$. For arbitrary values of r this equation is satisfied only if the quantities inside the two brackets vanish identically. This requirement yields two equations for determination of the quantities a_p and b_p. We obtain

$$a_p = \frac{M_{p-1}^{+*} M_p^{-*} e^{j\beta_q \ell_{p,p-1}} - M_{p-1}^{-*} M_p^{+*} e^{-j\beta_q \ell_{p,p-1}}}{M_{p-1}^{-*} M_{p-2}^{+*} e^{j\beta_q \ell_{p-1,p-2}} - M_{p-1}^{+*} M_{p-2}^{-*} e^{-j\beta_q \ell_{p-1,p-2}}} e^{-j\beta_e \ell_{p,p-2}} \qquad \text{(B.4)}$$

$$b_p = \frac{-M_{p-2}^{+*} M_p^{-*} e^{j\beta_q \ell_{p,p-2}} + M_{p-2}^{-*} M_p^{+*} e^{-j\beta_q \ell_{p,p-2}}}{M_{p-1}^{-*} M_{p-2}^{+*} e^{j\beta_q \ell_{p-1,p-2}} - M_{p-1}^{+*} M_{p-2}^{-*} e^{-j\beta_q \ell_{p-1,p-2}}} e^{-j\beta_e \ell_{p,p-1}} \qquad (B.5)$$

If a_p and b_p are chosen according to these equations, Eq (B.1) reduces to the following second-order homogeneous difference equation:

$$Y_{p,p}\eta_p + (b_p Y_{p-1,p-1} + Y_{p,p-1})\eta_{p-1} + (a_p Y_{p-2,p-2} + b_p Y_{p-1,p-2} + Y_{p,p-2})\eta_{p-2} = 0 \qquad (B.6)$$

where the quantities appearing in the coefficients depend only on parameters associated with the cavities $p-2$, $p-1$, and p.

Although the general expressions for a_p and b_p given in Eqs (B.4) and (B.5) are relatively complex, they simplify considerably if the coupling coefficients of all the gaps are the same, i e if $M_{p-2}^{+} = M_{p-1}^{+} = M_p^{+}$ and $M_{p-2}^{-} = M_{p-1}^{-} = M_p^{-}$. In this slightly less general case, to which we will confine our attention, a_p and b_p are given by

$$a_p = \frac{\sin \beta_q \ell_{p,p-1}}{\sin \beta_q \ell_{p-1,p-2}} e^{-j\beta_e \ell_{p,p-2}} \qquad (B.7)$$

$$b_p = -\frac{\sin \beta_q \ell_{p,p-2}}{\sin \beta_q \ell_{p-1,p-2}} e^{-j\beta_e \ell_{p,p-1}} \qquad (B.8)$$

In this case the transfer admittance $Y_{p,r}$ defined in Eq (2.67) can be written

$$Y_{p,r} = e^{-j\beta_e \ell_{p,r}} \left(2G_e \cos \beta_q \ell_{p,r} + \frac{1}{W} \bar{M}^2 \sin \beta_q \ell_{p,r}\right) \qquad (B.9)$$

where the beam loading G_e is given by Eq (2.70), and $\bar{M}^2$ is defined as the arithmetic mean of the squares of the coupling coefficients of the slow and the fast space-charge waves

$$\bar{M}^2 = \frac{1}{2}\left(|M^+|^2 + |M^-|^2\right) \qquad (B.10)$$

Using Eq (B.9) for evaluation of the coefficients in the difference equation (B.6), we obtain

$$Y_{p,p}\eta_p - 2e^{-j\beta_e \ell_{p,p-1}}$$

$$\times\left(\frac{1}{2}\frac{\sin\beta_q \ell_{p,p-2}}{\sin\beta_q \ell_{p-1,p-2}} Y_{p-1,p-1} - G_e \cos\beta_q \ell_{p,p-1} - j\frac{\overline{M}^2}{2W}\sin\beta_q \ell_{p,p-1}\right)\eta_{p-1}$$

$$+ e^{-j\beta_e \ell_{p,p-2}}\frac{\sin\beta_q \ell_{p,p-1}}{\sin\beta_q \ell_{p-1,p-2}}\left(Y_{p-2,p-2} - 2G_e\right)\eta_{p-2} = 0 \qquad \text{(B.11)}$$

If the generality is restricted still more by the assumption of equal cavity spacings, i e, $\ell_{p,p-1} = \ell_{p-1,p-2} = \text{---} = \ell$, Eq (B.11) simplifies to

$$Y_{p,p}\eta_p - 2e^{-j\beta_e \ell}\left[(Y_{p-1,p-1} - G_e)\cos\beta_q \ell - j\frac{\overline{M}^2}{2W}\sin\beta_q \ell\right]\eta_{p-1}$$

$$+ e^{-j2\beta_e \ell}\left[Y_{p-2,p-2} - 2G_e\right]\eta_{p-2} = 0 \qquad \text{(B.12)}$$

In the difference equation or recurrence formula derived here in various forms (Eqs (B.6), (B.11) and (B.12)), the RF gap voltages of any three consecutive cavities are related by linear expressions valid for arbitrarily tuned cavities.

References

(1) Pierce, J R - Traveling-wave tubes (book), D Van Nostrand Co, New York (1950)

(2) Slater, J S - Microwave electronics (book), D Van Nostrand Co, New York (1950)

(3) Kleen, W - Einführung in die Mikrowellen-Elektronik, Teil I (book), S Hirzel, Zürich (1952)

(4) Kleen, W
K Pøschl - Einführung in die Mikrowellen-Elektronik, Teil II (book), S Hirzel, Stuttgart (1958)

(5) Beck, A H W - Space-charge waves (book), Pergamon Press, London (1958)

(6) Hamilton, D R
J K Knipp
J B H Kuper - Klystrons and microwave triodes (book), MIT Rad Lab Series 7, McGraw-Hill Book Co, New York (1948)

(7) Beck, A H W - Velocity modulated thermionic tubes (book), Cambridge University Press (1948)

(8) Chodorow, M
E J Nalos - The design of high-power traveling-wave tubes, Proc IRE 44, 649-59 (1956)

(9) Chodorow, M
T Wessel-Berg - A high-efficiency klystron with distributed interaction, submitted for publication in Proc IRE

(10) Wessel-Berg, T - A general theory of klystrons with arbitrary, extended interaction fields, Technical Report 376, Stanford University, Microwave Laboratory, Stanford, Cal (1957)

(11) Heil, A A
O Heil - Eine neue Methode zur Erzeugung kurzer ungedampfter Elektromagnetischen Wellen von grosser Intensität, Zeit Phys 95, 752-73, (1935)

(12) Varian, R H
S F Varian - A high frequency oscillator and amplifier, J Appl Phys 10, 321-7 (1939)

(13) Webster, D L - Theory of klystron oscillations, J Appl Phys 10, 864-72 (1939)

(14) Hahn, W C - Small-signal theory of velocity-modulated electron beams, Gen Elec Rev 42, 258-70 (1939)

(15) Ramo, S - Space charge and field waves in an electron beam, Phys Rev 56, 276 (1939)

(16) Wessel-Berg, T - An analogy between multi-cavity klystrons and loaded transmission lines, Technical Report 352, Stanford University, Microwave Laboratory, Stanford, Cal (1956)

(17) Bloom, S
R W Peter - Transmission-line analog of a modulated electron beam, RCA Rev XV, 1, 95-112 (1954)

(18) Chu, L J - A kinetic power theorem, paper delivered at the IRE conference PGED, Durham, N H (1951)

(19) Louisell, W H
J R Pierce
- Power flow in electron beam devices, Proc IRE 43, 425 (1955)

(20) Haus, H A
D L Bobroff
- Small-signal power theorem for electron beams, J Appl Phys 28, 694-704 (1957)

(21) Kliver, J W
- Small signal power conservation theorem for irrotational electron beams, J Appl Phys 29, 618-22 (1958)

(22) Kreuchen, K H
B A Auld
N E Dixon
- A study of the broadband frequency response of the multicavity klystron amplifier, J Electronics 2, 529-67 (1957)

(23) Isaacs, A T
- Iterative methods for stagger-tuning multicavity klystron amplifiers, M A Sc Thesis, University of British Columbia, Vancouver, B C (1958)

(24) Louisell, W H
C F Quate
- Parametric amplification of space charge waves, Proc IRE 46, 707-16 (1958)

(25) Margenau, H
G M Murphy
- The mathematics of physics and chemistry (book) p 80, D Van Nostrand Co, New York (1943)

(26) Smullin, L D
C Fried
- Microwave noise measurements on electron beams, Trans IRE PGED 1, 4, 168 (1954)

(27) Rowe, H E
- Shot noise in electron beams at microwave frequencies, Sc D Thesis, MIT (1952); also MIT Research Lab Electronics Tech Rep 239 (1952)

(28) Gould, R W
- Traveling-wave couplers for longitudinal beam-type amplifiers, Proc IRE 47, 419-26 (1959)

(29) Bers, A
- Quarterly progress report 52, MIT Research Lab of Electronics, 39-43 (1959)

RS